Ice-sheet dynamics and climate fluctuations during the Weichselian glaciation along the southwestern Baltic Sea coast

I n a u g u r a l d i s s e r t a t i o n

zur

Erlangung des akademischen Grades eines

Doktors der Naturwissenschaften (Dr. rer. nat.)

der

Mathematisch-Naturwissenschaftlichen Fakultät

der

Ernst-Moritz-Arndt-Universität Greifswald

vorgelegt von

Michael Kenzler

geboren am 20.10.1981

in Ludwigslust

Greifswald, 19. April 2017

'The aim of science is not to open a door to infinite wisdom but to set a limit to infinite error.'

Bertolt Brecht (1898-1956)

Table of contents

I. List of figures

II.   List of tables

III. Abstract

This thesis aims to develop a palaeogeographic and chronostratigraphic model of the southwestern Baltic Sea area, to improve our understanding of the depositional history of the Late Pleistocene on both a local and a transregional scale. New sedimentological, palaeontological and numerical age data will be presented from three reference sites located at the coast of NE Germany. So far, the chronostratigraphic assignment of Saalian and Weichselian sediments of NE Germany has been based mainly on lithostratigraphic methods and on sparse numerical age data, resulting in a fragmentary age database. Modern sedimentological approaches, such as facies analyses, have been applied only at a few isolated profiles. Thus, a reliable reconstruction of the depositional environments and their stratigraphic positions is still missing for the study area, which makes the correlation between Pleistocene successions from NE Germany and other circum-Baltic regions problematic. To address these lithostratigraphic and geochronologic issues, three crucial profiles were re-investigated using a multiproxy approach, including sedimentological, geochronological, and palaeontological techniques. The Glowe and Kluckow sites are located on the peninsula of Jasmund (Rügen Island), whereas the Klein Klütz Höved (KKH) section is situated between Wismar and Travemünde at the coast of the Mecklenburg Bay. The age-constraining of critical horizons was conducted by luminescence dating of feldspar and quartz grain minerals. Together, these successions represent the Late Saalian to Late Weichselian period and give rise to the following picture.

The Glowe and Kluckow sections reveal that ice-free conditions dominated the study site between 47 and 42 ka. Deposition occurred in a steppe-like environment with moderate summers and cool winters. Meandering and braided river systems inhabited by various freshwater species, such as *Anodonta cygnea*, *Pisidium amnicum* and *Perca fluviatilis*, shaped the landscape. A subsequent cooling phase resulted in the establishment of a periglacial landscape and the formation of ice-wedges. This phase is shown in this thesis to be connected to the Klintholm advance documented at 34±4 ka in Denmark. Furthermore, the data indicate the formation of a lacustrine basin during the transition of MIS 3 to MIS 2 under sub-arctic climate conditions. A potential link to the Kattegat ice advance (29 – 26 ka) will be proposed. At 23±2 ka, the study area was characterised by proglacial and ice-contact lakes related to the Last

Glacial Maximum ice advance of the Scandinavian Ice Sheet (SIS). This is the first documented SIS advance of Weichselian age, which reached Jasmund at 22±2 ka.

The KKH sedimentary succession comprises deposits of Late Saalian to Late Weichselian age: after a period of deglaciation between ~139-134 ka (Termination II; MIS 6), which is preserved in a glaciofluvial sequence deposited in a braided river system, a lacustrine environment was established in an arctic to subarctic climate. During this time, the landscape was vegetated by typical Late Saalian flora communities. The Eemian interglacial is represented by lacustrine to brackish deposits covering the reference pollen zones 1 to 3. During this initial part of the Eemian, thermophile forest elements spread (*Quercus*, *Ulmus*), indicating a deciduous forest. The presence of brackish ostracods represents the influence of a marine transgression between 300 and 750 years after the beginning of the Eemian period. A hiatus of more than 90,000 years separates the Eemian from the overlying Late Weichselian sediments. During the Late Weichselian period, the deposition at KKH was dominated by glaciolacustrine and subglacial facies, where the first Weichselian ice advance occurred at 20±2 ka.

The sedimentological and geochronological findings in this thesis provide valuable information for the reconstruction of the palaeoenvironmental history from the Late Saalian to Late Weichselian period. The Late Saalian palaeoenvironmental setting is reconstructed, including Termination II and the initial phase of the Eemian interglacial. Furthermore, the Eemian marine transgression is shown to have occurred 300 to 750 years after the beginning of this interglacial. The first proven Weichselian advance of the SIS approached NE Germany between ~23 and ~20 ka. In contrast, there is no evidence to support a pre-LGM advance of Weichselian age to the study area, as proposed by several authors, neither at Glowe and Kluckow, nor at the KKH site. Based on the presented results, and contra what was previously assumed, the MIS 3 Ristinge and Klintholm advance of the SIS, documented in Denmark, did not reach NE Germany.

IV. Zusammenfassung

Das Ziel der vorliegenden Arbeit besteht in der Erstellung von paläogeographischen und chronostratigraphischen Modellen, welche das Verständnis der spätpleistozänen Ablagerungsgeschichte auf lokaler und regionalen Ebene im südwestlichen Ostseeraum verbessern sollen. Hierzu werden neue sedimentologische, paläontologische und numerische Alters-Daten von drei Referenz-Profilen der nordostdeutschen Küste präsentiert. Bislang basiert die chronostratigraphische Einordnung der saale- und weichselzeitlichen Sedimente in diesem Gebiet hauptsächlich auf lithostratigraphischen Methoden und einzelnen numerischen Altersdaten, woraus sich eine nur unvollständige Altersdatenbasis ergibt. Moderne sedimentologische Ansätze, wie z.B. Fazies Analysen, sind nur an einzelnen Profilen angewendet worden. Dies verhindert eine verlässliche Rekonstruktion der Ablagerungsmilieus und deren stratigraphische Einstufung, wodurch die Korrelationen zwischen pleistozänen Abfolgen Nordost-Deutschlands mit denen anderer zirkum-baltischen Regionen erheblich erschwert wird. Um diese lithostratigraphischen und geochronologischen Probleme zu lösen, wurden drei Profile mit Hilfe eines Multiproxy-Ansatzes, einschließlich sedimentologischen, geochronologischen und paläontologischen Techniken, untersucht. Die Kliffaufschlüsse Glowe und Kluckow befinden sich auf der Halbinsel Jasmund (Insel Rügen), wohingegen Klein Klütz Höved (KKH) an der Küste der Mecklenburger Bucht zwischen Wismar und Travemünde liegt. Die Alterseinstufung kritischer Horizonte gelang mit Hilfe der Lumineszenz Datierung von Feldspat- und Quarz-Mineralkörnern. Insgesamt repräsentieren die untersuchten Abfolgen den Zeitraum zwischen dem ausgehenden Saaleglazial und dem Letzten Glazialen Maximum (LGM).

Die Sequenzen von Glowe und Kluckow belegen eisfreie Bedingungen in der Phase zwischen 47 und 42 ka in einer steppen-ähnlichen Landschaft, mit moderaten Sommern und kühlen Wintern. Mäandrierende und verzweigte Flusssysteme, bewohnt von Süßwasserarten, wie z.B. *Anodonta cygnea*, *Pisidium amnicum* and *Perca fluviatilis*, gestalteten die Landoberfläche maßgeblich. Eine anschließende Abkühlungsphase führte zur Herausbildung einer periglazialen Landschaft und dem Entstehen von Eiskeil-Polygonnetzen. In der vorliegenden Arbeit wird gezeigt, wie diese Abkühlung mit dem dänischen Klintholm Vorstoss (34±4 ka) des Skandinavischen Inlandeises (SI) in Verbindung steht. Des Weiteren zeigen die Daten,

dass sich ein lakustrines Becken im Untersuchungsgebiet am Übergang vom MIS 3 zum MIS 2 unter sub-arktischen Klimabedingungen gebildet hat. Ein möglicher Zusammenhang mit dem Kattegat Eisvorstoß (29 – 26 ka) wird diskutiert. Um 23±2 ka dominierten im heutigen Gebiet von Jasmund proglaziale Seen, welche im Vorfeld des vorrückenden SI lagen. Der erste auf Jasmund nachgewiesen SI Vorstoß mit weichselzeitlichem Alter erfolgte um 22±2 ka.

Die sedimentären Einheiten am KKH Aufschluss umfassen Ablagerungen von der Spätsaalezeit bis zum LGM: Eine Phase der Deglaziation erfolgte zwischen ~139-134 ka (Termination II; MIS 6), wobei glaziofluviatilen (verzweigte Flusssysteme) und lakustrinen Ablagerunsbedingungen dominierten. Die Landschaft unterlag arktische bis subarktische Klimabedingungen und wurde geprägt von einer typischen spätsaalezeitlichen Florengemeinschaft. Lakustrine und brackische Sedimente, welche die Referenz-Pollen Zonen 1 bis 3 repräsentieren, belegen die Erhaltung von früh-eemzeitlichen Ablagerungen am KKH Aufschluss. Während dieser initialen Phase des Eem-Interglazials breiteten sich wärmeliebende Arten (*Quercus*, *Ulmus*) aus und bildeten einen Laubwald. Das Vorhandensein brackischer Ostrakoden verweist auf die Beeinflussung einer marinen Transgression zwischen 300 und 750 a nach dem Beginn des Eems. Ein Hiatus von 90 000 Jahre trennt die Ablagerungen des Eems von den darüber liegenden spätweichselzeitlichen Einheiten. Während des späten Weichsel Glazials wurde die Sedimentation von glaziolakustrinen und subglazialen Fazien dominiert. Der erste belegte Weichsel-Vorstoss ist auf 20±2 ka datiert worden.

Die sedimentologischen und geochronologischen Ergebnisse dieser Arbeit liefern wichtige Informationen zur Rekonstruktion der Ablagerungsbedingungen im Zeitraum vom ausgehenden Saaleglazial bis zum LGM. Unter anderem wurde die Landschaftsgeschichte während der Deglaziation des Saale-Glazials (Termination II) und des beginnenden Eems rekonstruiert. Die Eem-Transgression erfolgte im Untersuchungsgebiet zwischen 300 bis 750 a nach Beginn des Interglazials. Der erste nachgewiesene Weichsel-Vorstoß des SI erreichte NE Deutschland zwischen ~23 und ~20 ka. Hingegen gibt es keine Hinweise in den untersuchten Abfolgen, welche die Existenz eines weichselzeitlichen pre-LGM Eisvorstoßes belegen. Basierend auf den präsentierten Ergebnissen und im Kontrast zu dem was vorher angenommen wurde, erreichten sowohl der Ristinge, wie auch der Klintholm Vorstoss, nicht den norddeutschen Raum.

1   Introduction

1.1   Motivation

The investigation of the climatic evolution of the Pleistocene period (2.6 Ma – 12 ka; Cohen & Gibbard 2011), together with its depositional history, glacier dynamics and ecosystem development, provides critical information in the assessment of whether the current climate change is atypical, and to what extent it is anthropogenic in origin (IPCC 2013). The Scandinavian Ice Sheet (SIS) was one of the main ice masses in the northern hemisphere during the Pleistocene and covered large regions of the North European Plain, during the Elsterian (~400 – ~320 ka, Litt et al. 2007), Saalian (~300 – ~130 ka; Litt et al. 2007), and Weichselian periods (115 – 12 ka; Cohen & Gibbard 2012). Various stadial and interstadial sediments document the Late Pleistocene depositional history of this area. The investigation of these deposits will help to understand the complicated response of the SIS to climate fluctuations during the last interglacial-glacial cycle.

The Weichselian Glaciation and the associated phases of advances and retreats of the SIS (Tab. 1.1) have significantly shaped the landscape around the southwestern Baltic Sea. The dynamics of the SIS during the Weichselian Glaciation resulted in several distinct sedimentological successions, which contain detailed information about past biogeosystems, notably for the Late Pleistocene time. Understanding the distribution of the depositional environments and their corresponding chronostratigraphic positions can help reconstruct the palaeogeographic extent of the SIS during the Weichselian period (Hughes et al. 2016). For example, a subglacial till indicates the presence of the SIS, whereas fluvial or lacustrine layers refer to ice-free conditions (*e.g.* Wohlfarth 2010; Anjar et al. 2012; Kenzler et al. 2017). This information can improve our understanding of the interaction between inland ice masses and climate fluctuations, and the interpretation of current climate signals and the possible response of landscape dynamics and sea-level changes. These data are crucial for advancing the modeling of the future climate development and the response of the Greenlandic and Antarctic ice shields (IPCC 2013).

Distinctive morphological landmarks in NE Germany (Fig. 1.1; Lüthgens 2011) are evidence of the remarkable dynamics of the SIS, especially during Marine Isotope

Tab. 1.1 Overview of Scandinavian Ice Sheet advances reached NE Germany and their stratigraphic position

Formation[1]	SIS advances[1]	Age estimation[2]	NW European Stages	MIS
qw3	Mecklenburgian adv.	17 - 15 ka		MIS 2
qw2main	Pomeranian main adv.	20 - 18 ka		MIS 2
qw2max	Pomeranian max. adv.	20 - 18 ka	Weichselian Glaciation	MIS 2
qw1F	Frankfurt adv.	21 - 20 ka		MIS 2
qw1B	Brandenburg adv.	(34)[3] - 21 ka		MIS (3) - 2
qw0	Warnow adv.	<110 - >40 ka		MIS 5d - 3
		127 - 110 ka	Eemian Interglacial	MIS 5e
qs2	Warthe adv.	150 - 130 ka	Saalian Glaciation	MIS 6
qs1	Drenthe adv.	191 - >150 ka		MIS 6

[1] Müller (2004); Müller & Obst (2006)

[2] Müller (2004); Litt et al. (2007); Brauer et al. (2007); Kenzler et al. (2010)

[3] Lüthgens et al. (2010b)

Stage 2 (MIS 2, 29–14 ka; Cohen & Gibbard 2012). Within a few 1,000 years, the southwestern ice front of the SIS oscillated several 100 kms (Hughes et al. 2016), massively shaping the landscape of NE Germany, thus making it an outstanding region for sedimentological and chronostratigraphic studies. Especially the German Baltic Sea coast exhibits numerous excellent outcrops with Pleistocene successions that span long time ranges (*i.e.* Saalian to Weichselian, Tab. 1.1; Ludwig 1964). Often these sequences are more complete than those of more proximal (Sweden; Alexanderson et al. 2010) or distal sites (ice marginal positions in Brandenburg, Germany; Lüthgens & Böse 2011) in relation to the ice summit. Due to the lack of a reliable absolute age chronology, however, the reconstruction of the general stratigraphy of the Late Pleistocene in NE Germany has so far mainly been based on provenance analyses of glacial diamicts (tills) (TGL 25232, 1971; Panzig 1995; Müller 2004), and sparse numerical age data or pollen (*e.g.* Steinich 1992; Strahl et al. 1994; Krbetschek 1995; Lüthgens et al. 2011; Rinterknecht et al. 2014). Hence, there are substantial uncertainties concerning the timing of SIS advances and retreats in NE Germany, especially during the Weichselian period (Tab. 1.1; Müller 2004; Lüthgens & Böse 2011; Lüthgens et al. 2011; Stephan 2014; Kenzler et al. 2015; Hardt et al. 2016; Obst et al. 2017). Compared to the better-constrained records from Denmark and Sweden (*e.g.* Houmark-Nielsen 2010), the age database for Late Pleistocene deposits of NE Germany is fragmentary at best, leading to correlation problems of, for instance,

individual ice advances and their corresponding deposits between Denmark and Sweden and Germany. Although there has been a long tradition of studying Quaternary successions, notably at cliff sections of the German Baltic Sea coast, modern process-response sedimentological analyses, such as facies analysis, have been conducted in only a limited number of case studies. Hence, the correlation between Pleistocene successions is often impossible, even on a local scale. The main issues addressed in this thesis therefore are:

- *Transition from the Saalian to the Eemian period* – Very few accessible profiles exist that document the Late Saalian to Eemian period in NE Germany, so the penultimate deglaciation and the transition to interglacial conditions is poorly understood.

- *Early- to mid-Weichselian SIS advance in NE Germany* – Based on lithostratigraphic data from boreholes, Müller (2004) proposes an early to mid-Weichselian ice advance (W0, Warnow advance) of the SIS approaching NE Germany, which he correlates to the Middle Weichselian Ristinge ice advance in Denmark (Houmark-Nielsen 2003; Obst et al. 2017). However, due to the lack of absolute age constraints, it is unclear to what extent the reported MIS 3 ice advance in Denmark is correlatable to NE Germany.

- *Depositional environment during MIS 3* – The environmental and depositional conditions during the Weichselian interstadial phases are virtually uninvestigated in NE Germany. In contrast, studies from Sweden, Denmark and Norway have documented several warmer stages with ice-free conditions during MIS 4 and MIS 3. Deposits from this time have only been fragmentarily reported for NE Germany.

- *Two-folded Last Glacial Maximum (LGM)* – The presence of a two-folded LGM ice advance through NE Germany during the transition of MIS 3 and MIS 2, as proposed by Lüthgens et al. (2011), has not yet been unequivocally established.

- *Age assessment of LGM advances* – Several advances and retreats of the SIS have been documented in NE Germany during the LGM, but, due to the lack of a reliable numerical age data base, their ages have often only been estimated.

To address these issues, three reference profiles from the southwestern Baltic Sea coast were re-investigated using a combination of sedimentological, geochronological and palaeontological methods: Glowe and Kluckow (located on the peninsula of Jasmund, Rügen Island), and Klein Klütz Höved (KKH, situated between Wismar and Travemünde) (Fig. 1.1). Absolute dating methods are required to age-constrain the glacial dynamics, such as luminescence dating, cosmogenic exposure dating, or radiocarbon ages (Hardt & Böse 2016). This thesis applies luminesence dating to obtain absolute ages for the dynamics of the SIS in NE Germany, in addition to facies analyses, geological mapping and palaeontology. These results are combined with the available data from previous research, to develop a palaeogeographic/ chronostratigraphic model that will significantly improve our understanding of the Eemian to Weichselian period. Finally, the findings will help to assess the complicated response of the SIS to past climate signals recovered from the Greenland ice core records (*e.g.* NorthGRIP and NEEM; Andersen et al. 2004; Flückiger et al. 2004; Wolff et al. 2010; Guillevic et al. 2013), and thus contribute to the ongoing tasks and objectives of the IPCC concerning current climate change.

1.2   Research area and geological setting

The morphology of NE Germany has been significantly shaped by the Weichselian glaciation and its repeated phases of ice advances and retreats (Fig. 1.1). Beside Holocene deposits, vast areas in this region are covered by glacial and associated material, including (sub-)glacial, (glacio-)fluvial and (glacio-)lacustrine successions (Katzung & Müller 2004). Furthermore, interglacial deposits of Eemian age (127–110 ka, MIS 5e; Brauer et al. 2007) are locally exposed (Meng et al. 2009). Many Pleistocene outcrops are located at the coastline of Germany, exposed due to the Holocene sea level rise of the Littorina transgression (9.8 ka BP; Andrén et al. 2011). As a result, large portions of the coast are retreating (Ministerium für Landwirtschaft, Umwelt und Verbraucherschutz Mecklenburg-Vorpommern 2009), revealing several deposits of Saalian to Weichselian age. The three papers in this thesis focus on three representative coastal sections (Fig. 1.1), which are all part of glaciotectonic complexes formed during late-LGM re-advances of the SIS (Strahl et al. 1994; Kenzler et al. 2015, 2017).

The Glowe and Kluckow sections (Jasmund) – The cliff sections of Glowe and Kluckow belong to the glaciotectonic complex of Jasmund (Rügen Island), formed between ~20 and 18 ka ago (Pomeranian Phase; Müller & Obst 2006; Kenzler et al. 2010; Gehrmann et al. 2017). The Jasmund peninsula exhibits an outstanding study area that has been explored by Quaternary researchers since the end of 19th century (*e.g.* Credner 1889; Keilhack 1914; Ludwig 1964; Steinich 1972; Steinich 1992; Panzig 1995; Kenzler et al. 2010, 2015, 2017; Gehrmann et al. 2017). So far, however, few modern techniques have been applied to the sedimentological processes and the reconstruction of depositional environments at Jasmund. Although there are many local studies on the formation of the Pleistocene sequence, the inter-site correlations of intercalated (glacio-)fluvial and (glacio-)lacustrine layers remain unclear. Thus, both the timing of events and their spatial variation are far from resolved.
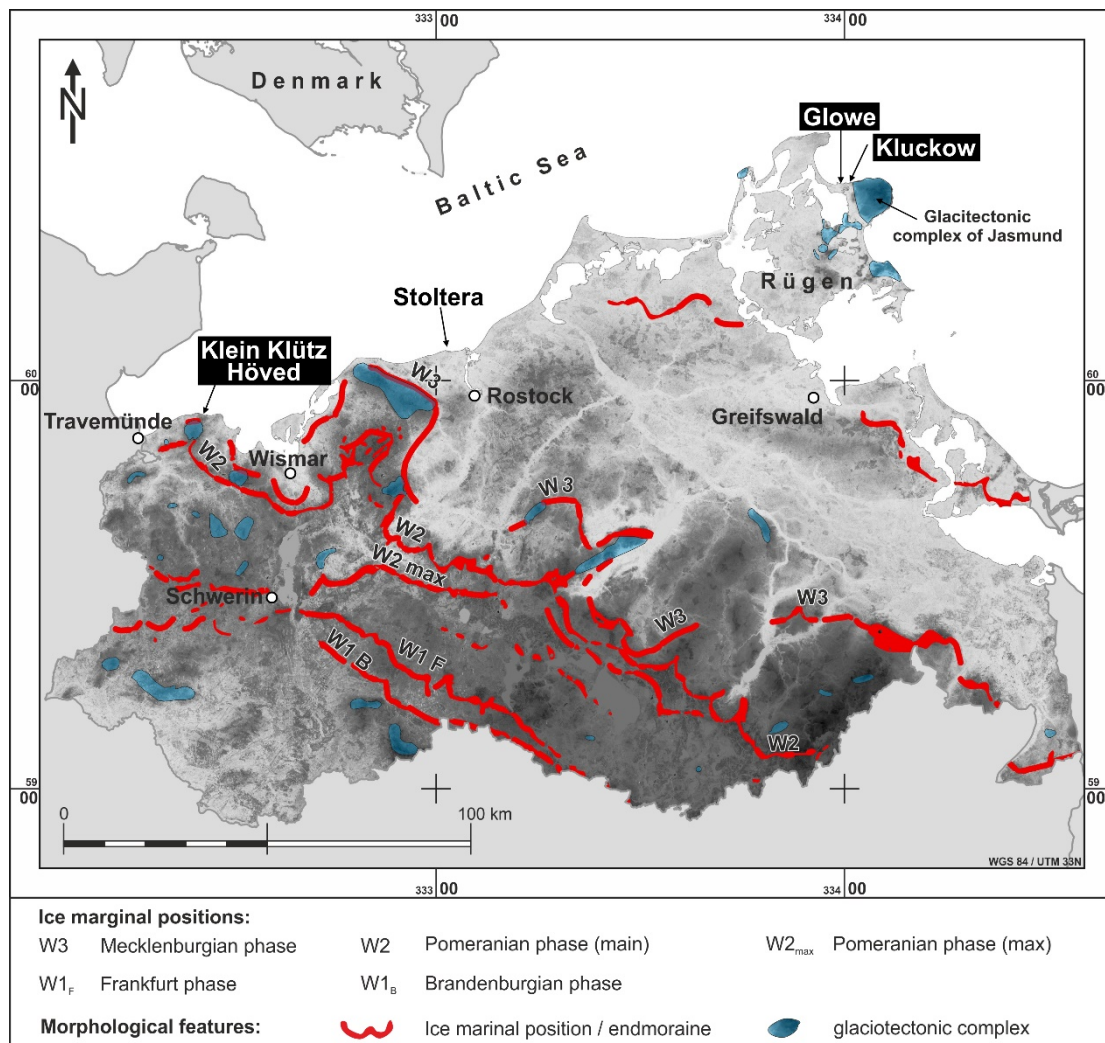
Fig. 1.1 Digital Elevation Model (DEM) of Mecklenburg-Vorpommern (NE Germany) with heights up to 180 m a.s.l. (dark grey), showing ice marginal positions of the Late Weichselian period, the areas affected by glaciotectonism, and the investigated localities of Klein Klütz Höved, Glowe and Kluckow (modified from Kettler 2014 based on LUNG-WMS/WFS-Service and NASA SRTM 3 arcsec)

The stratigraphic succession at Jasmund includes Cretaceous bedrock (limestone), paraconformably overlain by Pleistocene deposits. At least four till complexes (from bottom to top: M-0, M-1, M-2, and M-3; see Fig. 3.2 in Chapter 3) can be distinguished. Between these tills, mostly clayey to sandy lithostratigraphic units are intercalated (I-1 and I-2; see Fig. 3.2). Previous age estimations were based on sparse thermoluminescence (Krbetschek 1995) and radiocarbon data (Steinich 1992) for the sandwiched I-1 and I-2 units, and on provenance analyses (fine gravel analysis) of the till complexes (Panzig 1995). The age assessment of the individual tills ranges from Elsterian to Saalian or even early to mid-Weichselian for the lowermost tills (M-0 and M-1; *e.g.* Steinich 1992; Müller & Ost 2006; Niedermeyer et al. 2010), and up to Late Weichselian for the upper till layers (M-2 and M-3; Niedermeyer et al. 2010). In contrast, the intercalated deposits of lithostratigraphic units I-1 and I-2 are correlated to MIS 3 and MIS 2, respectively (Steinich 1992). Due to a glaciotectonic event caused by a late LGM re-advance of the SIS, the Pleistocene succession M-1 to I-2, together with the underlying Cretaceous bedrock, are unconformably overlain by the M-3 till complex. Hence, the base of the M-3 is a benchmark for this SIS re-advance. The genetic development of this glaciotectonic event is subject to on-going research (Gehrmann et al. 2017), as is the general relationship between the ice flow direction and the orientation of clasts in the subglacial traction tills (Brumme 2016). The current study contributes crucial sedimentological and geochronological data to further our understanding of the formation of the Jasmund glaciotectonic complex.

The Klein Klütz Höved section – The third study site at Klein Klütz Höved (KKH) is part of a glaciotectonic complex located between Travemünde and Wismar (Fig. 1.1 and Fig. 4.1B in Chapter 4). This structure was formed during a re-advance of the SIS between ~18 and 15 ka (Mecklenburgian Phase; Müller 2004). The KKH section exhibits a sequence of Saalian, Eemian and Weichselian deposits - a composition that is unique for NE Germany (Strahl et al. 1994; Meng et al. 2009; Menzel-Harloff & Meng 2015). This includes successions that record the transition of the Saalian glaciation to the Eemian interglacial with its marine-influenced deposits during the early Eemian (Strahl et al. 1994). Even though this Pleistocene site is excellent and the KKH section has been rather well investigated compared to Jasmund (Geinitz 1922; Gehl 1961; Ullerich 1991; Strahl et al. 1994; Menzel-Harloff & Meng 2015), it has gone unnoticed by the international research community (cf. *e.g.* Rattas et al. 2010; Head 2007;

Knudsen et al. 2011). However, the KKH profile provides significant insights into the last glacial-interglacial period (Saalian-Eemian), and the early to middle Weichselian ice advances and retreats. The deposits of the KKH succession include several tills (M-I to M-V) and corresponding intercalated sorted deposits of mainly clayey to gravelly grain size (I-I to I-IV, Fig. 4.3). Similar to Jasmund, the KKH Pleistocene succession is characterised by an unconformity between the uppermost till (M-V) and the underlying units (M-I to I-IV; Fig. 4.3). This boundary marks a comparable glaciotectonical event to the one in the Jasmund area as a result of a late-LGM re-advance of the SIS.

1.3   Thesis outline and structure

This thesis consists of four chapters. The remainder of the current chapter first outlines the three different papers that this thesis is based on. The methods employed in this thesis are summarised in section 1.4 (more detailed descriptions can be found in the individual papers), and the results are synthesised in section 1.5. Section 1.6 suggests possible directions for future work. **Chapters 2**, **3** and **4** correspond to three papers published in (or submitted to) peer-reviewed journals, which are summarised below:

Chapter 2 *Luminescence dating of Weichselian interstadial sediments from the German Baltic Sea coast* (Kenzler et al. 2015, Quaternary Geochronology):

This paper deals with the Kluckow cliff section on the Jasmund peninsula (Rügen). The investigated succession consists of Weichselian (glacio-)fluvial to (glacio-)lacustrine deposits in between a Saalian and Weichselian till unit. The aims of this paper are:

- Testing the applicability of luminescence dating (OSL and pIRIR) on Weichselian sediments from Jasmund and establishing a first reliable absolute age chronology in the area

- Palaeoenvironmental reconstruction during MIS 3 and early MIS 2, based on a detailed lithofacies analysis

- Age-constraining of Weichselian stadial and interstadial units and their relation to advances and retreats of the SIS, with particular focus on MIS 3 and MIS 2

- Determination of climate conditions and their implications for the Weichselian period at the study sites

- Correlation of the sediments on local (NE Germany) and transregional (southwestern Baltic Sea area) scales and their palaeogeographic implications

Chapter 3 *New age constraints from the SW Baltic Sea area – implications for Scandinavian Ice Sheet dynamics and palaeo-environmental conditions during MIS 3 and early MIS 2* (Kenzler et al. 2017, Boreas)

This paper investigates the Weichselian sequence preserved at the Glowe and Kluckow cliff sections (NE Jasmund), including absolute age estimations derived from luminescence dating. The previously presented results for the Kluckow section (Chapter 2) are significantly expanded by new sedimentological and palaeontological data. The results are discussed in the context of the SIS dynamics.

- Detailed lithofacies analysis and palaeoenvironmental reconstruction

- Establishment of a reliable numerical age chronology by luminescence dating

- Age constraining of Weichselian stadial and interstadial units and their relation to the dynamics of the SIS, with a special focus on MIS 3 and MIS 2

- Assessing the possibility of a two-folded LGM ice advance as proposed by Lüthgens et al. (2011)

Chapter 4 *A multi-proxy palaeoenvironmental and geochronological reconstruction of the Saalian-Eemian-Weichselian succession at Klein Klütz Höved (SW Baltic Sea, NE-Germany)* (Kenzler et al., in press)

This chapter presents the study of a cliff section at Klein Klütz Höved (SW Baltic Sea coast), which exhibits an outstanding sequence of Saalian to Weichselian age (including Eemian). The depositional environment is reconstructed based on sedimentological and palaeontological (pollen, ostracods) analyses, with the chronological framework obtained by luminescence dating of quartz (OSL) and K-rich feldspar mineral grains (pIRIR), independently controlled by the classification of Saalian and Eemian pollen zones.

- Detailed lithological description and interpretation of the succession (reconstruction of the palaeoenvironment)

- Establishment of a reliable numerical age chronology by luminescence dating

- Refining of existing palaeontological results (pollen, ostracods) with a focus on the (pre-)Eemian sediments

- Assessment of the existence of brackish-marine sediments of Eemian age at the site

- Climatic implications for the Saalian to Weichselian period

- Assessment of the previously presented numerical age chronology at the site

- Age-constraining of the first recorded Weichselian ice advance

1.4 Methods

The reconstruction of the depositional environments at Glowe, Kluckow and KKH was mainly based on detailed geological field mapping, palaeontological studies and facies analyses. For the latter, the sedimentological methods of Miall (1985, 1996) and Benn & Evans (2010) were used, in addition to thin section analyses to obtain a better insight into the specific lithological sequences, such as tills, lacustrine and fluvial deposits (*e.g.* van der Meer 1993; Menzies et al. 2006; Phillips et al. 2007). An estimation of the ages of the investigated sediments was made by luminescence dating, either from K-rich feldspar (infrared-stimulated luminescence, IRSL; Buylaert et al. 2011; Lamothe 2016), or from quartz grain minerals (optically stimulated luminescence, OSL; Murray & Wintle 2000; Wintle & Murray 2006). An independent age control was obtained by radiocarbon

dating (Glowe and Kluckow; Chapters 2 and 3), palynological results (Klein Klütz Höved; Chapter 4) and lithostratigraphic estimations (Chapters 2, 3 and 4). Much more detailed descriptions of the various techniques used in this study are presented in the respective papers (Chapters 2, 3 and 4).

1.5 Discussion of the overall results

This thesis provides valuable chronostratigraphic and palaeoenvironmental data on the last glacial-interglacial and glacial cycles in the southwestern Baltic Sea region. The results of the here presented investigations include detailed logging of three outstanding Pleistocene cliff profiles with modern sedimentological methods. These successions were furthermore dated by modern luminescence methods such as OSL and pIRIR for the first time, thus significantly expanding the numerical age database for NE Germany with 17 new luminescence ages, ranging from the Late Saalian to
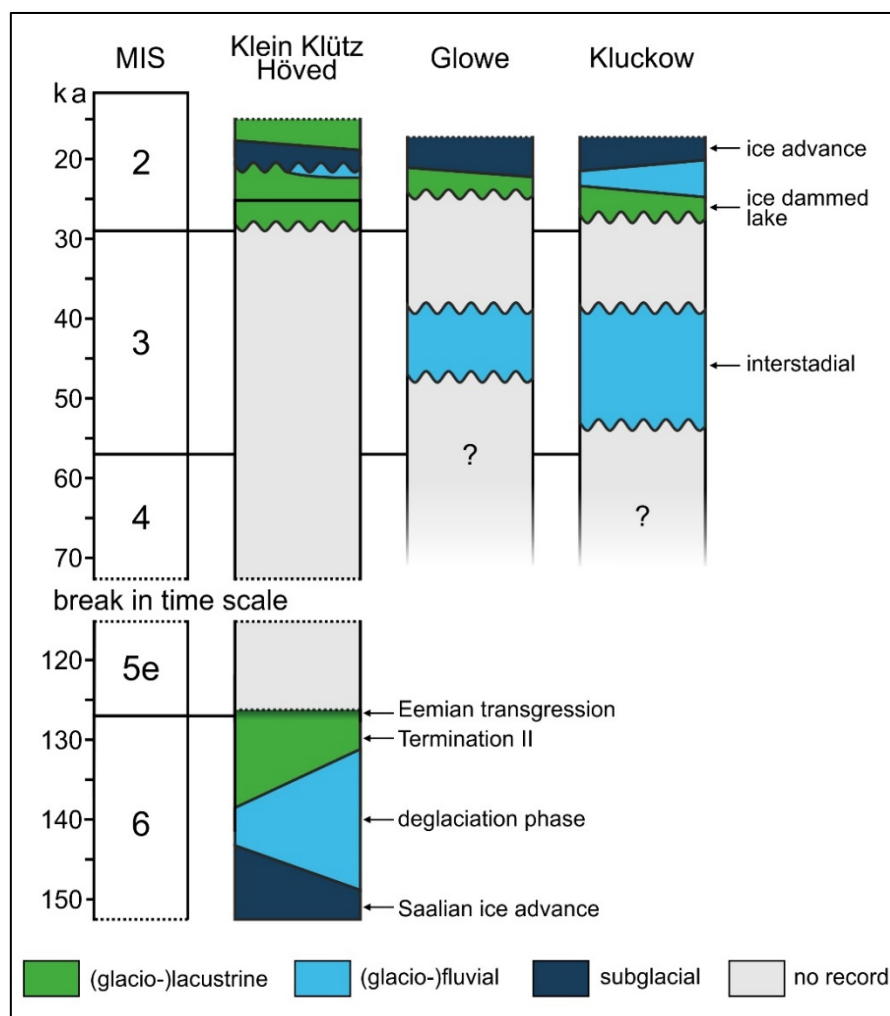
Fig. 1.2 Simplified overview of the main facies and their corresponding chronologies recorded at Klein Klütz Höved, Glowe and Kluckow. Note that MIS refers to Marine Isotope Stage.

Late Weichselian period (Fig. 1.2). The main results of this study, which have decidedly improved our understanding of the Late Saalian, early Eemian and Middle Weichselian (MIS 3) palaeoenvironments and glacier dynamics, as well as their transregional implications are recapitulated below, including a critical reflection of the findings and possible alternative interpretations.

Transition from the Saalian to the Eemian period – A major outcome of this study is the documentation and age-constraining of lacustrine sediments deposited during Termination II (TII, 136-129 ka; Landais et al. 2013) at the KKH section (Fig. 1.1 and Fig. 1.2; Chapter 4), lasting from the end of the Saalian glaciation (MIS 6) to the beginning of the Eemian interglacial (MIS 5e, ~127–110 ka; Brauer et al. 2007). Based on palynological analyses, a Late Saalian development was reconstructed from an open Arctic landscape with few *Juniperus* and *Betula* dwarf shrubs, to a subarctic environment with *Betula-Juniperus-Hippophaë* communities, to an increasingly vegetated landscape dominated by *Betula-Juniperus-Pinus* communities (Chapter 4). Sedimentary archives preserving TII successions are rare in the southwestern Baltic Sea area (Rattas et al. 2010), especially ones that are dated by physical methods such as luminescence dating. The successful application of a post-IR infrared-stimulated luminescence protocol (pIRIR$_{225}$; Buylaert et al. 2009) for dating pre-Eemian deposits validated the usefulness of K-rich feldspar for age determination (Lamothe 2016). Nevertheless, feldspar pIRIR dating suffers from anomalous fading (*i.e.* instability of the luminescence signal over time; Huntley & Lamothe 2003). To overcome the issue, the feldspar ages in this thesis were successfully fading-corrected with the method of Kars et al. (2008). The resulting luminescence ages of the TII lacustrine sediments, independently confirmed by pollen analyses, indicate a deposition during the end of the Saalian glaciation.

The Eemian transgression – The second main finding of this thesis was the confirmation of a brackish-influenced lacustrine facies for the early Eemian time at the KKH section. During this period, the study area was part of a former Trave estuary system that drained freshwater to the north (Fig. 4.1). The presence of the ostracod *Cyprideis torosa* indicates that a marine transgression most likely influenced this system and formed a brackish environment (Frenzel & Boomer 2005). This ostracod has a broad range of tolerance against salinity (nearly freshwater to hypersaline water conditions; Boomer et al. 2016), but it has been shown that the noded form of this

species is a clear proxy for brackish settings (Keyser & Aladin 2004; Frenzel et al. 2012). Although water bodies with brackish characteristics do not necessarily indicate a marine influence - an elevated salinity has been documented to occur in special geological settings, such as subrosion from Permian evaporates (Fuhrmann 2015) - a scenario of an external influx of saline water from an underground source is very unlikely in the KKH section, as Permian evaporites occur more than 3,000 m below surface (Zagora & Zagora 2004), and salt domes are not known in the direct vicinity of the area (Katzung & Granitzki 2004). Hence, the brackish water conditions at the KKH section are most probably the result of a marine transgression. This interpretation is consistent with deposits in Denmark from the same time period (Kristensen & Knudsen 2006; Head 2007; Knudsen et al. 2011). However, Eemian sediments of full marine origin were not preserved at KKH, as the Eemian sequence is truncated. The documented deposits span less than 750 years of the initial Eemian period, whereas the main part of this interglacial is not recorded (Fig. 1.2).

The early- and mid-Weichselian period – Late Weichselian lacustrine deposits superimpose the Eemian succession at KKH. As non-deposition seems an unlikely reason for this hiatus of nearly 90,000 years, an erosional phase probably removed the sediments. The presence of reworked marine Eemian molluscs within the sediment overlying the hiatus might indicate the previous existence of a more complete Eemian succession. The question what kind of depositional environment occurred during the main Eemian and early to middle Weichselian period remains open. The causes of the hiatus between the Eemian and Weichselian strata are also hard to determine. An SIS advance is a possibility, but a subglacial till would then be expected to overlie the hiatus, and not lacustrine deposits as recorded at KKH. Dispersed outsized clasts were found at the base of the lowermost Late Weichselian lake sediments, but a derivation from a reworked till seems unlikely. A more detailed investigation, perhaps with micromorphological methods, is necessary to determine the cause of the hiatus.

All three sections were examined to identify the existence of deposits that could be related to a Weichselian ice advance of pre-LGM age, as proposed by Müller (2004). On Jasmund (Glowe and Kluckow sections), the sedimentological and dating results indicated that most probably no ice advance reached this area during MIS 3 (57–29 ka; Cohen & Gibbard 2012); the first Weichselian ice advance was dated to MIS 2. Although there is a possibility of an ice advance between MIS 5d and MIS 4, no evidence for this has yet been found in the study area. No records of early to middle

Weichselian age are preserved at the KKH site. Therefore, the existence of a Weichselian pre-LGM ice advance is still pending.

In this context, the recent discussions reassessing the age of the Weichselian Brandenburgian and Frankfurt phases are of significant importance. Based on luminescence dating of glaciofluvial and aeolian sandur deposits correlated to the Brandenburgian and Frankfurt ice marginal positions (IPMs) in NE Germany, it has been proposed that these ice advances might have occurred earlier than previously assumed (Lüthgens et al. 2010a; Lüthgens et al. 2010b; Lüthgens et al. 2011; Lüthgens & Böse 2011; Hardt et al. 2016). For example, the maximum age of the Brandenburgian phase has been argued to lie between 41–24 ka (Lüthgens et al. 2010a; Lüthgens et al. 2010b; Lüthgens et al. 2011), and a two-fold LGM ice advance has been proposed during the transition of MIS 3 and 2 (*e.g.* Lüthgens et al. 2011). Evidence from Denmark indicates an SIS advance between 34 and 30 ka (Klintholm advance; Houmark-Nielsen & Kjær 2003; Houmark-Nielsen 2010), which has been correlated with the formation of glaciofluvial deposits at the Brandenburgian IMP (Lüthgens & Böse 2011; Hardt et al. 2016). The findings of the current study, however, provide no evidence for this scenario. Instead, the palaeoenvironmental reconstruction of the Jasmund area indicates that a braided river system predominated in the time between 54 and 38 ka. Furthermore, the palaeontological evidence points to warmer interstadial climate conditions. Although the transition between MIS 3 and MIS 2 was dominated by cold climate conditions and a deposition in a glaciolacustrine environment (Chapter 3), there are no indications for an MIS 3 advance reaching this part of NE Germany.

The Last Glacial Maximum – The age-constraining of documented MIS 2 ice advances across the study sites by luminescence dating yielded only limited results. The main reason for this are the various ice advances and retreats that occurred in the relatively short time period between 25-15 ka (Toucanne et al. 2015), resulting in the frequent overlapping of luminescence ages of different intercalated sediments deposited during this time. Therefore, the error of the luminescence ages, which is usually between 10 and 15%, covers a longer time period than the age difference of the individual ice advances. For example, an OSL age of 17±2 ka (19–15 ka; LUM 3178; Kluckow section) could correspond either to the Pomeranian (~20–18 ka) or the Mecklenburgian phase (~18–15 ka). The statistical probability of a true burial age of 19 ka is as high as

of 15 ka. Hence, a much greater age database is required to obtain a statistically solid age-constraining for the MIS 2 ice advances.

Applicability of luminescence dating – Another main aim of this thesis was to evaluate the applicability of luminescence dating to Weichselian sediments from coastal sections of NE Germany. For the determination of the luminescence ages, both quartz (OSL) and feldspar minerals (IRSL) were used. In general, the quartz luminescence characteristics, such as signal brightness, decay of the luminescence signal, recycling ratio, and IR depletion ratio, were suitable for dating. Several test measurements on selected samples from each section were conducted to test which preheat and cutheat temperatures were appropriate for the single aliquot regenerative (SAR) protocol. For most samples, the suitable preheat temperature ranged between 260 and 220 °C (corresponding cutheat between 200 and 240 °C). Apart from a small number of samples, it was possible to calculate a reliable age for nearly all luminescence samples. For a small number, particularly those with higher D_e values, a potential luminescence signal saturation of the quartz minerals was observed. This saturation effect would lead to an underestimation of the true burial age, as it was shown for three samples from the KKH site (Chapter 4). Based on pollen analysis, these samples were collected from pre-Eemian sediments, but their OSL ages indicated deposition during the early Weichselian period. The additional pIRIR$_{225}$ age determination from K-rich feldspar confirmed the pre-Eemian age of the deposits (Chapter 4). The discrepancy between the OSL and pIRIR ages suggests signal saturation issues of the quartz minerals, which in turn suggests a higher reliability of the pIRIR ages.

A final problem for the age calculation was the estimation of the water content during burial time. As water content is a critical factor that determines the establishment of the luminescence signal within the mineral grains over time, it should be treated very seriously. In this thesis, the average water content was estimated by taking into account the in situ water content (estimated as the minimum water content during burial time), the maximum content in the sediment, the type of over- and underlying deposits, and the height of the groundwater table. This estimation resulted in a relatively high water content value, close to saturation, that was used for the final age calculation.

1.6 Future work

The palaeogeographic and chronostratigraphic results presented in this thesis and their implications for the dynamics of the SIS during the Saalian, Eemian and Weichselian periods are a major contribution towards the reconstruction of the interglacial-glacial history of the southwestern Baltic Sea area. Naturally, some issues still need to be resolved, such as the existence of a Weichselian pre-LGM ice advance across NE Germany (Müller 2004). The identification of this SIS ice advance and its corresponding diamictic deposit based on fine gravel analyses by Müller (2004) raises the question why it is not documented in the cliff sections of the study area. Perhaps there are overinterpretations regarding the reliability of the fine gravel method across longer distances. Hence, the decision on whether there was a pre-LGM ice advance is still pending, as authors disagree on this (see Müller 2004; Obst et al. 2017). One promising cliff section that may resolve this issue is located at the Stoltera near Rostock (Fig. 1.1). Along the steep coast of the Stoltera, up to five different till units have been identified (Müller 2004; Strahl 2004; Brumme 2008). Based on its lithostratigraphic position, the so-called 'm2' till is potentially correlatable to a pre-LGM ice advance (Müller 2004). This till is intercalated between several meters thick fluvial and lacustrine deposits, which can be age-constrained by luminescence dating. Therefore, future research should focus on the Stoltera succession to establish a geochronological framework for these deposits. A pre-LGM SIS advance in NE Germany would be correlatable with pre-LGM advances in Denmark (Ristinge advance, Klintholm advance; Houmark-Nielsen 2010). Currently, the correlation of the Warnow advance with the Ristinge or Klinholm advances is highly speculative (Lüthgens & Böse 2011; Hardt et al. 2016; Obst et al. 2017). In this context, the Ellund advance of northern Germany (Stephan 2014), with a similar age estimation as the Warnow advance, should also be taken into consideration.

Finally, the results of this paper have shown that our understanding of the palaeoenvironment of the study area and the sedimentation patterns is still limited, particularly for the early to middle Weichselian period, where deposits are poorly preserved due to the erosional reworking by the subsequent LGM advances. The identification of early to middle Weichselian deposits in NE Germany thus is a worthwhile challenge.

1.7 Indication of work share with co-authors

Kenzler, M., Rother, H., Hüneke, H., Frenzel, P., Strahl, J., Tsukamoto, S., Li, Y., Meng, S., Gallas, J. & Frechen, M. (in press): A multi-proxy palaeoenvironmental and geochronological reconstruction of the Saalian-Eemian-Weichselian succession at Klein Klütz Höved (SW Baltic Sea, NE-Germany). *Boreas*.

Own contribution: data acquisition – 80%

measurements and figures – 80%

writing – 75%

concept and discussion – 75%

corresponding author

Henrik Rother supported the first author during assemblage of the main manuscript with discussions and linguistic support. Yan Li calculated the fading corrected pIRIR K-rich feldspar ages and prepared the raw version of Fig. 4.4. Peter Frenzel determined the macro- and microfossil (ostracods) content and delivered text modules for their interpretation. He also prepared parts of Fig. 4.12. Jaqueline Strahl identified all pollen grains, including their interpretation and palaeoenvironmental implications. Furthermore, she prepared an early version of Fig. 4.11. Sumiko Tsukamoto accompanied the luminescence measurements. All co-authors revised an early version of the manuscript.

(Michael Kenzler) (PD Dr. Heiko Hüneke)

Kenzler, M., Tsukamoto, S., Meng, S., Frechen, M. & Hüneke, H. 2017: New age constraints from the SW Baltic Sea area – implications for Scandinavian Ice Sheet dynamics and palaeo-environmental conditions during MIS 3 and early MIS 2. *Boreas 46 (1)*, 34–52.

Own contribution: data acquisition – 90%

measurements and figures	– 90%
writing	– 90%
concept and discussion	– 80%
corresponding author	

Stefan Meng determined the mollusc ensemble and prepared early versions of Fig. 3.16, Fig. 3.17 and Tab. 3.5. Furthermore, this co-author provided help during the writing of the palaeontological part of the paper (Chapter 3.3.3 and Chapter 3.4.2). All other co-authors supported the first author with expedient discussions and revised an early stage manuscript.

(Michael Kenzler)   (PD Dr. Heiko Hüneke)

Kenzler, M., Tsukamoto, S., Meng, S., Thiel, C., Frechen, M. & Hüneke, H. 2015: Luminescence dating of Weichselian interstadial sediments from the German Baltic Sea coast. *Quaternary Geochronology 30*, 215–256.

Own contribution:	data acquisition	– 95%
	measurements and figures	– 100%
	writing	– 90%
	concept and discussion	– 90%
	corresponding author	

The first author wrote the manuscript, prepared all figures and tables and conducted all analyses. Stefan Meng determined the mollusc species. Sumiko Tsukamoto accompanied the luminescence measurements. All other co-authors supported the first author with discussions and revised an early version of the manuscript.

(Michael Kenzler)   (PD Dr. Heiko Hüneke)

1.8 References

Andersen, K.K., Azuma, N., Barnola, J.-M., Bigler, M., Biscaye, P., Caillon, N., Chappellaz, J., Clausen, H.B., Dahl-Jensen, D., Fischer, H., Flückiger, J., Fritzsche, D., Fujii, Y., Goto-Azuma, K., Grønvold, K., Gundestrup, N.S., Hansson, M., Huber, C., Hvidberg, C.S., Johnsen, S.J., Jonsell, U., Jouzel, J., Kipfstuhl, S., Landais, a, Leuenberger, M., Lorrain, R., Masson-Delmotte, V., Miller, H., Motoyama, H., Narita, H., Popp, T., Rasmussen, S.O., Raynaud, D., Rothlisberger, R., Ruth, U., Samyn, D., Schwander, J., Shoji, H., Siggard-Andersen, M.-L., Steffensen, J.P., Stocker, T., Sveinbjörnsdóttir, A.E., Svensson, A., Takata, M., Tison, J.-L., Thorsteinsson, T., Watanabe, O., Wilhelms, F., White, J.W.C. 2004: High-resolution record of Northern Hemisphere climate extending into the last interglacial period. *Nature 431*, 147–151.

Alexanderson, H., Johnsen, T. & Murray, A.S. 2010: Re-dating the Pilgrimstad Interstadial with OSL: A warmer climate and a smaller ice sheet during Swidish Middle Weichselian (MIS 3)? *Boreas 39*, 367–376.

Andrén, T., Björck, S., Andrén, E., Conley, D., Zillén, L. & Anjar, J. 2011: The development of the Baltic Sea Basin during the last 130 ka. *In* Harff, J., Björck, S. & Hoth, P. (eds.): *The Baltic Sea Basin*, 75–97. Springer, Berlin.

Anjar, J., Adrielsson, L., Bennike, O., Björck, S., Filipsson, H. L., Groeneveld, J., Knudsen, K. L., Larsen, N. K. & Möller, P. 2012: Palaeoenvironments in the southern Baltic Sea Basin during Marine Isotope Stage 3: a multi-proxy reconstruction. *Quaternary Science Reviews 34*, 81–92.

Benn, D.I. & Evans, D.J.A. 2010: *Glaciers and Glaciations*. 802 pp. Hodder Education, London.

Boomer, I., Frenzel, P. & Feike, M. 2016: Salinity-driven size variability in Cyprideis torosa (Ostracoda, Crustacea). *Journal of Micropalaeontology*. DOI: 10.1144/jmpaleo2015-043

Brauer, A., Allen, J.R.M., Mingram, J., Dulski, P., Wulf, S. & Huntley, B. 2007: Evidence for last interglacial chronology and environmental change from Southern Europe. *Proceedings of the National Academy of Science 140*, 450–455.

Brumme, J. 2016: Three-dimensional microfabric analyses of Pleistocene tills from the cliff section Dwasieden on Rügen (Baltic Sea coast): micromorphological evidence for subglacial polyphaser deformation. Unpublished doctoral dissertation, 250 pp. University Greifswald.

Brumme, J. 2008: Geologische Neuaufnahme des Steilufers an der Stoltera von Wilhelmshöhe bis Geinitzort im Bereich I'-M'. Unpublished bachelor thesis, 73 pp. University of Greifswald.

Buylaert, J. P., Hout, S., Murray, A. S. & Van den Haute, P. 2011: Infrared stimulated luminescence dating of an Eemian (MIS 5e) site in Denmark using K-feldspar. *Boreas 40*, 46–56.

Buylaert, J.P., Murray, A.S., Thomsen, K. J. & Jain, M. 2009: Testing the potential of an elevated temperature IRSL signal from K-feldspar. *Radiation Measurements 44*, 560–565.

Cohen K.M. & Gibbard, P. 2011: Global chronostratigraphical correlation table for the last 2.7 million years. Subcommission on Quaternary Stratigraphy (International Commission on Stratigraphy), Cambridge. Available at:
http://quaternary.stratigraphy.org/correlation/POSTERSTRAT_v2011.jpg

Cohen, K.M. & Gibbard, P.L. 2012: Regional chronostratigraphical correlation table for the last 270,000 years. Available at:
http://www.nhm2.uio.no/norges/GTS2012_Quaternary-Poster-reg-GSA2012.pdf

Credner, H. 1889: Die Lagerungsverhältnisse in den Kreidefelsen auf Rügen. Zeitschrift der Deutschen geologischen Gesellsschaft 41 (B), 365–370.

Flückiger, J., Blunier, T., Stauffer, B., Chappellaz, J., Spahni, R., Kawamura, K., Schwander, J., Stocker, T.F. & Dahl-Jensen, D. 2004: N_2O and CH_4 variations during the last glacial epoch: Insight into global processes. *Global Biogeochemical Cycles 18 (1) GB 1020*.

Frenzel, P. & Boomer, I. 2005. The use of ostracods from marginal-marine, brackish waters as bioindicators of modern and Quaternary environmental change. *Palaeogeography, Palaeoclimatology, Palaeoecology 225 (1-4)*, 68–92.

Frenzel, P., Schulze, I. & Pint, A. 2012: Noding of *Cyprideis torosa* valves (Ostracoda) – a proxy for Salinity? New data from field observations and a long-term microcosm experiment. *International Review of Hydrobiology 97 (4)*, 314–329.

Fuhrmann, R. 2015: Die Ostracoden- und Molluskenfauna des eemzeitlichen Salzsees bei Cottbus. *Natur und Landschaft in der Niederlausitz 31*, 21–39.

Gehl, O. 1961: Neue Ergebnisse über das marine Eem und zur Gliederung des Jungpleistozäns in NW-Mecklenburg. *Geologie 18*, 550–562.

Geinitz, E. 1922: *Geologie Mecklenburgs I Teil: Diluvium und Allivium (Quartär)*. 200 pp. Hinstorff, Rostock.

Gehrmann, A., Hüneke, H., Meschede, M. & Phillips, E. 2017: 3D microstructural architecture of deformed glacigenic sediments associated with large-scale glacitectonism, Jasmund Peninsula (NE Rügen), Germany. *Journal of Quaternary Science 32*, 213–230.

Guillevic, M., Bazin, L., Landais, A., Kindler, P., Orsi, A., Masson-Delmotte, V., Blunier, T., Buchardt, S.L., Capron, E., Leuenberger, M., Martinerie, P., Prié, F. & Vinther, B.M. 2013: Spatial gradients of temperature, accumulation and δ^{18}O-ice in Greenland over a sieres of Dansgaard-Oeschger events. *Climate of the Past 9*, 1029–1051.

Hardt, J. & Böse, M. 2016: The timing of the Weichselian Pomeranian ice marginal position south of the Baltic Sea: A critical review of morphological and geochronological results. *Quaternary International*. DOI: 10.1016/j.quaint.2016.07.044

Hardt, J., Lüthgens, C., Hebenstreit, R. & Böse, M. 2016: Geochronological (OSL) and geomorphological investigations at the presumed Frankfurt ice marginal position in northeast Germany. *Quaternary Science Reviews 154*, 85–99.

Head, M.J. 2007: Last Interglacial (Eemian) hydrographic conditions in the southwestern Baltic Sea based on dinoflagellate cycsts from Ristinge Klint, Denmark. *Geological Magazine 144 (6)*, 987–1013.

Houmark-Nielsen, M. 2003: Signature and timing of the Kattegat Ice Stream: onset of the Last Glacial Maximum sequence at the southwestern margin of the Scandinavian Ice Sheet. *Boreas 32*, 227–241.

Houmark-Nielsen, M. & Kjær, K.H. 2003: Southwest Scandinavia, 40–15 kyr BP: palaeogeography and environmental change. *Journal of Quaternary Science 18*, 769–786.

Houmark-Nielsen, M. 2010: Extent, age and dynamics of Marine Isotope Stage 3 glaciation in the southwestern Baltic Basin. *Boreas 39*, 343–359.

Hughes, A.L.C., Gyllencreutz, R., Lohne, Ø.S., Mangerud, J. & Svendsen, J.I. 2016: The last Eurasian ice sheet – a chronological database and time-slice reconstruction, DATED-1. *Boreas 45*, 1–45.

Huntley, D.J. & Lamothe, M. 2003: Ubiquity of anomalous fading in K-feldspar and the measurement and correction for it in optical dating. *Canadian Journal of Earth Sciences 38*, 1093–1106.

IPCC, 2013: *Climate Change 2013: The Physical Science Basis. Contribution of Working Group I to the Fifth Assessment Report of the Intergovernmental Panel on Climate Change* [Stocker, T.F., Qin, D., Plattner, G.-K., Tignor, M., Allen, S.K., Boschung, J., Nauels, A., Xia, Y., Bex, V. & Midgley, P.M. (eds.)]. 1535 pp. Cambridge University Press, Cambridge.

Kars, R.H., Wallinga, J. & Cohen, K.M. 2008: A new approach towards anomalous fading correction for feldspar IRSL dating — tests on samples in field saturation. *Radiation Measurements 43*, 786–790.

Katzung, G. & Granitzki, K. 2004: Salze und Erze. *In* Katzung (ed.): *Geologie von Mecklenburg-Vorpommern*, 423–425. E. Schweizerbart'sche Verlagsbuch-handlung, Stuttgart.

Katzung, G. & Müller, U. 2004: Quartär. *In* Katzung (ed.): *Geologie von Mecklenburg-Vorpommern*, 221–225. E. Schweizerbart'sche Verlagsbuchhandlung, Stuttgart.

Keilhack, K. 1914: Die Lagerunsverhältnisse des Diluviums in der Steilküste von Jasmund auf Rügen. *In* Königlich Preussische Geologische Landesanstalt (ed.):

Jahrbuch der Königlich Preussischen Geologischen Landesanstalt zu Berlin für das Jahr 1912 33 (1), 114–158.

Kenzler, M., Rother, H., Hüneke, H., Frenzel, P., Strahl, J., Tsukamoto, S., Li, Y., Meng, S., Gallas, J. & Frechen, M. (in press): A multi-proxy palaeoenvironmental and geochronological reconstruction of the Saalian-Eemian-Weichselian succession at Klein Klütz Höved (SW Baltic Sea, NE-Germany). Boreas.

Kenzler, M., Tsukamoto, S., Meng, S., Thiel, C., Frechen, M. & Hüneke, H. 2015: Luminescence dating of Weichselian interstadial sediments from the German Baltic Sea coast. *Quaternary Geochronology 30*, 215–256.

Kenzler, M., Tsukamoto, S., Meng, S., Frechen, M. & Hüneke, H. 2017: New age constraints from the SW Baltic Sea area – implications for Scandinavian Ice Sheet dynamics and palaeo-environmental conditions during MIS 3 and early MIS 2. *Boreas 46 (1)*, 34–52.

Kenzler, M., Obst, K., Hüneke, H. & Schütze, K. 2010: Glazitektonische Deformation der kretazischen und pleistozänen Sedimente an der Steilküste von Jasmund nördlich des Königsstuhls (Rügen). *Brandenburger Geowissenschaftliche Beiträge 17*, 107–122.

Kettler, C. 2014: Fazies und Entstehung der Interstadialsedimente des I$_2$ an der Ostflanke des Glower Sattels (Profilmeter 120-140, Jasmund, Rügen). Unpublished bachelor thesis, 51 pp. University of Greifswald.

Keyser, D. & Aladin, N. 2004: Noding in *Cyprideis torosa* and its causes. *Studia Quaternaria 21*, 19–24.

Knudsen, K.L., Jiang, H., Kristensen, P., Gibbard, P.L. & Haila, H. 2011: Early Last Interglacial palaeoenvironments in the western Baltic Sea: benthic foraminiferal stable isotopes and diatom-based sea-surface salinity. *Boreas 40*, 681–696.

Krbetschek, M.R. 1995: Lumineszenz-Datierungen quartärer Sediment Mittel-, Ost- und Nordostdeutschlands. Unpublished doctoral dissertation, 122 pp. TU Bergakademie Freiberg.

Kristensen, P.H. & Knudsen, K.L. 2006: Palaeoenvironments of a complete Eemian sequence at Mommark, South Denmark: foraminifera, ostracods and stable isotopes. *Boreas 35*, 349–366.

Lamothe, M. 2016: Luminescence dating of interglacial coastal depositional systems: Recent developments and future avenues of research. *Quaternary Science Reviews 146*, 1–27.

Landais, A., Dreyfus, G., Capron, E., Jouzel, J., Masson-Delmotte, V., Roche, D.M., Prié, F., Caillon, N., Chappellaz, J., Leuenberger, M., Lourantou, A., Parrenin, F., Raynaud, D. & Teste, G. 2013: Two-phase change in CO_2, Antarctic temperature and global climate during Termination II. *Nature Geoscience 6*, 1062–1065.

Litt, T., Behre, K.-E., Meyer, K.-D., Stephan, H.-J. & Wansa S. 2007: Stratigraphische Begriffe für das Quartär des norddeutschen Vereisungsgebietes. *Quaternary Science Journal (Eiszeitalter und Gegenwart) 56 (1-2)*, 7–65.

Ludwig, A.O. 1964: Stratigrapische Untersuchungen des Pleistozäns der Ostseeküste von der Lübecker Bucht bis Rügen. *Geologie 13 (42)*, 1–143.

Lüthgens, C., Böse, M., Krbetschek, M., 2010a: On the age of the young morainic morphology in the area ascribed to the maximum extent of the Weichselian glaciation in north-eastern Germany. *Quaternary International 222*, 72–79.

Lüthgens, C., Krbetschek, M., Böse, M., Fuchs, M.C., 2010b: Optically stimulated luminescence dating of fluvioglacial (sandur) sediments from north-eastern Germany. *Quaternary Geochronology 5*, 237–243.

Lüthgens, C. 2011: The age of Weichselian main ice marginal positions in north-east Germany inferred from Optically Stimulated Luminescence (OSL) dating. Doctoral dissertation, 206 pp. FU Berlin.

Lüthgens, C. & Böse, M. 2011: Chronology of Weichselian main ice marginal positions in north-eastern Germany. *Quaternary Science Journal (Eiszeitalter und Gegenwart) 2–3*, 236–247.

Lüthgens, C., Böse, M. & Preusser, F. 2011: Age of the Pomeranian ice-marginal position in northeastern Germany determined by Optically Stimulated Luminescence (OSL) dating of glaciofluvial sediments. *Boreas 40*, 598–615.

Meng, S., Börner, A., Strahl, J. & Thieke, H.-U. 2009: Bio- und lithostratigraphische Untersuchungen an limnisch-fluviatilen Sedimenten aus dem Eem-Interglazial im unteren Peenetal (NE Deutschland). *Brandenburger Geowissenschaftliche Beiträge 16*, 63–78.

Menzel-Harloff, H. & Meng, S. 2015: Spätsaalezeitliche und eemzeitliche Makrofaunen aus dem Kliffaufschluss Klein Klütz Höved (NW-Mecklenburg) mit Erstnachweisen von *Belgrandia germanica* (Gastropoda: Hydrobiidae), *Pupilla loessica* (Gastropoda: Pupillidae) und *Lagurus lagurus* (Mammalia: Cricetidae) für Mecklenburg-Vorpommern. *Quaternary Science Journal (Eiszeitalter und Gegenwart) 44*, 82–94.

Menzies, J., van der Meer, J.J.M. & Rose, J. 2006: Till – as a glacial "tectomict", its internal architecture, and the development of a "typing" method for till differentiation. *Geomorphology 75*, 172–200.

Miall, A.D. 1996: *The Geology of Fluvial Deposits: Sedimentary Facies, Basin Analysis, and Petroleum Geolog*y. 582 pp. Springer, Berlin.

Miall, A.D. 1985: Architectural-Element Analysis: A New Method of Facies Analysis Applied to Fluvial Deposits. *Earth-Science Reviews 22*, 261–308.

Ministerium für Landwirtschaft, Umwelt und Verbraucherschutz Mecklenburg-Vorpommern 2009: *Regelwerk Küstenschutz Mecklenburg-Vorpommern – Übersichtsheft – Grundlagen, Grundsätze, Standortbestimmung und Ausblick*. 102 pp. Rostock.

Murray, A.S. & Wintle, A.G. 2000: Luminescence dating of quartz using an improved single-aliquot regenerative-dose protocol. *Radiation Measurements 32*, 57–73

Müller, U. 2004: Weichsel-Frühglazial in Nordwest-Mecklenburg. *Meyniana 56*, 81–115.

Müller, U. & Obst, K. 2006: Lithostratigraphy and bedding of the Pleistocene deposits in the area of Lohme (Jasmund/Rügen). *Journal for the Geological Science 34 (1-2)*, 39–54.

Niedermeyer, R.-O., Kanter, L., Kenzler, M., Panzig, W.-A., Krienke, K., Ludwig, A.-O., Schnick, H.H. & Schütze, K. 2010: Rügen Island (I) – Facies, stratigraphy,

structural architecture and geological hazard potential of Pleistocene deposits of the Jasmund cliff coast. *In* Lampe, R. & Lorenz, S. (eds.): *Eiszeitlandschaften in Mecklenburg-Vorpommern*, 50–71. Geozon Science Media, Greifswald.

Obst, K., Nachtweide, C. & Müller, U. 2017: Late Saalian and Weichselian glaciations in the German Baltic Sea documented by Pleistocene successions at the southeastern margin of the Arkona Basin. *Boreas 46*, 18–33.

Panzig, W.-A. 1995: Zum Pleistozän von Rügen. *Terra Nostra 6*, 177–200.

Phillips, E., Merritt, J., Auton, C. & Golledge, N. 2007: Mircostructures in subglacial and proglacial sediments: understanding faults, folds and fabric, and the influence of water on the style of deformation. *Quaternary Science Reviews 26*, 1499–1528.

Rattas, M., Kalm, V., Kihno, K., Liivrand, E., Tinn, O., Tänavsuu-Milkeviciene, K. & Sakson, M. 2010: Chronology of Late Saalian and Middle Weichselian episodes of ice-free lacustrine sedimentation recorded in the Arumets section, southwestern Estonia. *Estonian Journal of Earth Science 59 (2)*, 125–140.

Rinterknecht, V., Börner, A., Bourlès, D. & Braucher, R. 2014: Cosmogenic [10]Be dating of ice sheet marginal belts in Mecklenburg-Vorpommern, Western Pomerania (northeast Germany). *Quaternary Geochronology 19*, 42–51.

Steinich, G. 1992: Die stratigraphische Einordnung der Rügen-Warmzeit. *Zeitschrift für geologische Wissenschaften 20*, 125–154.

Steinich, G. 1972: Endogene Tektonik in den Unter-Maastricht-Vorkommen auf Jasmund. *Geologie 20 (71/72)*, 1–207.

Stephan, H.-J. 2014: Climato-stratigraphic subdivision of the Pleistocene in Schleswig-Holstein, Germany and adjoining areas. *Quaternary Science Journal (Eiszeitalter und Gegenwart) 63*, 3–18.

Strahl, J., Keding, E., Steinich, G., Frenzel, P. & Strahl, U. 1994: Eine Neubearbeitung der eem- und frühweichselzeitlichen Abfolge am Klein Klütz Höved, Mecklenburger Bucht. *Quaternary Science Journal (Eiszeitalter und Gegenwart) 44*, 62–78.

Strahl, U. 2004: Kliff der Stoltera westlich Warnemünde. *In* Katzung, G. (ed.): *Geologie von Mecklenburg-Vorpommern*, 302–306, E. Schweizerbart'sche Verlagsbuchhandlung, Stuttgart.

TGL 25232. 1971: *Fachbereichsbestand Geologie, Analyse des Geschiebebestandes quartärer Grundmoränen*. Blatt 1–6, Berlin.

Toucanne, S., Soulet, G., Freslon, N., Silva Jacinto, R., Dennielou, B., Zaragosi, S., Eynaud, F., Bourillet, J.-F. & Bayon, G. 2015: Millennial-scale fluctuations of the European Ice Sheet at the end of the glacial, and their potential impact on global climate. *Quaternary Science Reviews 123*, 113–133.

Ullerich, H. 1991: Die sandig-siltigen Zwischensedimente am Kliff des Klein-Klütz-Höved (Mecklenburger Bucht). Unpublished diploma thesis, 98 pp. University of Greifswald.

van der Meer, J.J.M. 1993: Microscopic evidence of subglacial deformation. *Quaternary Science Reviews 12*, 553–587.

Wintle, A.G. & Murray, A.S. 2006: A review of quartz optically stimulated luminescence characteristics and their relevance in single-aliquot regeneration dating protocols. *Radiation Measurements 41*, 369–391.

Wohlfarth, B. 2010: Ice-free conditions in Sweden during Marine Oxygen Isotope Stage 3? *Boreas 39*, 377–398.

Wolff, E.W., Chappellaz, J., Blunier, T., Rasmussen, S.O. & Svensson, A., 2010: Millennial-scale variability during the last glacial: the ice core record. *Quaternary Science Reviews 29*, 2828–2838.

Zagora, I. & Zagora, K. 2004: Zechstein. *In* Katzung (ed.): *Geologie von Mecklenburg-Vorpommern*, 132–139. E. Schweizerbart'sche Verlagsbuchhandlung, Stuttgart.

2 Luminescence dating of Weichselian interstadial sediments from the German Baltic Sea coast

Michael Kenzler[1, 2], Sumiko Tsukamoto[2], Stefan Meng[1], Christine Thiel[2], Manfred Frechen[2] & Heiko Hüneke[1]

[1]University of Greifswald, Institute of Geography and Geology, F.-L. Jahn Str. 17a, 17487 Greifswald, Germany

[2]Leibniz Institute for Applied Geophysics (LIAG), Geochronology and Isotope Hydrology, Stilleweg 2, 30655 Hannover, Germany

Abstract

A cliff outcrop called Kluckow, in the Baltic Sea area, with a (glacio-) fluvial to (glacio-) lacustrine succession, provides a unique opportunity to resolve uncertainties in the timing and extent of several poorly constrained Weichselian ice advances. Based on a detailed lithofacies analysis, we selected four sampling horizons for luminescence dating to determine a depositional chronology. We measured both coarse grain quartz and potassium-rich feldspar for age determination using optically stimulated luminescence (OSL) and post-IR infrared stimulated luminescence (pIRIR). Furthermore we addressed potential problems such as incomplete bleaching and quartz saturation effects. The resulting luminescence chronology, supported by one radiocarbon age, illustrates a depositional time interval of the investigated sequence between ~62 and ~22 ka. Within this sequence a mussel-bearing fluvial sand indicate interstadial climate conditions at approximately 46 ka. The upper part of the section is composed of a 4 m thick glaciolacustrine silty clay and an overlying glaciofluvial sand;

the latter yielded an OSL age of ~22 ka. Shortly after these sequences formed, the subsequent ice advance (indicated by the overlying till sheet) reached the study area. Based on our new chronology and lithofacies analysis, we conclude that the Scandinavian Ice Sheet did not reach the study area between ~62 and ~22 ka.

Keywords: Southwestern Baltic Sea; Weichselian; Fluvial; Optically stimulated luminescence (OSL); MIS 3; Interstadial

2.1 Introduction

The southwestern Baltic Sea and its vicinity are key areas for understanding the complex interactions between climate conditions and the advance and retreat of the Scandinavian Ice Sheet (SIS) during the Weichselian Glaciation (115–11.7 ka) (Houmark-Nielsen 2010). Due to the large climate variability, especially during Marine Isotope Stage 3 (MIS 3, 60–27 ka), various stadial and interstadial phases have been defined in this area (Wolff et al. 2010). The stratigraphy during this time has been well described in Denmark and southern Sweden (*e.g.*, Larsen et al. 2009; Anjar et al. 2012). However, sedimentary records of Early and Middle Weichselian age (MIS 5d– MIS 3, 115–27 ka) are rare in northeastern Germany and chronological data are also sparse (Ludwig 2006). Most of the dated deposits in this region are ice marginal sediments connected to the Late Weichselian (MIS 2, 27–11.7 ka) (Lüthgens & Böse 2011).

Rügen Island, located at the southwestern border of the Baltic Sea basin (Fig. 2.1), has several cliff outcrops with deposits correlated to Saalian and Weichselian periods (Panzig 1995), but aside from a few thermoluminescence (TL) and radiocarbon ages from Weichselian deposits (Krbetschek 1995; Steinich 1992), no numerical chronologies are available for these sediments. Hence the age of most of the different till sheets and intercalated deposits is still under debate (Müller 2004), resulting in uncertainty in the timing of the events they reflect. Chronological constraint of these sediments will allow for new understanding of the Weichselian sedimentary history in northeastern Germany. Further, a comparison with data from Denmark, Sweden and Poland will be made possible; this is an important framework for the reconstruction of former climate and event history.

The key aspect of our research is a comparative dating approach for glaciofluvial, fluvial and lacustrine deposits, including a comparison of quartz and feldspar luminescence dating results, in order to evaluate the bleaching conditions (*e.g.* Lüthgens et al. 2010). This study represents the first application of optically stimulated luminescence (OSL) dating to sediments from Rügen Island, and one of few applications to northeast German Middle Weichselian deposits (Lüthgens et al. 2011). Based on these dates and detailed stratigraphy, we critically reassess the chronostratigraphical position of these sediments on Rügen Island and place them in the context of the Weichselian glacial history of the SIS to improve our understanding of the response of the SIS to the global climate.

2.2 Study area

2.2.1 Previous studies and chronostratigraphic framework

The dynamics of the SIS in the southwestern Baltic Sea area during the Early and Middle Weichselian glaciation are still discussed controversially. Stephan (2014) and Müller (2004), for example, indicated Early to Middle Weichselian ice advances in north and northeastern Germany, but these have not been fully confirmed. However, Houmark-Nielsen (2010) correlated these ice advances with the Ristinge advance (50±4 ka) in Denmark. Furthermore, Houmark-Nielsen (2010) described the Klintholm ice advance on Møn (Denmark) (32±4 ka), but this ice advance has not been found in Germany to date. There are also indications of pre-Last Glacial Maximum (LGM) ice advances in Poland at ~36 to 32 ka (Marks 2012). A correlation of these ice advances is very difficult; one reason is the lack of suitable age data in the German region. Several locations with interstadial sediments of Early and Middle Weichselian age are reported in Denmark and Sweden, *e.g.*, at Pilgrimstad (44±8 ka, Alexanderson et al. 2010) and Sejerø (~41.5 cal ka BP, Bennike et al. 2007), but little evidence of these interstadials exists in northeastern Germany (Steinich 1992).

There are several main Weichselian ice marginal positions (IMP) in Germany which have been connected to MIS 2 (27–11.7 ka) (Fig. 2.1). The oldest confirmed Weichselian IMP in Germany is the Brandenburg IPM, which represents the maximum extent of the Weichselian ice sheet. OSL dating of quartz from glaciofluvial sediments for the Brandenburg IMP yielded ages between 34±3 ka and 28±4 ka (Lüthgens et al.

2010), whereas the surface exposure dating (^{10}Be) of boulders gave ages between 21.9 and 18.2 ka (Heine et al. 2009). Lüthgens & Böse (2011) have interpreted these results as the maximum (OSL) and minimum (^{10}Be) age of the Brandenburg IMP. According to Houmark-Nielsen et al. (2012), the age of the maximum Weichselian ice extent in Denmark, represented by the East Jylland IMP (Fig. 2.1), ranges between 22 and 20 ka. In Poland, Marks (2012) assumed an age of 24 to 19 ka for the same IMP.
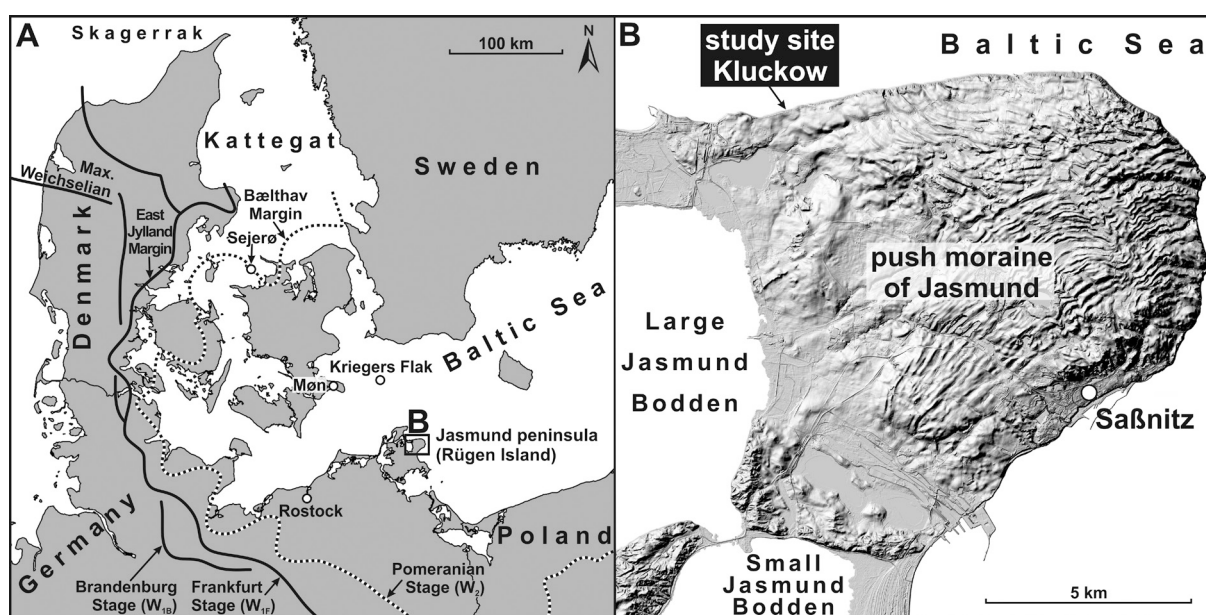
Fig. 2.1 (A) Map of the southwestern Baltic Sea area with ice marginal positions of the Weichselian glaciation (based on Houmark-Nielsen 2010; Houmark-Nielsen et al. 2012); (B) Digital elevation model (DEM) of the Jasmund push–moraine complex with the location of the sample site, Kluckow (based on @GeoBasis-DE/M-V 2015, processed by J. Hartleib).

2.2.2 Geographical and geological settings

The cliff outcrop Kluckow (Lat: 54°34.53 N, Lon: 13°31.24 E) is located at the Jasmund peninsula (Rügen Island, Germany) (Fig. 1). The Jasmund area is formed by a push–moraine complex up to 161 m high characterised by Lower Maastrichtian bedrock (~69.5 Ma) and overlying Pleistocene sediments (Panzig 1995). The 70 m long and 21 m high Kluckow cliff section is composed of an 8 m thick (glacio-) fluvial to (glacio-) lacustrine succession intercalated between two tills which are correlated to Saalian and Weichselian in age (Panzig 1995) (Fig. 2.2). The first detailed sedimentological
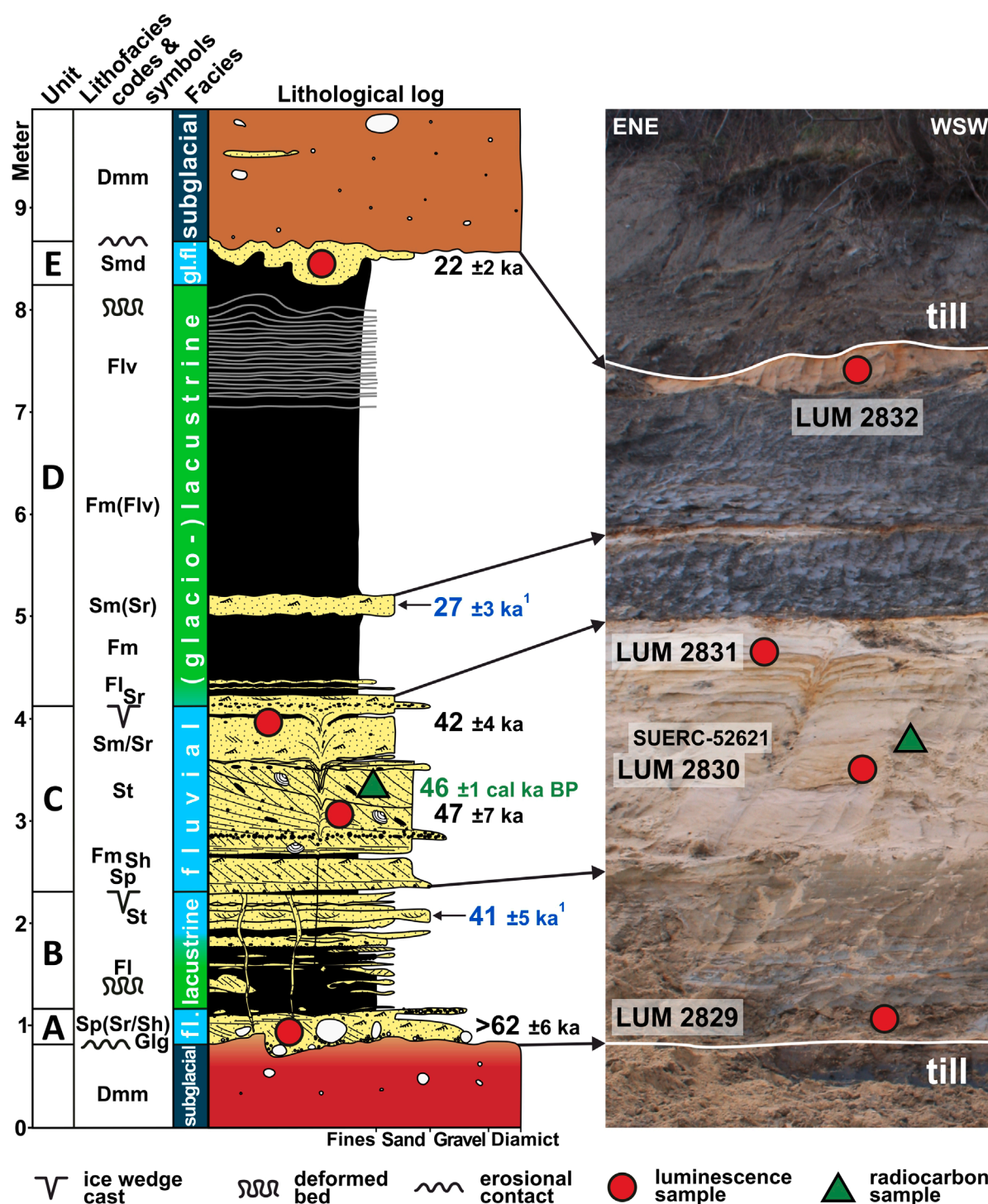
Fig. 2.2 Investigated part of the Kluckow section showing a synoptic lithological log with interpretations of the depositional environments, lithofacies codes according to Benn & Evans (2010), corresponding lithostratigraphic units (A to E), in comparison with a picture of the cleaned cliff surface of the Kluckow section with luminescence (LUM) and radiocarbon (SUERC) sample locations. The OSL ages were calculated from the mean D_e values of the 2.5 mm aliquot quartz measurements. A calibrated radiocarbon age is also shown. The complete Pleistocene Kluckow section continues upward and downward and will be described and discussed elsewhere.

[1]Thermoluminescence ages (Krbetschek 1995).

and palaeontological description of the site was provided by Steinich (1992), who divided the section into several lithostratigraphical units. Based on two TL ages by Krbetschek (1995), the accumulation of these deposits occurred during MIS 3, between 41±5 ka and 27±3 ka (cf. Fig. 2.2).

We conducted detailed lithofacies analysis focusing on the sedimentary structures and textural characteristics of individual depositional units and their palaeoenvironmental interpretations (Fig. 2.2). The sediments were analysed and termed according to the facies codes and classification scheme of Benn & Evans (2010). The overall result of our facies analysis agrees well with the descriptions and interpretations of Steinich (1992), but includes some minor modifications: We divide the investigated sequence into five lithostratigraphic units (A to E) with corresponding depositional environments (Fig. 2.2).

We interpret unit A as a fluvial or a glaciofluvial deposit. A sample LUM 2829 was taken from a position more than 30 cm away from the underlying till surface to avoid radiation influence from the till (Fig. 2.2). Unit B is a mainly lacustrine sediment that was subsequently deformed by cryoturbation in a periglacial environment. The ice-wedge casts above this unit indicate a period of periglacial conditions. Unit C represents a mainly fluvial environment during an interstadial climate. The top of this unit reflects a cooling of the climate, evidenced by the presence of ice-wedge casts, and signifies a possible periglacial land surface with a temporary halt in sedimentation. Two samples (LUM 2830 and LUM 2831) were collected from unit C (Fig. 2.2). During sampling, we avoided any possible contamination of the sample with material from the ice-wedge casts. Within unit C, we found undeformed *Anodonta* sp. (bivalvular preservation with intact organic ligaments), which we submitted for accelerator mass spectrometer (AMS) radiocarbon analysis at the Scottish Universities Environmental Research Centre (SUERC) in Glasgow. Because of the non-reworked character of the subfossil, we assume a contemporaneous burial age of the bivalves and the host sediment (LUM 2830). We interpret the overlying unit D as a glaciolacustrine basin deposit, whereas unit E is most likely a glaciofluvial deposit that was accumulated before the following ice advance. The undulation of both the upper part of the underlying clay (unit D) and the sand of unit E may have been caused by a proglacial deformation and/or by loading when the glacier overrode these deposits. One sample (LUM 2832) was taken from unit E (Fig. 2.2).

2.3 Methods

2.3.1 Comparative dating approach

Because the investigated sediments may have been deposited in an environment influenced by the ice margin of the SIS, it is possible that they were insufficiently bleached, as discussed *e.g.* by Lüthgens et al. (2010). A statistical analysis of the equivalent-dose (D_e) distribution to find the true burial dose is possible (Galbraith et al. 1999) but should be treated with caution because the reason for De scattering is not fully understood (Murray et al. 2012). The most commonly used statistical models are the Central Age Model (CAM) and the Minimum Age Model (MAM) described in Galbraith et al. (1999). Murray et al. (2012) recommended the comparison between quartz and feldspar ages as an independent approach to identify the bleaching condition of the samples because of the different bleaching behaviour of quartz and feldspar.

2.3.2 Experimental setup

Sample preparation and luminescence measurements were carried out under subdued red light. A standard procedure was implemented for cleaning and separating sand-sized (150–200 mm) quartz and potassium-rich feldspar grains. The quartz separates were additionally etched with 40% hydrofluoric acid (HF) for 60 min to remove any remaining feldspar contaminations and the outer ~10 µm of the grains affected by alpha radiation. The luminescence signals were measured on a Risø TL/OSL DA-20 reader system fitted with a ^{90}Sr/^{90}Y beta source (Bøtter-Jensen et al. 2010).

For estimation of the water content during the burial time, both natural and saturated water content were measured. We presume that during most of the time after deposition, the water content was higher than today, as these sediments were deposited in fluvial, glaciolacustrine and potentially extended periglacial conditions. Hence, we used 10% lower water content than the saturated water content for age calculation with ±10% uncertainty (Tab. 2.1).

Tab. 2.1 Details about radionuclide concentrations, water content, altitude, depth of sample locations and the resulting total dose rates for quartz and feldspar.

Sample ID	Altitude (mamsl)	Depth below ground (m)	potassium (%)	thorium[1] (ppm)	uranium[2] (ppm)	Water content in situ (%)	Maximum water content (%)	Water content used for age calculation (%)	Quartz dose rate (Gy/ka)	Feldspar dose rate[3] (Gy/ka)
LUM 2829	2.5	20.5	1.32 ± 0.07	3.48 ± 0.17	1.14 ± 0.06	13.0	42.4	32 ± 10	1.32 ± 0.13	2.04 ± 0.15
LUM 2830	4.5	18.5	0.76 ± 0.04	1.22 ± 0.06	0.38 ± 0.02	4.0	36.0	26 ± 10	0.73 ± 0.11	1.45 ± 0.16
LUM 2831	5.8	17.2	1.21 ± 0.06	1.98 ± 0.10	0.63 ± 0.03	4.0	38.3	28 ± 10	1.13 ± 0.12	1.85 ± 0.16
LUM 2832	10.3	12.7	1.74 ± 0.09	3.37 ± 0.17	1.07 ± 0.05	13.9	37.4	27 ± 10	1.70 ± 0.15	2.42 ± 0.16

[1] Thorium concentration was calculated from the activities of 228Ac, 208Tl and 212Pb

[2] Uranium concentration was calculated from the activities of 214Pb and 214Bi

[3] The potassium concentration within the feldspar is assumed with 12.5±0.5% (Huntley and Baril 1997)
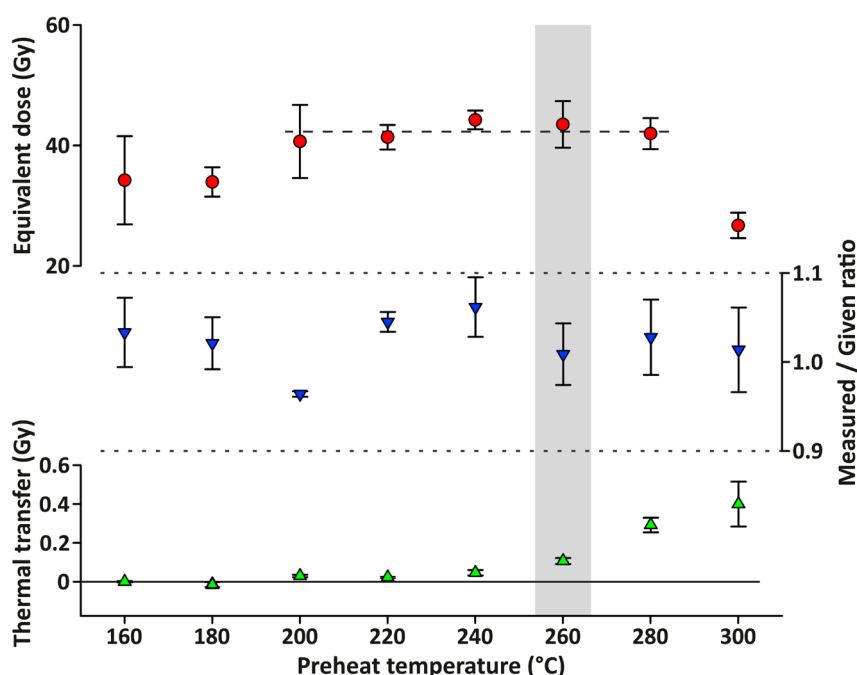
Fig. 2.3 Summary for the preheat plateau, dose recovery and thermal transfer test for sample LUM 2830. Based on the results shown here the preheat temperature at 260 °C (grey shading) and a cutheat temperature at 240 °C were selected for the SAR protocol. Each data point represents the mean of three 6 mm aliquots with standard error bars.

To determine the dose rate, the concentration of uranium, thorium and potassium were measured with a high resolution gamma spectrometer. Based on the conversion factors of Guérin et al. (2011), the concentrations were converted to sediment dose rates. The cosmic part of the dose rates was determined using the approach of Prescott & Stephan (1982) and Prescott & Hutton (1994). The a-value of 0.09±0.02 based on estimation of Balescu et al. (2007) was used for the K-feldspar dose rate. The results of the dosimetry and the dose rates are stated in Tab. 2.1.

A standard single aliquot regenerative dose (SAR) protocol (Murray & Wintle 2000) was applied to determine D_e of quartz (Tab. 2.2). The criteria for approval of the applied SAR protocol for each aliquot were the following: recycling ratio between 0.9

and 1.1, recuperation <5% of the natural signal, and IR depletion ratio >0.9 (Wintle & Murray 2006; Duller 2003). Aliquots of both 2.5 mm (~70–150 quartz grains counted under the microscope) and 6 mm (several hundreds of quartz grains) were measured. Signal and background integrals of 0.0–0.32 s and 0.32–0.96 s were used for the D_e determination. A series of test measurements, *i.e.* preheat plateau, dose recovery and thermal transfer tests, were performed to find the most suitable preheat temperature (Fig. 2.3). Based on these test results a preheat temperature of 260 °C and a cutheat temperature of 240 °C were selected for the D_e determination.

Tab. 2.2 (A) SAR protocol for coarse-grain quartz measurements, (B) Post-IR IRSL SAR protocol for coarse-grain potassium-rich feldspar.

Run	Treatment	
	(A) Quartz	(B) Feldspar
1	Dose (except before first run)	Dose (except before first run)
2	Preheat (260°C for 10s)	Preheat (320°C for 60s)
3	Optical stimulation with IR-diodes for 100s at 125°C	Optical stimulation with IR-diodes for 120s at 50°C
4	Optical stimulation with blue LEDs for 40s at 125°C	Optical stimulation with IR-diodes for 240s at 290°C
5	Give test dose	Give test dose
6	Cutheat at 240°C	Preheat (320°C for 60s)
7	Optical stimulation with blue LEDs for 40s at 125°C	Optical stimulation with IR-diodes for 120s at 50°C
8	Return to run 1	Optical stimulation with IR-diodes for 240s at 290°C
9		Return to run 1

The dating of potassium-rich feldspar was conducted with the post-IR infrared stimulated luminescence protocol at 290 °C (pIRIR$_{290}$) adopted from Thiel et al. (2011). The IR$_{50}$ signal obtained as a part of the pIRIR$_{290}$ protocol was also used for D_e and age calculation. For each sample, nine aliquots were bleached for 4 h in a solar simulator (Hönle SOL2) to perform dose recovery, residual dose, and fading rate measurements. The mean measured-to-given ratio for the pIRIR$_{290}$ signal after subtracting the residual dose is within 10% of unity (Fig. 2.4). The fading rate (g-value) for IR$_{50}$ and pIRIR$_{290}$ was determined following the approach of Auclair et al. (2003) for all samples.
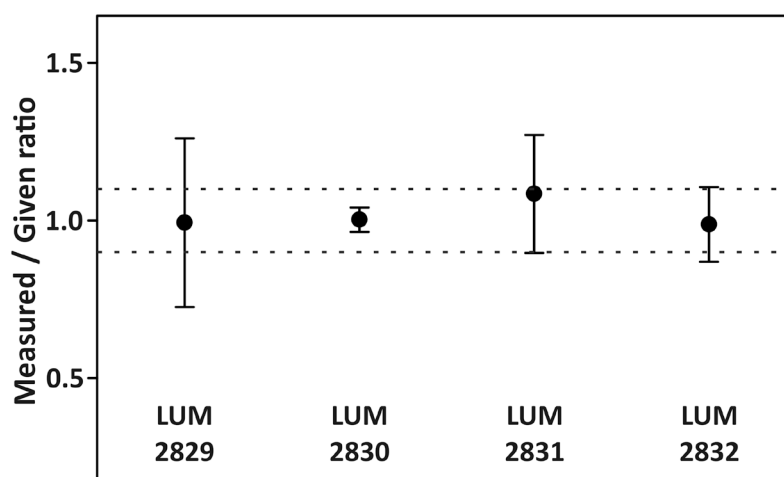
Fig. 2.4 Dose recovery ratios for the pIRIR$_{290}$ signal. Each data point refers to the mean of three 2.5 mm aliquots of potassium-rich feldspar with standard error bars. The residual dose measured after 4 hours of bleaching in a Hönle SOL2 solar simulator was removed for each sample. The dashed line represents ±10% of unity.

2.4 Results and Discussion

2.4.1 Radiocarbon dating

The organic skin of several *Anodonta* sp. (unit C) submitted for radiocarbon dating (sample number: SUERC-52621/GU34333) yielded a ^{14}C age of 42.8±0.5 ka, which is near the uppermost limit of radiocarbon dating. However, the AMS measurement revealed sufficient ^{14}C content to calculate a ^{14}C age. We applied OxCal4.2 (Bronk Ramsey 2009) using IntCal13 (Reimer et al. 2013) for ^{14}C correction, giving a calibrated ^{14}C age of 46.1±1 ka (Fig. 2.2).

2.4.2 Luminescence measurements of quartz

The observed quartz luminescence signal decayed rapidly (Fig. 2.5), implying a domination by a fast component. The D_e distribution for 2.5 and 6 mm aliquots of sample LUM 2829 and LUM 2830 is shown in Fig. 2.6A and the results are summarised in Tab. 2.3. For sample LUM 2829, the 2.5 mm aliquot D_e distribution is obviously skewed, and an overdispersion of 34% was calculated using the CAM. The radial plot of this sample indicates no distinct D_e clusters (Fig. 2.6B). The host sediment for this sample is fluvial sand with the possibility of glacial influence during deposition, making it very likely that the sample was insufficiently bleached in a glaciofluvial environment.
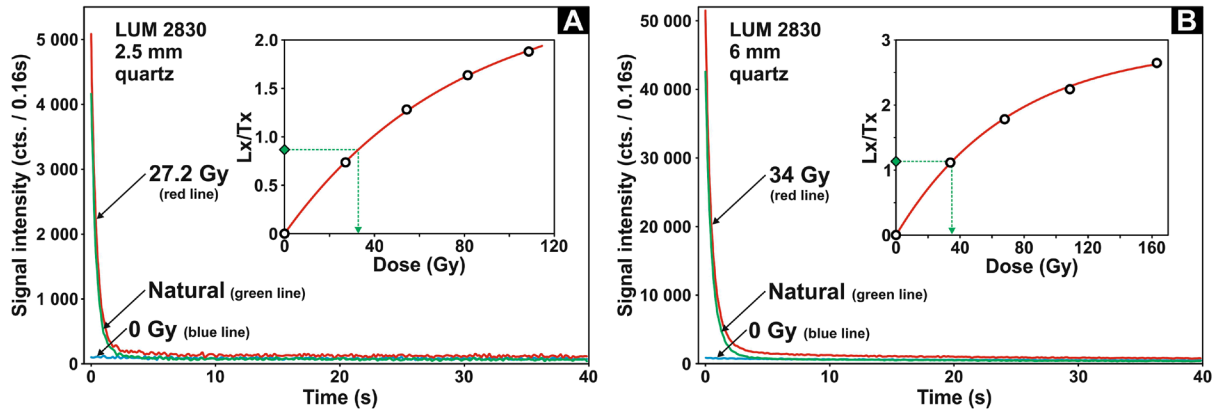
Fig. 2.5 Decay and dose response curves for a typical (A) 2.5 mm and (B) 6 mm aliquot with quartz grains of sample LUM 2830.
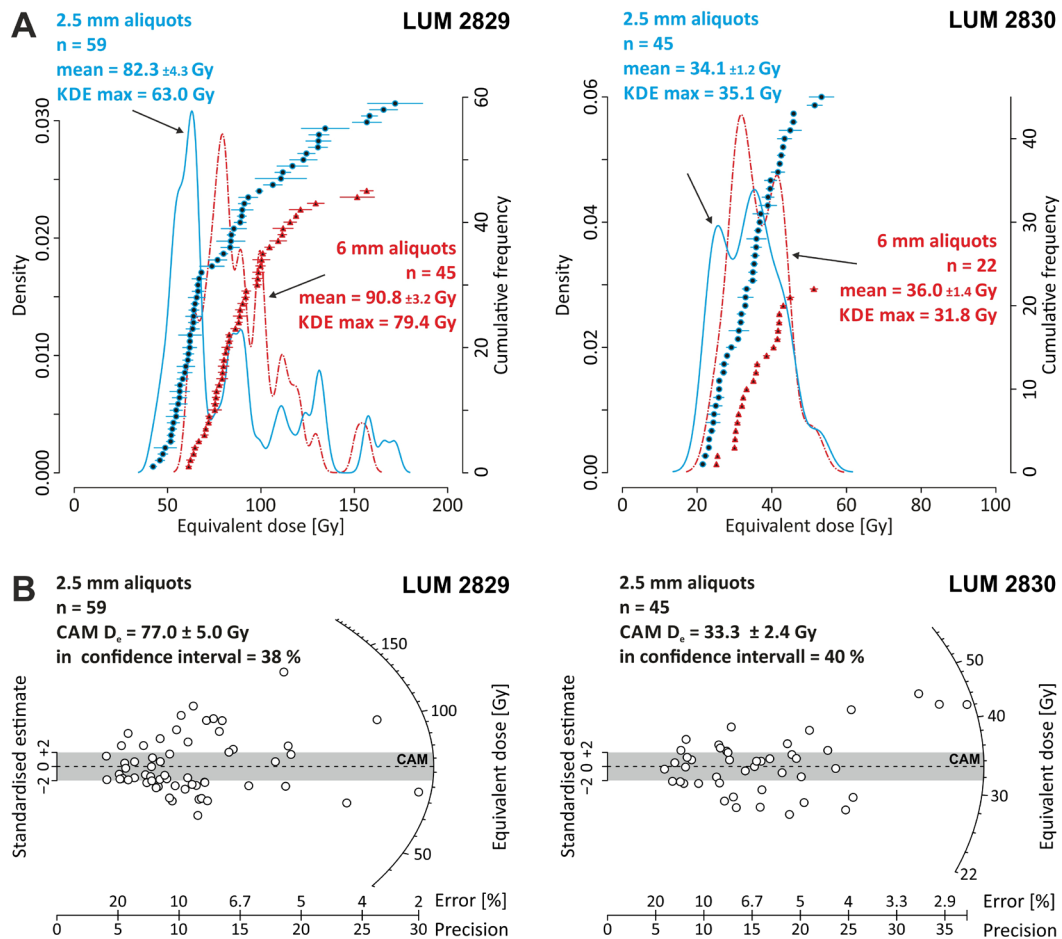
Fig. 2.6 (A) Kernel density estimation (KDE) and empirical cumulative D$_e$ distribution for 2.5 and 6 mm aliquots of samples LUM 2829 and LUM 2830, showing a nearly Gaussian distribution for LUM 2830 and a skewed one for LUM 2829. The KDE max refers to the maximum value of the kernel density estimate. (B) Radial plots of samples LUM 2829 and LUM 2830. The 2-sigma estimate (grey shading) is centred on the Central Age Model (CAM) equivalent dose (D$_e$). The CAM D$_e$ and the mean D$_e$ value are in agreement within the error for the 2.5 mm aliquots of both samples. Modified plots drawn in RStudio (2012) using the package 'Luminescence' by Kreutzer et al. (2014).

Tab. 2.3 Small-aliquot (2.5 mm) and medium-aliquot (6 mm) quartz D_e data and comparison using the mean D_e value and CAM for age calculation

Sample	Aliquot size	No. of aliquots[1]	mean D_e (Gy)	mean age (ka)[2]	CAM D_e (Gy)	overdispersion (%)	CAM age (ka)
LUM 2829	6 mm	49 (45)	90.8 ± 3.2	68.8 ± 6.2			
	2.5 mm	92 (59)	82.3 ± 4.3	**62.4 ± 6.1**	77.0 ± 3.6	34.1 ± 2.0	58.4 ± 5.5
LUM 2830	6 mm	22 (22)	36.0 ± 1.4	49.3 ± 7.3			
	2.5 mm	82 (45)	34.1 ± 1.2	**46.7 ± 6.9**	33.3 ± 1.2	22.1 ± 1.2	45.5 ± 6.7
LUM 2831	6 mm	38 (38)	46.5 ± 1.2	41.0 ± 4.1			
	2.5 mm	92 (54)	47.7 ± 1.8	**42.0 ± 4.3**	45.7 ± 1.5	23.2 ± 1.2	40.3 ± 4.1
LUM 2832	6 mm	48 (47)	36.4 ± 0.9	21.4 ± 1.7			
	2.5 mm	96 (47)	36.5 ± 1.3	**21.6 ± 1.8**	35.6 ± 1.2	22.1 ± 1.2	21.0 ± 1.7

[1] Total number of measured aliquots and aliquots that passed criteria (in parentheses)

[2] Bold numbers refer to the most reliable age

However, other possible interpretations for the D_e scattering include 1) mixing with different deposits (cryoturbation, ice-wedge casts), 2) dose rate inhomogeneities, or 3) saturation effects of quartz grains (Murray et al. 2012). As our sampling attempted to minimise the impact of sediment mixture due to cryoturbation with the choice of a suitable sampling point, this first possibility is not likely. If the D_e distribution is affected by inhomogeneities in the beta dosimetry, the mean D_e value should be used for age calculation, because the determination of the dose rate resulted in an average value for the surrounding sediment (Murray et al. 2012). To test for the presence of potentially saturated quartz grains, a SAR protocol with a high regeneration dose up to 520 Gy for all samples was conducted (Wintle & Murray 2006). From the resulting dose response curves described by a single saturating exponential, averaged $2D_0$ values in the range of 140±29 Gy (LUM 2829) to 167±45 Gy (LUM 2832) were calculated (Fig. 2.7). These $2D_0$ are all larger than the mean D_e values (Tab. 2.3), however, ~20% of the D_e values for sample LUM 2829 exceed the $2D_0$ value. The corresponding quartz mean D_e age remains therefore unreliable. For samples LUM 2830, LUM 2831 and LUM 2832, quartz saturation effects can be excluded because all D_e values are much lower than the corresponding $2D_0$ value. The shape of the D_e value variations for both 2.5 mm and 6 mm aliquots of sample LUM 2830, LUM 2831 and LUM 2832 are similar and show nearly Gaussian distributions. The calculated overdispersion for the 2.5 mm aliquots is ~22–23% (Tab. 2.3). There are no significant differences between the mean D_e values of the 2.5 and 6 mm aliquots (Tab. 2.3). Single grain measurements of glaciofluvial sediment performed by Lüthgens et al. (2011) resulted in 2.8–5.0% accepted quartz grains. The deposit is connected to the Pomeranian IMP and located

near Eberswalde, 200 km to the south of Kluckow. Hence, we assume a possible similar range of suitable quartz for both locations. If true, each of our 2.5 mm aliquots represents an average signal of 2–8 quartz grains. Therefore, a potential averaging effect still exists for most of the aliquots. Nevertheless, the minor difference in the dose distributions between the D_e values of 2.5 mm and 6 mm aliquots might be indicative of good bleaching conditions prior to deposition.
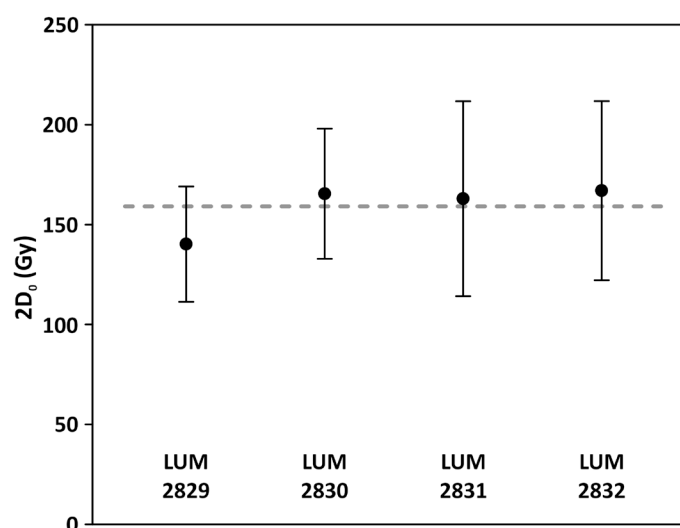
Fig. 2.7 Plot of $2D_0$ values for quartz, calculated from dose response curves fitted using a single saturating exponential and a high regeneration dose of 520 Gy. Each data point represents the mean of three 2.5 mm aliquots with 1σ standard error. The grey dotted line refers to the mean $2D_0$ value of all samples.

2.4.3 Luminescence measurements of feldspar

For age calculation, the mean D_e of six 2.5 mm aliquots per sample was used with 1-σ standard error. A representative decay and dose response curve of the IR_{50} and the $pIRIR_{290}$ signal are shown in Fig. 2.8. The residual doses estimated from the IR_{50} and $pIRIR_{290}$ signal varied between 2 and 25 Gy (Fig. 2.9). For the $pIRIR_{290}$, the g-values ranged between $0.2\pm0.4\%$ and $1.2\pm0.5\%$ per decade, whereas the corresponding g-values for IR_{50} are between $1.7\pm0.5\%$ and $3.4\pm0.8\%$ per decade (Tab. 2.4). As a result, the IR_{50} ages were corrected for anomalous fading using the method of Huntley & Lamothe (2001), whereas no correction was done for the $pIRIR_{290}$ ages. For all samples the fading corrected IR_{50} and nonfading corrected $pIRIR_{290}$ age are consistent within the uncertainties (Tab. 2.4).
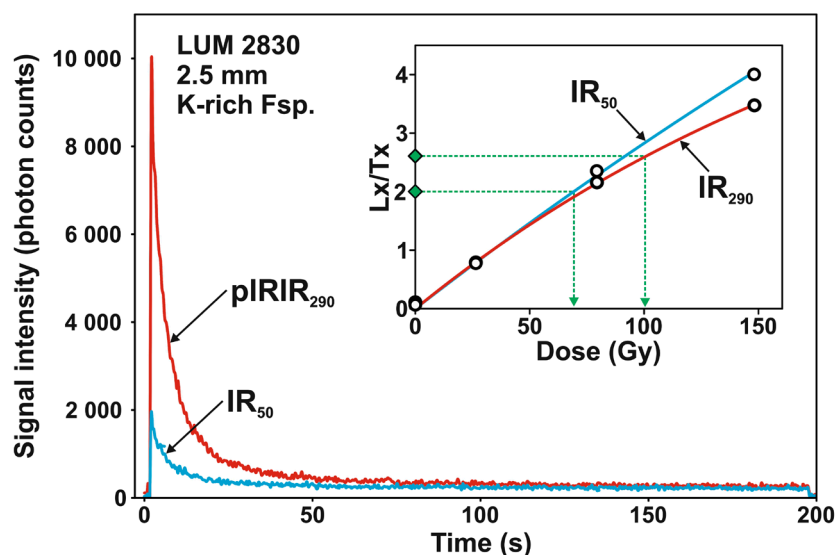
Fig. 2.8 Decay and dose response curves for the IR_{50} and $pIRIR_{290}$ signal of sample LUM 2830.
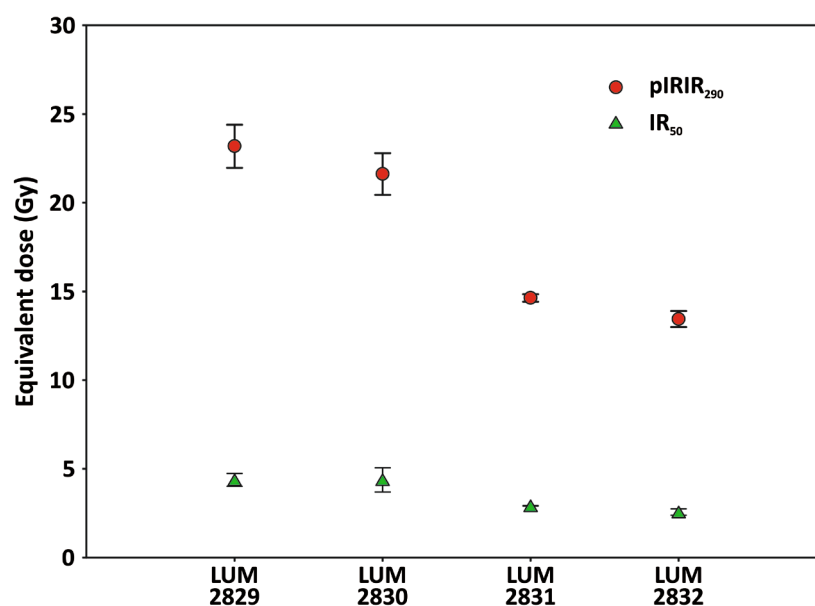
Fig. 2.9 Measured residual equivalent doses for the IR_{50} and $pIRIR_{290}$ signal after 4 hours of bleaching in a Hönle SOL2 solar simulator. Each data point conforms to the mean of three aliquots with corresponding standard error.

Tab. 2.4 Summary of the feldspar luminescence measurements with D_e values, g-values, $pIRIR_{290}$ ages and fading corrected ages for IR_{50}.

Sample	Aliquot size	No. of aliquots[1]	$pIRIR_{290}$ D_e (Gy)	$pIRIR_{290}$ g-value (%/decade)	$pIRIR_{290}$ age (ka)	IR_{50} D_e (Gy)[2]	IR_{50} g-value (%/decade)	IR_{50} age (ka) corr
LUM 2829	2.5 mm	6 (6)	206.3 ± 11.5	1.2 ± 0.5	101 ± 9[3]	171.9 ± 25.0	3.4 ± 0.8	122 ± 23
LUM 2830	2.5 mm	6 (5)	106.4 ± 1.2	0.2 ± 0.4	73.6 ± 8.1	77.5 ± 5.3	2.6 ± 0.6	69.6 ± 9.6
LUM 2831	2.5 mm	6 (6)	95.3 ± 4.8	1.1 ± 0.2	51.4 ± 5.1	75.4 ± 6.0	1.7 ± 0.5	47.9 ± 6.3
LUM 2832	2.5 mm	6 (6)	66.4 ± 2.3	0.4 ± 0.4	27.4 ± 2.1	45.3 ± 1.2	2.9 ± 0.6	25.0 ± 2.3

[1] Total number of measured aliquots and aliquots that passed criteria (in parentheses)   [2] IR_{50} signal was obtained from the $pIRIR_{290}$ protocol

[3] The $pIRIR_{290}$ age should be treated as maximum age of sample LUM 2829

2.4.4   Reliability of age calculation based on quartz and feldspar measurements

The comparison of the quartz ages (2.5 mm aliquots), calculated using the mean D_e and CAM, compared with the feldspar ages of the IR_{50} and $pIRIR_{290}$ signal, may be interpreted as follows (Fig. 2.10): For sample LUM 2829 a significant difference between the mean D_e quartz ages (62.4±6.1 ka) and the corresponding fading corrected IR_{50} (122±23 ka) and $pIRIR_{290}$ signal (101±9 ka) is obvious. The large difference between the quartz and feldspar ages of sample LUM 2829 makes it impossible to evaluate the degree of bleaching of the quartz grains. Because the quartz D_e scattering of sample LUM 2829 cannot be fully explained, the corresponding age remains unreliable. Hence, for this sample, we used the mean D_e value for age calculation (Tab. 2.3). The resulting mean D_e quartz age of 62.4±6.1 ka should be treated as a minimum age. The true burial ages of this sample very likely lies between 62.4±6.1 ka and the uncorrected $pIRIR_{290}$ age of 101±9ka. The feldspar ages of sample LUM 2830 overestimate the quartz ages by several thousand years (Fig. 2.10), whereas the difference between quartz and feldspar ages for LUM 2831 and LUM 2832 are very small or even agree within uncertainties. Thus we presume that both quartz and feldspar grains were well-bleached (Murray et al. 2012) and the overdispersion of 22 and 23% for both samples represent a well-bleached sediment. This would also suggest that the quartz of sample LUM 2830 with an overdispersion of 22% might also be sufficiently bleached (Arnold & Roberts 2009). For samples LUM 2830, LUM 2831 and LUM 2832 the ages calculated with the CAM and the mean D_e values are indistinguishable and thus we use the ages based on the mean D_e values (Tab. 2.3) for interpretation. The quartz OSL ages for all samples range from 62.4±6.1 ka (unit A) to 21.6±1.8 ka (unit E), and are stratigraphically consistent. The calibrated radiocarbon age in unit C (46.1±1.0 cal ka BP) is in good agreement with the corresponding OSL age of sample LUM 2830 (46.7±6.9 ka). The agreement between OSL and TL ages (Fig. 2.2) might be another evidence for good bleaching conditions because the TL signal is known to bleach slower than the OSL signal (*e.g.* Jain et al. 2007).
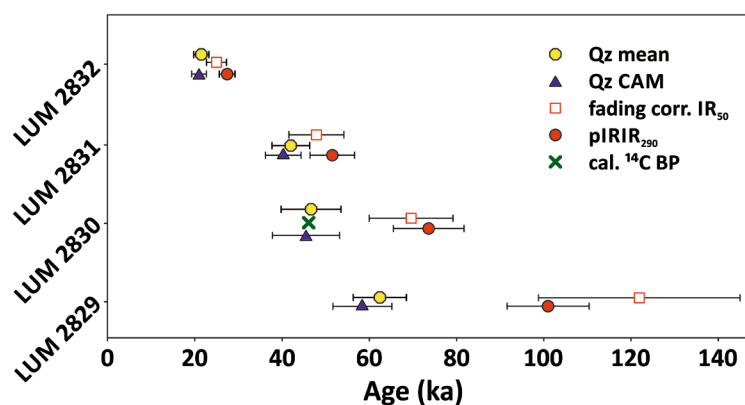
Fig. 2.10 Comparison of quartz and feldspar ages calculated from D_e estimates of 2.5 mm aliquots. One radiocarbon age is plotted as independent age control.

2.4.5 Geochronological implications for Weichselian ice dynamic

During the Early or Middle Weichselian, (glacio-) fluvial unit A, with an age of 101±9 ka ($pIRIR_{290}$) and a minimum age of 62.4±6.1 ka (quartz mean D_e), was deposited at the study site. A TL age from unit B (41±5 ka; Krbetschek 1995) suggests a hiatus between unit A and B. The sediments of units A and B show no evidence for the presence of an ice sheet in this area during the depositional interval from at least 62.4±6.1 ka until 46.7±6.9 ka. Nevertheless, it is possible that deposits like diamictons or tills connected to an ice advance had been removed by an erosion. From a sedimentological view point, we think this is not likely because there is no clear evidence, except at the base of unit A, for significant erosion with a corresponding boulder bed or fluvial lag deposit. However, it is not possible at this stage to determine whether the underlying till is of Saalian or Early Weichselian age, as discussed by Müller (2004) and Steinich (1992). The hiatus between units B and C, accompanied by ice-wedge casts, indicates a former periglacial land surface. The corresponding cooler climate conditions could be related to the Ristinge advance (50±4 ka) in Denmark (Houmark-Nielsen 2010) but we found no evidence in the section of Kluckow that the Ristinge advance reached the region of Jasmund. Anjar et al. (2012) also did not find reliable indications for the Ristinge advance in the area of Kriegers Flak, 60 km north-northwest of Kluckow (Fig. 2.1). The finding of *Anodonta* sp. shells within the fluvial sediments of unit C indicates a warming phase between 46.7±6.9 ka and 42.0±4.3 ka. Both the OSL age of sample LUM 2830 and the radiocarbon age indicate that the deposition of the main part of unit C may correlate with the Pilgrimstad (44±8 ka) (Alexanderson et al. 2010) or Sejerø Interstadial (41.5 cal ka BP) (Bennike et al. 2007). The ice-wedge casts on top of

subunit C suggest a hiatus in connection with a cooling phase and a former periglacial land surface, which can be related with the Klintholm advance at 32±2 ka (Houmark-Nielsen 2010), but there is no sedimentological evidence that this ice advance extended to Kluckow. The overlying clay of subunit D (2.2) represents a glaciolacustrine depositional environment, very likely related to an ice advance. A TL age of Krbetschek (1995) and the quartz OSL age of sample LUM 2832 indicate that unit D was deposited between 27±3 ka and 22±2 ka. Anjar et al. (2012) also demonstrated the formation of a glaciolacustrine clay succession at Kriegers Flak, related to a large ice-dammed lake between 28.5 and 26 ka. Thus, the glaciolacustrine sediments of unit D were most likely deposited during the Kattegat ice advance and the resulting damming of the Kattegat and southwestern Baltic Basin (Houmark-Nielsen 2010). The area of Kluckow marks the possible southern margin of this ice-dammed lake. The following main ice advance of the SIS related to the LGM is represented by the till overlying subunit E (Fig. 2.2), which reached the area of Jasmund soon after 21.6±1.8 ka (LUM 2832). The palaeogeographical reconstructions of Houmark-Nielsen (2010) for the southwestern Baltic Sea area support this hypothesis. In this context, the quartz OSL ages of 34±3 ka and 28±4 ka (Lüthgens et al. 2010) for the advance of the Brandenburg phase appears to be too old, whereas those of 20.1±1.6 ka and 19.4±2.4 ka for an outwash plain attributed to the Pomeranian phase (Lüthgens et al. 2011) are in good agreement.

2.5 Conclusion

This study uses luminescence dating and lithofacies analysis of a (glacio-) fluvial to (glacio-) lacustrine sequence at the Kluckow section on Rügen Island (Germany) to provide new temporal constraints and a palaeoenvironmental interpretation of the Early and Middle Weichselian glaciation in northeastern Germany, resolving some controversial questions in the history of the Scandinavian Ice Sheet. Both quartz and feldspar minerals were used for luminescence dating; the comparison of the two minerals allows for assessing the bleaching history of the sediment. The new dating results and lithofacies analysis have the following main implications for the dynamics of the SIS: (1) The investigated sequence was mainly deposited during the Marine Isotope Stage 3 (60–27 ka); (2) Facies analysis shows no evidence for an ice advance

reaching the research area from >62.4 ka to 21.6±1.8 ka; (3) A periglacial land surface accompanied by ice-wedges was formed between >62.4±6.1 ka and 46.7±6.9 ka; (4) A warmer phase with potentially interstadial climate conditions existed at 46.1±1.0 ka; (5) Between 42.0±4.3 ka and 27±3 ka, the development of another periglacial land surface with ice-wedges suggests a cooling phase; (6) A glaciolacustrine lake was present between 27±3 ka and 21.6±1.8 ka; (7) Finally the first clear Weichselian ice advance of the SIS reached the study site after 21.6±1.8 ka.

2.6 Acknowledgements

2.7 References

Alexanderson, H., Johnsen, T. & Murray, A.S. 2010: Re-dating the Pilgrimstad Interstadial with OSL: a warmer climate and a smaller ice sheet during the Swedish Middle Weichselian (MIS 3)? *Boreas 39*, 367–376.

Anjar, J., Adrielsson, L., Bennike, O., Björck, S., Filipsson, H.L., Groeneveld, J., Knudsen, K.L., Larsen, N.K. & Möller, P. 2012: Palaeoenvironments in the southern Baltic Sea Basin during marine isotope stage 3: a multi-proxy reconstruction. *Quaternary Science Reviews 34*, 81–92.

Arnold, L.J. & Roberts, R.G. 2009: Stochastic modelling of multi-grain equivalent dose (D_e) distributions: implications for OSL dating of sediment mixtures. *Quaternary Geochronology 4*, 204–230.

Auclair, M., Lamothe, M. & Huot, S. 2003: Measurement of anomalous fading for feldspar IRSL using SAR. *Radiation Measurements 37*, 487–492.

Balescu, S., Ritz, J.-F., Lamothe, M., Auclair, M. & Todbileg, M. 2007: Luminescence dating of a gigantic palaeolandslide in the Gobi-Altay mountains, Mongolia. *Quaternary Geochronology 2*, 290–295.

Bennike, O., Houmark-Nielsen, M. & Wiberg-Larsen, P. 2007: A Middle Weichselian interstadial lake deposit on Sejerø, Denmark: macrofossil studies and dating. *Journal of Quaternary Science 22 (6)*, 647–651.

Benn, D.I. & Evans, D.J.A. 2010: *Glaciers and Glaciations*. 802 pp. Hodder Education, London.

Bøtter-Jensen, L., Thomsen, K.J. & Jain, M. 2010: Review of optically stimulated luminescence (OSL) instrumental developments for retrospective dosimetry. *Radiation Measurements 45*, 253–257.

Bronk Ramsey, C. 2009: Bayesian analysis of radiocarbon dates. *Radiocarbon 51 (1)*, 337–360.

Duller, G.A.T. 2003: Distinguishing quartz and feldspar in single grain luminescence measurements. *Radiation Measurements 37*, 161–165.

Galbraith, R.F., Roberts, R.G., Laslett, G.M., Yoshida, H. & Olley, J.M. 1999: Optical dating of single and multiple grains of quartz from Jinmium Rock Shelter, Northern Australia: Part I, experimental design and statistical models. *Archaeometry 41*, 339–364.

Guérin, G., Mercier, N. & Adamiec, G. 2011: Dose-rate conversion factors: update. *Ancient TL 29*, 5–8.

Heine, K., Reuther, A.U., Thieke, H.U., Schulz, R., Schlaak, N. & Kubik, P.W. 2009: Timing of Weichselian ice marginal positions in Brandenburg (northeastern Germany) using cosmogenic in situ [10]Be. *Zeitschrift für Geomorphologie N. F. 53 (4)*, 433–454.

Houmark-Nielsen, M. 2010: Extent, age and dynamics of Marine Isotope stage 3 glaciation in the southwestern Baltic Basin. *Boreas 39*, 343–359.

Houmark-Nielsen, M., Linge, H., Fabel, D., Schnabel, C., Xu, S., Wilcken, K.M. & Binnie, S. 2012: Cosmogenic surface exposure dating the last deglaciation in

Denmark: discrepancies with independent age constraints suggest delayed periglacial landform stabilization. *Quaternary Geochronology 13*, 1–17.

Huntley, D.J. & Baril, M.R. 1997: The K content of the K-feldspars being measured in optical dating or in thermoluminescence dating. *Ancient TL 15*, 11–13.

Huntley, D.J. & Lamothe, M. 2001: Ubiquity of anomalous fading in K-feldspar and the measurement and correction for it in optical dating. *Canadian Journal of Earth Sciences 38 (7)*, 1093–1106.

Jain, M., Duller, G.A.T. & Wintle, A.G. 2007: Dose response, thermal stability and optical bleaching of the 310°C isothermal TL signal in quartz. *Radiation Measurements 42*, 1285–1293.

Krbetschek, M.R. 1995: *Lumineszenz-Datierungen quartärer Sedimente Mittel-, Ost- und Nordostdeutschlands*. Ph.D. thesis. TU Bergakademie Freiberg, 122 pp.

Kreutzer, S., Schmidt, C., Fuchs, M.C., Dietze, M., Fischer, M. & Burow, C. 2014: Package for Luminescence Dating data analysis (Version 0.3.3) [Computer software].

Larsen, N.K., Knudsen, K.L., Krohn, K.L., Kronborg, C.F., Murray, A.S. & Nielsen, O.B. 2009: Late quaternary ice sheet, lake and sea history of southwest Scandinavia – a synthesis. *Boreas 38*, 732–761.

Ludwig, A.O. 2006: Cyprina-clay and I1 beds in the Pleistocene sequence in Northeast Rügen and the island Hiddensee (southwestern Baltic Sea). *Zeitschrift für Geologische Wissenschaften 34*, 349–377.

Lüthgens, C. & Böse, M. 2011: Chronology of Weichselian main ice marginal positions in north-eastern Germany. *Quaternary Science Journal (Eiszeitalter und Gegenwart) 60 (2–3)*, 236–247.

Lüthgens, C., Böse, M. & Preusser, F. 2011: Age of the Pomeranian ice-marginal position in northeastern Germany determined by optically stimulated luminescence (OSL) dating of glaciofluvial sediments. *Boreas 40*, 598–615.

Lüthgens, C., Krbetschek, M., Böse, M. & Fuchs, M.C. 2010: Optically stimulated luminescence dating of fluvioglacial (sandur) sediments from north-eastern Germany. *Quaternary Geochronology 5*, 237–243.

Marks, L. 2012: Timing of the Late Vistulian (Weichselian) glacial phases in Poland. *Quaternary Science Reviews 44*, 81–88.

Murray, A.S., Thomsen, K.J., Masuda, N., Buylaert, J.P. & Jain, M. 2012: Identifying well-bleached quartz using the different bleaching rates of quartz and feldspar luminescence signals. *Radiation Measurements 47*, 688–695.

Murray, A.S. & Wintle, A.G. 2000: Luminescence dating of quartz using an improved single-aliquot regenerative-dose protocol. *Radiation Measurements 32*, 57–73.

Müller, U. 2004: Weichsel-frühglazial in Nordwest-Mecklenburg. *Meyniana 56*, 81–115.

Panzig, W.-A. 1995: Zum Pleistozän von Rügen. *Terra Nostra 6*, 177–200.

Prescott, J.R. & Hutton, J.T. 1994: Cosmic ray distribution to dose rates for luminescence and ESR dating: large depths and long-term variations. *Radiation Measurements 23*, 497–500.

Prescott, J.R. & Stephan, L.G. 1982: The contribution of cosmic radiation to the environmental dose for thermoluminescent dating – Latitude, altitude and depth dependences. *Proceedings of the Second Specialist Seminar on Thermoluminescence Dating (Council of Europe) 6*, 17–25.

Reimer, P.J., Bard, E., Bayliss, A., Beck, J.W., Blackwell, P.G., Bronk Ramsey, C., Buck, C.E., Cheng, H., Edwards, R.L., Friedrich, M., Grootes, P.M., Guilderson, T.P., Haflidason, H., Hajdas, I., Hatté, C., Heaton, T.J., Hoffmann, D.L., Hogg, A.G., Hughen, K.A., Kaiser, K.F., Kromer, B., Manning, S.W., Niu, M., Reimer, R.W., Richards, D.A., Scott, E.M., Southon, J.R., Staff, R.A., Turney, C.S.M. & van der Plicht, J. 2013: IntCal13 and Marine13 radiocarbon age calibration curves 0–50,000 years cal BP. *Radicarbon 55 (4)*, 1869–1887.

RStudio, 2012: RStudio: Integrated development environment for R (Version 0.98.501) [Computer software]. Boston, MA.

Steinich, G. 1992: Die stratigraphische Einordnung der Rügen-Warmzeit. *Zeitschrift für Geologische Wissenschaften 20*, 125–154.

Stephan, H.-J. 2014: Climato-stratigraphic subdivision of the Pleistocene in Schleswig-Holstein, Germany and adjoining areas. *Quaternary Science Journal (Eiszeitalter und Gegenwart) 63 (1)*, 3–18.

Thiel, C., Buylaert, J.-P., Murray, A.S., Terhorst, B., Hofer, I., Tsukamoto, S. & Frechen, M. 2011: Luminescence dating of the Stratzing loess profile (Austria) – testing the potential of an elevated temperature post-IR IRSL protocol. *Quaternary International 234*, 23–31.

Wintle, A.G. & Murray, A.S. 2006: A review of quartz optically stimulated luminescence characteristics and their relevance in single-aliquot regeneration dating protocols. *Radiation Measurements 41*, 369–391.

Wolff, E.W., Chappellaz, J., Blunier, T., Rasmussen, S.O. & Svensson, A., 2010: Millennial-scale variability during the last glacial: the ice core record. *Quaternary Science Reviews 29*, 2828–2838.

3   New age constraints from the SW Baltic Sea area – implications for Scandinavian Ice Sheet dynamics and palaeo-environmental conditions during MIS 3 and early MIS 2

Michael Kenzler[1], Sumiko Tsukamoto[2], Stefan Meng[1], Manfred Frechen[2] & Heiko Hüneke[1]

[1]University of Greifswald, Institute of Geography and Geology, F.-L. Jahn Str. 17a, 17487 Greifswald, Germany

[2]Leibniz Institute for Applied Geophysics (LIAG), Geochronology and Isotope Hydrology, Stilleweg 2, 30655 Hannover, Germany

Abstract

The study of two cliff outcrops from the Jasmund Peninsula provides new information on the ice-sheet dynamics and palaeo-environmental conditions during MIS 3 and the ensuing transition to MIS 2 in the southwestern Baltic Sea region. We identified interstadial fluvial sediments, with mollusc and vertebrate fauna, which were deposited between 47 and 42 ka in a steppe-like landscape. A subsequent cooling phase led to the formation of a proglacial lake, between 30 and 22 ka, indicated by varve-like, rhythmically bedded silty clay. This proglacial lake formation can be correlated to the blocking of the Baltic Basin by the Kattegat ice advance, previously dated to c. 29–26 ka. The transition from proglacial to terminoglacial lacustrine deposits reflects the immediate advance of the Scandinavian Ice Sheet (SIS) into the study area after the transition from MIS 3 to early MIS 2. The SIS finally reached the area at 23±2 ka

(Brandenburgian phase; advance from the northeast). A subsequent ice retreat accompanied by the deposition of meltwater sediments was followed by a re-advance of the SIS, resulting in a glaciotectonic deformation event across the study area. The age control for our study is based on optically stimulated luminescence (OSL). The investigated Pleistocene sediments show ice-free conditions during MIS 3 and early MIS 2, indicating that neither the Ristinge nor the Klintholm advance reached the SW Baltic Sea coast of Jasmund.

3.1 Introduction

The advance and retreat of the Scandinavian Ice Sheet (SIS) during the Weichselian glaciation (115–11.7 ka; Cohen & Gibbard 2012) resulted in a variety of deposits in the southwestern Baltic Sea basin, including subglacial tills, glaciolacustrine clays, fossil-bearing fluvial sands, and gravels. These sediments provide vital information about the highly diverse depositional environments during this period. The interpretation of these dynamically migrating depositional systems strongly depends on reliable age data. Such data are presented in this paper for two key localities on Rügen Island, Glowe and Kluckow, together with sedimentological and palaeontological details.

Apart from the main oscillations of the SIS during Marine Isotope Stage 2 (MIS 2, 29–14 ka; Cohen & Gibbard 2012), several ice advances have been reported from Fennoscandia during MIS 3 (57–29 ka, Cohen & Gibbard 2012) into Denmark (Houmark-Nielsen & Kjær 2003; Larsen et al. 2009; Houmark-Nielsen 2010, 2011; Wohlfarth 2010), northern Germany (Müller 2004; Ehlers et al. 2011; Stephan 2014), northern Poland (Marks 2012) and the Baltic states (*e.g.* Zelčs & Markots 2004; Kalm 2006) (Fig. 3.1). It is difficult to reconstruct the Weichselian ice advances by direct age determination, due to the lacking of datable material in subglacial tills; instead, the timing of the ice advances has been constrained by dating the sediments below and above till sheets with *e.g.* luminescence or radiocarbon (^{14}C) dating methods. Therefore, the intercalated interstadial deposits between glacial tills are of great importance to constrain the ice advances (Houmark-Nielsen & Kjær 2003).

For the reconstruction of the SIS extent between 40 and 10 ka, Hughes et al. (2016) used a Geographical Information System (GIS) database with more than 5000 ages. For the northern and northeastern parts of Germany, only a few absolute ages

are available (*e.g.* Steinich 1992; Krbetschek 1995; Preusser 1999; Heine et al. 2009; Lüthgens et al. 2010a, b, 2011b; Lüthgens & Böse 2011; Rinterknecht et al. 2014; Kenzler et al. 2015; Livingstone et al. 2015). Hence, the reconstructed ice-sheet time-slices are not as accurate as they are for well-dated areas such as Denmark, in particular during MIS 2.

This paper presents the results of detailed investigations on two outcrops in the southwestern Baltic Sea area (Fig. 3.1) based on lithofacies analysis, luminescence dating, palaeontology and sediment microfacies. We significantly expand and refine the recently published luminescence, sedimentological and palaeontological results of Kenzler et al. (2015) for the Kluckow site. We reconstruct the depositional history of the Jasmund area and its implications for the dynamics of the SIS at local and regional scales during MIS 3 and early MIS 2. This is the first reconstruction of the depositional environment and the timing of the SIS entering the study area during MIS 2.
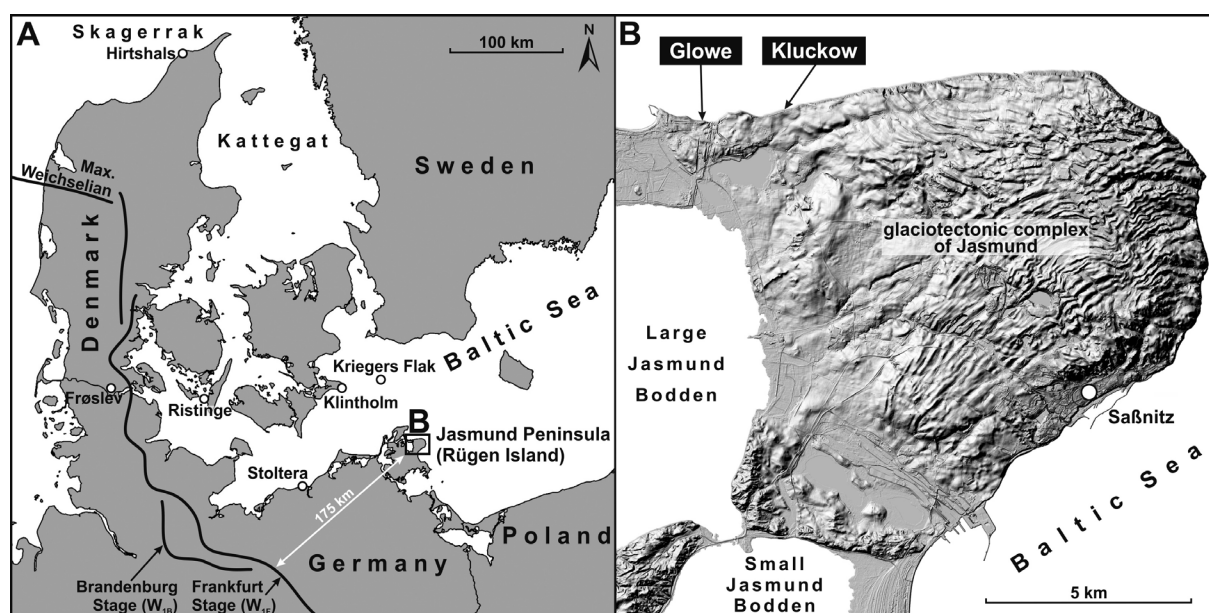
Fig. 3.1 A. Map of the southwestern Baltic Sea region showing the location of Jasmund (Rügen Island), the maximum Weichselian ice extent (black solid line; based on Houmark-Nielsen 2010) and localities mentioned in the text. B. A digital elevation model of Jasmund with the locations of the study sites Glowe and Kluckow; the hillshade relief with 10-fold exaggeration shows the glaciotectonically structured morphology of the peninsula (based on LiDAR data from @GeoBasis-DE/M-V 2015 processed by J. Hartleib).

3.2 Study area

The study sites are located on the Jasmund Peninsula, in the northeast of Rügen Island (southwestern Baltic Sea; Fig. 3.1A). The peninsula consists of a glaciotectonic complex at least 161 m high (Fig. 3.1B), with imbricated lower Maastrichtian Cretaceous bedrock (c. 70 Ma; Reich & Frenzel 2002) and overlying Pleistocene deposits (Panzig 1995). Since the Holocene sea-level rise of the Littorina transgression (9.8 ka BP; Andrén et al. 2011), the Jasmund Peninsula has been laterally eroded by the Baltic Sea, revealing Pleistocene deposits along active sea cliffs. This Pleistocene record can be lithostratigraphically differentiated into at least four till complexes. They are numbered (from bottom to top) M-0, M-1, M-2 and M-3, and are interbedded with lithostratigraphical units mainly consisting of clay, sand and gravel, which are termed I-1, I-2 and I-3 (Fig. 3.2; Panzig 1995; Kenzler et al. 2010). Together with the underlying Cretaceous bedrock, the M-0 to I-2 strata form a heavily deformed stack of imbricate units, in turn disconformably truncated by the M-3 till complex (Fig. 3.2). This distinct unconformity represents a glaciotectonic event, caused by a re-advance of the SIS during MIS 2 (Ludwig 2011).

The existing stratigraphical classifications of the individual tills and their proposed relation to the intercalated sediments are often contradictory (Ludwig 2005; Kenzler et al. 2010). Based on provenance analyses, sparse radiocarbon (^{14}C), thermoluminescence (TL) and optically stimulated luminescence (OSL) ages from previous studies, the stratigraphy of Jasmund can be summarized as follows (Fig. 3.2): The isolated preserved M-0 till unit, exposed only at very few cliff outcrops around Jasmund, is assumed to have formed during the Elsterian (MIS 10) and/or Saalian (MIS 8/6) (Niedermeyer et al. 2010). The erosional contact between the M-0 till and the underlying Cretaceous chalk is sharp, although para-conform. The M-1 unit that overlies the M-0 can be subdivided into two subunits: M-1u and M-1o (Panzig 1995). The lower subunit M-1u is most likely correlated with a Saalian ice advance (MIS 6), whereas the upper subunit M-1o has been proposed to be either Saalian (Panzig 1991; Müller & Obst 2006) or Early to Middle Weichselian (Steinich 1992; Müller 2004). For the first well-marked intercalated (glaci-)fluvial to (glacio-)lacustrine lithostratigraphical unit I-1, several ^{14}C, TL and OSL ages are available, ranging from c. 62 to c. 19 ka (Steinich 1992; Krbetschek 1995; Kenzler et al. 2015). The overlying M-2 till unit consists of two individual till sheets (Panzig 1995). The following I-2 unit was deposited

in a glacifluvial to glaciolacustrine environment. The disconformably overlying M-3 till complex, at Glowe subdivided into three subunits (M-3u, M-3m and M-3o; Panzig 1995), completes the Pleistocene succession of Jasmund. The depositional time of the M-2, I-2 and M-3 is still under discussion because of the lack of reliable age data (Müller & Obst 2006). Oscillations of the SIS during the Brandenburg/Frankfurt and Pomeranian phases (c. 25 to c. 17 ka) relate to the M-2, I-2 and the lower part of the M-3 complex (M-3u). However, the top of the M-3 till complex (M-3 m and M-3o) has a Late Weichselian age, so it can be correlated to a re-advance of the SIS during the Mecklenburgian phase (c. 17 to c. 15 ka; Niedermeyer et al. 2010; Kenzler et al. 2010). Based on previous studies, the Glowe and Kluckow sections are summarized below.

3.2.1 Glowe site

At the northwestern coast of the Jasmund Peninsula (Fig. 3.1B; latitude 54°34.350N, longitude 13°29.120E), east of Glowe harbour, the east–west orientated Glowe cliff with its chalk anticline and Pleistocene deposits crops out along a cliff length of more than 170 m (Fig. 3.3A). The cliff exhibits Cretaceous bedrock with overlying Pleistocene deposits of possible Elsterian to Weichselian age (Niedermeyer et al. 2010), which were glaciotectonically dislocated and uplifted during an MIS 2 re-advance of the SIS (Panzig 1995). Panzig & Kanter (1997) distinguished up to nine different till units at the Glowe section (Fig. 3.3A), including three intercalated clayey to sandy units. The subdivision was based on provenance analyses of till beds, using the fine-gravel spectrum between 4 and 10 mm. Two TL ages from the lowermost intercalated sandy bed between the M-1o till and M-2-1 unit indicate a depositional time between 55±9 and 19±3 ka (Krbetschek 1995). The sedimentary log presented in the current study was recorded between 100 and 110m in the profile (see Fig. 3.3A and Fig. 3.4A).
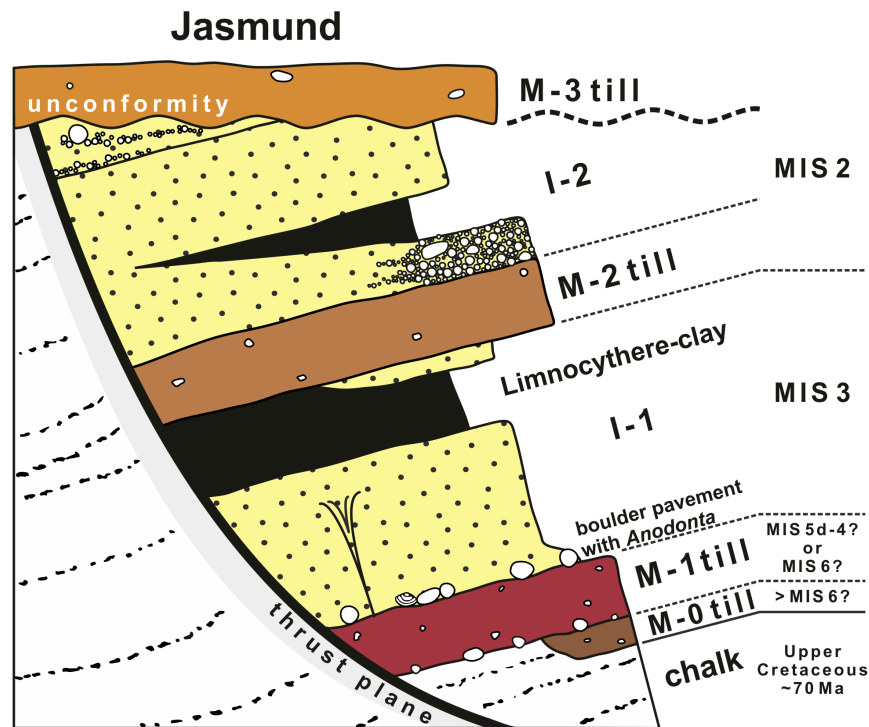
Fig. 3.2 Generalized stratigraphical scheme of a glaciotectonically rafted imbricate structure at Jasmund, comprising Upper Cretaceous chalk and paraconform Pleistocene deposits, bounded by a thrust plane and a disconformably overlying Late Weichselian till complex. Age classification based on Reich & Frenzel (2002), Niedermeyer et al. (2010) and Kenzler et al. (2015). For explanation of lithological units see Fig. 3.3, Fig. 3.5 and Fig. 3.13.
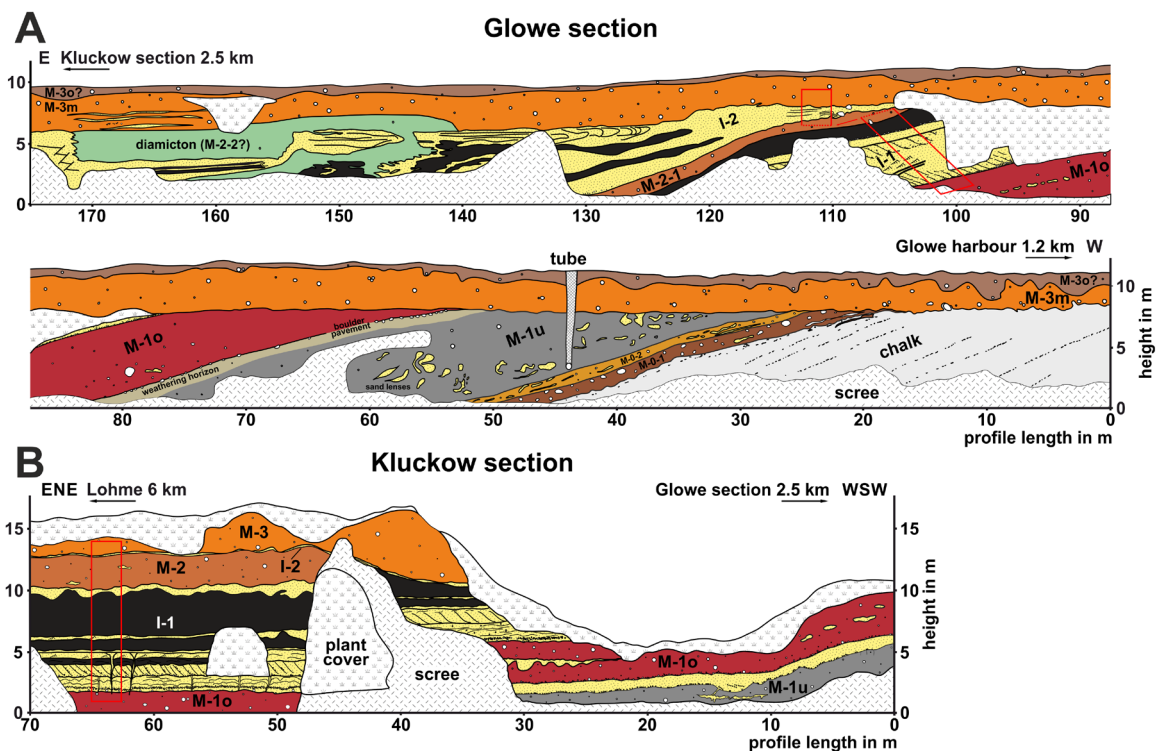
Fig. 3.3 Sketch of the (A) Glowe and (B) Kluckow cliff sections. The sketches show the outcrop situation during the years 2010 and 2011. The labelling of lithostratigraphical units is based on Panzig & Kanter (1997) for the Glowe section and Kenzler et al. (2015) for the Kluckow section. The red boxes indicate the locations of the lithofacies analyses.
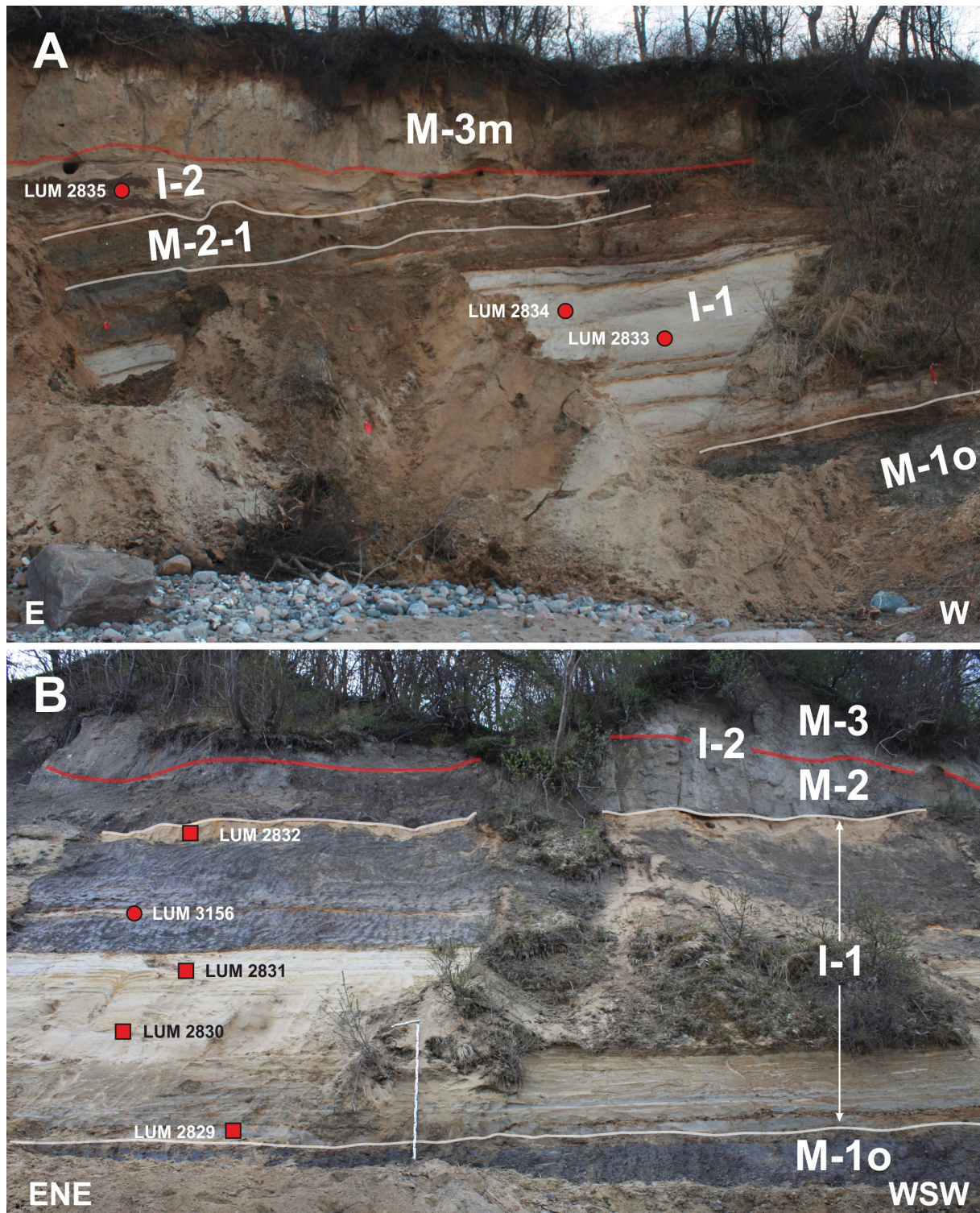
Fig. 3.4 Photographs of the (A) Glowe (profile metres 95–110, Fig. 3.3A) and (B) Kluckow (profile metres 50–70, Fig. 3.3B) cliff sections with lithostratigraphical units according to Panzig & Kanter (1997) for Glowe and to Kenzler et al. (2015) for Kluckow. The filled dots highlight the sample position for luminescence dating with the corresponding laboratory numbers of this study, whereas the filled squares indicate the luminescence sample locations of Kenzler et al. (2015). The semi-transparent red lines represent the base-M-3 glaciotectonic unconformity.

3.2.2 Kluckow site

The 700-m-long cliff exposure of Kluckow is located approximately 2.5 km east of the Glowe section (Fig. 3.1B; 54°34.530 N, 13°31.240 E). The record is composed of Cretaceous bedrock and paraconformably overlying Pleistocene sediments, including a distinct glaciotectonic unconformity below the M-3 till unit (Fig. 3.3B and Fig. 3.4B). Steinich (1992) performed the first sedimentological and palaeontological investigation; his sedimentological results were expanded by Kenzler et al. (2015) based on a lithofacies analysis: between two tills (M-1o and M-2), interstadial sediments were deposited in a (glaci-)fluvial to (glacio-)lacustrine environment. Based on luminescence (TL, OSL and post-IR infrared stimulated luminescence) and a single ^{14}C age, this interstadial succession has been assigned a Middle Weichselian age within MIS 3 and MIS 2 (Krbetschek 1995; Kenzler et al. 2015). Moreover, Kenzler et al. (2015) argued that there is no unambiguous sedimentological proof that supports a Middle Weichselian ice advance that reached the study area from a northwestern direction during that time, as proposed by Müller (2004) and Houmark-Nielsen (2010).

3.3 Materials and methods

To reconstruct the depositional environments of the Pleistocene sediments of Kluckow and Glowe and to obtain palaeoclimatic information, a combination of geological mapping, detailed lithofacies analysis, micromorphology, biofacies and OSL dating was used. The local and regional lithostratigraphical correlation of the Pleistocene tills was based on the detailed provenance studies of Panzig (1991).

3.3.1 Lithofacies analysis

The classification and interpretation of the lithofacies in this study focused on primary depositional features such as sedimentary structures, textural characteristics of individual beds, grain size and bedding (Miall 1996). Based on the facies codes and classification scheme of Benn & Evans (2010), the exposed sediments were subdivided into different units. For the Weichselian succession at the Kluckow site, we used the previous sedimentological interpretations and dating results in Kenzler et al.

(2015) and Steinich (1992), supplemented with new information about lithofacies, macro- and micropalaeontology, as well as age data, from this study.

3.3.2   Thin section preparation and micromorphology

For the micromorphological investigation, one sample from the M-1o till at Kluckow and three samples from glaciolacustrine sediments at Glowe (units G-D and G-E) were taken. The micromorphology of Pleistocene glacial and periglacial sediments can provide a powerful tool to help understand the dynamics and deposition mechanisms during ice advances and retreats (*e.g.* Menzies et al. 2006, 2010; Phillips et al. 2007; Phillips & Hughes 2014; Livingstone et al. 2015). For the description of the micromorphological features, the terminology of van der Meer (1993) and Menzies et al. (2006) was used. The preparation technique of the 7X5 cm thin sections (TSs) was mainly based on van der Meer (1987, 1993), Carr & Lee (1998) and Menzies (2000).

3.3.3   Macrofossils and pollen

A total of ~150 L of sediment, obtained from the middle part of unit K-C at the Kluckow section, was rinsed in the field using sieves with mesh sizes of 0.5 and 1.0 mm. The subsequent examination of the resulting fractions took place at the University of Greifswald (Germany). Dr Lutz Maul carried out the investigation of mammalian macrofossils. Especially at the lower middle part of the Kluckow section, cm-scale disc-like clay-silt intraclasts occurred. The pollen content of these intraclasts was investigated. A standard pollen preparation and extraction technique was applied at the pollen laboratory of the State Laboratory Berlin-Brandenburg (LLBB) in Kleinmachnow (Germany). Dr Jaqueline Stahl analysed and interpreted the pollen spectrum.

3.3.4   Luminescence dating

Four samples were taken for luminescence dating from the clean cliff surface at the Glowe (LUM 2833, LUM 2834, LUM 2835) and Kluckow (LUM 3156) sections in stainless steel tins. The luminescence measurements were carried out at the Leibniz

Institute for Applied Geophysics (LIAG) in Hannover (Germany). For the preparation of pure coarse-grained quartz (100–150 or 150–200 µm), the standard technique of cleaning and separation steps was applied (Kunz et al. 2010). The OSL signal of medium-sized aliquots (6 mm in diameter) was measured with a Risø TL/OSL DA-20 reader equipped with a ^{90}Sr/^{90}Y beta source (Bøtter-Jensen et al. 2010). For dose rate determination, we used the same procedure and conversion factors as in Kenzler et al. (2015).

As the sand layer of sample LUM 3156 was only 30 cm in thickness, which could lead to an inhomogeneity of sediment dose rate, we took two additional sediment samples from the under- and overlying silty clay for dose rate determination. To model the total concentration of uranium, thorium and potassium for the LUM 3156 sample, we used 66.6% of the measured values of the adjacent sand and 16.6% from both the under- and overlying silty clay. We added a further uncertainty of 20% to the total nuclide concentration of this sample, to accommodate potential uncertainties of the used model (Tab. 3.1).

Tab. 3.1 Summary data for dosimetry, water content determination, dose rates, equivalent doses, number of aliquots that passed the rejection criteria, and OSL ages for all luminescence samples.

Sample ID	Altitude (m a.s.l.)	Depth below ground (m)	K (%)	Th (ppm)	U (ppm)	Grain size (µm)	Aliquot size (mm)	Natural H$_2$O content (%)	Saturated H$_2$O content (%)	H$_2$O content used for age calculation (%)	Quartz dose rate (Gy/ka)	# of aliquots [1]	mean D$_e$ (Gy)	OSL age (ka)	CAM (ka)	Section
LUM 2833	4.1	5.0	1.08 ± 0.05	1.19 ± 0.06	0.38 ± 0.02	150 - 200	6	6.0	39.3	22±10	1.09 ± 0.13	27 (27)	46.2 ± 1.5	42.5 ± 5.2	41.9 ± 5.1	Glowe
LUM 2834	5.1	4.1	1.23 ± 0.06	2.05 ± 0.10	0.63 ± 0.03	150 - 200	6	4.6	41.6	23±10	1.30 ± 0.13	23 (24)	56.0 ± 1.6	43.3 ± 4.7	43.2 ± 4.6	Glowe
LUM 2835	6.2	3.8	1.32 ± 0.07	2.74 ± 0.14	0.99 ± 0.05	150 - 200	6	4.6	42.2	23±10	1.65 ± 0.13	24 (24)	33.3 ± 1.0	22.8 ± 2.3	22.5 ± 2.3	Glowe
LUM 3156[2]	8.9	15.0	1.53 ± 0.23[3]	5.39 ± 0.81[3]	1.60 ± 0.24[3]	100 - 150	6	15.2	35.1	30±5	1.70 ± 0.21	24 (24)	41.6 ± 1.2	24.4 ± 3.7	24.2 ± 3.7	Kluckow
LUM 3156a[4]			1.12 ± 0.06	2.97 ± 0.15	0.90 ± 0.04	66.6% on total nuclide amount of LUM 3156										
LUM 3156b[5]			2.50 ± 0.13	10.52 ± 0.53	2.97 ± 0.15	16.7% on total nuclide amount of LUM 3156										
LUM 3156c[6]			2.21 ± 0.11	9.96 ± 0.50	3.06 ± 0.15	16.7% on total nuclide amount of LUM 3156										

[1] Total number of measured aliquots and aliquots that passed criteria (in parentheses) [2] Determination of uranium, thorium and potassium concentrations based on three independent nuclide measurements
[3] Include uncertainty of 20 %   [4] Nuclide measurement of host sediment (sand)   [5] Nuclide measurement of underlying sediment (silty clay)   [6] Nuclide measurement of overlying sediment (silty clay)

As the water content of sediment significantly influences its effective dose rate, we measured the natural water content and determined the saturated content with cylinder volumeters (Tab. 3.1). The natural water content was assumed to correspond to the minimum content at the time of burial. Therefore, we used the average value of the natural and saturated water contents for the age calculation of samples LUM 2833, LUM 2834 and LUM 2835 (Tab. 3.1). As the sand layer of sample LUM 3156 was sandwiched between two silty clay deposits that were nearly impermeable, we assumed a high water content near saturation at the time of burial (Tab. 3.1). We added a 5% (LUM 3156) or 10% error (LUM 2833, LUM 2834 and LUM 2835) to the water content, to take uncertainties into account (Tab. 3.1).

The determination of the quartz equivalent dose (D_e) of the 6-mm aliquots followed the experimental specifications and rejection criteria for aliquots described in Kenzler et al. (2015) (Tab. 3.2; Murray & Wintle 2000).

Tab. 3.2 Modified single-aliquot regenerative-dose (SAR) protocol used for optically stimulated luminescence (OSL) dating of coarse-grained quartz.

Run	Treatment for quartz
1	Dose (expect before first run)
2	Preheat (260 °C for 10 s)
3	Optical stimulation with IR-diodes for 100 s at 125 °C
4	Optical stimulation with blue LEDs for 40 s at 125 °C
5	Give test dose
6	Cutheat at 240 °C
7	Optical stimulation with blue LEDs for 40 s at 125 °C
8	Return to run 1

3.4 Results

3.4.1 Glowe section

The sedimentological investigation at the Glowe section focused on the sediment succession between lithostratigraphical units M-1o and M-3m (Fig. 3.3A), which are termed I-1, M-2-1 and I-2. These deposits were subdivided into five units (G-A to G-E), summarized in Tab. 3.3 and Fig. 3.5.

Thin section analyses. – Sample TS 2 was taken from the lower part of unit G-D (Fig. 3.5 and Fig. 3.6). Its brecciated fabric with layers of finely laminated clay and silt intraclasts in a clayey to sandy matrix is clearly visible (Fig. 3.7). The roundness of the intraclasts is very variable, ranging from angular to well rounded. Some intraclasts display cracks, which are most likely related to shrinking processes that occurred during the drying of the sample.

Tab. 3.3 Descriptions and interpretations of the lithofacies from the investigated sequence at Glowe (Fig. 3.5), with information about the depositional age. Facies codes after Benn & Evans (2010).

Unit	Codes	Lithofacies	Interpretation	Age
G-E	Sh Sm Fl GRh	>2.2 m horizontally-bedded or low-angle cross-laminated sand with intercalations of fine-laminated silt and distinct horizontally-bedded sandy fine-grained gravel layers (cm-scale); deformation structures such as folds and normal faults, truncated by the glaciotectonic unconformity	**Glacio-lacustrine environment** (terminoglacial): traction-bedded sand formed at meltwater outlets or by density flows in a glacier-proximal setting; plus rain-out of debris of icebergs and ice-rafts (dropstones); glaciotectonised	23±2 ka (OSL)
G-D	Dms	0.5 - 0.9 m massive to stratified diamicton; distinct sand stringers and clast-supported gravel lenses; occurrence of finely-laminated clay and silt intraclasts; locally intensely deformed and brecciated	**Glacio-lacustrine environment** (terminoglacial): deposition of water-lain till and debris flows in an ice-marginal lacustrine basin; dumpstones represented by distinct gravel lenses; stratified diamicts with sand stringers as a result of traction-flow activity	
	Fp (d)	0.5 - 0.8 m greyish-brown, rhythmically-laminated clay and silt (including finely-laminated clay and silt intraclasts) with isolated outsized clasts of Scandinavien provenance (up to 15 cm in diameter), some showing impact structures and draped lamination	Rythmically-bedded lacustrine bottomsets with suspension deposits of clay and silt, rain out of debris and dropstones from undermelting of icebergs and ice-rafts	
G-C	Fl Fp Sp Sm GRm	up to 0.9 m dark brownish-grey, rhythmically-laminated clay and silt; (a) layers of finely-laminated clay and silt intraclast (mm-scale, subangular to angular) with masepic plasmic fabric; (b) distinct bed of fine- to medium-grained sand with loadcasts and ball-and-pillow structures	**Glacio-lacustrine environment**: rhythmically-bedded lacustrine bottomsets with suspension deposits of clay and silt; (a) repeated resedimentation of rhythmite-derived intraclasts, formed by undermelting of ice-rafts or by debris flows; (b) events of density flows indicated by massive sand layers, partly deformed by liquefaction	19±3 ka (TL)[1]
G-B	Sp Sr Sh Fl	3.3 m dominated by tabular cross-bedded sand with mud clasts at its base; intercalations of horizontally- and ripple-laminated sand; few distinct beds of finely-laminated clay and silt	**Fluvial environment**: mainly tabular cross-bedded sand beds from superimposed 2-D dunes; fine-grained deposits from suspension settling during slack-water stages; deposition in shallow, perennial, sand-bed braided river system (resembling the classical "Platte-type" according to Miall 1996); a characteristic feature is the down-stream accretion of bars	42±4 ka (OSL) 43±5 ka (OSL) 55±9 ka (TL)[1]
G-A	GRm (Sp)	up to 0.3 m massive, sandy, fine-grained gravel with minor medium- to coarse-grained planar cross-bedded sand; isolated stones (up to 15 cm in diameter) stick out of the underlying till	**Fluvial environment**: lag deposit overlying a ravinement surface, reworking of older sediments and the underlying till surface, traction-bedded sediments	

[1] From Krbetschek (1995).

Sample TS 3 from the upper part of unit G-D is dominated by stratified diamicton layers with sand-rich layers and stringers (Fig. 3.8). The frequent occurrence of clay and silt intraclasts is also visible. Some of the larger clasts are composed of Cretaceous chalk, indicative of a relatively short transport distance, due to the sensitivity of chalk to physical weathering. The sand layers and stringers have a very low clay and silt content (Fig. 3.8).

Unit G-E is a horizontally stratified to massive, silty to gravelly sand with frequent cm-scale diamicton-like layers (Fig. 3.5, Fig. 3.6 and Fig. 3.9). Clay intraclasts and fragmented clay-rich layers with an often well-developed internal plasmic fabric can be observed sample in TS 4 (Fig. 3.9). Several reverse faults are visible, indicating compression.
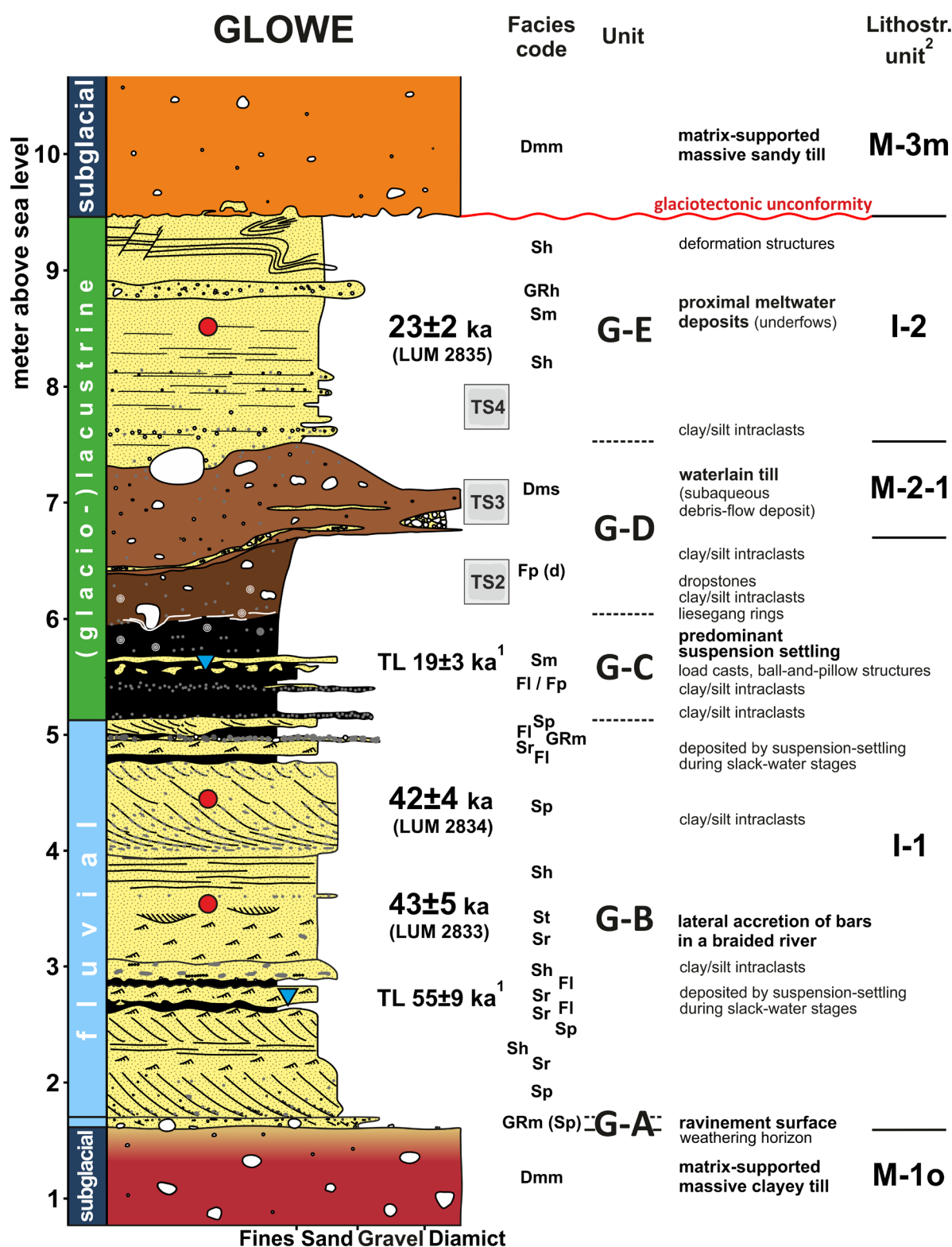
Fig. 3.5 Stratigraphical log from Glowe (profile metres 100–110, Fig. 3.3) indicating lithostratigraphical units, depositional environments, and OSL (red dots) and TL ages (blue triangles). The grey squares indicate the position where thin section (TS) samples were taken.

[1] Krbetschek (1995); [2] Panzig (1995). Facies codes after Benn & Evans (2010).
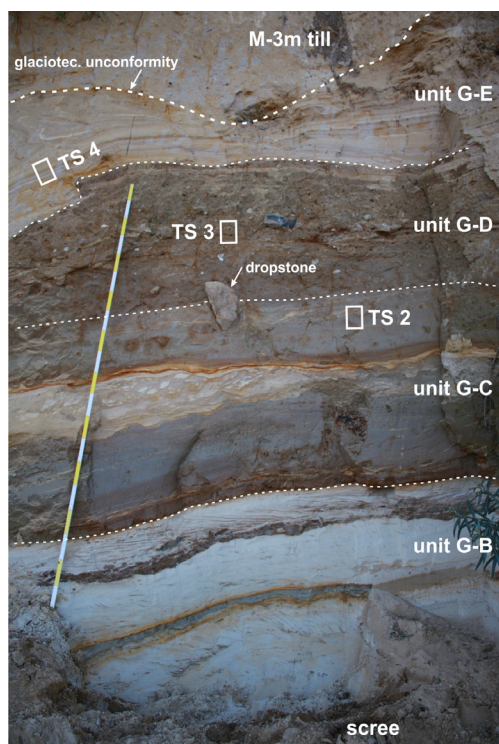
Fig. 3.7 Photograph of the upper part of unit G-B up to unit G-E at the Glowe section between 105 and 107 m in the profile (see Fig. 3.3).

Fig. 3.6 High-resolution scan of thin section TS 2 from the upper part of unit G-C at the Glowe section (see Fig. 3.6).

Fig. 3.8 High-resolution scan of thin section TS 3 sampled from the middle part of unit G-D at Glowe (see Fig. 3.6, Fig. 3.7). The documented part displays the stratified character of the diamicton, with sand-rich layers, dispersed larger clasts and matrix-supported diamictic domains.
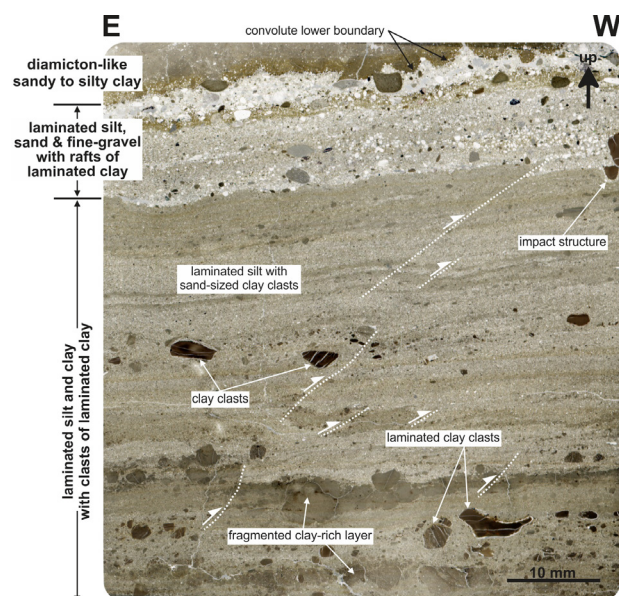
Fig. 3.9 High-resolution scan of thin section TS 4 collected from unit G-E at Glowe (see Fig. 3.6, Fig. 3.7). The major features are: horizontally laminated silt and clay layers, which are locally fragmented, and mm- to cm-scale intercalated sand-rich and matrix-supported diamictic layers. Several of the clay to silt intraclasts have an angular to subangular shape, indicating a short transport distance. The structure around the clay intraclasts in the right corner may be interpreted as an impact structure. Note the glaciotectonic reverse faults (white dotted lines) formed during a subsequent ice advance.

OSL signal characteristics and age calculations. – For sample LUM 2834, test measurements (Fig. 3.11) of medium-sized aliquots (6 mm) were performed to evaluate the suitability of preheat and cut-heat temperatures used during the SAR protocol. A preheat temperature of 260 °C held for 10 s and a cut-heat temperature of 240 °C were then chosen for the SAR protocol for all samples (Tab. 3.2). The rapid decrease of the OSL signal suggests a domination of the fast components (Fig. 3.12). From the dose-response curves, there is no indication of natural luminescence signals that are at, or close to, saturation (Fig. 3.12).
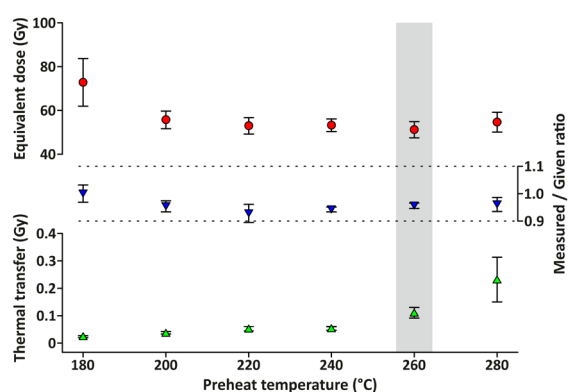
Fig. 3.10 Summary of the preheat plateau, dose recovery and thermal transfer test for sample LUM 2834.
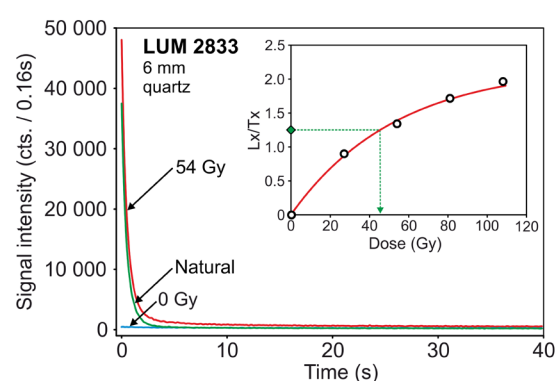
Fig. 3.11 A representative decay curve for natural (green), 0 Gy (blue) and 54 Gy (red) dosed signals and a growth curve for sample LUM 2833.

The total dose rates, comprising the environmental and cosmic dose rates, range between 1.09±0.13 and 1.65±0.13 Gy ka^{-1} (Tab. 3.1). These are similar to the values in Kenzler et al. (2015) for comparable sediments. The measured natural water content ranged between 4 and 6%, whereas the saturated water content reached values between 39 and 42% (Tab. 3.1). For all samples, the D_e distribution of all accepted aliquots is almost Gaussian-like (Fig. 3.13). There is no significant difference between the mean D_e-value and central age model (CAM) D_e-value. The overdispersion of 12 to 17% is relatively small, as may be expected for 6-mm aliquots (Cunningham & Wallinga 2010). Hence, we used the mean D_e-value to determine the burial age. The calculated ages range from 43±5 ka (LUM 2833) to 23±2 ka (LUM 2835) at the Glowe section (Tab. 3.1). As sample LUM 2835 was taken from meltwater deposits, insufficient bleaching could be a problem (Fuchs & Owen 2008). However, the calculated age fell at the lower end of the expected age range, which most likely rules

out a significant overestimation of the true burial age. However, from a methodological point of view we cannot rule out incomplete bleaching for this sample.
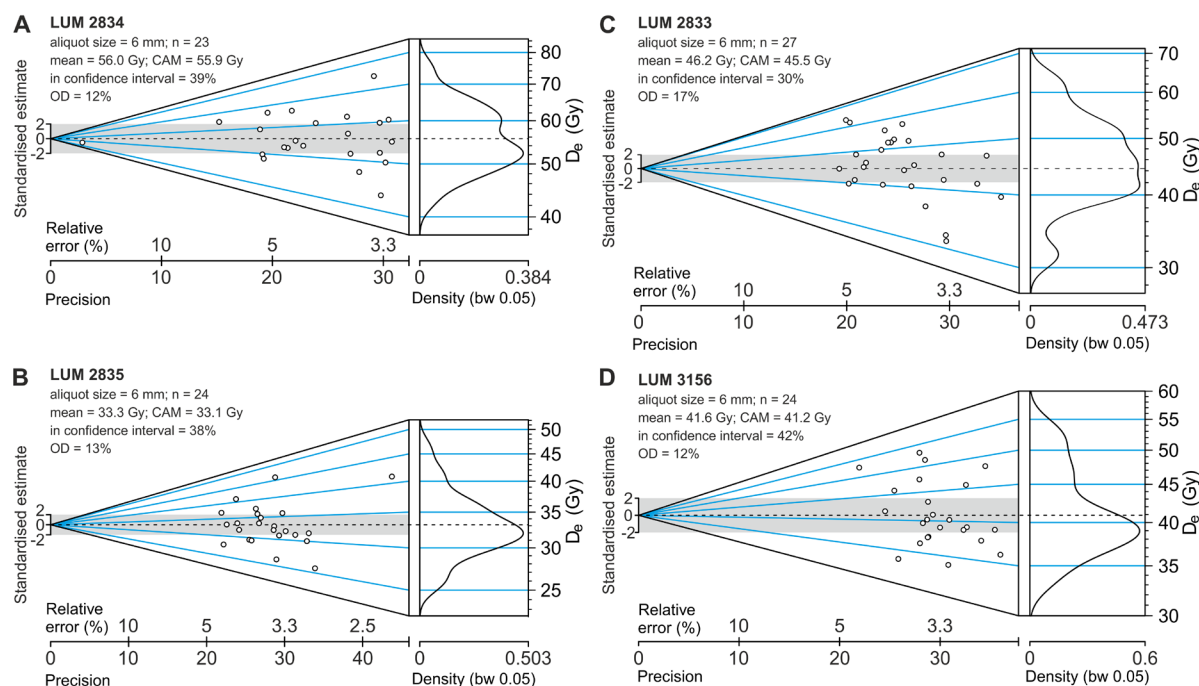
Fig. 3.12 Abanico plots with statistic information about mean D_e-value (mean), the number of aliquots that passed the rejection criteria (n), central age model (CAM), confidential interval and overdispersion (OD) for samples LUM 2833, LUM 2834, LUM 2835 (all Glowe site) and LUM 3156 (Kluckow site).

3.4.2 Kluckow section

A detailed lithofacies analysis of the Kluckow section was performed by Kenzler et al. (2015). In this study, we extended the description to the overlying till complexes (M-2 and M-3) and intercalated sediments (I-2). Furthermore, we added new results about fossil content, sedimentary processes and microfabric analyses to the existing data, as well as one new OSL age. A detailed summary of the sedimentary features and their interpretations is given in Tab. 3.5 and Fig. 3.13.

Thin section analyses. – At the top of unit K-C, vertically orientated wedge-structures penetrate the underlying units downward into the M-1o till (Fig. 3.4, Fig. 3.13, Fig. 3.14D). Sample TS 1 was taken 0.15 m below the boundary between the M-1o till and the overlying unit K-A and included the lowermost part of the wedge-shaped structure

(Fig. 3.14D). TS 1 represents an up to 10-mm wide secondary-filled dyke within a matrix-supported diamicton (Fig. 3.15). The dyke is filled with fine- to medium-grained sand, including mm-scale clay to silt intraclasts. Furthermore, isolated fine-grained gravel clasts occur. In contrast to the surrounding diamicton, the sediment of the dyke fill is clast-supported with a low content of clay and silt. Due to circulating pore water, the peripheral area of the fracture and the diamicton are stained by iron precipitations.

OSL signal characteristics and age calculations. – A detailed overview of the OSL signal characteristics of the sediments of the Kluckow section is given in Kenzler et al. (2015). In the current study, we used the same measurement setup and SAR protocol for D_e determination. The luminescence properties of sample LUM 3156 confirmed the result of the previous work, *e.g.* a bright quartz OSL signal that decayed rapidly. Therefore, a dominant fast component can be assumed. The calculated age of sample LUM 3156 is 24.4±3.7 ka.

Tab. 3.4 Description and interpretation of the lithofacies from the investigated sequence at Kluckow (see Fig. 3.13), with information about the depositional age. Facies codes after Benn & Evans (2010).

Unit	Codes	Lithofacies	Interpretation	Age
K-E	Sm (d)	up to 0.4 m reddish-yellow, fine- to medium-grained sand; macroscopically homogeneous and unstratified; strong undulation and load structures; sharp contact at base and top	**(Glacio-) fluvial environment**: sediment gravity-flow deposits, deposited immediately before and during an ice advance (frontal apron sand); glaciotectonised	22±2 ka (OSL)[2]
K-D	Flv Fm Sr Fl Sr (St)	4.2 m massive to rhythmically-laminated silty clay with intercalated ripple cross-laminated fine-grained sand layer, up to 0.4 m thick; sharp contact at base and top	**Glacio-lacustrine environment**: domination of suspension-settling of clay and silt, interrupted by hyperconcentrated density-flow deposits	24±4 ka (OSL) 27±3 ka (TL)[1]
K-C	Sr Sp Sh Fm	1.8 m tabular cross-bedded to ripple-laminated, middle- to fine-grained gravelly sand; few intercalated clay layers in cm-scale, lens-shaped clayey silt intraclast (up to 8 cm in diameter); wedge-shaped structures vertically penetrate the sediment and underlying deposits (up to 3.8 m in vertical length); remnants of molluscs and few vertebrates (see Table 5), erosional contact at base and top	**Fluvial environment**: lateral accretion in a point-bar setting, reworking of cut bank sediments consisting of material of abandoned channels or ponds, indicated by clayey silt intraclasts (intraformational orgin); fine-grained deposits from suspension-settling during slack-water stages	42±4 ka (OSL)[2] 46±1 cal. ka BP[2] 47±7 ka (OSL)[2]
K-B	St Fp	1.3 m interstratified grey-brown, laminated clay and silt and yellowish, fine- to medium-grained, massive to trough cross-bedded sand; faint ripple lamination; intensively deformed and convoluted; vertical penetration of wedge-shaped structures (orginated at the top of unit B)	**(Glacio-)lacustrine environment with potential (glacio-)fluvial influence**: domination of suspension-settling from the water column; to the top shift to higher flow velocities (underflows or density flows); intensively deformed and mingled due to post-sedimentary periglacial condition resulting in cryoturbation and the establishment of ice-wegdes	41±5 ka (TL)[1]
K-A	Sp (Sr, Sh) Glg	up to 0.3 m massive to planar cross-bedded gravelly sand; at base and top non-continuous coarse gravel beds; isolated stones (up to 30 cm in diameter) stick out of the underlying till	**Fluvial environment**: lag deposit overlying a ravinement surface, reworking of older sediments and the underlying till surface, traction-bedded sediments	>62±6 ka (OSL)[2]

[1] From Krbetschek (1995).
[2] From Kenzler *et al.* (2015).
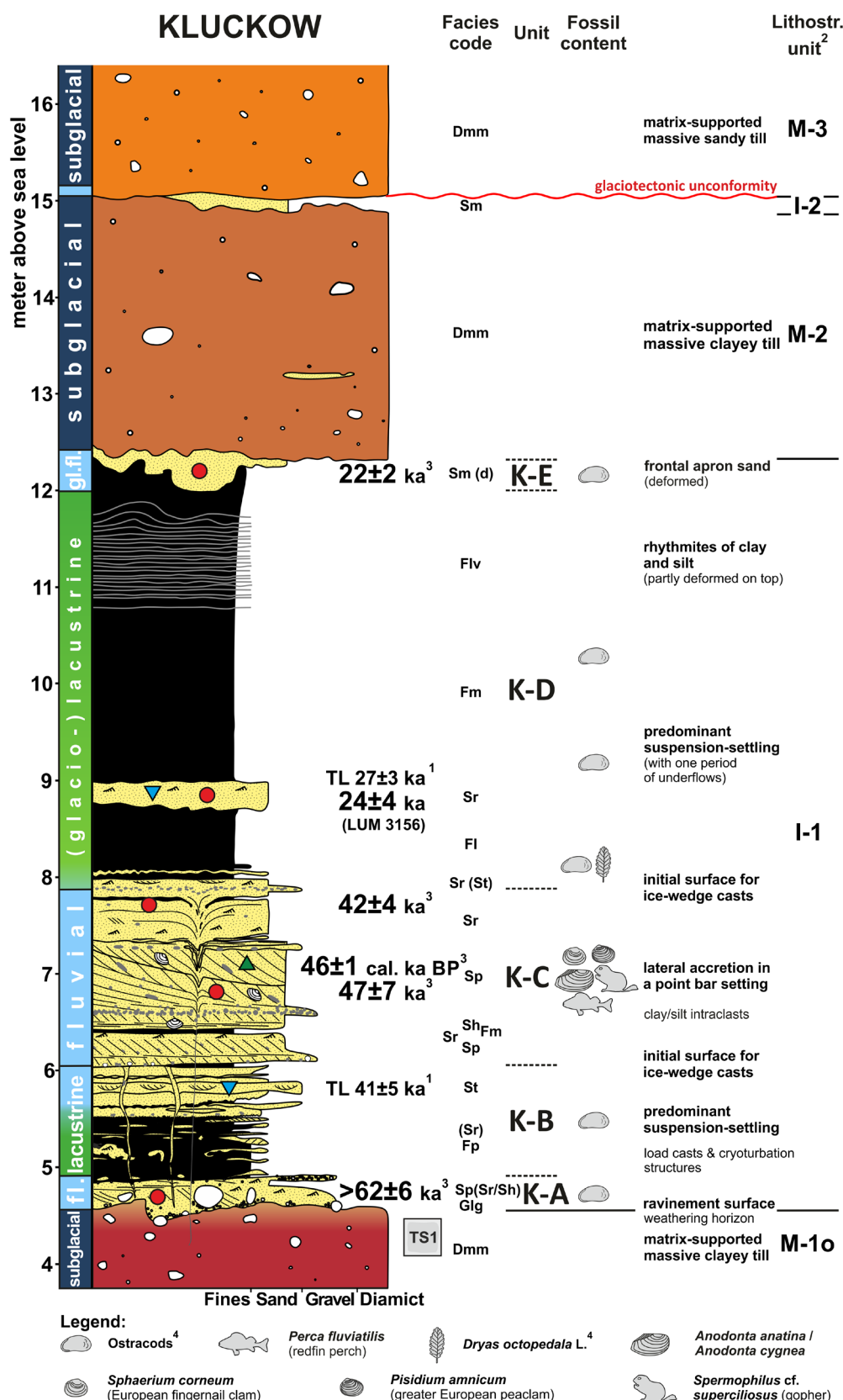
Fig. 3.13 Stratigraphical log from Kluckow (modified and extended from Kenzler et al. 2015) indicating lithofacies, lithostratigraphical units, depositional environments, fossil content, and OSL (red dots), TL (blue triangles) and radiocarbon (green triangle) ages. The grey square indicates the position where a thin section (TS) sample was taken. [1] Krbetschek (1995); [2] Panzig (1995); [3] Kenzler et al. (2015); [4] Steinich (1992). Facies codes after Benn & Evans (2010).
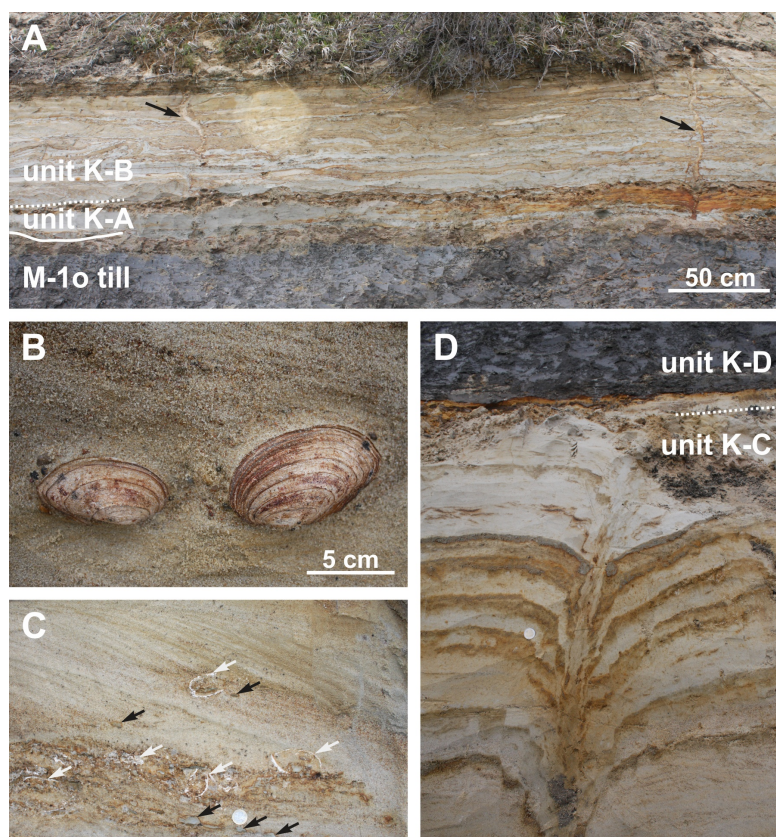
Fig. 3.14 Photographs of wedge-shaped structures and *Anodonta* sp. resting *in situ* from the Kluckow section. A. Two ice-wedge casts (black arrows) penetrating units K-B and K-A. B. Two double-valved *Anodonta* sp. embedded *in situ* in the middle part of unit K-C with preserved organic skin. C. Several cut *Anodonta* sp. shells (white arrows) and disc-shaped clay intraclasts (black arrows) in the tabular crossbedded gravelly sand of unit K-C at Kluckow. D. Uppermost part of the wedge-shaped structure originating at the boundary between units K-C and K-D. Note that various normal faults bound the fracture of the structure, which is interpreted as an ice-wedge cast (coin for scale).

Fig. 3.15 Sediment-filled dyke within the M-1o till at the Kluckow section interpreted as an ice-wedge cast. The fissure is the lowermost part of the wedge-shaped structure shown in Fig. 9D that originates at the boundary between units K-C and K-D. The dyke thins out and passes into a fissure 0.2 m below the TS 1 sample location.
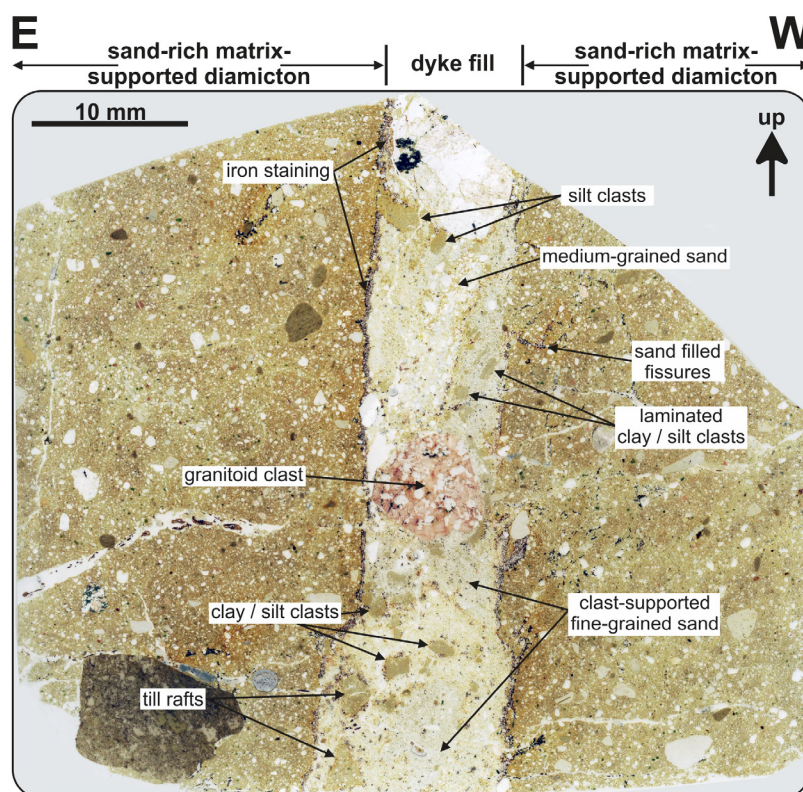
Macro- and microfossil content. – Unit K-C contains remnants of molluscs and a few vertebrates (Fig. 3.16 and Fig. 3.17), which are particularly abundant between 6.3 and 7.2 m in the profile (Fig. 3.13). We examined the fossil content of the sand and the lens-shaped clayey silt intraclasts. The mollusc spectrum of the sand and the intraclasts is nearly identical, consisting of three freshwater gastropod and seven to eight freshwater bivalve species (Tab. 3.5).

A high concentration of undeformed *Anodonta* sp. was found, mostly double-valved and in living position (Fig. 3.14B, C and Fig. 3.16A–E). The organic ligaments and the periostracum are preserved (Fig. 3.16D, E). The carbonate of the shells itself is highly disintegrated and broke apart into small calcite-prisms during recovery attempts (Fig. 3.16C). In addition to *Anodonta anatina* (pond mussel; Fig. 3.16B), we identified *Anodonta cygnea* (swan mussel; Fig. 3.16A). *A. anatina* inhabits both fluvial and lacustrine environments and tolerates oligotrophic and eutrophic water conditions. In contrast, *A. cygnea* prefers oxbow lakes and smaller water bodies but also inhabits slow-flowing rivers (Zettler et al. 2006). Today both mussel species are widespread, their habitats ranging from northern Europe below the northern polar circle, to Portugal and Turkey. *A. anatina* also occurs in parts of Siberia (Lopes-Lima 2014).

The *Pisidium* genus is represented by the species *P. amnicum* and *P. henslowanum*, while the *Sphaerium* genus includes *S. solidum* and *S. corneum*. Furthermore, we identified the gastropods *Valvata piscinalis* and *Radix* sp., which, together with *S. corneum*, inhabit a broad spectrum of lacustrine environments with standing and flowing water. *P. amnicum* and *S. solidum*, by contrast, prefer fluvial environments with flowing water (Fig. 3.17). Additionally, isolated remnants of vertebrates, such as a fully preserved fish scale of *Perca fluviatilis* (perch), were found in the middle part of unit K-C (Fig. 3.16G). The perch being a predator, the presence of other (non-predatory) fish species can be assumed in this habitat. One incisor (incisive) of the young Pleistocene *Spermophilus* cf. *superciliosus* (gopher) (Fig. 3.16F) was also recovered. The pollen spectrum of the lens-shaped clayey silt intraclasts of unit K-C showed a melange of (allochthonous) pre-Quaternary (12%) and Quaternary (88%) floral elements. Apart from interstadial species, the Quaternary pollen comprises typically interglacial species, which are very probably reworked (Tab. 3.6). Due to this melange character of the pollen spectrum, a classification as a distinct Weichselian interstadial was impossible.
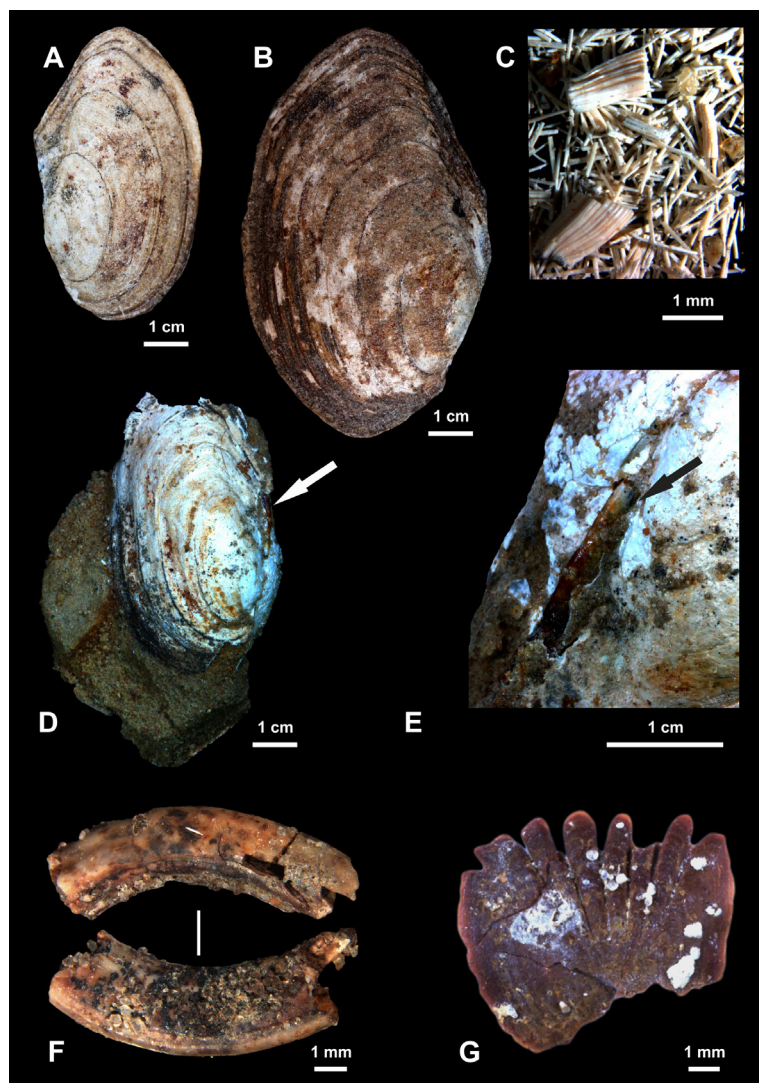
Fig. 3.16 Large freshwater mussels (*Anodonta*) and vertebrate remnants recovered from the tabular cross-bedded sand of unit K-C (profile metres 6.3–7.2) at the Kluckow section. A. *Anodonta cygnea*, left valve. B. *Anodonta anatina*, right valve. C. Calcite-prisms of disintegrated *Anodonta* sp. shell. D. *Anodonta* cf. *cygnea*, double-valved with intact organic ligament (white arrow). E. Enlarged photograph of the organic ligament (black arrow) of an *Anadonta* cf. *cygnea*. F. *Spermophilus superciliosus*, upper incisor. G. *Perca fluviatilis*, ridge scale.

Fig. 3.17 Pea mussels (*Sphaeriidae*) and freshwater shells from the fluvial sand of unit K-C at Kluckow site. A. *Pisidium amnicum*, left valve, A1 external view, A2 internal view. B. *Sphaerium corneum*, right valve, B1 external view, B2 internal view. C. *Sphaerium solidum*, fragment of left valve, C1 external view, C2 internal view. D. *Sphaerium solidum*, external view of a fragment. E and F. *Valvata piscinalis.* G1 and G2. *Radix* sp. (scale bar is 1 mm).
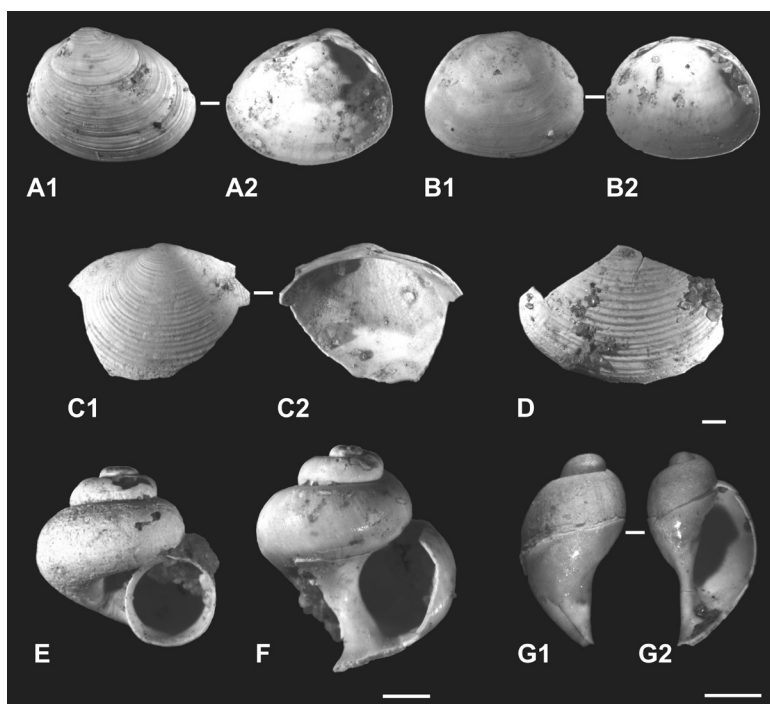
Tab. 3.5 Summary of the macrofossil content of the fluvial sand and the clayey silt intraclasts of the middle part of unit K-C at the Kluckow section (Fig. 3.13).

Kluckow section middle part of unit K-C (metre in profile 6.3 - 7.2) (planar cross-bedded gravelly medium- to fine-grained sand)		
Fauna	clayey silt intraclasts	sand
Molluscs		
Gastropoda		
Valvata piscinalis (O.F. Müller 1774)	10	36
Radix sp. 1	1	
Radix sp. 2	1	
Bivalvia		
Unionidae		frgm.
Anodonta sp.		frgm.
Anodonta anatina (Linnaeus 1758)		com.
Anodonta cygnea (Linnaeus 1758)		X
Sphaerium sp.	frgm.	frgm.
Sphaerium corneum (Linnaeus 1758)	10	20
Sphaerium solidum (Normand 1844)	4	150
Pisidium sp.	frgm.	frgm.
Pisidium amnicum (O.F. Müller 1774)	7	120
Pisidium henslowanum (Sheppard 1823)	275	64
Vertebrates		
Pisca		
Frgm. undet.	X	X
Perca fluviatilis (Linnaeus 1758)		1 scale
Mammalia		
Spermophilius superciliosus (Kaup 1839)		1 incisive
sieved sediment in liters	5	150

Tab. 3.6 Pollen spectrum of several clayey silt intraclasts collected from tabular cross-bedded gravelly sand of unit K-C at the Kluckow section (sample # 1000 96 967).

taxa	
AP in %	
Betula sp.	1,2
Pinus sp.	82,1
Ulmus sp.	0,4
Alnus sp.	0,4
Corylus sp.	2,3
Carpinus sp.	1,2
Picea sp.	1,2
Abies sp.	1,6
Σ BP in %	**90,3**
NAP in %	
Poaceae	1,2
Cyperaceae	1,9
Ericaceae p. p.	4,3
Helianthemum sp.	1,2
Polygonum sp.	0,8
Amaranthaceae	0,4
Σ NAP in %	**9,7**
Σ AP + NAP =100%	**257**
helophytes, aquatic plants, pteridophytes, moos in %	
Myriophyllum sp.	0,4
Azolla vel. *Salvinia* , Massulae-Bruch	0,4
Equsietum sp.	0,4
Botrychium sp.	3,5
Monoletes, o. P.	4,7
algae, plankter and other micro-remnants in %	
Pediastrum boryanum	2,3
Pediastrum boryanum var. *longicorne*	5,4
Pediastrum kawraiskyi	34,6
Botryococcus sp.	+
sponge spicule	+
reworked pre-quaternary taxa in %	
Taxodiaceae/Cupressaceae	
Sciadopytis sp.	1,2
Nyssa sp.	0,4
Liquidambar sp.	2,3
Pterocarya sp.	0,4
Ilex sp.	0,4
Tricolporates	1,2
Tricolpates	0,4
Triporates	0,4
Triletes	1,2
Dinozysten	4,7

3.5 Interpretation

3.5.1 Glowe section

The lowermost unit G-A was deposited in a fluvial setting after a reworking of the surface of the M-1o till. The chronological and genetic relationship of this unit to the underlying till is unclear (Fig. 3.5).

Unit G-B shows sedimentary structures indicative of deposition in a shallow, perennial braided river system with a sand-dominated bed. Superimposed 2-D dunes are characteristic of this environmental setting. The flow velocity must have temporarily decreased, and the water level dropped, as indicated by layers of laminated fine-grained deposits (Tab. 3.3). Fine-grained sediments of abandoned channels or ponds in the vicinity of the active river channel were occasionally eroded, transported and redeposited after a short distance. Unit G-B was previously TL dated to 55±9 ka (Krbetschek 1995). Two OSL samples yielded ages of 43±5 and 42±4 ka (MIS 3).

Unit G-C is interpreted as a glaciolacustrine deposit formed in a proglacial lake dominated by suspension settling of fine-grained detritus and short-lived phases of density flow supply. Krbetschek (1995) provided a TL age of 19±3 ka for this unit. The erosive transition between unit G-B and G-C indicates a hiatus of unknown duration.

The overlying unit G-D was deposited in a terminoglacial lacustrine basin (see Livingstone et al. 2012, 2015; Carrivick & Tweed 2013 for case studies). A deposition in a subglacial lake can most likely be ruled out because sediments deposited below a glacier should give an overestimation of the true burial age (cf. age of LUM 2835 from unit G-E; Livingstone et al. 2015). The lower part of unit G-D could be related to water-level variations and a reworking of the clay to silt layers at the lake beach during rising water levels. Additionally, slumping processes or grounded icebergs may have disturbed the primary sediment lamination (Fig. 3.7). An outsized clast generated an impact structure at the base of unit G-D (Fig. 3.8) and is interpreted as a dropstone. Hence, the terminoglacial lake was in contact with an active ice margin that released floating icebergs and debris into a local lake basin.

Previous studies have interpreted the upper part of unit G-D (Fig. 3.5, Fig. 3.6 and Fig. 3.9) as a subglacial till (Panzig 1995) or as a sediment formed by repeated re-sedimentation of till blocks (Ludwig 2005). Based on the documented micromorphological evidence, we interpret the diamictic part of unit G-D as a subaqueous debrisflow deposit with intercalated rain-out sediments. During the glacier

advances and fluctuations at the lake margin, debrisflows occurred that entered the lake. In addition, instabilities at the front of the ice mass may have triggered slides and slumps of various sizes (Brodzikowski & van Loon 1987). The fine-gravel spectrum of the upper part of unit G-D is comparable to the spectrum of the lithostratigraphical M-2 till at Kluckow (Panzig 1991). These data indicate that in both cases, the sediments were derived from the same advancing ice sheet.

The overlying unit G-E is interpreted as a terminoglacial meltwater deposit. Due to the proceeding ice advance at the Glowe site, the still existing ice-contact lake was filled with horizontally bedded or massive silty to gravelly sand. Thin sandy debrisflow layers were formed during this period (Fig. 3.5, Fig. 3.6 and Fig. 3.8). The calculated OSL age of this unit is 23±2 ka (LUM 2835). Subsequently, the SIS overrode the lake sequence and deposited a subglacial till (M-2-2) on top of unit G-E. Occurring further to the east (Fig. 3.3A), this till is not present at the sampling site due to erosional truncation during the Late Weichselian glaciotectonic event (Fig. 3.3A and Fig. 3.6). The faulting and folding of the upper part of unit G-E (glaciotectonic) are related to the ice advance that occurred during or after the glaciotectonic event.

3.5.2 Kluckow section

The weathered uppermost parts of the M-1o till indicate pedogenic processes, which would point to a significant exposure time of several 100s or even 1000s of years. The overlying unit K-A is interpreted as a fluvial deposit. The erosive contact with the underlying M-1o till suggests a reworking phase that resulted in a ravinement surface. Whether unit K-A is chronologically and genetically closely related to the underlying M-1o till (Steinich 1992), or whether there is a substantial hiatus of several 1000s of years between the two units, cannot be shown conclusively. Unit K-A was dated by OSL to a minimum age of >62±6 ka by Kenzler et al. (2015). Based on a pIRIR$_{290}$ measurement of K-rich feldspar, this work suggested a maximum age for this unit of <101±6 ka (Early Weichselian). Hence, the underlying M-1o till could be of Saalian age, which suggests that the hiatus above it includes the Eemian and parts of the Early Weichselian period. However, an Early Weichselian age of the M-1o till cannot be ruled out.

The sedimentary features of unit K-B point to a deposition in a small lacustrine basin, within a sandy lake-shore environment at the top, due to increasing fluvial

supply. Steinich (1992) found indications (ice-wedge casts) of a hiatus between units K-A and K-B. Furthermore, he documented several ostracod species, such as Limnocythere baltica, indicating a deposition in a freshwater body under arctic/sub-arctic climate conditions. Thus, a deposition of unit K-B under cooler climate conditions is possible. The period between the deposition of units K-B and K-C was dominated by erosion or non-sedimentation and the establishment of an ice-wedge polygon net in a periglacial landscape. Krbetschek (1995) TL dated unit K-B to 41±5 ka. This age should however be treated as an approximation because of methodological issues (Jain et al. 2007). Hence, for unit K-B, a depositional age within MIS 3 between c. 62 and c. 47 ka is suggested.

Unit K-C is interpreted as a fluvial deposit, which was formed in a meandering river system with point bars and cut banks. Laminated clay and silt layers, deposited in abandoned channels or ponds nearby the active river bed, were eroded and redeposited after a short distance (clay intraclasts). The mollusc assemblage indicates a meandering river system, with species that inhabit oxbow lakes and species that favour flowing river channels. A higher content of coccal green algae *Pediastrum kawraiskyi* (~35%) and *P. boryanum* var. *longicorne* within the disc-shaped clayey silt intraclasts are evidence for cooler temperatures. The cooler climate conditions are consistent with the occurrence of *Spermophilus* cf. *superciliosus*, which inhabits steppe-like landscapes. Furthermore, the autochthone pollen genera such as *Botrychium* indicate an open- land-dominated environment. The climate conditions during the deposition of unit K-C seem to be dominated by cool winters and short moderate summers. Similar interstadial climate conditions have been described for coeval sediments on Jasmund by Keding (1993), who investigated the macro-flora content of peat in contemporaneous deposits. He identified plants living under sub-arctic climate conditions.

Two OSL samples from unit K-C yielded ages of 47±7 and 42±4 ka (Kenzler et al. 2015). The deposition age of unit K-C thus ranges between 54 and 38 ka. An additional radiocarbon dating using a freshwater mussel gave an age of 46±1 cal. ka BP (Fig. 3.13). After the deposition of unit K-C, the climate deteriorated, changing the depositional environment. A periglacial landscape with ice-wedge polygons shaped the surface at the Kluckow site, most likely accompanied by an onset of permafrost conditions (Murton 2013). A period of non-sedimentation occurred, which formed a hiatus of several 1000 years between unit K-C and the overlying unit K-D.

Unit K-D is interpreted as a glaciolacustrine deposit. The sedimentation at Kluckow was dominated by suspension settling and one period of gravity-underflow deposition (Fig. 3.13). This underflow can be attributed to a fluvially influenced event with a high sediment influx. The varve-like appearance of the top part of unit K-D indicates an advance of the ice sheet and a more seasonally influenced sediment influx. Steinich (1992) collected remnants of Dryas octopedala L. from the base of unit K-D (Fig. 3.13), which is a typical plant of the arctic climate (Skrede et al. 2006). Furthermore, Steinich (1992) described ostracod species such as *Limnocythere baltica* from this unit at the Kluckow site, likewise indicating an arctic climate and a lacustrine environment. By counting all distinguishable laminas, he inferred a sedimentation period of more than 2000 years for the 4-m-thick unit K-D. This requires a strictly annual deposition of the laminas. In fact it cannot be ruled out that an event-driven deposition also occurred; such depositions can also lead to a much shorter accumulation time. For unit K-D, one OSL age gave 24±4 ka (LUM 3156), which is consistent with the TL age of 27±3 ka from Krbetschek (1995). A deposition at the end of MIS 3 and/or the beginning of MIS 2 is therefore proposed.

The following unit K-E was formed shortly before, or during, the advance of the SIS and has been interpreted as a glacifluvial sediment (Kenzler et al. 2015). During the subsequent overriding by a glacier, the sand of unit K-E and the rhythmically laminated upper part of unit K-D were glaciotectonically folded. One OSL sample from unit K-E yielded an age of 22±2 ka (Kenzler et al. 2015). The overlying till complex M-2 and M-3, together with the intercalated I-2 deposits, should therefore be younger than 22±2 ka. A correlation to re-advances of the SIS during or after the LGM (MIS 2) is very likely. After depositing the M-2 till complex, the SIS retreated. Lithostratigraphical unit I-2 was deposited after this retreat and before the following readvance (M-3 till).

3.6 Discussion

The sedimentological and chronological results of this study enable a reconstruction of the depositional history during MIS 3 and parts of MIS 2 at Jasmund, which completes our picture of the southwest Baltic Sea area. In particular, the dynamics of

the SIS in the study area during the transition of MIS 3 and early MIS 2 can now be reconstructed.

3.6.1 Reliability of available age data

In the Kluckow section, Kenzler et al. (2015) dated the organic ligament of an *Anadonta* sp. at 46±1 cal. ka BP and argued that the shell was not redeposited. Non-reworked organic material is one important criterion to obtain a reliable age with radiocarbon, as dating redeposited organic fragments only indicates a maximum depositional age for the sediment (Houmark-Nielsen 2010). Additionally, dating bulk samples of organic-rich sediments has the potential problem of reworking, which makes the resulting age less reliable. Hence, the reliability of the ^{14}C age of the shell at Kluckow site as an independent age control is high, although the age is very close to the upper limit of the method.

OSL dating, however, also has some major methodological issues. The main problem is insufficient bleaching of quartz grains, which can occur if the sediment was deposited in an environment with a limited exposure to sunlight (Fuchs & Owen 2008). This, in turn, may result in an overestimation of the burial age. A proper sedimentological investigation is therefore crucial to determine suitable positions for taking luminescence samples, which should be well bleached before burial (Fuchs & Owen 2008). To overcome the problem of partial bleaching, different statistical models are in use (Galbraith & Roberts 2012). The identification of well-bleached quartz is possible by comparing the luminescence signal of quartz and feldspar grains (Murray et al. 2012). Thus, Kenzler et al. (2015) argued that at least the upper two samples (LUM 2831 and LUM 3832) of the Kluckow section contained well-bleached quartz, whereas the lowermost sample (LUM 2829) potentially suffered from partial bleaching.

Another important issue is the reconstruction of the water content at the time of burial. Due to a dampening effect of water with respect to the dose rate, a 1% discrepancy from the true water content over time results in a 1% deviation from the true burial age. Furthermore, the detection of a radionuclide disequilibrium within the ^{238}U decay chain can cause an over- or underestimation of the sediment dose rate (Lüthgens et al. 2011a), whereas saturation effects of the quartz OSL signal result in an underestimation of the true burial age (Wintle & Murray 2006). For sample LUM 2829 (Kluckow site) Kenzler et al. (2015) identified potential quartz saturation effects

by comparing growth curves (Wintle & Murray 2006). Hence, sample LUM 2829 indicates a minimum age.

The TL ages determined by Krbetschek (1995) for the Glowe and Kluckow sites should be treated as approximate values because of the uncertainties and methodological problems involved in dating lacustrine and fluvial sediments with TL (Jain et al. 2007).

3.6.2 Early and Middle Weichselian period

Deposits of Early Weichselian age have so far not been documented in the study area, which makes an environmental reconstruction almost impossible. Either this period was dominated by erosional processes, or the Early Weichselian deposits were later eroded.

The first proven Weichselian sediments (unit K-A) were dated to a minimum age of c. 62 ka and indicate a fluvial phase in the study area. From a sedimentological point of view, a comparable depositional environment for units K-A and G-A is likely, and therefore a simultaneous deposition is possible. The till below these units is of Early Weichselian or even Saalian age (Müller 2004). A correlation of this till with the Ristinge advance of Denmark (Houmark-Nielsen 2010) does not seem likely, as this advance occurred at 50±4 ka. In addition, the Ellund advance of northern Germany (Stephan 2003, 2014) is thought to be of Middle Weichselian age, as indicated by TL (Marks et al. 1995) and OSL ages (Preusser 1999) of meltwater deposits. Instead, age estimation of the Early to Middle Weichselian Warnow advance (NE Germany) is based on fine-gravel analyses and relative age estimations (Müller 2004). Hence, the question whether the Ellund, Warnow and Ristinge advances represent a single contemporaneous SIS advance (Houmark-Nielsen 2010) or different advances (Kenzler et al. 2015) is still unresolved. Nonetheless, a relationship between the Ristinge advance and the M-1o till of Jasmund cannot be excluded. Anjar et al. (2012) found evidence for a deglaciation phase during the early Middle Weichselian at Kriegers Flak (Fig. 3.1A) and correlated the lowermost till with the Ristinge advance (Fig. 3.18). Due to uncertainties concerning two OSL ages of 72±5 and 86±6 ka (Anjar et al. 2012) in terms of bleaching and saturation effects, a Saalian age is also possible for this till. Considering the pIRIR$_{290}$ age of unit K-A (101±9 ka; Kenzler et al. 2015) at

Kluckow, however, a correlation of the Ristinge advance with the M-1o is not plausible (Fig. 3.18); rather, this till seems to be correlated with a Saalian ice advance.
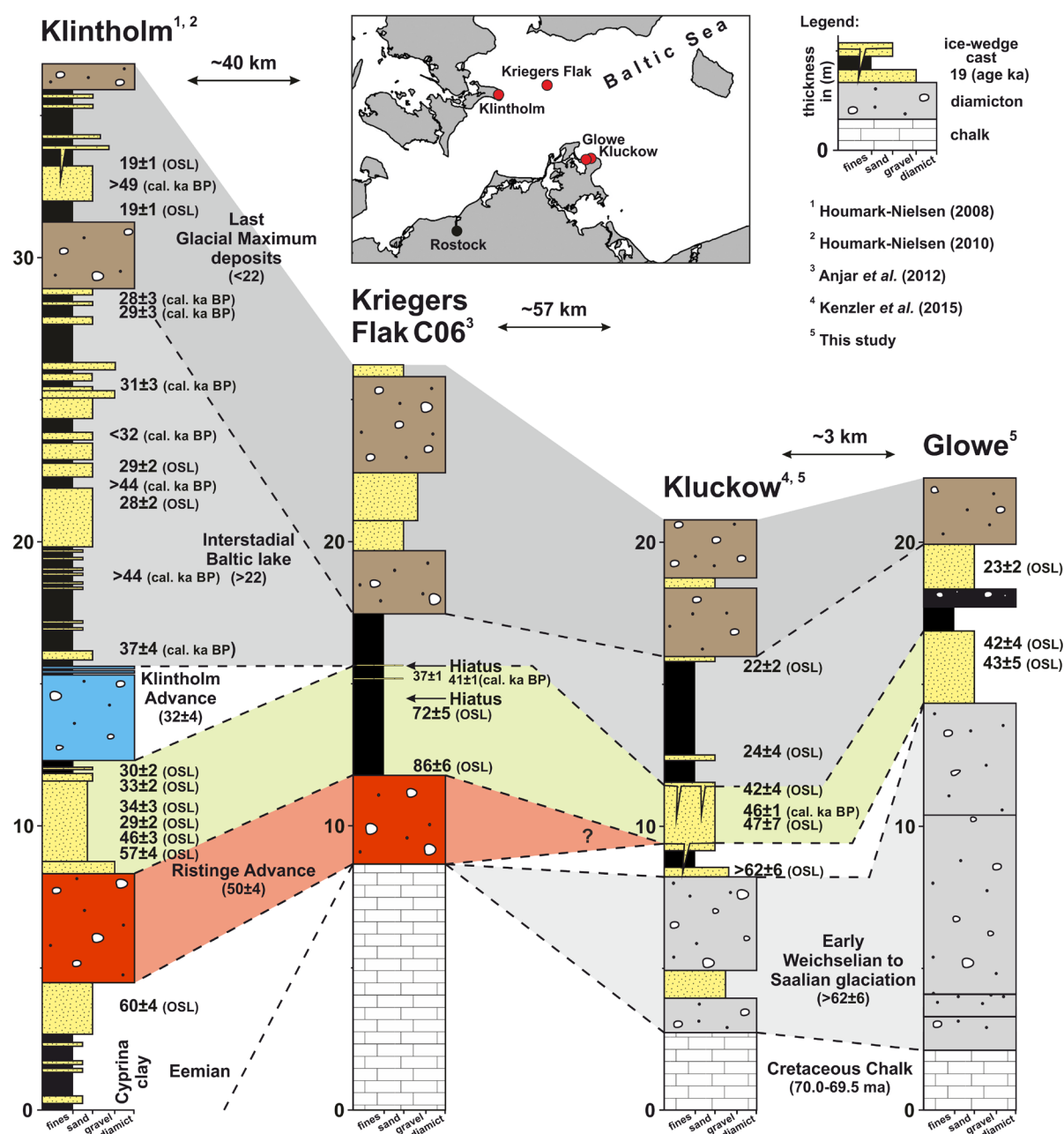
Fig. 3.18 Correlation of simplified stratigraphical logs from Pleistocene deposits at Klintholm (Houmark-Nielsen 2008, 2010), Kriegers Flak (Anjar et al. 2012), Kluckow (Kenzler et al. 2015; Krbetschek 1995; this study) and Glowe (Krbetschek 1995; this study). Based on sedimentological results and age data, a direct association of the Klintholm and Ristinge advance with deposits on Jasmund is not possible. Due to the lack of additional age data, the correlation of different MIS 2 age tills is not yet possible.
[1] Houmark-Nielsen (2008); [2] Houmark-Nielsen (2010); [3] Anjar et al. (2012); [4] Kenzler et al. (2015); [5] this study.

3.6.3 Marine Isotope Stage 3

The depositional environment during MIS 3 was dominated by lacustrine and fluvial processes interrupted by phases of non-sedimentation or erosion. Cold climate conditions occurred between c. 62 and c. 47 ka (unit K-B), which correspond to a possible cold time interval at Kriegers Flak, exhibiting a cold brackishwater facies (Anjar et al. 2012). While in Jasmund a periglacial landscape with ice-wedge casts existed at c. 47 ka, an ice advance has been documented at Ristinge at 50±4 ka (Fig. 3.1A; Houmark-Nielsen 2010). At Jasmund, this ice advance could be represented by the hiatus between units K-B and K-C. This in turn would mean that the ice never entered the study area during this time (Kenzler et al. 2015). Indeed, Anjar et al. (2012) discussed the possibility that the lowermost till recorded at Kriegers Flak could be correlated to the Ristinge advance, but their OSL ages (86±6 and 72±5 ka) of the directly overlying deposits contradict this.

The time between 47 and 38 ka was dominated by a steppe-like landscape with braided river systems (units G-B and K-C). Contemporaneous interstadial deposits with comparable environmental conditions have been reported from Scandinavia: based on macrofossils and pollen, Odgaard (1982) reconstructed a steppe-like landscape with short, warm summers in northern Denmark near Hirtshals. Likewise, Kolstrup & Havemann (1984) proposed an interstadial period around 47 ka, based on radiocarbon dating of pieces of *Juniperus* recovered from an alluvial fan near Frøslev (southern Jutland, Denmark). A landscape with lakes and open vegetation was also inferred from a sediment core drilled at eastern Møn (Klintholm) by Houmark-Nielsen et al. (2016). Finally, the Greenlandic inland ice-core indicates interstadial climate condition during Greenland Interstadial 12 (around 47–45 ka) (Hättestrand & Robertsson 2010). These results suggest that the SIS did not cover the southwestern Baltic Sea region between 47 and 42 ka.

A subsequent cooling phase resulted in a periglacial landscape with ice-wedge polygon nets associated with non-deposition and/or erosion, represented by a hiatus at the boundaries between units K-C and K-D and between units G-B and G-C. These hiatuses include the time between c. 42 and c. 30 ka. While Houmark-Nielsen (2010) proposed an ice advance at Klintholm (southeastern Denmark) at 32±4 ka, Anjar et al. (2012) found no evidence for an ice advance during this period at Kriegers Flak; instead, they found a hiatus in contemporaneous sediments. This indicates that the hiatus at Jasmund and Kriegers Flak could be related to the Klintholm advance (Fig.

3.18) and the corresponding cooler climate conditions. If true, however, this ice advance did not reach the Jasmund area. This would mean that the palaeogeographical map of Hughes et al. (2016) for the period between 32 and 30 ka, where the SIS advances into the study area, needs to be revised, as the actual ice margin lies further to the north/northeast at this time.

However, several OSL ages from glacifluvial sediments from northeast Germany, related to ice-marginal positions of the Weichselian, indicate a possible pre-LGM ice advance between 34±3 and 28±4 ka (Lüthgens et al. 2010a, b; Lüthgens & Böse 2011). These authors also discussed the possibility of a two-phase LGM for northeast Germany, with a possible ice advance reaching the local LGM position at around late MIS 3 to early MIS 2. This would mean that the deposits of this initial LGM ice advance have been eroded away at Jasmund, potentially represented by the hiatuses between units G-B and G-C, and between units K-C and K-D, or that the ice did not pass through this area. According the findings presented here, the latter is more likely. To check the hypothesis of a two-phase LGM in northeast Germany, a broader age database of suitable outcrops is needed, such as the Stoltera section near Rostock (Fig. 3.1A; Müller 2004), as well as sections corresponding to the ice-marginal positions of Weichselian age.

3.6.4   Transition from MIS 3 to MIS 2

Between c. 30 and c. 22 ka, the study area was a glaciolacustrine environment, represented by units K-D, K-E, G-C, G-D and G-E. Anjar et al. (2012) also recorded glaciolacustrine clays at Kriegers Flak, with an age of 28.5–26 ka. These deposits indicate the presence of one or more glacially influenced freshwater lakes across the southwest Baltic Sea area, including Jasmund (Kenzler et al. 2015). The Kattegat ice stream (29–26 ka; Houmark-Nielsen 2003; Hughes et al. 2016), which came from the Oslo region and moved southward, blocked the Norwegian Channel. As a consequence, meltwater accumulated in depressions of the Baltic basin and formed freshwater lakes. From the available data, it is not clear whether the glaciolacustrine deposits of Kriegers Flak (unit C in Anjar et al. 2012) and Jasmund (mainly units G-C and K-D) have accumulated in the same or in separate basins. Nevertheless, the more likely scenario seems to be a bigger lake, whereby Jasmund would correspond to its southern rim.

3.6.5 The Last Glacial Maximum

At Kluckow, the transition from a glaciolacustrine to a subglacial depositional environment of the subsequent ice advance (M-2) was interrupted by a short glaciofluvial phase (unit K-E). At Glowe, on the contrary, a gradual transition from a proglacial lake (unit G-C) to a terminoglacial ice-contact lake (unit G-D) and terminoglacial meltwater sediments occurred immediately before the ice advance (M-2 at Kluckow). The SIS reached Kluckow between 24–20 ka (Kenzler et al. 2015), indicated by the M-2 till, and Glowe between 25–21 ka, indicated by unit G-E. Corresponding ages for the LGM in Denmark range from 22 to 20 ka (Houmark-Nielsen 2011). The palaeogeographical maps of Hughes et al. (2016) indicate that the SIS arrived at the study area between 25 and 23 ka, which is in excellent agreement with the results presented here. The timing is furthermore supported by Toucanne et al. (2015), who summarized the possible SIS advances in the southwest Baltic Sea area between 40 and 14 ka, and who stated that the SIS reached the LGM position in northern Germany and Denmark between 23 and 21 ka. Indeed, Lüthgens et al. (2011b) proposed that the global LGM is not equal to the local LGM in terms of ice extent. The most prominent ice advance of northeast Germany was dated to about 20 ka by these authors – reaching the Pomeranian ice-marginal position (IMP), which is not the southernmost IMP. During MIS 2, at least two post-LGM re-advances of the SIS (Toucanne et al. 2015) occurred on Jasmund. These advances were interrupted by a phase of ice retreat, as recorded by two subglacial tills (M-2 and M-3 at Kluckow, M-3 at Glowe) and an interbedded glacifluvial unit (I-2 at Kluckow) (Fig. 3.2, Fig. 3.3).

3.7 Conclusion

The sedimentological and geochronological results from the Glowe and Kluckow sections indicate the following main ice dynamics of the SIS, and palaeo-environmental conditions during MIS 3 and early MIS 2:

- Ice-free conditions occurred in the study area during MIS 3 and early MIS 2.

- Between c. 62 and c. 47 ka, deposition occurred in small lakes under arctic or sub-arctic climate conditions. By the end of this period, a periglacial landscape

with an ice-wedge polygon net was formed, reflecting cryoturbation and non-sedimentation.

• Deposition in various fluvial environments such as meandering and braided river systems occurred between 46±1 and 42±4 ka. Climate conditions involved short, moderate summers and cool winters. The landscape was steppe-like.

• Between 42±4 and 24±4 ka, a cooling phase occurred, resulting in a periglacial landscape with ice wedges. This colder period may have occurred due to the approaching SIS during the Klintholm advance at 32±4 ka in Denmark. Non-deposition or erosional processes dominated the study area during this period.

• During the transition of MIS 3 to MIS 2, a glaciolacustrine succession accumulated at Kluckow. The lake water was inhabited by cold-water ostracods, indicating arctic to sub-arctic climate conditions. A link to the damming effect of the Kattegat advance (29–26 ka) is likely.

• In front of the advancing SIS, short-lived proglacial to ice-contact lakes were formed at 23±2 ka. The sedimentation was dominated by suspension settling of clay and silt, rain-out of debris from icebergs, and debrisflows.

• The SIS covered the study area at 22±2 ka. After a deglaciation period with ice decay, a re-advance occurred, which caused a regional glaciotectonic event. This event formed the glaciotectonic complex of Jasmund and the consequent glaciotectonic unconformity at the base of the M-3 till unit.

The results of this study have contributed to the reconstruction of the depositional environments during MIS 3 and the transition to MIS 2 in the southwest Baltic Sea basin. The reconstructed time-slices in the vicinity of Jasmund from Hughes et al. (2016) need to be revised, in particular for the period between 32 and 30 ka, as it has been shown here that the SIS did not reach the study area during this time. Instead, the time when the SIS reached the study area was constrained to 22±2 ka.

3.8 Acknowledgements

3.9 References

Andrén, T., Björck, S., Andrén, E., Conley, D., Zillén, L. & Anjar, J. 2011: The development of the Baltic Sea Basin during the last 130 ka. In Harff, J., Björck, S. & Hoth, P. (eds.): *The Baltic Sea Basin*, 75–97. Springer, Berlin.

Anjar, J., Adrielsson, L., Bennike, O., Björck, S., Filipsson, H. L., Groeneveld, J., Knudsen, K. L., Larsen, N. K. & Möller, P. 2012: Palaeoenvironments in the southern Baltic Sea Basin during Marine Isotope Stage 3: a multi-proxy reconstruction. *Quaternary Science Reviews 34*, 81–92.

Benn, D. I. & Evans, D. J. A. 2010: *Glaciers and Glaciations*. 802 pp. Hodder Education, London.

Bøtter-Jensen, L., Thomsen, K. J. & Jain, M. 2010: Review of optically stimulated luminescence (OSL) instrumental developments for retrospective dosimetry. *Radiation Measurements 45*, 253–257.

Brodzikowski, K. & van Loon, A. J. 1987: A systematic classification of glacial and periglacial environments, facies and deposits. *Earth-Science Reviews 24*, 297–381.

Carr, S. J. & Lee, J. A. 1998: Thin-section production of diamicts: problems and solutions. *Journal of Sedimentary Research 68*, 217–220.

Carrivick, J. L. & Tweed, F. S. 2013: Proglacial lakes: character, behaviour and geological importance. *Quaternary Science Reviews 78*, 34–52.

Cohen, K. M. & Gibbard, P. L. 2012: *Regional chronostratigraphical correlation table for the last 270,000 years*. Available at: http://www.nhm2.uio.no/norges/GTS2012_Quaternary-Poster-reg-GSA2012.pdf

Cunningham, A.C. & Wallinga, J. 2010: Selection of integration time intervals for quartz OSL decay curves. *Quaternary Geochronology 5*, 657–666.

Ehlers, J., Grube, A., Stephan, H.-J. & Wansa, S. 2011: Pleistocene laciations of North Germany – new results. *In* Ehlers, J., Gibbard, P. L. & Hughes, P. D. (eds.): *Quaternary Glaciations – Extent and Chronology*, 149–162. *Developments in Quaternary Science 15*. Elsevier, Amsterdam.

Fuchs, M. & Owen, L. A. 2008: Luminescence dating of glacial and associated sediments: review, recommendations and future directions. *Boreas 37*, 636–659.

Galbraith, R. F. & Roberts, R. G. 2012: Statistical aspects of equivalent dose and error calculation and display in OSL dating: an overview and some recommendations. *Quaternary Geochronology 11*, 1–27.

Hättestrand, M. & Robertsson, A.-M. 2010: Weichselian interstadials at Riipiharju, northern Sweden – interpretation of vegetation and climate from fossil and modern pollen records. *Boreas 39*, 296–311.

Heine, K., Reuther, A. U., Thieke, H. U., Schulz, R., Schlaak, N. & Kubik, P. W. 2009: Timing of Weichselian ice marginal positions in Brandenburg (northeastern Germany) using cosmogenic in situ [10]Be. *Zeitschrift für Geomorphologie, Neue Folge 53*, 433–454.

Houmark-Nielsen, M. 2003: Signature and timing of the Kattegat Ice Stream: onset of the Last Glacial Maximum sequence at the southwestern margin of the Scandinavian Ice Sheet. *Boreas 32*, 227–241.

Houmark-Nielsen, M. 2008: Testing OSL failures against a regional Weichselian glaciation chronology from southern Scandinavia. *Boreas 37*, 660–677.

Houmark-Nielsen, M. 2010: Extent, age and dynamics of Marine Isotope Stage 3 glaciation in the southwestern Baltic Basin. *Boreas 39*, 343–359.

Houmark-Nielsen, M. 2011: Pleistocene glaciations in Denmark: a closer look at chronology, ice dynamics and landforms. *In* Ehlers, J., Gibbard, P. L. & Hughes, P. D. (eds.): *Quaternary Glaciations: Extent and Chronology, 47–58*. Elsevier, Amsterdam.

Houmark-Nielsen, M. & Kjær, K. H. 2003: Southwest Scandinavia, 40–15 kyr BP: palaeogeography and environmental change. *Journal of Quaternary Science 18*, 769–786.

Houmark-Nielsen, M., Bennike, O., Lemdahl, G. & Lüthgens, C. 2016: Evidence of ameliorated Middle Weichselian climate and sub-arctic environment in the western Baltic region: coring lake sediments at Klintholm,Møn, Denmark. *Boreas 45*, 347–359.

Hughes, A. L. C., Gyllencreutz, R., Lohne, Ø. S., Mangerud, J. & Svendsen, J. I. 2016: The last Eurasian ice sheet – a chronological database and time-slice reconstruction, DATED-1. *Boreas 45*, 1–45.

Jain, M., Duller, G. A. T. & Wintle, A. G. 2007: Dose response, thermal stability and optical bleaching of the 310 degrees C isothermal TL signal in quartz. *Radiation Measurements 42*, 1285–1293.

Kalm, V. 2006: Pleistocene chronostratigraphy in Estonia, southeastern sector of the Scandinavian glaciation. *Quaternary Science Reviews 25*, 960–975.

Keding, E. 1993: The vegetation of a Weichselian Middle Pleniglacial Interstadial from the Isle of Rügen/Western Pommerania reconstructed by macro remains. *Meyniana 45*, 87–105.

Kenzler, M., Obst, K., Hüneke, H. & Schütze, K. 2010: Glazitektonische Deformation der kretazischen und pleistozänen Sedimente an der Steilküste von Jasmund nördlich des Königsstuhls (Rügen). *Brandenburger Geowissenschaftliche Beiträge 17*, 107–122.

Kenzler, M., Tsukamoto, S., Meng, S., Thiel, C., Frechen, M. & Hüneke, H. 2015: Luminescence dating of Weichselian interstadial sediments from the German Baltic Sea coast. *Quaternary Geochronology 30*, 215–256.

Kolstrup, E. & Havemann, K. 1984: Weichselian Juniperus in the Frøslev alluvial fan (Denmark). *Bulletin of the Geological Society of Denmark 32*, 121–131.

Krbetschek, M. R. 1995: *Lumineszenz-Datierungen quartärer Sedimente Mittel-, Ost- und Nordostdeutschlands*. Ph.D. thesis. TU Bergakademie Freiberg, 122 pp.

Kunz, A., Frechen, M., Ramesh, R. & Urban, B. 2010: Luminescence dating of late Holocene dunes showing remnants of early settlement in Cuddalore and evidence of monsoon activity in south east India. *Quaternary International 222*, 194–208.

Larsen, N. K., Knudsen, K. L., Krohn, K. L., Kronborg, C. F., Murray, A. S. & Nielsen, O. B. 2009: Late Quaternary ice sheet, lake and sea history of southwest Scandinavia – a synthesis. *Boreas 38*, 732–761.

Livingstone, S. J., Clark, C. D., Piotrowski, J. A., Tranter, M., Bentley, M. J., Hodsen, A., Swift, D. A. & Woodward, J. 2012: Theoretical framework and diagnostic criteria for the identification of palaeo-subglacial lakes. *Quaternary Science Reviews 53*, 88–110.

Livingstone, S. J., Piotrowski, J. A., Bateman, M. D. & Ely, J. C. 2015: Discriminating between subglacial and proglacial lake sediments: an example from the Dänischer Wohld Peninsula, northern Germany. *Quaternary Science Reviews 112*, 86–108.

Lopes-Lima, M. 2014: *Anodonta anatine. The IUCN Red List of Threatened Species. Version 2014.3*. Available at: http://www.iucnredlist.org (downloaded 18.03.2015).

Ludwig, A. O. 2005: On the interpretation of the cliff section east of Glowe/isle of Rügen (Baltic Sea). *Journal for the Geological Science (Zeitschrift der Geologischen Wissenschaften) 33*, 263–272.

Ludwig, A. O. 2011: Two striking push moraines: Peski/Belorussland and Jasmund/Rügen Island, NE Germany – common features and differences. *Quaternary Science Journal (Eiszeitalter und Gegenwart) 60*, 464–487.

Lüthgens, C. & Böse, M. 2011: Chronology of Weichselian main ice marginal positions in north-eastern Germany. *Quaternary Science Journal (Eiszeitalter und Gegenwart) 2–3*, 236–247.

Lüthgens, C., Böse, M. & Krbetschek, M. 2010a: On the age of the young morainic morphology in the area ascribed to the maximum extent of the Weichselian glaciation in north-eastern Germany. *Quaternary International 222*, 72–79.

Lüthgens, C., Böse, M., Lauer, T., Krbetschek, M., Strahl, J. & Wenske, D. 2011a: Timing of the last interglacial in Northern Europe derived from Optically Stimulated Luminescence (OSL) dating of a terrestrial Saalian–Eemian–Weichselian sedimentary sequence in NE-Germany. *Quaternary International 241*, 79–96.

Lüthgens, C., Böse, M. & Preusser, F. 2011b: Age of the Pomeranian ice-marginal position in northeastern Germany determined by Optically Stimulated Luminescence (OSL) dating of glaciofluvial sediments. *Boreas 40*, 598–615.

Lüthgens, C., Krbetschek, M., Böse,M. & Fuchs,M. C. 2010b: Optically stimulated luminescence dating of fluvioglacial (sandur) sediments from north-eastern Germany. *Quaternary Geochronology 5*, 237–243.

Marks, L. 2012: Timing of the Late Vistulian (Weichselian) glacial phases in Poland. *Quaternary Science Reviews 44*, 81–88.

Marks, L., Piotrowski, J. A., Stephan, H.-J., Fedorowicz, S. & Butrym, J. 1995: Thermoluminescence indications of the Middle Weichselian (Vistulian) glaciation in Northwest Germany. *Meyniana 47*, 69–82.

van der Meer, J. J. M. 1987: Micromorphology of glacial sediments as a tool in distinguishing genetic varieties of till. *Geological Survey of Finland Special Paper 3*, 77–89.

van der Meer, J. J. M. 1993: Microscopic evidence of subglacial deformation. *Quaternary Science Reviews 12*, 553–587.

Menzies, M. 2000: Micromorphological analyses of microfabrics and microstructures indicative of deformation processing in glacial sediments. *In* Maltmann, A. J., Hubbard, B. & Hambrey, J. M. (eds.): *Deformation of Glacial Material*s, 279–292. *Geological Society, Special Publications 176*.

Menzies, J., van der Meer, J. J. M. & Rose, J. 2006: Till–as a glacial 'tectomict', its internal architecture, and the development of a 'typing' method for till differentiation. *Geomorphology 75*, 172– 200.

Menzies, J., van der Meer, J. J. M., Domack, E. & Wellner, J. S. 2010: Micromorphology: as a tool in the detection, analyses and interpretation of (glacial) sediments and man-made material. *Proceedings of the Geologists' Association 121*, 281–292.

Miall, A. D. 1996: *The Geology of Fluvial Deposits: Sedimentary Facies, Basin Analysis, and Petroleum Geology*. 582 pp. Springer, Berlin.

Müller, U. 2004: Weichsel-Frühglazial in Nordwest-Mecklenburg. *Meyniana 56*, 81–115.

Müller, U. & Obst, K. 2006: Lithostratigraphy and bedding of the Pleistocene deposits in the area of Lohme (Jasmund/Rügen). *Journal for the Geological Sciences (Zeitschrift der Geologischen Wissenschaften) 34*, 39–54.

Murray, A. S. & Wintle, A. G. 2000: Luminescence dating of quartz using an improved single-aliquot regenerative-dose protocol. *Radiation Measurements 32*, 57–73.

Murray, A. S., Thomsen, K. J., Masuda, N., Buylaert, J. P. & Jain, M. 2012: Identifying well-bleached quartz using the different bleaching rates of quartz and feldspar luminescence signals. *Radiation Measurements 47*, 688–695.

Murton, J. 2013: Ice wedges and ice-wedge casts. *In* Elias, S. A. & Mock, C. J. (eds.): *Encyclopedia of Quaternary Science*, 436–451. Elsevier, Amsterdam.

Niedermeyer, R.-O., Kanter, L., Kenzler, M., Panzig, W.-A., Krienke, K., Ludwig, A.-O., Schnick, H.H. & Schütze, K. 2010: Rügen Island (I) – Facies, stratigraphy, structural architecture and geological hazard potential of Pleistocene deposits of the Jasmund cliff coast. *In* Lampe, R. & Lorenz, S. (eds.): *Eiszeitlandschaften in Mecklenburg-Vorpommern*, 50–71. Geozon Science Media, Greifswald.

Odgaard, B.V. 1982: A middle Weichselian moss assemblage from Hirtshals, Denmark, and some remarks on the environment 47.000 BP. *Danmarks Geologiske Undersøgelse, Årbog 1981*, 5–45.

Panzig, W.-A. 1991: Zu den Tills auf Nordostrügen. *Journal for the Geological Sciences (Zeitschrift der Geologischen Wissenschaften) 19*, 331–346.

Panzig, W.-A. 1995: Zum Pleistozän von Rügen. *Terra Nostra 6*, 177–200.

Panzig, W.-A. & Kanter, L. 1997: Stop 18 – Glowe (NW Jasmund). *In* Piotrowski, J. A. (ed.): *Field Symposium on Glacial Geology at the Baltic Sea Coast in Northern Germany, 7–12 September 1997*, 49–55. *The Peribaltic Group, INQUA Commission on Glaciation, Excursion Guide*, Kiel.

Phillips, E. & Hughes, L. 2014: Hydrofracturing in response to the development of an overpressurised subglacial meltwater system during drumlin formation: an example from Anglesey, NW Wales. *Proceedings of the Geologists' Association 125*, 296–311.

Phillips, E., Merritt, J., Auton, C. & Golledge, N. 2007: Microstructures in subglacial and proglacial sediments: understanding faults, folds and fabrics, and the influence of water on the style of deformation. *Quaternary Science Reviews 26*, 1499–1528.

Preusser, F. 1999: Lumineszenzdatierung fluviatiler Sedimente; Fallbeispiele aus der Schweiz und Norddeutschland. *Kölner Forum für Geologie und Paläontologie 3*, 1–62.

Reich, M. & Frenzel, P. 2002: Die Fauna und Flora der Rügener Schreibkreide. *Archiv für Geschiebekunde 3*, 73–284.

Rinterknecht, V., Börner, A., Bourlès, D. & Braucher, R. 2014: Cosmogenic [10]Be dating of ice sheet marginal belts in Mecklenburg-Vorpommern, Western Pomerania (northeast Germany). *Quaternary Geochronology 19*, 42–51.

Skrede, I., Eidesen, P.B., Portela, R.P. & Brochmann, C. 2006: Refugia, differentiation and postglacial migration in arctic-alpine Eurasia, exemplified by the mountain avens (Dryas octopetala L.). *Molecular Ecology 15*, 1827–1840.

Steinich, G. 1992: Die stratigraphische Einordnung der Rügen-Warmzeit. *Journal for the Geological Sciences (Zeitschrift der Geologischen Wissenschaften) 20*, 125–154.

Stephan, H.-J. 2003: Zur Entstehung der eiszeitlichen Landschaft Schleswig-Holsteins. *Schriften des Naturwissenschaftlichen Vereins für Schleswig-Holstein 68*, 101–118.

Stephan, H.-J. 2014: Climato-stratigraphic subdivision of the Pleistocene in Schleswig-Holstein, Germany and adjoining areas. *Quaternary Science Journal (Eiszeitalter und Gegenwart) 63*, 3–18.

Toucanne, S., Soulet, G., Freslon, N., Silva Jacinto, R., Dennielou, B., Zaragosi, S., Eynaud, F., Bourillet, J.-F. & Bayon, G. 2015: Millennial-scale fluctuations of the European Ice Sheet at the end of the glacial, and their potential impact on global climate. *Quaternary Science Reviews 123*, 113–133.

Wintle, A.G. & Murray, A. S. 2006: A review of quartz optically stimulated luminescence characteristics and their relevance in single-aliquot regeneration dating protocols. *Radiation Measurements 41*, 369–391.

Wohlfarth, B. 2010: Ice-free conditions in Sweden during Marine Oxygen Isotope Stage 3? *Boreas 39*, 377–398.

Zelčs, V. & Markots, A. 2004: Deglaciation history of Latvia. *In* Ehlers, J. & Gibbard, P. L. (eds.): *Quaternary Glaciations – Extent and Chronology*, 225–243. Elsevier BV, Oxford.

Zettler, M.L., Jueg, U., Menzel-Harloff, H., Göllmitz, U., Petrick, S., Weber, E. & Seemann, R. 2006: *Die Land- und Süßwassermollusken Mecklenburg-Vorpommerns*. 318 pp. Obotritendruck, Schwerin.

4 A multi-proxy palaeoenvironmental and geochronological reconstruction of the Saalian-Eemian-Weichselian succession at Klein Klütz Höved, NE Germany

Michael Kenzler[1], Henrik Rother[1], Heiko Hüneke[1], Peter Frenzel[2], Jaqueline Strahl[3], Sumiko Tsukamoto[4], Yan Li[4], Stefan Meng[1], Julia Gallas[5] & Manfred Frechen[4]

[1]University of Greifswald, Institute of Geography and Geology, F.-L. Jahn Str. 17a, 17487 Greifswald, Germany

[2]Institute of Earth Sciences, Friedrich Schiller University of Jena, Burgweg 11, 07749 Jena, Germany

[3]Landesamt für Bergbau, Geologie und Rohstoffe Brandenburg (LBGR), Geological Survey, Inselstraße 26, 03046 Cottbus, Germany

[4]Leibniz Institute for Applied Geophysics (LIAG), Geochronology and Isotope Hydrology, Stilleweg 2, 30655 Hannover, Germany

Abstract

Here we present a multi-proxy investigation of the Klein Klütz Höved (KKH) coastal cliff section (NE Germany), involving lithofacies analysis, micromorphology, micropalaeontology, palynology and luminescence dating of quartz and feldspar. Our results show that the local stratigraphy is subdivided into three depositional phases: (i) Following a Saalian ice advance (MIS 6) by the Scandinavian Ice Sheet, the penultimate deglaciation (Termination II) at the site occurred between ~139-134 ka, leading to the establishment of a braided river system and lacustrine basins under

arctic-subarctic climate conditions. (ii) The initial phase of the Eemian interglacial at KKH is represented by lacustrine deposits containing warm-water ostracods and a pollen spectrum indicating gradual expansion of woodlands eventually containing thermophile deciduous forest elements. A correlation of the local pollen assemblages with Eemian reference records from central Europe suggests that less than 750 years of the last interglacial period are preserved at KKH. The occurrence of brackish ostracods dates the onset of the Eemian marine transgression at the section at ~300–750 years after the beginning of the last interglacial period. (iii) The Eemian record is directly overlain by a ~10 m thick sedimentary succession of MIS 2 age, implying a significant hiatus of ~90 ka, encompassing the time from middle and upper MIS 5e to late MIS 3. During the Late Weichselian, KKH features a depositional shift from (glacio-)lacustrine to subglacial to recessional terminoglacial facies, with a first documented Weichselian ice advance postdating 20±2 ka. Overall, the KKH section represents an exceptional sedimentary archive for palaeoenvironmental reconstructions, covering the period from the Saalian glaciation and subsequent Termination II to the early Eemian and Late Weichselian. The results refine the existing palaeogeographical and geochronological models of the late Quaternary history in the southwestern Baltic Sea area and allow correlations to other reference records in the wider region.

4.1 Introduction

The reconstruction of sedimentary and palaeoenvironmental conditions for deposits of Eemian age (127-110 ka; Brauer et al. 2007; Marine Isotope Stage (MIS) 5e) yields valuable information about the characteristics of the last interglacial period. Understanding Eemian sea-level dynamics, climatic and palaeoenvironmental trends, as well as the timing of its onset and termination, is critical for evaluating past interglacials and for the forward modelling of our future climate. To enhance the available information on the Eemian period, a robust geochronological database is mandatory. Infrared-stimulated luminescence (IRSL) dating of K-rich feldspar is one promising approach to establish a absolute age chronology beyond 100 ka (Buylaert et al. 2011; Lüthgens et al. 2011; Lamothe 2016), while in a limited number of cases, thermoluminescence (TL), electron spin resonance (ESR) and Thorium/Uranium

(^{230}Th/U) dating methods have also been successfully applied to date Eemian sediments (Krbetschek 1995; Winn et al. 2000; Degering & Krbetschek 2007; Börner et al. 2015).

This study focuses on an investigation of the Klein Klütz Höved (KKH) cliff section at the south-west Baltic Sea coast, where a Saalian to Weichselian depositional succession is preserved (Ullerich 1991; Strahl et al. 1994; Krbetschek 1995; Menzel-Harloff & Meng 2015). The sediment succession includes terrestrial and brackish deposits of early Eemian age (Strahl et al. 1994), which are overlain by Weichselian tills and associated clayey to sandy deposits. The present study re-evaluates this section using detailed lithofacies logging, micromorphology, luminescence dating, and micropalaeontological analyses. Based on these new data we reconstruct palaeoenvironmental and depositional conditions, with an emphasis on characterising the timing between the Late Saalian and the Eemian period.

We also address so-far unresolved questions relating to the depositional shift from the Eemian interglacial to the Weichselian glaciation, including the possible occurrence of marine-transgressional Eemian sediments at KKH. The information from the investigated coastal section provides an important link between other well-studied Eemian sites in Denmark (*e.g.* Murray & Funder 2003; Eiríksson et al. 2006; Larsen et al. 2009) and contemporaneous records from central Germany (*e.g.* Wansa & Wimmer 1990; Eissmann 2002; Hermsdorf & Strahl 2008; Novenko et al. 2008; Lüthgens et al. 2011; Strahl et al. 2011).

4.2 The Klein Klütz Höved coastal section

4.2.1 Geology and geomorphology

The KKH section is located in the south of the Mecklenburg Bay (south-west Baltic Sea, Fig. 4.1). Morphologically, this area is part of the ice-marginal belt associated with the Pomeranian and Mecklenburgian phases of the Late Weichselian glaciation (MIS 2), which represent local late-Last Glacial Maximum (LGM) re-advances of the Scandinavian Ice Sheet (SIS) (Toucanne et al. 2015; Fig. 4.1A). During the Mecklenburgian ice advance (between 17 and 15 ka; Kenzler et al. 2010; Börner et al.
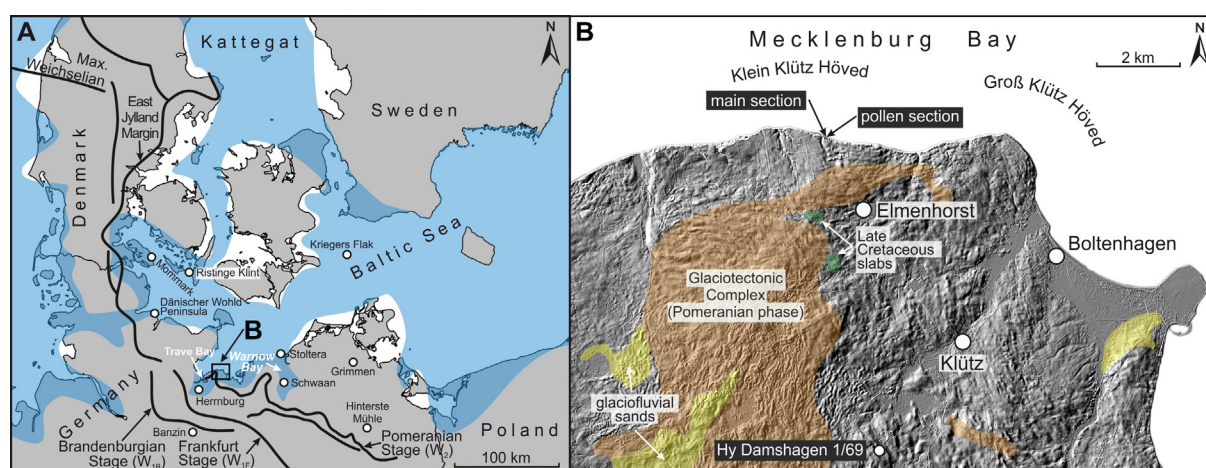
Fig. 4.1 A. Map of the south-west Baltic Sea region showing the study area and other sites mentioned in the text. The blue shaded area indicates the Eemian sea (based on Seidenkrantz et al. 2000; Funder et al. 2002; Meng et al. 2009) with revisions in the vicinity of Klein Klütz Höved and the former Trave Bay. The solid black line marks the maximum extent of the Scandinavian Ice Sheet during the Weichselian period (based on Houmark-Nielsen 2010). B. Digital elevation model of the study area visualising the local glaciotectonic complex of Pomeranian age (based on LiDAR data from @GeoBasis-DE/M-V 2016 processed by C. Kettler) and locations of the studied cliff sections and the drilling site of Hy Damshagen 1/69.

2014), parts of the region were affected by large-scale glaciotectonic deformation, as evidenced by widespread thrust faulting, folding and the uplifting of blocks of Pleistocene deposits (Strahl 2004). As a result of the glaciotectonic imbrication, Pleistocene units were locally uplifted by up to 30 m from their original position. Along the coast at KKH these blocks are exposed at sea cliffs up to 30 m high (Fig. 4.1B), displaying large-scale glaciotectonic structures representing tight anticline-syncline pairs which are occasionally separated by thrust faults (Ullerich 1991).

The Quaternary geology of the KKH site has been studied since the beginning of the 20th century and various authors have described the local presence of Late Saalian to Eemian fluvial, lacustrine and marine deposits (MIS 6 to 5e), stratigraphically located between Saalian and Weichselian tills (*e.g.* Geinitz 1922; Gehl 1961; Ludwig 1964; Ullerich 1991; Strahl et al. 1994; Krbetschek 1995; Menzel-Harloff & Meng 2015). We investigated the most studied section of the KKH cliff, which has a width of about 20 m and a height of 15 m (54°00.67' N, 11°06.98' E). The outcrop is divided into two subsections (Fig. 4.2) with the general stratigraphic succession comprising five glacial diamict units, referred to as M-I to M-V, interbedded with glaciofluvial to (glacio-)lacustrine and brackish-marine deposits, labelled I-I to I-IV (Fig. 4.3; Strahl et al. 1994; Strahl 2004; Rühberg 2004). Of these, the lowermost glacial diamict (M-I), interpreted as a subglacial till, has previously been correlated to a SIS advance during

the Saalian glaciation (MIS 6, Warthe phase). The overlying unit I-I is divided into a glaciofluvial to glaciolacustrine Late Saalian lower part, a lacustrine to brackish middle part of early Eemian age, and a (glacio-)fluvial to (glacio-)lacustrine Weichselian upper part (Strahl et al. 1994). The M-II till above is associated with an ice advance during the LGM (MIS 2, Brandenburgian/Frankfurt phase), while the stratigraphically following proglacial strata and tills (I-II to M-V) represent several phases of SIS late-LGM ice front oscillations (Fig. 4.3; Strahl et al. 1994; Strahl 2004). The overall chronostratigraphic correlations of the tills at KKH have primarily been based on provenance analyses of the fine-gravel content (Ullerich 1991).
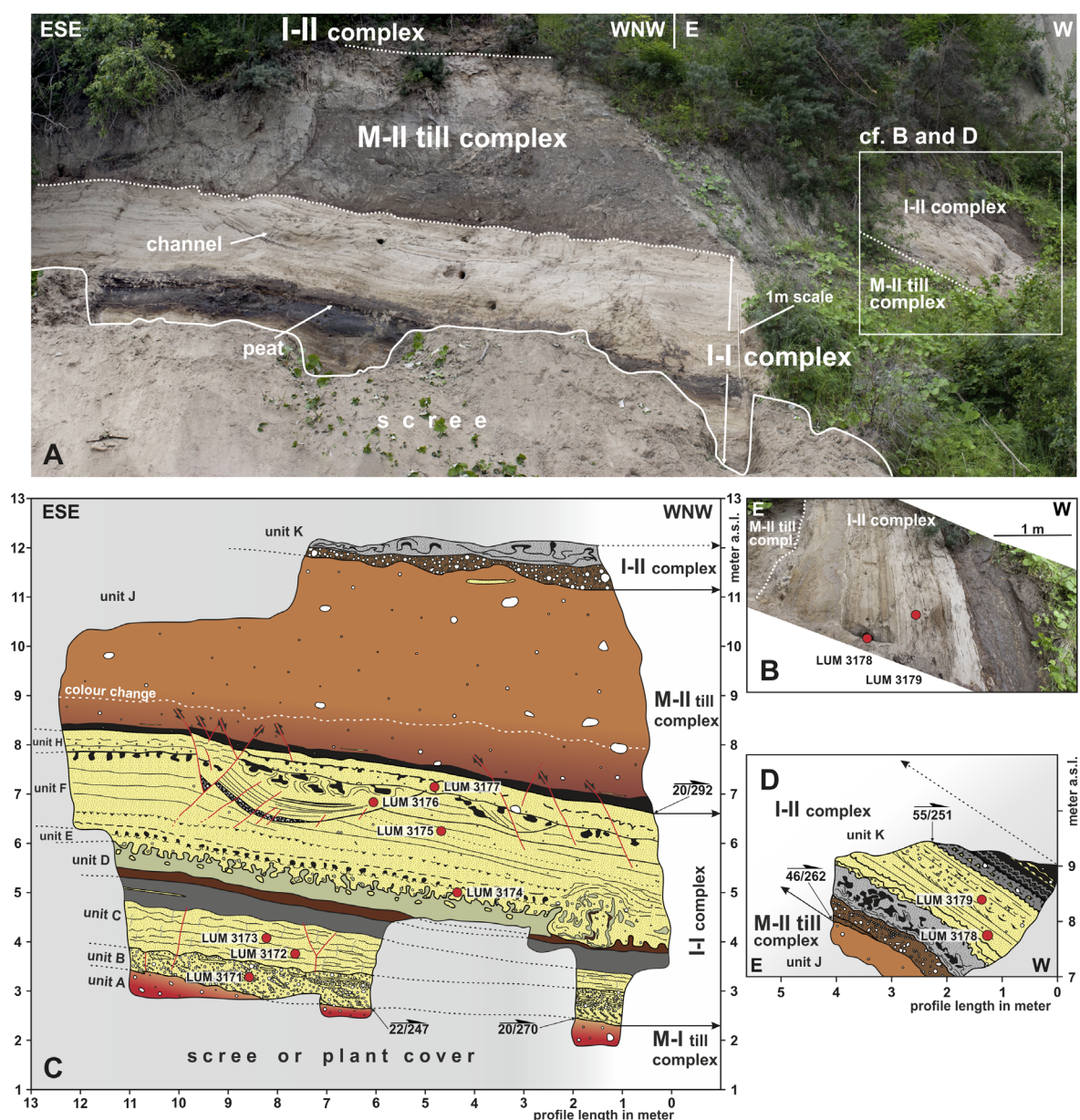
Fig. 4.2 Photographs of the Klein Klütz Höved main section (A, B) and corresponding lithostratigraphic sketches (C, D) displaying stratification, sediment architecture and the locations of all luminescence samples (LUM 3171 to LUM 3179). An expanded legend is available in Fig. S4.1 in the supplements.

4.2.2 Previous palaeontological and geochronological investigations

The most detailed palaeontological investigation at KKH was undertaken by Strahl et al. (1994), who focused on the fossil-bearing lithostratigraphic unit I-I (unit B to H in this study, Fig. 4.5). Based on the documented pollen, macro-flora, ostracods, foraminifera, molluscs and fishes, their study suggested a general shift from a (glacio-)fluvial to a lacustrine and finally brackish-influenced depositional environment during the Late Saalian to Eemian period. The main part of the Eemian record at KKH comprises a peat (subunit D1, Fig. 4.5) and an overlying organic mud (subunit D2, Fig. 4.5), above which reworked marine molluscs of Eemian age were found within a deformed horizon showing ball-and-pillow structures ("cryoturbated horizon", unit E; Strahl et al. 1994). More recently, Menzel-Harloff & Meng (2015) re-investigated the macrofauna at KKH (molluscs, mammals, fish remains), thereby significantly expanding the fossil inventory. In total, about 40 different terrestrial, lacustrine and marine mollusc species and remnants of steppe lemming (*Lagurus lagurus*) were found, indicating a shift from a cool climate during the Late Saalian to warmer climatic conditions during the initial phase of the Eemian interglacial.
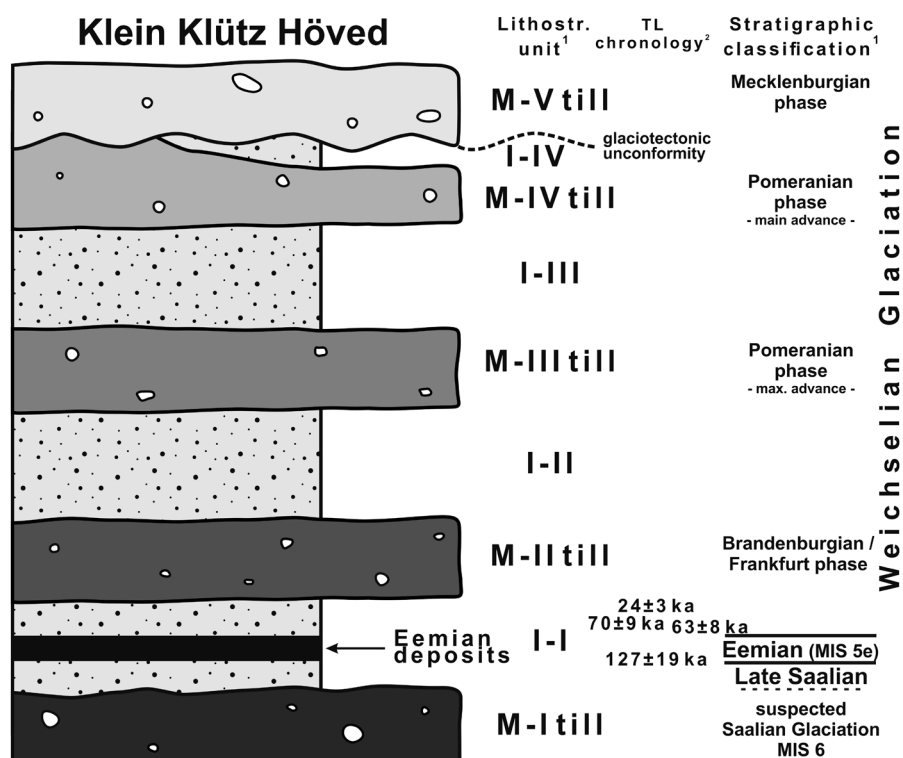
Fig. 4.3 Standard profile showing chronostratigraphic interpretations of the Pleistocene succession at Klein Klütz Höved based on fine gravel analyses ([1]Strahl 2004) and thermoluminescence dating ([2]Krbetschek 1995).

Until now, only few attempts have been made to obtain numerical age control for the deposits exposed at the Klein Klütz Höved section. Two samples from the peat horizon in subunit D1 (Fig. 4.5) gave finite radiocarbon ages of >40 ka BP, consistent with the presumed Eemian age of this unit (Krbetschek 1995). In addition, four TL ages from lithostratigraphic unit I-I, yielded age estimates from 127±19 ka to 24±3 ka (Strahl et al. 1994; Krbetschek 1995; Fig. 4.3). Based on the state of the art at that time, the study by Krbetschek (1995) applied both the total bleach method and/or the additive dose technique, which has been shown to be problematic for dating glacial sediments (Mejdahl et al. 1992; Prescott & Robertson 1997; Houmark-Nielsen 2010). The significant methodological improvements in luminescence dating of the last decade, including the development of the optically stimulated luminescence technique using quartz (OSL; Murray & Wintle 2000), and new IRSL dating protocols using feldspar (Buylaert et al. 2009), warrant a thorough re-evaluation of the existing chronologies at the KKH section as presented in this study.

4.3   Material and methods

4.3.1   Sedimentological logging and lithofacies analysis

After excavation, cleaning and mapping of the section, a detailed geological logging, and lithofacies analysis were undertaken. Logging focused on primary depositional (*e.g.* composition, structure, texture, bedding, and lamination) and erosional features (bed boundaries). The resulting data were then used to characterise individual lithofacies using a customized scheme (Tab. 4.1) based on Miall (1985, 1996) and Benn & Evans (2010).

4.3.2   Micromorphological analysis

A total of six samples (TS 1-6) were taken for thin section analysis, four samples from lithostratigraphic unit I-I and two samples from the M-II till (Fig. 4.5 Summary log of the main section at Klein Klütz Höved with information on lithology, luminescence chronology, micropalaeontological MP-units, local pollen assemblage zones (LPAZ), and thin section sample positions (TS). An expanded legend is available in Fig. S8.). After careful recovery, the samples were dried and gradually impregnated with a resin mixture (Oldopal P80-21, Oldopal co-activator 1% and Butanox M-50), using a vacuum

oven. After cutting, grinding and lapping, the samples were mounted on glass slides and grounded to a thickness of 20 to 25 μm. The terminology and interpretation of the observed micromorphological features follow the approaches introduced by van der Meer (1993), Menzies et al. (2006) and Stoops (2010).

4.3.3 Palaeontological material and methods

Pollen analysis. – To refine the existing palynological information from KKH (Strahl et al. 1994), samples were obtained from a nearby exposure (pollen section, 54°00.67' N, 11°07.05' E; Fig. 4.1B), which was temporarily accessible in 1997 and 2012 and is located 80 m east of the main outcrop (main section; Fig. 4.1B). Based on distinct marker horizons, which can be traced along the face of the cliff, the position of the sampled layers can be stratigraphically correlated with the main section. Additional control provides pollen stratigraphy presented in Strahl et al. (1994). Sampling was carried out at regular intervals of approximately five centimetres, providing a total of 45 pollen samples (Fig. 4.11). Laboratory preparation was undertaken at the Federal Institute of Geosciences and Natural Resources in Hannover (Germany) including HCl, KOH, HF treatment, acetolysis and ultrasonic sieving (6 μm) to extract liquid preparations (suspensions). On average 335 arboreal pollen (AP) and non-arboreal pollen (NAP) grains were counted using a Leica DMRB microscope (magnification 20, 40 and 100). The results are presented in percentage terms, in which the ratio AP to NAP (including Cyperaceae) corresponds to the basic sum of 100%. Pollen, spores and cysts of local components such as aquatic plants, marsh plants, ferns, moss, algae and reworked pre-Quaternary palynomorphs were excluded from the basic sum. The results of our pollen analyses are shown in a conventional pollen diagram (Fig. 4.11). Curves are enlarged tenfold to enhance visibility of values below 1%.

Micro- and macrofauna analysis. – In total, 31 sediment samples were taken from the main section at KKH for micro- and macropalaeontological analyses (Fig. 4.12). They cover all lithological units (B to H) between the tills (units A and J). A sediment volume of 100 mL from each sample was washed with sieves (63 μm, 200 μm and 1 mm mesh sizes) to extract microfossils. All ostracods, foraminifers, fruits and seeds were picked from the >200 μm size fraction of the dried residue using a stereo-microscope. In cases where more than 300 ostracod valves, foraminifer tests or fruits and seeds were present, the samples were further divided into subsamples using a micro-splitter.

Macrofossils, such as mollusc or plant fragments, were either counted or documented semi-quantitatively. The size fraction of 63-200 µm was checked for taxa not present within the >200 µm residue, but these were not separately counted. The material analysed is stored in the collections of the Institute of Geography and Geology, University of Greifswald, Germany. Taxonomic identification and their ecological characterisation is primarily based on Frenzel et al. (2010) for Ostracoda, Murray (1979) for Foraminifera, Glöer & Meier-Brook (1994) for molluscs and Frenzel (2006) for other taxa. Statistical evaluations, including the Spearman Rank correlation and cluster analysis on taxon distribution (log-transformed abundance) were conducted using the PAST 3.05 software (Hammer et al. 2001).

Luminescence dating. – In the past 15 years, luminescence dating has become one of the standard techniques to establish a geochronological framework for resolving the climatic development and glacial dynamics of the SIS during the last glacial-interglacial cycle (Buylaert et al. 2011; Lüthgens et al. 2011; Hughes et al. 2016; Kenzler et al. 2017). Most luminescence dating studies use quartz or K-rich feldspar grains; however, both minerals have distinct advantages and disadvantages (Murray et al. 2012). For the present study, we measured quartz to determine the equivalent dose (D_e) for all samples (LUM 3171 to LUM 3179; Fig. 4.5). Additionally, we measured the post-IR infrared stimulated luminescence (pIRIR) signal from K-rich feldspar for samples LUM 3171 to LUM 3174, to test whether signal saturation affected the quartz grains. A serious drawback in the luminescence dating of feldspar is its tendency towards anomalous fading, which involves a random loss of trapped energy, leading to an underestimation of the true burial age (Jain et al. 2015). Models developed to correct for anomalous fading are published by Huntley & Lamothe (2001) and Kars et al. (2008), which we further consider in the discussion of our results.

Nine luminescence samples were obtained using stainless steel tubes, which were inserted into the cleaned face of the outcrop (Fig. 4.5). For a determination of the environmental dose rate, additional sediment was collected from the direct vicinity of each sample position. Because the sediment water content can significantly influence the effective dose rate, further separate sample material was taken with a volumetrically defined cylinder to estimate the current in situ and the theoretically saturated water content value. To extract pure quartz and K-rich feldspar of 100-150 µm (LUM 3172 to LUM 3179) and 100-200 µm (LUM 3171) grain size, we used standard sample preparation techniques (*e.g.* Zhang et al. 2014), including drying,

sieving, chemical treatment with HCl, H_2O_2 and sodium oxalate. Separation of quartz, K-rich feldspar and heavy minerals was achieved using a heavy density liquid (sodium polytungstate solution). The extracted quartz fraction was then etched using 40% HF for 60 minutes, followed by treatment with HCl and a final sieving step.

The samples for dose rate determination were dried for 24 hours at 130 °C, followed by the sealed storage of 700 g homogenised sediment in Marinelli beakers for at least four weeks to prevent the development of a radon-disequilibrium. Natural radionuclide concentrations were measured by high-resolution gamma spectrometry. The results were converted into sediment dose rates by using the conversion factors of Guérin et al. (2011). The contribution of cosmic radiation was calculated using the approach of Prescott & Hutton (1994). To determine the feldspar dose rate, we used an estimated a-value (alpha-efficiency) of 0.09±0.02 (Balescu et al. 2007) and a potassium concentration of 12.5±0.5% (Huntley & Baril 1997). An accurate estimation of the water content of the sampled units over the entire time of its burial is an important but challenging task (Kenzler et al. 2017). This is especially the case for settings such as at KKH, where the investigated units were glaciotectonically dislocated and uplifted, which is likely to have altered their position relative to the groundwater table (Kenzler et al. 2015, 2017).

The luminescence measurements were performed with a Risø TL/OSL DA-20 reader equipped with a $^{90}Sr/^{90}Y$ beta source (Bøtter-Jensen et al. 2010). Pure quartz grains were mounted on stainless steel discs (6 mm spot) using an adhesive silicone oil. Determination of D_e was undertaken using a single aliquot regenerative dose (SAR) protocol (Tab. 4.2; Murray & Wintle 2000), including an early background approach (signal integral: 0.0-0.32 s, background integral: 0.32-0.96 s; Cunningham & Wallinga 2010). We applied a set of test measurements (preheat plateau, dose recovery, and thermal transfer) for representative samples LUM 3176 and LUM 3179, to select the most suitable preheat temperature for the SAR protocol (Fig. S1). The following quality criteria were applied during the SAR protocol: dose recovery within 10% of unity, IR depletion ratio >0.9, recuperation <5% of the natural signal (Duller 2003; Wintle & Murray 2006).

For K-rich feldspar D_e measurements, we used aliquots of 2.5 mm size. Measurements were conducted using a pIRIR procedure (Tab. 4.2; Buylaert et al. 2009), involving a preheat at 250 °C, followed by an IR bleach step at 50 °C for 100 s (IR_{50}). The post-IR IRSL signal was then measured at 225 °C for 200 s ($pIRIR_{225}$). After

a four-hour bleaching interval in a solar simulator (Hönle SOL2), dose recovery tests and residual dose determinations were performed using three bleached aliquots per sample. K-rich feldspars were checked for anomalous fading (Auclair et al. 2003). In the current study, the final K-rich feldspar ages were fading-corrected using the approach of Kars et al. (2008) based on Huntley (2006). Accordingly, the unfaded dose response curve (DRC) was constructed based on the measured DRC to eliminate the anomalous fading component, and includes the determination of the saturation value and saturation dose (D_0). The simulated DRC was then derived following procedures by Kars et al. (2008), who employed the quantum-mechanical tunnelling model suggested in Huntley (2006) (Fig. 4.4).
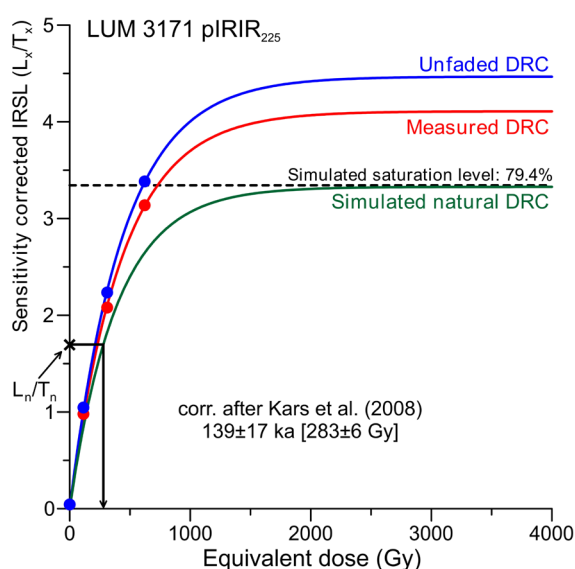
Fig. 4.4 Measured, unfaded and simulated dose response curves (DRC) for representative sample LUM 3171 using the fading-correction model by Kars et al. (2008). The saturation level is indicated by the dashed black line.

4.4 Results

4.4.1 Sedimentological description

Based on our detailed lithofacies analysis, the logged sedimentary succession at KKH was divided into ten lithological units (labelled A to K), which, where appropriate, were further divided into subunits. In general, the deposits mainly represent the shift from a subglacial (unit A) over a glaciofluvial (unit B), lacustrine (unit C to H) to subglacial (unit J) and finally glaciolacustrine (unit K) environment. An important finding of this study is the recognition of a major hiatus between the top of the unit D (Eemian) and the overlying sands of unit E (Late Weichselian; see discussion below). Detailed information on depositional features of all lithological units and subunits and their sedimentological interpretation, supported by additional evidence from microfacies

analyses (Fig. 4.6, Fig. 4.7, Fig. 4.8, Fig. 4.9 and Fig. 4.10), is given in Tab. 4.3 and Fig. 4.5.

Fig. 4.5 Summary log of the main section at Klein Klütz Höved with information on lithology, luminescence chronology, micropalaeontological MP-units, local pollen assemblage zones (LPAZ), and thin section sample positions (TS). An expanded legend is in Fig. S4.1 in the supplements.

based on [1]Miall (1985, 1996) and Benn & Evans (2010); [2]Menzel-Harloff & Meng (2015); [3]Strahl (2004).

Tab. 4.1 Lithofacies codes used in the current study with explanations about sedimentary features (based on Miall 1985, 1996 and Benn & Evans 2010).

Code	Grain size	Description
	Lithofacies codes	
Dcm	clay to boulders	clast-supported, massive diamicton
Dmm	clay to boulders	matrix-supported, massive diamicton
GRch	gravel (2 - 8 mm)	massive and infilling channels
GRcu	gravel (2 - 8 mm)	upward coarsening
GRm	gravel (2 - 8 mm)	massive and homogeneous
GRmi	gravel (2 - 8 mm)	massive with isolated, imbricated clasts
GRp	gravel (2 - 8 mm)	cross-bedded
Sd	sand	deformed bedding
Sfl	sand	flasar bedded
Sh	sand	horizontally/plane-bedded or low angle cross-laminated
Sl	sand	horizontal and draped lamination
Sm	sand	massive
Sp	sand	planar cross-bedded
Sr	sand	ripple cross-laminated
Ssr	sand	starved ripples
Frg	sand	graded and climbing ripple
Fl	clay to silt	fine laminated
Fm	clay to silt	massive
Fp	clay to silt	intraclasts or lens
Fcf	mud	massive, with freshwater molluscs
Fsc	silt, mud	laminated to massive
C	mud	swamp deposits
--- (s)		sheared
--- (d)		with dropstones
--- (w)		with detwatering structures

Tab. 4.2 Single aliquot regenerative dose (SAR) protocol applied for the equivalent dose (D_e) estimation of coarse-grained quartz and feldspar minerals (based on Murray & Wintle 2000 and Buylaert et al. 2009).

Run	Treatment	
	Quartz	K-rich feldspar
1	Dose (except before first run)	Dose (except before first run)
2	Preheat (260 °C for 10 s)	Preheat (250 °C for 60 s)
3	Stimulation with IR-diodes for 100 s at 125 °C	Stimulation with IR-diodes for 100 s at 50 °C
4	Optical stimulation with blue LEDs for 40 s at 125 °C	Stimulation with IR-diodes for 200 s at 225 °C
5	Give test dose	Give test dose
6	Cutheat at 240 °C	Preheat (250 °C for 60 s)
7	Optical stimulation with blue LEDs for 40 s at 125 °C	Stimulation with IR-diodes for 100 s at 50 °C
8	Return to run 1	Stimulation with IR-diodes for 200 s at 225 °C
9		Return to run 1

▼▼ Tab. 4.3 Lithological description, sedimentary facies interpretation and luminescence age chronology of the Klein Klütz Höved depositional succession. The grey-shaded units (A and J) indicate tills deposited by the SIS during the Saalian and Weichselian glaciations

(Sub-) units	Codes	Lithofacies and macrofossils	Interpretation	Age
K4	Fm(d), Fp(d), Ssr	~0.7 m of a thick, dark-brownish, massive **clay** with lenticularly-bedded, fine-grained sand (lenses) and distinct wavy sand layers; occurrence of isolated outsized clasts (up to 5 cm in diameter) and layers with dispersed fine-laminated clay intraclasts; fine-grained sand layer with starved ripple-lamination	**Glacio-lacustrine environment (ice-contact lake):** Rhythmically-bedded lacustrine bottomsets, interrupted by underflow or homopycnal-flow deposition representing varying flow rates and/or sediment supply (alternation of current and quiet-water conditions); rainout of dropstones from melting of ice rafts	
	GRmi(d)	~0.2 m thick bed consisting of weakly-imbricated finely-laminated **clay and silt intraclasts** (mostly 0.3 to 3 cm in diameter), isolated outsized **granite clast** up to 7 cm in diameter	Resedimention of rhythmite-derived intraclasts during rising lake level (erosional event); rainout of dropstones from melting ice rafts	
K3	Sh, Sl, Sfl(d), Sr, Fm, Frg, Sm, Sd	1.9 m parallel to ripple-laminated fine- to medium-grained **sand** with isolated lenses of coarse-grained sand and fine-grained gravel; massive clay layers in mm to cm-scale; distinct beds of wave-ripple cross-laminated sand and mud; deformation structures at the base	Traction-bedded sand (wave ripples) and rainout of debris of ice-rafted material (dropstones), suspension settling of clay and silt during quiet-water periods; density induced deformation at the base	**21±2 ka** (OSL) **17±2 ka** (OSL)
K2	Fm, Fp(w)	0.4 m massive to finely-laminated clay and silt with deformation structure (diapir, sag and flame)	Bottomsets with suspension deposits of clay and silt in a lake-like setting; soft-sediment deformation due to slumping and dewatering processes	
K1	Sm, Dcm, Dms	0.3 m poorly-sorted, clast-rich, diamictic **gravel** beds (cm to dm scale); frequent chalk clasts; mm-scale sand layers with dispersed diamictic intraclasts and fine-grained gravel	Gravitational mass movement (cohesive debris flow and/or slumping) with minor fluvial reworking in an ice-proximal setting	
J1	Dmm	Up to 5 m thick, brown-grey, clay-rich diamicton; fine-gravel content with Nordic provenance; compacted (TS 6, Fig. 4.10)	**Subglacial environment:** Deposition during an ice advance in a subglacial setting (subglacial traction till)	
J2	Dmm(s), Fm	Several dm thick, stratified, brown-reddish, clayey diamicton with scattered clast, sheared sand lenses and a basal clay layer (TS 5, Fig. 4.9)	Pseudo-stratification due to shearing at the base of the ice sheet (subglacial traction till)	
H	Sh, Sl, Sm	0.5 m thick parallel-laminated **sand** with layers showing wavy laminated sand and fines; lower portion of unit is dominated by massive gravelly sand	**(Glacio-) lacustrine environment:** Traction-bedded sand and suspension settling of clay and silt during periods of quiet-water deposition	**19±2 ka** (OSL)
G2	Fl, Fp Sh	Up to 1 m parallel-laminated **clay and silt**; distinct sand layer at base (thinning out to the channel rim); towards the top, cm-scale sediment deformation (disrupted and folded clay beds)	**Fluvial environment (fluvial distributary channel):** Suspension settling of clay and silt (channel-fill of an abandoned channel, oxbow); deformation at top induced by differences in density and possible dewatering processes (load casts)	**20±2 ka** (OSL)
G1	GRch	Cm-thick, massive, sandy, fine-grained **gravel**, containing rafts of diamictic material and finely-laminated clay / silt intraclasts at the base; sharp erosional basal contact	Erosion of channel bed and subsequent deposition of channel lag deposits in a point bar setting of a meandering river; diamicton-type rafts as well as clay and silt intraclasts derived from the eroded cut bank	
F	Sl, Sfl, Fp, Sh, Sr	1.5 m of parallel to wave-ripple cross-laminated, fine-grained **sand** with intercalated **clay and silt lenses** (mainly in ripple troughs); distinct layers of clay; towards top of the unit increasing amounts of clay and silt intraclasts (TS 4, Fig. 4.8)	**Lacustrine environment:** Combination of bedload-transported sand and suspension settling of clay and silt in a marginal shallow lake setting	**27±2 ka** (OSL)

E	Sd, Fp, Sm	Up to 0.5 m massive, medium- to coarse-grained **sand** and fine-grained gravel; irregularly undulating base with intense load structures (plus ball-and-pillow structures in D); weak flaser bedding near top of unit; Eemian shell fragments[1]	**Lacustrine environment:** Combination of traction-bedded sand and gravel and suspension settling of fines; syn- and post- depositional soft-sediments deformation at the basal contact (load casts); basal lag deposit (fine-grained gravel)	**24±2 ka** (OSL) 21±2 ka (pIRIR$_{225}$)
Eemian / Weichselian boundary				
D2	Fcf, Fsc	Up to 0.5 m of massive to laminated, **organic-rich mud** with shell fragments; mat-like mm- scale layers of algae; intercalated dark-brown peat lenses in cm-scale at the basal part (TS 3, Fig. 15B)	**Lacustrine to brackish environment:** Suspension settling of clay, silt and organic detritus from water column; laminated mat-like beds indicate events of algae blooms; redeposited peat; brackish influenced	
D1	C	Up to 0.15 thick, dark-brown **peat layer** with wood fragments (up to 0.15 m in length, partly imbricated) and plant detritus (slightly coalified)	Peat with some allochthonous (washed in) wood fragments deposited in a beach-like setting	>40 ka BP[2]
Saalian / Eemian boundary				
C2	Fcf	Up to 0.3 m, massive to faint-laminated, reddish-brown mud interbedded with mm-scale laminae of fine-grained sand; diffuse bioturbation; remnants of molluscs (*Pisidium stewarti*)[1] and scattered plant detritus (TS 2, Fig. 4.6A)	**Lacustrine environment:** Suspension settling of clay, silt and plant detritus; traction-bedded sand during phases of hyperpycnal flow events or higher sediment supply (underflows)	
C1	Sfl, Sl, Fl, (Sr)	~0.9 m of (rhythmically) interbedded fine-grained **sand, silt and clay**, yellowish-grey; faint wave-ripple cross-lamination; locally bioturbated; mollusc remnants (P*upilla loessica, Vertigo genesii, Vallonia tenuilabris*)[2], scattered plant detritus, mm-scale vertical root-like tubes, oogonian of charophyceae (TS 1, Fig. 4.7)	Combination of bedload-transported sand and suspension settling of clay, silt and plant detritus in a marginal shallow lake setting; plant growth on lake bottom	**134±12ka** (pIRIR$_{225}$) 135±12ka (pIRIR$_{225}$)
B2	Sh, Sl, (Sp), Fm, GRcu, GRmc	~0.4 m of massive, sandy, fine-grained **gravel** (grading upwards into medium-grained gravel) overlain by horizontally-bedded to low-angle, cross-laminated gravely sand; cm-scale lenses of clay in troughs and small depressions	**Glacio-fluvial environment (braided river setting):** Gravel deposition under supercritical flow conditions during flood event, forming longitudinal bars in a shallow braided channel; subsequent waning of the flood resulting in formation of traction bedded sand at the top of the bar; suspension settling of clay in small depressions during slack-water periods	
B1	Sl, Sp, GRp	0.4 to 0.5 m of tabular cross-bedded, sandy, fine-grained **gravel** with few outsized clast and cm-scale lenses of massive fine-grained sand	Migration of transverse gravel bars (foresets) from sediment-loaded currents; deposition of traction-bedded sand due to waning of stream velocity, water depth and/or meltwater discharge	**139±17ka** (pIRIR$_{225}$)
A	Dmm	>2 m thick, massive, matrix-supported clay-rich **diamicton** with dispersed clasts (cm- to dm-scale); fine-gravel content with Baltic provenance; greenish grey to grey in colour (uppermost 0.2 to 0.4 m spots with reddish oxidation staining), compacted	**Subglacial environment:** Deposition during ice advance in a subglacial setting (subglacial traction till), uppermost part weathered	Saalian Glaciation (MIS 6)

[1]Menzel-Harloff & Meng (2015); [2]Krbetschek (1995)
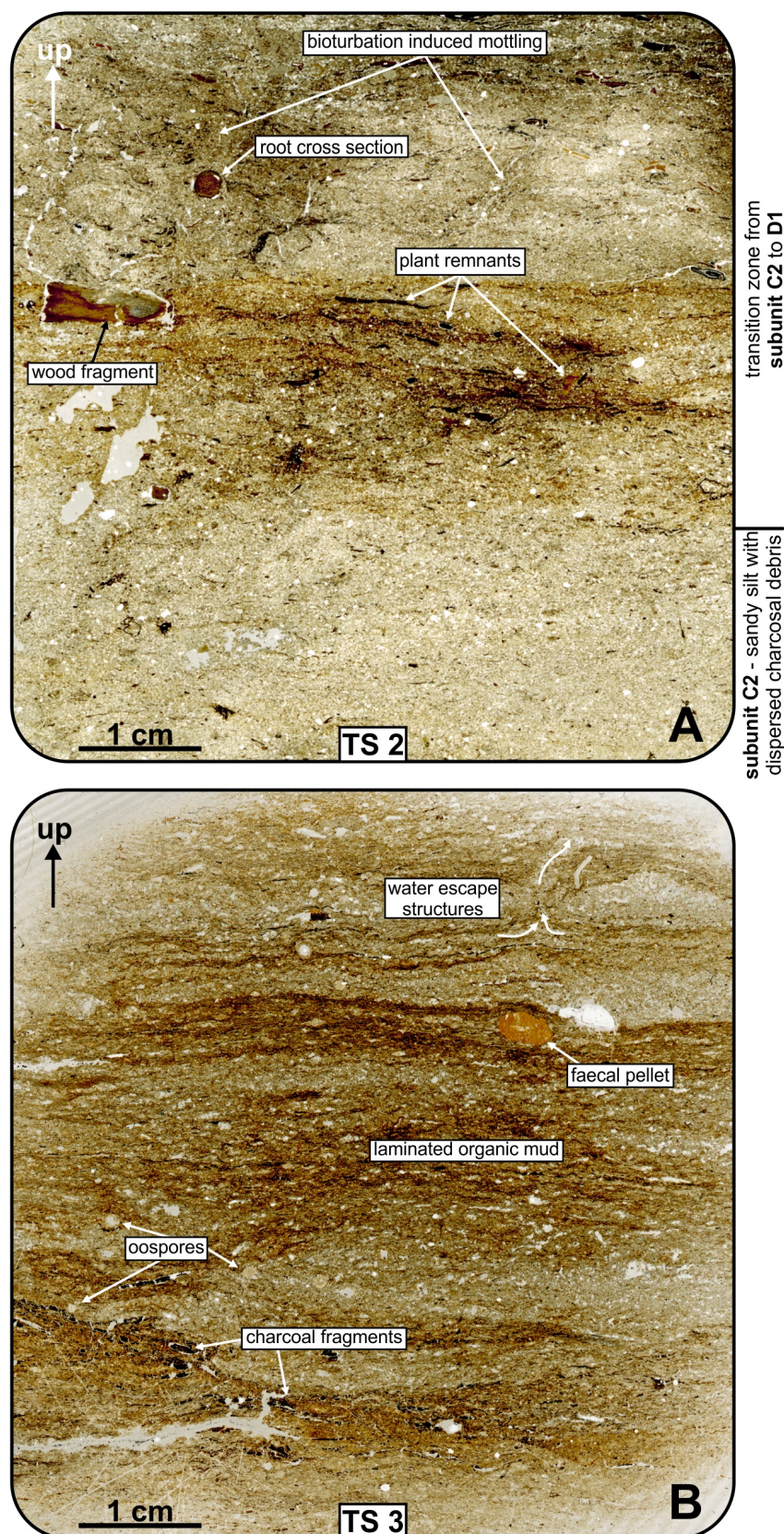
Fig. 4.6 A. Thin section scan of sample TS 2 obtained from the transition zone between subunit C2 and subunit D1. Note the increase of plant matter starting in the middle part of the scan and disturbed stratification towards the top, suggesting diffuse bioturbation and a reduced rate of accumulation. B. Thin section scan of sample TS 3 from the lower part of unit D2. The image displays the laminated character of unit D2, with dispersed oospores, plant remnants and a diatom-rich faecal pellet.
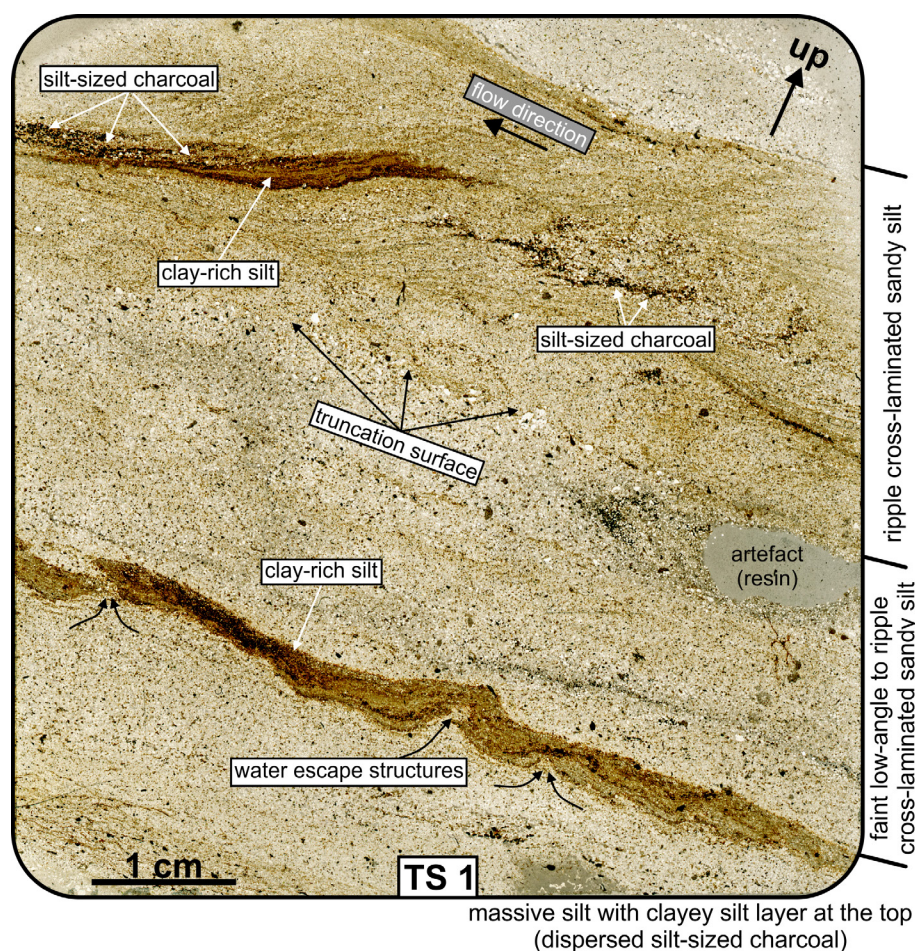
Fig. 4.7 Thin section scan of sample TS 1 obtained from the laminated lower part of subunit C1. Note the ripple cross-laminated sandy silt, which is locally draped by clay-rich silt layers.

Fig. 4.8 Thin section scan of sample TS 4 showing traction-bedded sands of unit F, which are intercalated with layers of clay and silt. Visible are couplets with a fining-upwards trend, indicating repeated waning of the flow velocity. Water escape structures may result from high rates of deposition.
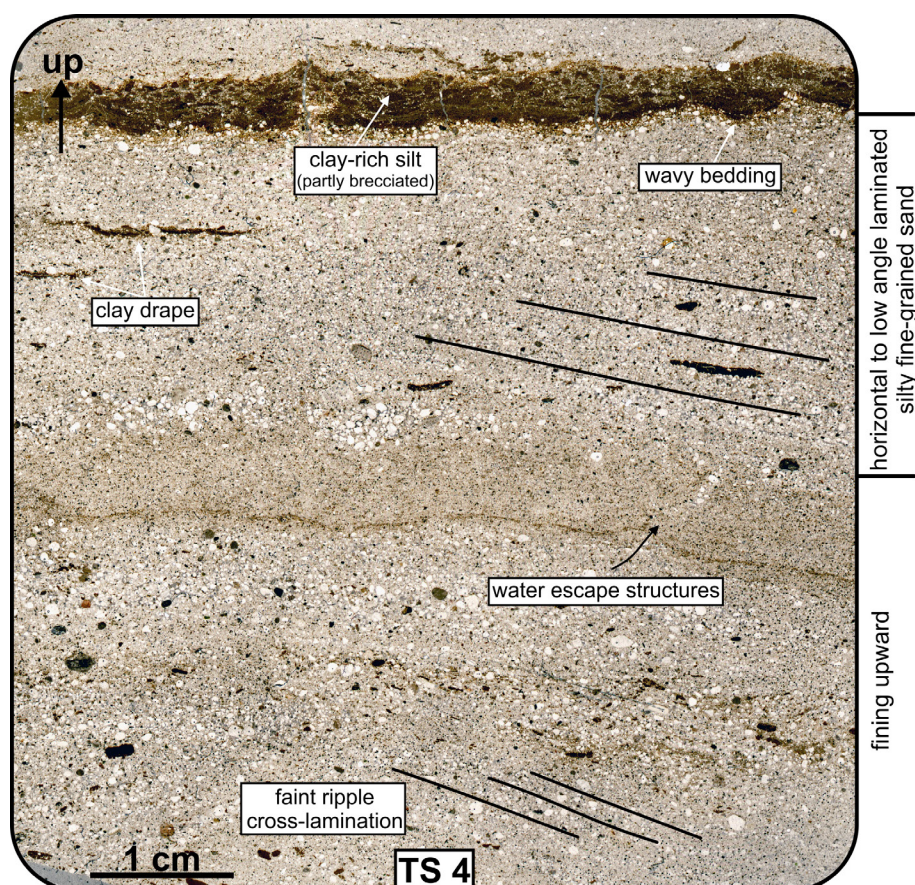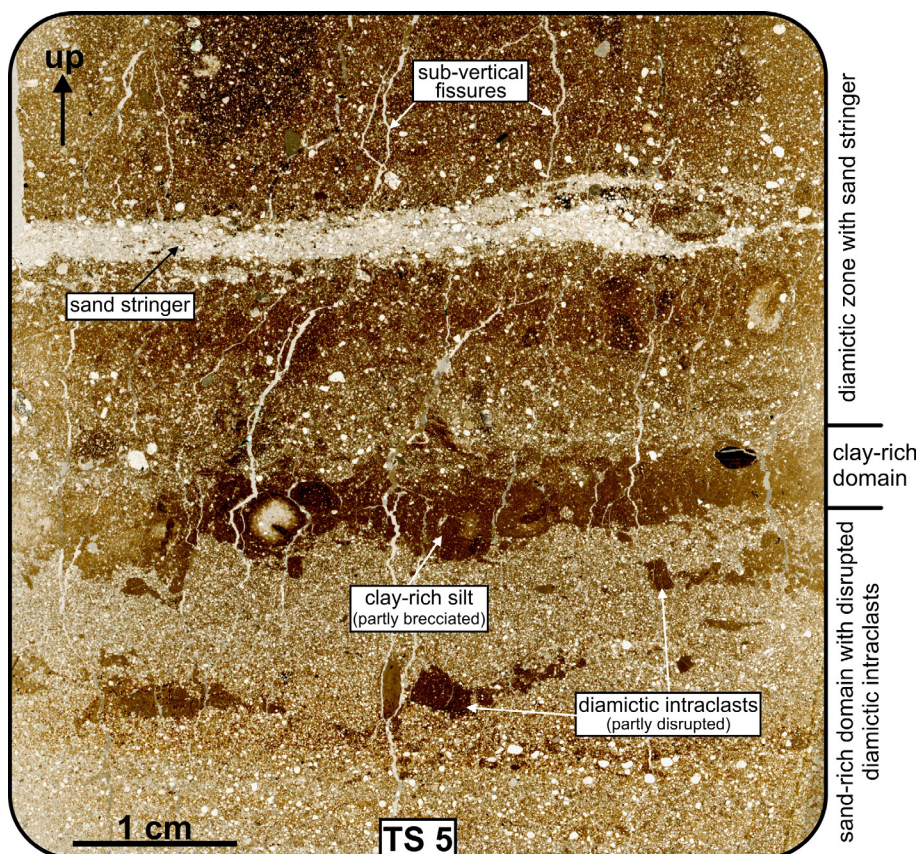
Fig. 4.9 Thin section scan of sample TS 5 from the basal zone of the subglacial traction till of subunit J1. The pseudo-stratified domains comprise better-sorted sand, clay-rich silt and poorly-sorted diamictic material incorporated by subglacial shearing processes.
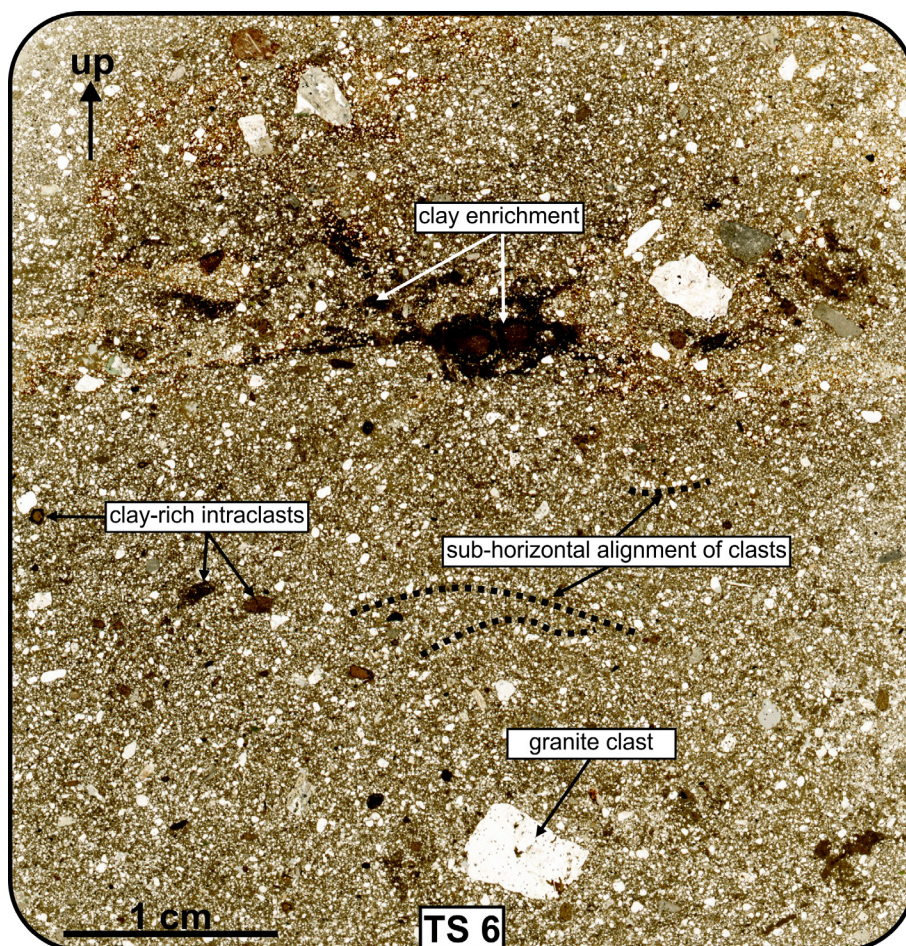
Fig. 4.10 Thin section scan of sample TS 6 showing the clast-rich and massive subglacial traction till of subunit J2, with a high content of angular to subangular gravel clasts.
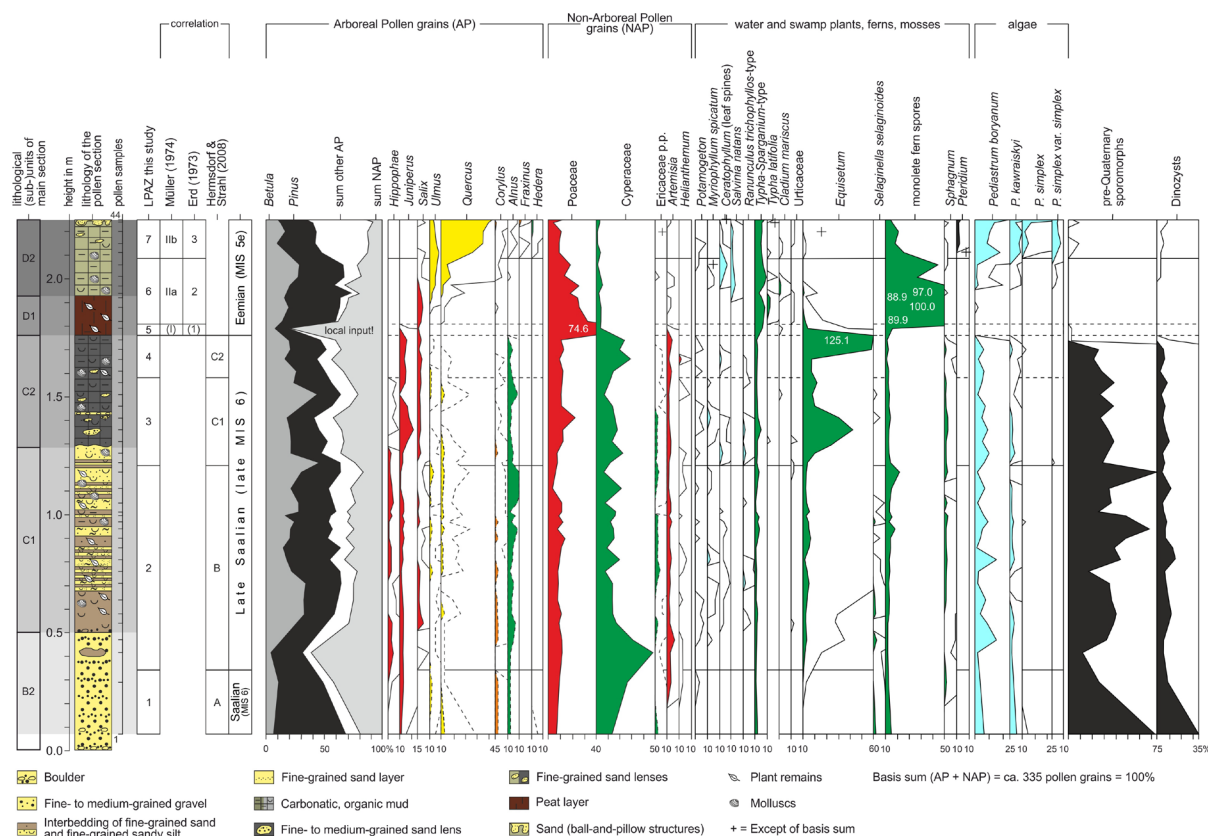
Fig. 4.11 Pollen diagram showing selected taxa from the pollen section at Klein Klütz Höved Fig. 4.1B) with resulting local pollen assemblage zones (LPAZ) and their correlation to the reference pollen stratigraphies (Pollen Zones, PZ) by Müller (1974), Erd (1973) and Hermsdorf & Strahl (2008). Basis sum AP + NAP = ±335 = 100%, excluding swamp- and water plants, sporae, algae and other micro remains, values <1% with tenfold exaggeration; + = out of basis sum; dotted lines = presumably also reworked pollen from older interglacial rsp. from Tertiary.

4.4.2 Palaeontological results

Pollen analysis. – The counted pollen at KKH derive from three different sources, with reworked pollen grains dominating in the lower part of lithostratigraphic unit I-I (subunit B2; Fig. 4.5), locally sourced pollen forming the majority in the lower part of subunit D1, and a regional pollen signal dominating in the lacustrine strata of unit C, and upwards from the middle part of subunit D1 to D2. We identify seven local pollen assemblages zones (LPAZ). Based on their palaeobotanical features and succession of tree taxa, we associate LPAZ 1 with the end of the Saalian pleniglacial, LPAZ 2-4 with the Late Saalian stage, and LPAZ 5-7 with the Eemian interglacial. These correlations follow the regional Saalian Pollen Zones (PZ) by Hermsdorf & Strahl (2008) and the Eemian PZ from Erd (1973). The detailed results of the pollen counting are given in Tab. S4.1 (supplementary information).

• LPAZ 1 – Saalian pleniglacial PZ A (treeless environment)

The reconstructed vegetation history at the KKH starts in the upper part of the glaciofluvial deposits (B2, Fig. 4.5) that overlie the lowermost till, with LPAZ 1 indicating a treeless environment of an open arctic landscape dominated by herbs (NAP) and *Selaginella selaginoides*. In addition, very few dwarf shrubs of *Juniperus* and *Betula* appeared (Fig. 4.11, Tab. S4.1). The local setting was characterised by Cyperaceae, while water plants were still missing, aside from an algae flora containing *Pediastrum boryanum* and *P. kawraiskyi* indicative of cool temperatures. Larger amounts of reworked, mainly Tertiary sporomorphes, dinocysts, some Mesozoic taxa, and older Quaternary interglacial forms (i.a. *Azolla filiculoides* – Holsteinian age?) are common within this zone and up to LPAZ 4. As the distribution of *Pinus* closely follows the pollen curves of the reworked pre-Quaternary sporomorphs (Fig. 4.11), we consider this taxa to be an allochthonous element. LPAZ 1 correlates with the lower portion of lithostratigraphic subunit B 2 (Fig. 4.11).

• LPAZ 2 – Late Saalian PZ B (*Hippophaë* communities)

An increasingly vegetated environment under subarctic climate conditions is recorded by LPAZ 2 (Fig. 4.11), showing a trend of expanding *Hippophaë* communities, *Betula* and *Salix*, accompanied by a more frequent occurrence of herbs (most notably Poaceae, *Artemisia*, and some *Helianthemum*). LPAZ 2 also indicates the spread of a local swamp and water flora with Cyperaceae, *Equisetum*, *Typha-Sparganium*-type and *Myriophyllum spicatum* among others (Tab. S4.1). LPAZ 2 corresponds to lithological subunits B2 (upper part) and C1 (Fig. 4.11).

• LPAZ 3 – Late Saalian PZ C1 (*Betula-Juniperus-Hippophaë* communities)

The following LPAZ 3 comprises an expansion of *Betula-Juniperus-Hippophaë* communities, showing a gradually ameliorating (warmer) climate and a shift from shrub-like to dendriform birches. Within the existing water plant communities, we observe a spread-out of *Equisetum*, Cyperaceae and *Typha-Sparganium*-type, while the composition of the herb flora remained largely unaltered, with the exception of the new occurrence of Tubuliflorae, Rosaceae p. p. and *Thalictrum* (Tab. S4.1).

• LPAZ 4 – Late Saalian PZ C2 (*Betula-Juniperus-Pinus* communities)

The overlying LPAZ 4 shows an increase of *Betula-Juniperus-Pinus* communities, with a weakly developed *Pinus* pollen signal but no macro remains of this tree taxon. The higher amounts of *Pinus* presumably trace back to an increased input from long-distance transported pollen grains, accompanied by a simultaneous decline of pre-Quaternary sporomorphes. The local surroundings are furthermore dominated by Cyperaceae-*Equisetum* communities, which we interpret as a sign of more ponding in the area. Overall, LAPZ 3 and 4 correlate with the uppermost part of lithological subunit C1 and subunit C2 (Fig. 4.11).

• LPAZ 5 – Eemian PZ 1 (*Betula*)

LPAZ 5 correlates with the lower part of lithological subunit D1 (Fig. 4.5) and is marked by a very pronounced rise of Poaceae (Fig. 4.11), indicating the spread of sweet grass taxa under cool-temperate climate conditions during peat accumulation. It is likely that this phase coincides with a climatic amelioration (warming), which is also indicated by the simultaneous decline of the Lateglacial taxa *Juniperus* and *Artemisia*. Taken together we interpret these indicators to represent a climatic setting consistent with the early onset of the Eemian interglacial, but we note that the dominance of locally sourced pollen grains hinders an unambiguous biostratigraphic interpretation of LPAZ 5 (Fig. 4.11).

• LPAZ 6 – Eemian PZ 2 (*Pinus-Betula*)

The overlying LPAZ 6 displays a prominent rise of *Pinus*, forming boreal forest communities together with *Betula* and *Salix*. Local swamp areas are represented by Poaceae, *Typha-Sparganium*-type, *Typha latifolia*, *Cladium mariscus* and ferns. The observed replacement of Cyperaceae, *Equisetum* and water plants is likely to reflect the successive infilling of the water basin at KKH, followed by the accumulation of peat. In the upper part of LPAZ 6, levels of *Ulmus* and *Quercus* increase together with thermophile and open quiet-water elements such as *Salvinia natans* and *Ceratophyllum* sp. (leaf spines). LPAZ 6 encompasses the upper portion of subunit D1 and the lower part of D2 (Fig. 4.5, Fig. 4.11).

• LPAZ 7 – Eemian PZ 3 (*Pinus-Quercetum*)

LPAZ 7 shows the Eemian expansion of *Quercus* accompanied by *Ulmus* and the first traces of *Alnus*. The rise of *Corylus* typical of the later stages of PZ 3 (Erd 1973) is missing, suggesting that PZ 3 is incompletely preserved at the investigated pollen section. Various *Pediastrum* species (*e.g. P. boryanum*, *P. kawraiskyi*, and *P. simplex*) are becoming more widespread and the occurrence of dinocysts is also noted. Finally, we find evidence for *Hedera*, already present sporadically in LPAZ 6, highlighting a growing influence of oceanic climate conditions at KKH during this time. LPAZ 7 correlates with the upper half of subunit D2 (Fig. 4.5, Fig. 4.11).

Microfossils. – We documented at least fifteen ostracod and two foraminifer taxa in the KKH section (Fig. 4.12). Beside those groups, other fossils include gyrogonites and oospores of charophytes, fruits and seeds, ephippia of cladocerans, insect remains, an oribatid mite, molluscs and reworked pre-Quaternary microfossils of mainly Upper Cretaceous age. Calcareous fossils show frequent traces of dissolution, while aragonitic shells are extremely rare. Delicate microfossils are often broken, probably by sediment compaction. A cluster analysis examining the abundance of the various fossil groups revealed three sample clusters dividing the profile into four micropalaeontological units (MP-units): (i) MP-unit 1 (samples 1-10), (ii) MP-unit 2 (samples 11-20), and (iii) MP-unit 3 (samples 21-25c), and MP-unit 4 (samples 26-29) (Fig. 4.12).

• MP-unit 1

MP-unit 1 (Fig. 4.12), in the lower part of the profile, contains a small number of plant fragments, which slightly increases towards the top of the MP-unit, but never becomes more than twenty pieces per sample. Present in low numbers are also reworked Upper Cretaceous foraminifers (*e.g. Bolivina incrassata* Reuss, 1851), with a maximum number of thirteen specimens in sample 7 and some not identifiable (poorly preserved) small mollusc fragments across most samples.

• MP-unit 2

MP-unit 2 contains numerous plant remains, freshwater ostracods and molluscs in most samples. The preservation of the mollusc remains improves in the upper part of this MP-unit. Juvenile stages of unspecified freshwater snails, some small terrestrial snails (sample 13) and *Pisidium* valves (sample 14 and 17) occur. Samples 14 to 18

contain a diverse fauna dominated by freshwater ostracods such as candonids (*Limnocythere inopinata*, *Limnocytherina sanctipatricii* and *Ilyocypris* sp.), increasing upwardly in number to over 300 specimens per sample. Interesting is the occurrence of males of *Limnocythere inoptinata* in the upper part of the MP-unit. Sample 16 is characterised by a high gyrogonite number. Apart from a few mollusc fragments, the last two samples of this MP-unit lack calcareous fossils.
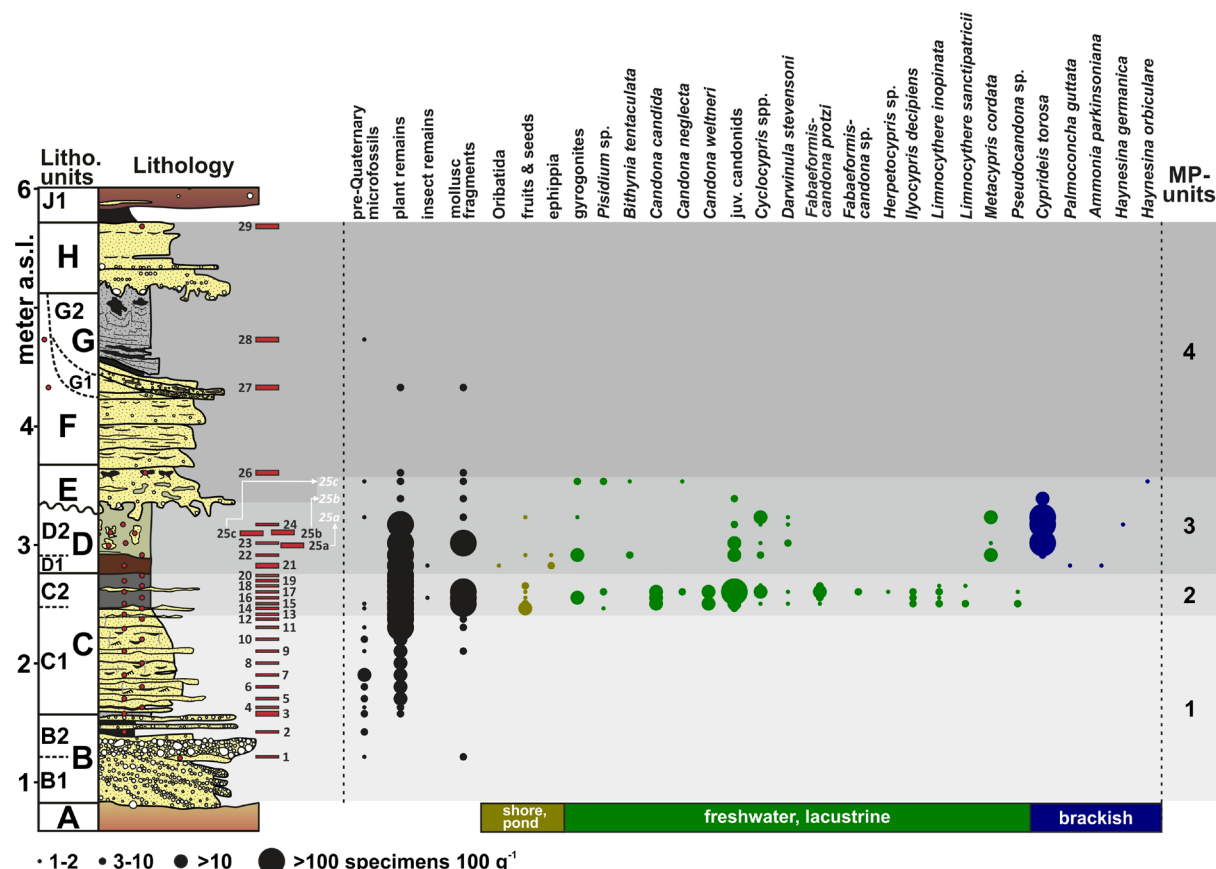
Fig. 4.12 Microfossil distribution within lithological units B to H of the main section at Klein Klütz Höved and inferred micropalaeontological units (MP-units). Red bars with corresponding sample labels depict the sample position (where bar height indicates sample thickness). Note that the micropalaeontological results for samples 25a, b and c are visually separated (white arrows and sample labelling) and placed above sample 24.

• MP-unit 3

MP-unit 3 also yields high but upwardly decreasing amounts of plant litter. As new features, MP-unit 3 records the occurrence of the ostracod *Cyprideis torosa* and locally elevated numbers of *Metacypris cordata* and *Cyclocypris* spp. (Fig. 4.12). Ephippia of cladocerans are typical for the basal part of this MP-unit, where an oribatid mite was found as well. In addition, foraminifers and opercula of the snail *Bithynia tentaculata*

occur in low numbers within MP-unit 3. Interestingly, the sands comprising the ball-and-pillow structures within subunit D2 contain an ostracod spectrum that closely resembles that of the surrounding muds (samples 25a – 25c; Fig. 4.12; see discussion).

• MP-unit 4

MP-unit 4 (samples 26-29) contains a high proportion of reworked pre-Quaternary microfossils and low amounts of plant fragments, which disappear entirely towards the top.

Overall, the fauna documented in the KKH section closely resembles the species listed by Strahl et al. (1994) and leads to a comparable reconstruction of the site evolution: A cold freshwater water fauna (MP-unit 2) evolves from a (late) glacial fauna of low diversity (MP-unit 1; Fig. 4.5). The following MP-unit 3 also contains freshwater microfossils and the brackish water ostracod *Cyprideis torosa*, which indicate ameliorating interglacial climatic conditions. By contrast, the overlying and nearly fossil-barren MP-unit 4 provides clear evidence for a return to deposition under cold-climate conditions.

4.4.3 Luminescence dating

In all cases, a fast decay of the luminescence signal was observed within the first second, indicating that the signal was dominated by the fast OSL component (Fig. 4.14; Cunningham & Wallinga 2010). Based on initial test measurements on two representative samples (LUM 3176 and LUM 3179; Fig. 4.13), we chose a preheat temperature of 260 °C, which was held for 10 s, and a cutheat of 240 °C. The average recycling ratio of all accepted aliquots was 1.03±0.04 (n = 178).

As expected, the residual dose of the IRSL and post-IR IRSL signals increased for samples with higher De values, as demonstrated by our stratigraphically oldest sample (LUM 3171), yielding an average residual dose of 11 Gy, while the stratigraphically younger sample LUM 3174 showed an average residual dose of 5 Gy. The results of the dose recovery test for the $pIRIR_{225}$ protocol were within 10% of unity after subtraction of the residual dose, indicating that the given dose was well-recovered with the applied protocol. The recuperation values ranged from 1.5 to 3.3%, which is satisfactory. The athermal instability for the $pIRIR_{225}$ signal, displayed by the g-value,

was relatively small with values between 1.0 – 1.4% per decade. The corresponding g-values for the IR_{50} signal were significantly higher (3.0 – 4.0% per decade; Tab. 4.6).

The natural (in situ) water content of all samples was between 2 and 8% of the dry weight (Tab. 4.4). Given that all samples were recovered from the dry face of the outcrop, we assume that the measured natural water content represents the minimum value over the length of burial. Conversely, the maximum water content (saturation level) was calculated for all samples to range between 15 and 32%. Based on the geological setting of the sampled sediments, it is reasonable to assume that the investigated units were at or near water saturation levels for most of the burial time. Thus, in our dose rate estimation, we used the individual maximum water content, including a 5% error, to account for potential uncertainties (Tab. 4.4). We found no evidence of significant radionuclide disequilibria within the ^{238}U decay chain.

The averaging effect from using 6-mm-aliquots may mask potential problems due to partial bleaching, even if, as is the case in our dataset, the measured overdispersion is relatively low (between 9 and 17% for most samples, Tab. 4.5). We found no significant difference between the statistical mean D_e values and the corresponding D_e values calculated using the central age model (Tab. 4.5; Galbraith et al. 1999). Therefore, we used the mean D_e of each sample for the final age calculation. For three samples (LUM 3171, LUM 3172 and LUM 3173), the mean quartz D_e reached values between 116 and 146 Gy, suggesting that these samples may approach saturation levels (Buylaert et al. 2011). Cross-checking with the corresponding K-rich feldspar ages (Murray et al. 2012) also indicated that the quartz results represent an age underestimation. Hence, for samples LUM 3171, LUM 3172 and LUM 3173, we used the mean K-rich feldspar D_e values to derive final ages. To correct for anomalous fading, we compare correction models by Huntley & Lamothe (2001) and Kars et al. (2008), showing that the latter ages are 5 - 10% higher (Tab. 4.6). Although some studies have shown that the Huntley & Lamothe (2001) model may also be used to correct samples >100 ka (Buylaert et al. 2011), the use of this method should be restricted to the linear part of the dose response curve, usually representing materials no older than 20-50 ka. Given that samples LUM 3171, LUM 3172 and LUM 3173 were obtained from units that are pre-Eemian in age, as independently evidenced by their stratigraphic context and palaeontological inventory (see discussion), we base our final K-rich feldspar age calculation on the Kars et al. (2008) fading correction model (Fig. 4.5, Tab. 4.6).
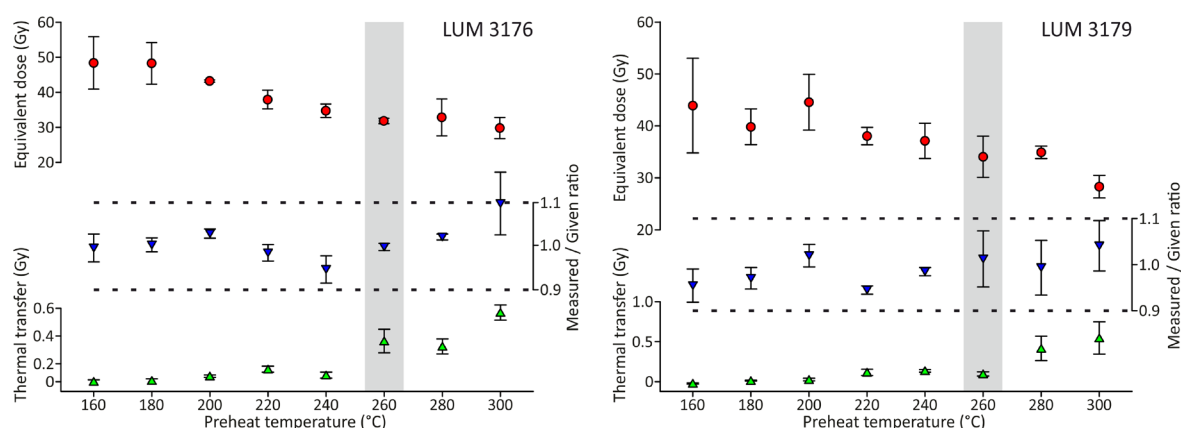
Fig. 4.13 Summary of luminescence test measurements (preheat plateau, dose recovery and thermal transfer) for coarse-grained quartz of samples LUM 3176 and LUM 3179. Each data point represents the mean value from three individually measured 6 mm aliquots. Based on these results, a preheat temperature of 260 °C (grey shaded) and a cutheat of 240 °C was used in the SAR protocol.
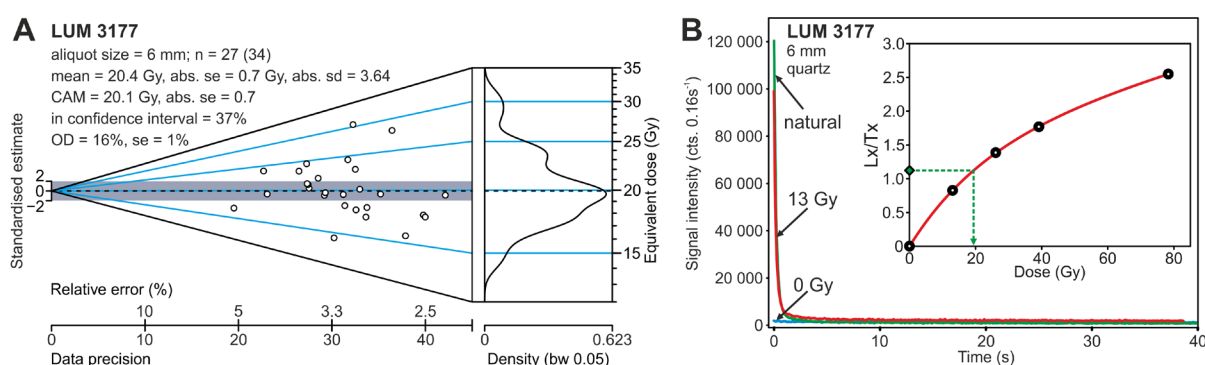
Fig. 4.14 A. Abanico plot for the coarse-grained quartz sample LUM 3177, illustrating results of the equivalent dose measurements. B. Decay curve for natural (green), 0 Gy (blue) and 13 Gy (red) dosed signals for the same sample.

Tab. 4.4 Dosimetry results for quartz and feldspar, information on water content, geographic altitudes and sample depth below ground used for luminescence age determination at KKH.

Sample ID	Altitude (m a.s.l.)	Depth below ground (m)	Potassium (%)	Thorium[1] (ppm)	Uranium[2] (ppm)	Water content *in situ* (%)	Water content used for age calculation (%)	Quartz dose rate (Gy ka^{-1})	Feldspar dose rate[3] (Gy ka^{-1})
LUM 3179	11.0	8.5	1.45±0.07	5.17±0.26	1.71±0.09	6.5	28±5	1.71±0.12	-
LUM 3178	11.0	8.5	1.38±0.07	3.78±0.19	1.33±0.07	4.8	28±5	1.52±0.11	-
LUM 3177	9.0	10.5	0.95±0.05	2.14±0.11	0.79±0.04	4.9	24±5	1.05±0.09	-
LUM 3176	8.0	11.5	1.47±0.07	3.71±0.19	1.23±0.06	5.9	24±5	1.61±0.12	-
LUM 3175	8.0	11.5	1.15±0.06	3.96±0.20	1.29±0.06	3.4	23±5	1.39±0.10	-
LUM 3174	7.0	12.5	1.44±0.07	4.82±0.24	1.43±0.07	5.1	23±5	1.69±0.12	2.25±0.13
LUM 3173	5.2	14.3	1.24±0.06	2.75±0.14	0.91±0.05	3.9	24±5	1.31±0.10	1.86±0.12
LUM 3172	5.0	14.5	1.30±0.07	2.91±0.15	0.95±0.05	7.8	21±5	1.41±0.11	1.96±0.12
LUM 3171	4.5	15.0	1.21±0.06	3.09±0.15	0.96±0.05	2.6	17±5	1.39±0.11	2.03±0.20

[1] Thorium concentration was calculated from the activities of ^{228}Ac, ^{208}Tl and ^{212}Pb

[2] Uranium concentration was calculated from the activities of ^{214}Pb and ^{214}Bi

[3] The potassium concentration within the feldspar is assumed with 12.5±0.5% (Huntley & Baril 1997)

Tab. 4.5 Sample information, luminescence data and resulting OSL ages. Final ages are given as central age model values and unweighted arithmetic means.

Sample	Aliquot size	No. of aliquots[1]	Mean D_e (Gy)	CAM D_e (Gy)	Overdispersion (%)	Total dose rate	Mean age (ka)[2]	CAM age (ka)
LUM 3179	6 mm	23 (24)	36.1±1.3	35.5±1.3	17.3	1.71±0.12	**21.1±1.7**	20.8±1.6
LUM 3178	6 mm	22 (24)	25.4±0.8	25.2±0.8	13.3	1.52±0.11	**16.7±1.5**	16.5±1.3
LUM 3177	6 mm	27 (34)	20.4±0.7	20.1±0.7	16.5	1.05±0.09	**19.4±1.7**	19.1±1.7
LUM 3176	6 mm	23 (24)	31.5±1.2	31.1±1.1	16.9	1.61±0.12	**19.6±1.6**	19.3±1.6
LUM 3175	6 mm	22 (24)	37.0±1.5	36.5±1.3	16.1	1.39±0.10	**26.5±2.3**	26.2±2.2
LUM 3174	6 mm	24 (24)	41.0±0.8	40.9±0.8	8.6	1.69±0.12	**24.3±1.8**	24.2±1.8
LUM 3173	6 mm	14 (16)	124±6	122±6	17.4	1.31±0.10	94.5±8.8	93.0±8.6
LUM 3172	6 mm	14 (16)	116±3	115±3	10.0	1.41±0.11	82.2±6.8	81.4±6.7
LUM 3171	6 mm	16 (16)	146±9	142±9	23.8	1.39±0.11	105±13	102±13

[1] Total number of measured aliquots and aliquots that passed criteria (in parentheses)

[2] Bold numbers refer to the most reliable age

Tab. 4.6 Results of post-IR IRSL equivalent dose (D_e) measurements of 2.5 mm aliquots, including the mean D_e, mean g-values, uncorrected and fading-corrected ages, for both the pIRIR$_{225}$ signal and the IR$_{50}$ signal. Bold numbers indicate fading-corrected ages (Kars et al. 2008), which are interpreted to represent the most reliable age estimates

Sample	Aliquot size	No. of aliquots[1]	pIRIR$_{225}$ D_e (Gy)	pIRIR$_{225}$ g-value (% decade^{-1})	pIRIR$_{225}$ age (ka) uncorr.	pIRIR$_{225}$ age (ka) corr.[2]	pIRIR$_{225}$ age (ka) corr.[3]	IR$_{50}$ D_e (Gy)[4]	IR$_{50}$ g-value (% decade^{-1})
LUM 3174	2.5 mm	6 (6)	42.1±1.2	1.1±0.3	18.7±1.5	21.9±1.9	20.6±1.8	35.4±1.7	3.0±0.4
LUM 3173	2.5 mm	6 (6)	215.9±7.6	1.0±0.0	116±8	**134±12**	128±12	210±11	3.1±0.4
LUM 3172	2.5 mm	6 (6)	213.7±4.4	1.4±0.2	113±10	**135±12**	130±12	201±3	4.0±0.2
LUM 3171	2.5 mm	6 (6)	228.0±6.6	1.2±0.2	112±11	**139±17**	126±13	225±5	3.3±0.1

[1] Total number of measured aliquots and aliquots that passed criteria (in parentheses)   [2] fading corrected after Kars et al. (2008) based on Huntley (2006)

[3] fading corrected after Huntley & Lamothe (2001)   [4] IR$_{50}$ signal was obtained from the pIRIR$_{225}$ protocol

4.5 Discussion

4.5.1 Reliability of the age data

Based on palaeontological zonation of the KKH section presented here and by Strahl et al. (1994) and Menzel-Harloff & Meng (2015), the luminescence ages for the basal units B and C (samples LUM 3171, LUM 3172 and LUM 3173) fall into the Late Saalian period (PZ A-B, MIS 6). The fading-corrected pIRIR$_{225}$ K-rich feldspar ages (Tab. 4.6) for the samples yield ages of 139±17 ka (LUM 3171), 135±12 ka (LUM 3172), and 134±12 ka (LUM 3173), which are in excellent agreement with the palaeontological results. However, the resulting quartz luminescence ages range from 105 to 82 ka (Tab. 4.5), indicating an age underestimation of ~30%, which is probably related to the quartz saturation effects (Murray & Funder 2003; Murray et al. 2007). The samples from the stratigraphically overlying units E and F (LUM 3174, LUM 3175) yielded much

younger but overlapping ages of 24±2 and 27±2 ka, followed by two samples from units G and H (LUM 3176, LUM 3177), which gave consistent ages of 20±2 and 19±2 ka. The dated materials were accumulated in (glacio-)fluvial to glaciolacustrine depositional environments, where issues due to incomplete exposure to sunlight during transport (*i.e.* partial bleaching) are common (Fuchs & Owen 2008; Murray et al. 2012). However, the good agreement between the OSL and the fading-corrected pIRIR$_{225}$ age for sample LUM 3174 (Tab. 4.5, Tab. 4.6) indicates no serious bleaching problems (Murray et al. 2012). We also note that the observed individual age scatter for the sampled subunits is small, and that the ages for the units E to H are chronostratigraphically consistent.

The uppermost unit K yields OSL ages of 17±2 ka (LUM 3178) and 21±2 ka (LUM 3179). During the accumulation of unit K (Fig. 4.5, Tab. 4.3) in an ice-contact lacustrine environment proximal to the ice front, partial bleaching has probably occurred. For OSL sample LUM 3179, a small overestimation of the true burial age seems to be possible, especially in comparison to samples LUM 3177 (19±2 ka) and 3178 (17±2 ka). Therefore, with regard to the overall chronology of the KKH section, the age of 17±2 ka (LUM 3178) of unit K is more likely than 21±2 ka (LUM 3179).

4.5.2   Palaeoenvironmental and geochronological implications

Based on the palynological results and the presented luminescence age chronology, the KKH section can be stratigraphically subdivided into four parts (see Fig. 4.5, Fig. 4.11, Fig. 4.12, Tab. 4.3): (i) a lowermost Saalian pleniglacial succession (PZ A; subunits A, B1 and lower B2), (ii) a Late Saalian succession (PZ B to C2; upper part of subunits B2 and C, encompassing MP-units 1 to 2), (iii) an early Eemian part (PZ 1-3; unit D and MP-unit 3), and (iv) a Late Weichselian succession (units E to K and MP-unit 4) above a substantial hiatus.

Deposition during the Saalian pleniglacial period (MIS 6). – The deposition of the basal subglacial traction till (unit A) was associated with an SIS advance during the Saalian glaciation, which matches earlier analyses of till provenance-indicators (fine gravel analyses; Ullerich 1991; Müller 2004a). This is followed by a period of glacial retreat, which established a braided river system that drained meltwaters from the decaying ice front. Sedimentary features of subunits B1 and B2, including normally-graded and horizontally-bedded fine-gravel to gravelly sand transported in an upper flow regime

(Tab. 4.3, Fig. 4.5), indicate deposition associated with frequent variations in meltwater volume (flood events). A glaciofluvial context is indirectly supported by high amounts of reworked Tertiary and older interglacial (Holsteinian?) palynomorphs (PZ A and B), and the presence of fractured pre-Quaternary microfossils (MP-unit 1). The pollen content of lower subunit B2 (PZ A) shows a treeless landscape with abundant Poaceae, *Selaginella selaginoides*, *Artemisia* and dwarf shrubs of *Betula* and *Juniperus*, pointing to arctic climate conditions during the late MIS 6 deglaciation (Termination II; Landais et al. 2013). This is consistent with the reported fading-corrected K-rich feldspar age of 139±17 ka for subunit B.

The following unit C, deposited during the Late Saalian PZ B to C2, shows a shift towards a lacustrine environment, characterised by suspension-settling of fines (clay, silt) and the deposition of traction-bedded sands, associated with higher energy inflow events (Fig. 4.7). Wave action affected the deposition of subunit C1 (Fig. 4.15A), indicative of a shallow lake basin (water depth <5 m; de Raaf et al. 1977), possibly in context of an oxbow lake or kettle depression (melting dead ice). Plants such as Cyperaceae, *Equisetum* and *Typha-Sparganium*-type point to marshy lakeshore conditions and fluctuating water levels. The appearance of freshwater ostracods (MP-unit 2) and a dominance of shrub communities in the lake surroundings, including *Betula*, *Juniperus* and *Salix*, imply a gradual warming trend within an open woodland environment (Fig. 4.11, Fig. 4.12). Towards the top of unit C, the pollen data indicate a climatic setting approaching a cool temperate climate, which is consistent with the occurrence of cold water ostracods (MP-unit 2) and cool-climate molluscs (Menzel-Harloff & Meng 2015; Fig. 4.5) within PZ-C2. Two luminescence ages of 135±12 and 134±12 ka confirm the pollen stratigraphy and suggest that unit C accumulated during the Late Saalian period.

The Eemian stage (MIS 5e). – The transition from unit C to D is characterised by a marked increase of wood fragments and other plant detritus (Fig. 4.15B), as shown in thin section TS 2, which was obtained from the uppermost part of unit C (Fig. 4.6A). Sedimentologically, this phase was accompanied by a drop in lake level, leading to a period of dominantly organic accumulation (peat of subunit D1, PZ (1)-2). Subsequently, lake levels rose again, re-establishing calm water deposition along with a higher input of fine-grained organic detritus (subunit D2; Fig. 4.6B). Based on the presented luminescence chronology for the underlying unit C (135±12 and 134±12 ka), and the biostratigraphical correlation to Eemian PZ (1)-3 after Erd (1973), the

deposition of subunit D occurred during the Eemian interglacial (MIS 5e, Fig. 4.11). Typically, the interglacial onset is indicated by the spread of birch, followed by boreal pine forests and the expansion of thermophile deciduous forest elements dominated by *Quercus* and *Ulmus*. During this time, most cold-water ostracod taxa disappear and are replaced by warm-water indicators such as *Metacypris cordata* (Griffiths & Evans 1995) and *Cyprideis torosa*, the latter requiring water temperatures >12 °C for hatching (Theisen 1966). Ameliorating climate conditions are also inferred from our documentation of marshy plants such as *Cladium mariscus* and the waterfern *Salvinia natans*, together with the appearance of the regional interglacial index species *Belgrandia germanica* (snail) within subunit D2 (Menzel-Harloff & Meng 2015). Palynologically, the Eemian succession at KKH ends within PZ 3, before the typical spread of *Corylus* within this pollen zone. We find no in situ evidence of the subsequent PZ 4 to 9, indicating that the local interglacial record is truncated with at least 10 ka of the younger Eemian missing. Based on a correlation to the Eemian reference site at Bispingen, where the duration of interglacial pollen zones is constrained by varve counting (Müller 1974), the accumulation of unit D at KKH occurred within less than 750 years after the beginning of the Eemian period.

A critical issue for the interpretation of subunit D2 is the occurrence of the ostracod *Cyprideis torosa* (noded form) along with *Metacypris cordata*, some marine dinocysts and foraminifers during PZ 2 and 3. This may suggest a brackish-influenced environment during deposition (indicating beta-oligohaline salinity; Gramann 2000; Frenzel et al. 2010, 2012; Pint et al. 2012). Menzel-Harloff & Meng (2015), however, documented exclusively terrestrial to lacustrine molluscs from unit D at KKH, with no evidence of a brackish or marine influence. Furthermore, the occurrence of *Salvinia natans* (this study) and fish remains (*e.g. Tinca tinca*, *Esox lucius*, *Rutilus rutilus*; Strahl et al. 1994; Menzel-Harloff & Meng 2015) are typical indicators of shallow still waters or slowly-flowing streams, possibly within an oxbow lake setting. This is not surprising because present-day beta-oligohaline waters (<2‰) of the southern Baltic Sea coast are also dominated by freshwater taxa and are not normally populated by brackish water molluscs. In this context, we infer an estuary setting during the Eemian transgression, where marine waters sporadically inflow and mix with freshwater. Our finding of ephippia and occasional mite remnants point to a reed fringe habitat in a close-to-shore setting (Frenzel 2006).

Interestingly, we identify a similar brackish microfossil assemblage within both the mud of subunit D2 and the sandy ball-and-pillow structures preserved within this subunit (Fig. 4.5). Based on this it is likely that the isolated sediment bodies within unit D derived from an overlying sand layer, which also deposited in brackish environment during the Eemian. However, a precise interpretation is complicated because the presently overlying sands of unit E yielded a Late Weichselian luminescence age, implying that the original Eemian sand layer was subsequently removed by erosion or sank entirely into subunit D2 (Fig. 4.12).

The Late Weichselian stage (MIS 2). – Unit E comprises fine-grained but relatively poorly-sorted lacustrine sand, including dispersed outsized gravel clasts (less than 50 mm in size) at the base, which we interpret as a lag deposit that formed at a lake margin (Tab. 4.3). The contact between units D and E is characterised by intense soft-sediment deformation (Fig. 4.15C), previously seen as evidence for cryoturbation (Ullerich 1991; Strahl et al. 1994). However, we note that the observed structures would also be consistent with an interpretation as load casts due to density-driven inversion processes. In the absence of other features suggesting a former periglacial land surface – which may be expected if cryoturbation caused the observed deformation – we favour liquefaction processes as the more plausible explanation for the deformed contact between units D2 and E.

An important new finding of this study is that the discrete erosional contact between unit D and unit E marks a significant hiatus of more than 90.000 years. This suggests that unit D accumulated during the warm Eemian period (Strahl et al. 1994; Menzel-Harloff & Meng 2015), while all subsequent units (E to K) formed during the Late Weichselian glaciation (MIS 2; Fig. 4.5, Tab. 4.3). These results differ from an earlier study by Krbetschek (1995), who reported two TL ages of 70±9 ka and 63±8 ka for unit E, implying a far less substantial hiatus between units D and E. We attribute this discrepancy to the sensitivity decrease caused by heating during the TL-dating of these sediments (*e.g.* Jain et al. 2007), suggesting that the earlier TL results with a tendency for significant age overestimation, are less reliable than the luminescence chronology presented in this study. Finally, the presence of Eemian marine molluscs (Menzel-Harloff & Meng 2015) and sporomorphes of PZ 3-4 (Strahl et al.1994) within unit E points to a reworking of Eemian fossils embedded into Late Weichselian deposits. Reworking of these fossils is also indicated by our observation that the quartz
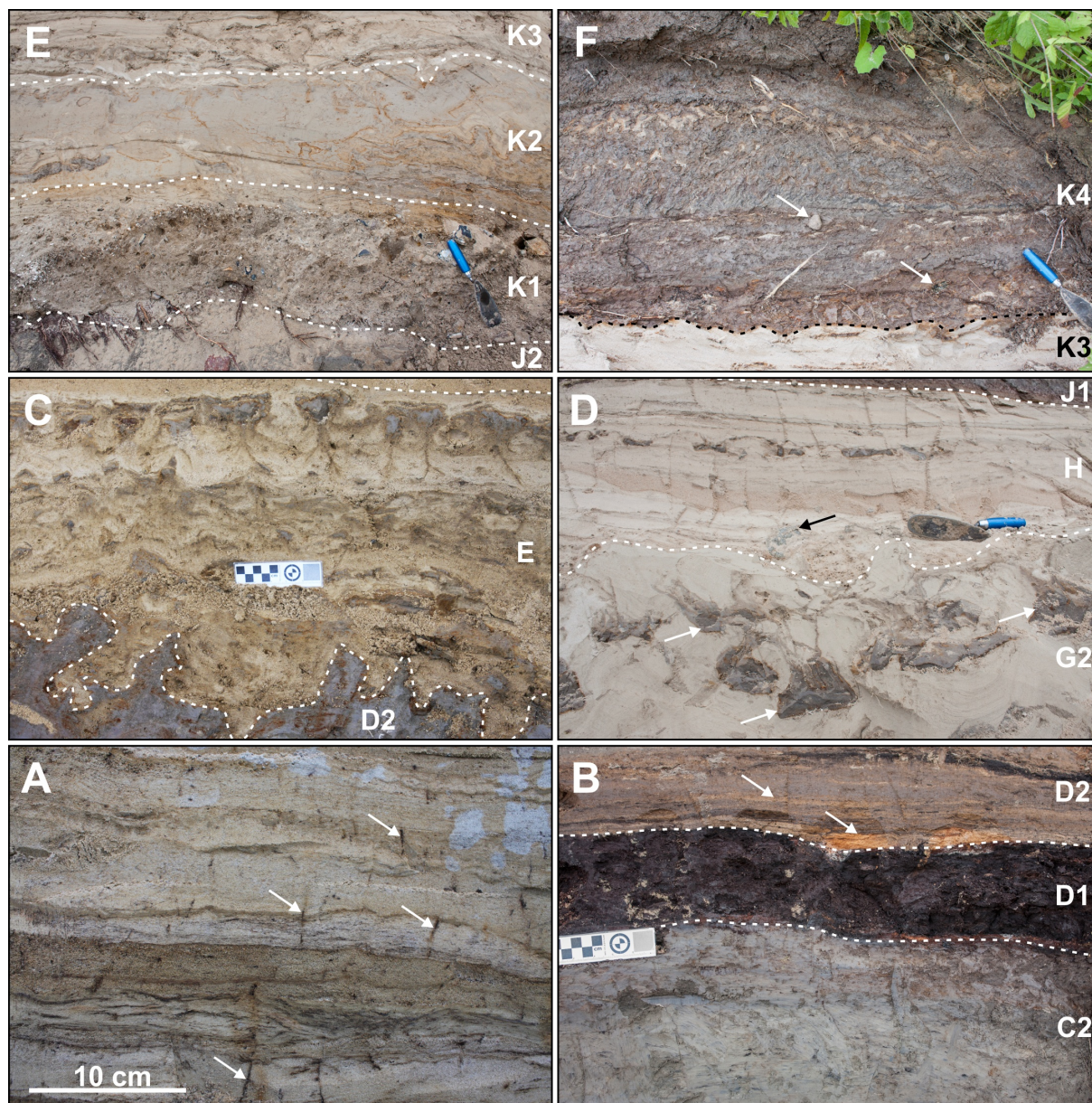
Fig. 4.15 A. Lacustrine sediments from subunit C1 showing draped wavy lamination and tube-like vertical structures (white arrows) indicating fossil root penetration. B. Contact between the Late Saalian subunit C2 (mud) and the overlying Eemian subunit D1 (peat). Note the light-yellowish laminated layering near the base of subunit D2 (white arrows), indicating former algae blooms. C. Soft-sediment deformation at the contact between subunit D2 and unit E. A hiatus of more than 90 ka marks the boundary between these units. D. Fine-grained lacustrine infill at the top of the fluvial channel (subunit G2), showing density-driven deformation (ball-and-pillow structures; see white arrows). Note the isolated gravel clast at the base of unit H (black arrow). E. Basal part of the terminoglacial lacustrine unit K above the Weichselian till of subunit J2. The waterlain sedimentation of unit K starts with debris flow deposits (subunit K1), followed by finely-laminated clay and silt with soft-sedimentary deformation (subunit K2), and traction-bedded sand and silt (subunit K3). F. Undulating erosional contact between subunits K3 and K4. The overlying fines indicate a rising lake level, sporadically interrupted by the input of sandy material forming lenticular bedding. Note the isolated gravel clasts interpreted as dropstones (white arrows).

and feldspar ages from this unit are in excellent agreement (OSL: 24±2 ka, fading-corrected pIRIR225: 22±2 ka), with no evidence for significant residual signals, suggesting that well-bleached grains were mixed with locally-reworked Eemian molluscs.

A precise interpretation of the mechanism that led to the formation of the aforementioned hiatus is difficult because of the deformed character of the contact between unit D and E. In addition, the presence of isolated sand bodies within unit D, which show a different microfossil content than the sands of unit E, points to a multi-phased overprinting of the sedimentary contact that marks the Eemian to Late Weichselian hiatus. The available evidence from the units that directly bracket the hiatus indicates an erosional phase during the Late Weichselian, which led to the removal of parts of the Eemian sequence. Under this scenario, it is conceivable that significant portions of potential early to mid-Weichselian deposits were also eroded from KKH, but this issue cannot yet be fully resolved.

A continuation of deposition in a shallow lacustrine basin is indicated by unit F, which combines evidence of the accumulation of bedload-transported sand and suspension settling of fines. Wave ripples occur throughout unit F, suggesting sedimentation near or at a lake margin possible influenced by fluctuating water levels or variable wind strength (Fig. 4.8). The early MIS 2 lacustrine phase (unit E and unit F) was interrupted by a short-lived erosional event of fluvial origin, as evidenced by small meandering channels (unit G) incised into the lacustrine sediments of unit F (Fig. 4.2, Fig. 4.5). The infill of one of these channels gave an OSL age of 20±2 ka (LUM 3176). Subsequently, both unit F and unit G were truncated by a minor erosional event, which formed a land surface and sediments with periglacial cryoturbation features (Fig. 4.15D), associated with increasingly colder climate conditions. The overlying unit H, comprising lacustrine sediments with an OSL age of 19±2 ka (LUM 3177), accumulated proglacially in front of the approaching SIS margin. MP-unit 4 includes the above-described lithological units E to H (Fig. 4.5, Fig. 4.12), which closely resemble the fossil-barren MP-unit 1 (not considering reworked Cretaceous microfossils in both MP-units).

A subsequent ice advance across the site glaciotectonically deformed the upper part of unit H and deposited an up-to-5 m thick till complex (unit J). The basal portion (subunit J1) of this subglacial traction till (sensu Evans et al. 2006) shows evidence of subglacial shearing and the incorporation of sediment derived from the underlying unit

H (glaciotectonic lamination; see thin section TS 5 in Fig. 4.95). The till of subunit J1 grades into the till of subunit J2, which constitutes a more massive, homogenous and compacted till facies (Fig. 4.106). Based on our OSL dating of units H and K, which directly sandwich unit J, the SIS advance across the KKH site occurred between 20±2 and 17±2 ka (LUM 3177 and LUM 3178, resp.). Chronostratigraphically, unit J represents the first Weichselian till at the KKH succession, underpinning earlier results that correlated this till with the Brandenburgian/Frankfurt phase (MIS 2; Strahl et al. 1994; Krbetschek 1995).

A subsequent phase of ice retreat is represented by a heterogeneous fining-upward succession of diamicts, sand and fines (unit K; Fig. 4.5, Tab. 4.3). We infer a terminoglacial depositional environment dominated by lacustrine sedimentation, associated with oscillating lake levels with a varying input by meltwater streams and gravitational mass movements. Subunit K1 comprises faintly-stratified gravelly debris flow diamictons, probably derived from the nearby ice front during the ice decay phase. The presence of abundant and locally sourced fragile chalk clasts (up to 30% of all gravel clast) within subunit K1 indicate a relatively short distance of transport. Furthermore, the dispersed occurrence of reworked diamictic (till) clasts within subunit K1 confirms a close spatial and chronological relationship between subunits J2 and K1.

The subsequent deposition of subunit K2 is dominated by suspension-settling of fines, resulting in massive to finely-laminated clay and silt. Due to syn- to post-sedimentary dewatering and slumping, the sediments of this subunit were deformed as evidenced by ubiquitous soft-sediment deformational structures (Fig. 4.15E). This is followed by periodic variations in sediment supply and water inflow with repeated slackwater phases leading to rhythmically bedded sediments (subunit K3). We interpret at least some of the isolated gravel lenses and larger clasts within subunit K3 to have been deposited by the rain-out of debris from melting ice-rafts. Nevertheless, the water depth of the basin was probably low, as indicated by the presence of symmetrical ripples with peaked crests, which are formed by wave action (Reineck & Singh 1975).

The terminoglacial lake phase of unit K3 was interrupted by an erosional event, marked by a sharp contact to the overlying subunit K4 (Fig. 4.15F). This indicates a short episode of lake level lowering or a sudden drainage event of the basin. The previously deposited lacustrine succession was partially eroded, brecciated and

deposited as a layer of gravel-sized clay and silt intraclasts after a short distance transport. As such, we interpret the lowermost part of subunit K4 as a conglomerate-like layer that formed during the refilling of the lake (transgression). Although quiet-water conditions dominate, there is evidence for occasional glaciofluvial inflow and the input of rafted debris from icebergs (subunit K4), implying that the lake was still in ice contact. Two OSL samples from unit K give tendentially stratigraphically reversed ages of 17±2 ka (LUM 3178) and 21±2 ka (LUM 3179). When viewed in the context of the overall Weichselian OSL chronology, it appears likely that the older of the two ages represents a slight overestimate of the true burial age (Fig. 4.5). Regardless of how sample LUM 3179 is treated, unit K represents a terminoglacial lacustrine succession that was deposited after the Brandenburgian/Frankfurt phase, and is thus part of the post-LGM sequence (*i.e.* Pomeranian phase) according to Toucanne et al. (2015).

4.5.3 Larger regional context

A compilation of available glacial records from northern Europe shows that the last major phase of ice expansion during the Saalian glaciation ends at around 140 – 135 ka (Lambeck et al. 2006). These dates are in excellent agreement with the age determinations from the basal portion at KKH, which formed during the Saalian deglaciation (MIS 6, Termination II). The regional context within the southern Baltic area is provided by only a limited number of studies that are constrained by absolute age dating of late MIS 6 successions (summarized in Rattas et al. 2010). Similarly, there are only few Eemian surface outcrops across this region, with the majority of the available information on last interglacial conditions derived from borehole data (Andrén et al. 2011). Eemian exposures in Denmark are frequently part of glaciotectonically dislocated blocks (Larsen et al. 2009), including the sites at Mommark (Eiríksson et al. 2006), Ristinge (Nielsen et al. 2007) and Gammelmarke (Murray & Funder 2003). In NE-Germany the situation is very similar, with most of the information obtained from borehole data (Müller 2004b; Meng et al. 2009). Although outcropping Eemian records have previously been documented from sites at Hinterste Mühle (Strahl 2000), Schwaan (Frenzel & Ansorge 2004), Grimmen (Steinich 1995), Banzin (Börner et al. 2015) and Klein Klütz Höved (Strahl et al. 1994; Menzel-Harloff & Meng 2015), the record remains fragmentary. The succession at KKH thus offers an excellent opportunity to improve the available information on the transition from Saalian to Eemian palaeoenvironments in the southwestern Baltic Sea region.

The KKH succession starts with sediments that record a Saalian ice advance, the subsequent Termination II (Landais et al. 2013) and the onset of the Eemian interglacial. Compared with Antarctic ice core data (Landais et al. 2013) and Atlantic marine records (Sanchez-Goñi et al. 2000; Oppo et al. 2006), where the Eemian onset was dated between 136 and 130 ka, terrestrial European sites show a delayed beginning of the Eemian at 127 ka (Brauer et al. 2007). Together with Hinterste Mühle (Fig. 4.1B; Strahl 2000), KKH represents the only site in NE Germany where the penultimate glacial-interglacial transition is palynologically firmly established, extended here by a first numerical age chronology based on luminescence dating. Apart from this record, physical age information is only available for several other sites, including the terrestrial succession at Vevais (NE Brandenburg, Germany), yielding a luminescence age of 126±16 ka for the base of the Eemian (Lüthgens et al. 2011), and a site at Banzin (Fig. 4.1A), where two ^{230}Th/U ages indicate peat accumulation at around 121–118 ka (Börner et al. 2014).

An important aspect in the interpretation of the KKH results is an evaluation to what extent a marine influence from the Eemian transgression can be detected at the site. Our finding of ostracods, which are tolerant of oligohaline salinity and marine dinocysts within subunit D2 indicate the establishment of brackish conditions at the transition from PZ 2 to 3, coinciding with the rise of *Quercus* in truncated PZ 3 (Fig. 4.11). This succession resembles the micropalaeontological record from Ristinge Klint, where the initial Eemian marine ingression is characterised by a gradual shift from a freshwater to a marginal marine environment, associated with a marked increase of Quercus pollen (Kristensen et al. 2000; Kristensen & Knudsen 2006; Head 2007). Kristensen et al. (2000) suggested that a first onset of the marine transgression at the Ristinge site (Fig. 4.1A) occurred c. 300 years after the start of the Eemian period. This was confirmed by a hydrographical reconstruction based on foraminiferal stable isotopes and diatoms by Knudsen et al. (2011) for the Ristinge section. Furthermore, Kristensen et al. (2000) proposed that the early marine ingression entered the southwestern Baltic Sea basin from the east via a connection through the White Sea. However, Funder et al. (2002) showed that this connection was established much later.

On balance, we suggest an estuary setting during the early Eemian at KKH (PZ 2-3), probably linked to the palaeo-Trave estuary (Trave Bay, Fig. 4.1A), which is well-documented from borehole data in the Herrnburg area, located 30 km to the SW of our site (summarized in Meng et al. 2009). Together with information recovered in 1969

from a drill core near Damshagen (~10 km SSE from KKH, 54°56.51' N, 11°08.33' E; Fig. 4.1B), indicating brackish conditions at the base of the Eemian (bore log report Hy Damshagen 1/69; LUNG M-V 2016), it is possible to revise the outline of the local Eemian coastline, showing that the early marine limit reached further to the south than previously thought (Fig. 4.1B). Within this context, the KKH site represents a key record for delineating the character and timing of the early Eemian transgression phase into the southwestern Baltic basin, and its correlation to coeval marine successions from Denmark and other circum-Baltic areas. In contrast to Eemian successions in Denmark (*e.g.* Kristensen et al. 2000; Funder & Balic-Zunic 2006; Nielsen et al. 2007), where full marine conditions were established c. 2500 years after the beginning of the interglacial, KKH provides only indirect evidence of this stage, based on reworked marine molluscs identified within the basal portion of the overlying Late Weichselian succession (unit E, Fig. 4.5; Strahl et al. 1994; Menzel-Harloff & Meng 2015).

At KKH, we find no evidence for an early- to mid-Weichselian SIS advance into the SW Baltic Sea, as previously proposed by Müller (2004a, b; 'Warnow advance'), Houmark-Nielsen (2010; 'Ristinge advance', Fig. 4.16) and more recently by Obst et al. (2017). Although it is conceivable that the associated glacial deposits were removed (*i.e.* during the erosional phase that generated the hiatus between unit D and E), it is noteworthy that, so far, there is no unambiguous evidence that such an ice advance reached the NE-German mainland (*e.g.* Kenzler et al. 2015, 2017). We would also like to point out that the complete removal of potential early- to mid-Weichselian till deposits at KKH would require an erosional force that is typically associated with an ice advance or exceptionally high-energy fluvial/littoral processes, capable of transporting away glacial debris including metre-sized boulders. However, the deposits directly overlying unit D are clearly of lacustrine origin (unit E) and hold no evidence for coarse till-derived boulder lag deposits.

During late MIS 3/early MIS 2, deposition at KKH was dominated by the accumulation of nearly fossil-barren lacustrine sediments under ice-free conditions (units E to F). This resembles reconstructions by Anjar et al. (2012) from Kriegers Flak (for location see Fig. 4.1A), who also document a (glacio-)lacustrine setting between 29 and 26 ka in the SW Baltic Sea region, reflecting the formation of a large ice-dammed lake during the southward advance of the Kattegat ice stream into northern Denmark (Houmark-Nielsen 2003; Fig. 4.16). Considering that the original position of the KKH succession, prior to its later glaciotectonic southward dislocation and uplift,

was approximately 30 m below modern sea level, it is not implausible that the MIS 3/MIS 2 lacustrine deposits at KKH accumulated along the southwestern margin of this palaeo-lake within the present-day Mecklenburgian Bay. If confirmed, this model refines the palaeogeographic maps by Houmark-Nielsen (2003), which show a less extensive suthwestely lake extent than is tentatively proposed here.
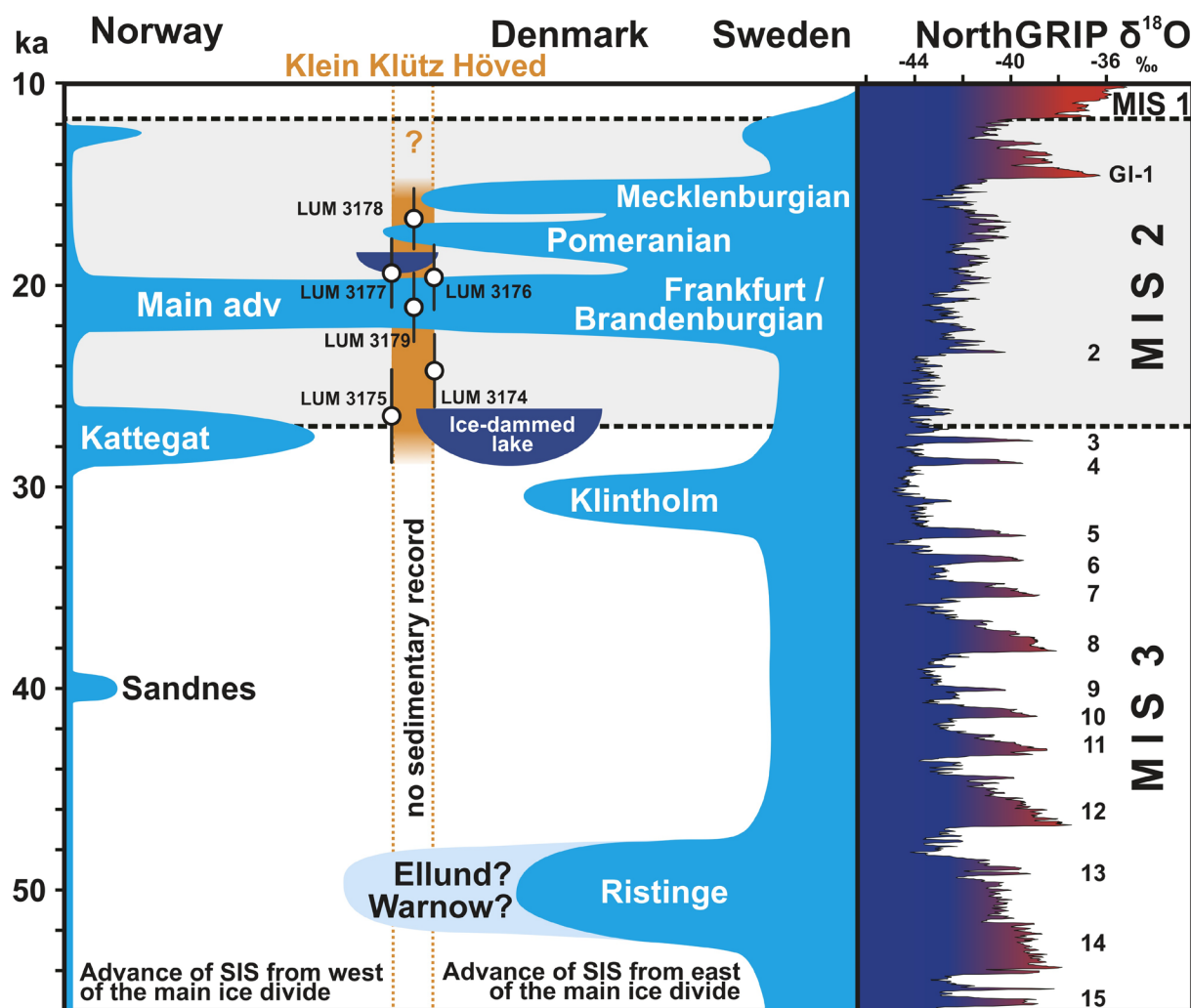

Fig. 4.16 Advances of the Scandinavian Ice Sheet into the southwestern Baltic Sea area during MIS 3 and MIS 2 (based on Houmark-Nielsen 2010) compared to the KKH luminescence chronology of samples LUM 3174 to LUM 3179, and the δO18 signal derived from the NorthGRIP ice core project (Wolff et al. 2010).

The presented luminescence chronology from KKH suggests that the first documented Weichselian ice advance of the SIS occurred approximately at 20±2 to 19±2 ka (Fig. 4.16). This matches chronological findings from the north-German Dänischer Wohld Peninsula and at Rügen Island (Fig. 4.1A), where proglacial

lacustrine sediments, associated with the advancing SIS, yielded a luminescence age of 23±2 ka (Livingstone et al. 2015; Kenzler et al. 2017). We see no evidence for a late MIS 3/early MIS 2 ice advance into NE Germany as discussed by Lüthgens & Böse (2011), and more recently by Hardt et al. (2016). Rather, the KKH record corroborates other data sets from across the southwestern Baltic Sea, which indicate a maximum expansion of the southwestern SIS sector between 25 and 20 ka (Houmark-Nielsen 2010; Toucanne et al. 2015), broadly coinciding with the overall Eurasian ice sheet maximum at c. 21 ka (Hughes et al. 2016). The subsequent ice retreat from the KKH site is dated to 17±2 ka and correlates well with an age estimates representative of the post-LGM sequence 1 or 2 according to Toucanne et al. (2015).

4.6 Conclusions

This paper presented results of a study of a Pleistocene succession at Klein Klütz Höved (southwestern Baltic Sea coast, Germany), based on detailed sedimentological and palaeontological reconstructions, and supported by luminescence dating of quartz (OSL) and feldspar minerals (pIRIR$_{225}$). Based on our findings, we summarize the palaeoenvironmental and depositional history of the site as follows:

• After a Saalian ice advance (MIS 6), the subsequent local deglaciation (Termination II) occurred at 139±17 ka, resulting in the development of a glaciofluvial braided river system. Soon thereafter, a shallow lake formed under arctic to subarctic climate conditions between 135±12 and 134±12 ka, characterised by a shift from a shrub- and herb-dominated landscape (PZ A) to *Hippophaë* communities (PZ B) and finally to an open woodland with *Betula*, *Juniperus* and *Salix* (PZ C1 and C2).

• Lake levels rose during the ensuing transition into the Eemian interglacial. The documented Eemian PZ 1 to 3 (Erd 1973) span less than 750 years of the last interglacial period. During this time the climate ameliorated at KKH, as evidenced by an increasingly forested landscape, which was eventually dominated by thermophile deciduous forest elements (*Quercus*, *Ulmus*), and the occurrence of warm-water ostracods. Palynologically, the local succession represents an incomplete interglacial record where at least 10 ka of the later Eemian are missing.

- The upper portion of the exposed Eemian record contains brackish indicators, which mark the onset of the Eemian marine transgression at KKH, approximately 300 – 750 years after the beginning of the last interglacial period. The resulting ingression is likely to have occurred within a former estuary setting, which best explains the observed coexistence of brackish and freshwater biota. This interpretation highlights the importance of the KKH site as a key record capturing the early onset of the marine Eemian transgression into the southwestern Baltic Sea region.

- At KKH, sediments dating into the early- to mid-Weichselian period (MIS 5d to 3) are missing, representing a hiatus of c. 90 ka between the early Eemian and overlying Late Weichselian (MIS 2) succession.

- Deposition during early MIS 2 occurred in a glaciolacustrine basin, which was possibly connected to an ice-dammed lake that formed during the Kattegat ice advance (29 – 26 ka) in the southwestern Baltic Sea basin.

- The first documented SIS advance of Weichselian age reached the study area at approximately 20±2 to 19±2 ka during the Brandenburgian/Frankfurt phase of the LGM (MIS 2). This was followed by an ice retreat resulting in the formation of an ice-contact lake with a minimum age of 17±2 ka.

4.7 Acknowledgements

4.8 References

Andrén, T., Björck, S., Andrén, E., Conley, D., Zillén, L. & Anjar, J. 2011: The development of the Baltic Sea Basin during the last 130 ka. *In* Harff, J., Björck, S. & Hoth, P. (eds.): *The Baltic Sea Basin*, 75–97. Springer, Berlin.

Anjar, J., Adrielsson, L., Bennike, O., Björck, S., Filipsson, H. L., Groeneveld, J., Knudsen, K. L., Larsen, N. K. & Möller, P. 2012: Palaeoenvironments in the southern Baltic Sea Basin during Marine Isotope Stage 3: a multi-proxy reconstruction. *Quaternary Science Reviews 34*, 81–92.

Auclair, M., Lamothe, M. & Hout, S. 2003: Measurement of anomalous fading for feldspar using SAR. *Radiation Measurements 37*, 487–492.

Balescu, S., Ritz, J. F., Lamothe, M., Auclair, M. & Todbileg, M. 2007: Luminescence dating of a gigantic palaeolandslide in the Gobi-Altay mountains, Mongolia. *Quaternary Geochronology 2*, 290–295.

Benn, D. I. & Evans, D. J. A. 2010: *Glaciers and Glaciations*. 802 pp. Hodder Education, London.

Börner, A., Hrynowiecka, A., Kuznetsov, V., Stachowicz-Rybka, R., Maksimov, F., Grigoriev, V., Niska, M. & Moskal-del Hoyo, M. 2015: Palaeoecological investigation and [230]Th/U dating of Eemian interglacial peat sequence of Banzin (Mecklenburg-Western Pomerania, NE-Germany). *Quaternary International 386*, 122–136.

Börner, A., Rinterknecht, V., Bourelès, D. & Braucher, R. 2014: First results from surface exposure dating of glacial boulders in ice marginal belts of Mecklenburg-Western Pomerania (NE-Germany) using in-situ cosmogenic Beryllium-10. *Journal for the Geological Science (Zeitschrift für geologische Wissenschaften) 41*, 123–143.

Bøtter-Jensen, L., Thomsen, K. J. & Jain, M. 2010: Review of optically stimulated luminescence (OSL) instrumental developments for retrospective dosimetry. *Radiation Measurements 45*, 253–257.

Brauer, A., Allen, J. R. M., Mingram, J., Dulski, P., Wulf, S. & Huntley, B. 2007: Evidence for last interglacial chronology and environmental change from Southern Europe. *Proceedings of the National Academy of Science 140*, 450–455.

Buylaert, J. P., Hout, S., Murray, A. S. & Van den haute, P. 2011: Infrared stimulated luminescence dating of an Eemian (MIS 5e) site in Denmark using K-feldspar. *Boreas 40*, 46–56.

Buylaert, J.-P., Murray, A. S., Thomsen, K. J. & Jain, M. 2009: Testing the potential of an elevated temperature IRSL signal from K-feldspar. *Radiation Measurements 44*, 560–565.

Cunningham, A. C. & Wallinga, J. 2010: Selection of integration time intervals for quartz OSL decay curves. *Quaternary Geochronology 5*, 657–666.

Degering, D. & Krebetschek, M. 2007: Luminizenzdatierungen an limnischen Sedimenten von Klinge/Niederlausitz. *Natur und Landschaft in der Niederlausitz 24*, 120–128.

Duller, G. A. T. 2003: Distinguishing quartz and feldspar in single grain luminescence measurements. *Radiation Measurements 37*, 161–165.

Eiríksson, J., Kristensen, P.H., Lykke-Andersen, H., Brooks, K., Murray, A., Knudsen K. L. & Glaister, C. 2006: A sedimentary record from a deep Quaternary valley in the southern Lillebælt area, Denmark: Eemian and Early Weichselian lithology and chronology at Mommark. *Boreas 35*, 320–331.

Eissmann, L. 2002: Quaternary geology of eastern Germany (Saxony, Sanon-Anhalt, South Brandenburg, Thüringia), type area of the Elsterian and Saalian Stages in Europe. *Quaternary Science Reviews 21*, 1275–1346.

Erd, K. 1973: Pollenanalytische Gliederung des Pleistozäns der Deutschen Demokratischen Republik. *Journal for the Geological Sciences (Zeitschrift der Geologischen Wissenschaften) 1*, 1087–1103.

Evans, D. J. A., Phillips, E. R., Hiemstra, J. F. & Auton, C. A. 2006: Subglacial till: Formation, sedimentary characteristics and classification. *Earth-Science Reviews 78*, 115–176.

Frenzel, P. 2006: Organismenreste aus holozänen Sedimenten der Ostsee als Paläomilieuindikatoren. *Meyniana 58*, 97–128.

Frenzel, P. & Ansorge, J. 2004: Die pleistozänen Fossilien der Cardiengrube von Schwaan bei Rostock (südliche Ostsee). *Archiv für Geschiebekunde 3*, 829–840.

Frenzel, P., Keyser, D. & Viehberg, F. A. 2010: An illustrated key and (palaeo)ecological primer for Recent to Postglacial Ostracoda (Crustacea) of the Baltic Sea. *Boreas 39*, 567–575.

Frenzel, P., Schulze, I. & Pint, A. 2012: Noding of *Cyprideis torosa* valves (Ostracoda) – a proxy for salinity? New data from field observations and a long-term microcosm experiment. *International Review of Hydrobiology 97*, 314–329.

Fuchs, M. & Owen, L. A. 2008: Luminescence dating of glacial and associated sediments: review, recommendations and future directions. *Boreas 37*, 636–659.

Funder, S. & Balic-Zunic, T. 2006: Hypoxia in the Eemian: mollusc faunas and sediment mineralogy from *Cyprina* Clay in the southern Baltic region. *Boreas 35*, 367–377.

Funder, S., Demidov, I. & Yelovicheva, Y. 2002: Hydrography and mollusc faunas of the Baltic and the White Sea – North Sea seaway in the Eemian. *Palaeogeography, Palaeoclimatology, Palaeoecology 184*, 275–304.

Galbraith, R. F., Roberts, R. G., Laslett, G. M., Yoshida, H. & Olley J. M. 1999: Optical dating of single and multiple grains of quartz from Jinmium Rock Shelter, northern Australia: Part I, experimental design and statistical models. *Archaeometry 41*, 339–364.

Gehl, O. 1961: Neue Ergebnisse über das marine Eem und zur Gliederung des Jungpleistozäns in NW-Mecklenburg. *Geologie 18*, 550–562.

Geinitz, E. 1922: *Geologie Mecklenburgs I Teil: Diluvium und Allivium (Quartär)*. 200 pp. Hinstorff, Rostock.

Glöer, P. & Meier-Brook, C. 1994: *Süßwassermollusken. Ein Bestimmungsschlüssel für die Bundesrepublik Deutschland*. 136 pp. Deutscher Jugendbund für Naturbeobachtung, Hamburg.

Gramann, F. 2000: Ostrakoden der Art *Cyprideis torosa* als Indikatoren für Salzgehalt und Klima-Nachweis eines Binnensalinars im Pleistozän Nordostniedersachsens. *Zeitschrift für Angewandte Geologie 46*, 49–58.

Griffiths, H. I. & Evans, J. G., 1995: The late-glacial and early Holocene colonisation of the British Isles by freshwater ostracods. *In* Ríha, J. (ed.): *Ostracoda and Biostratigraphy*, 291–302, A. A. Balkema Publishers, Rotterdam.

Guérin, G., Mercier, N. & Adamiec, G. 2011: Dose-rate conversion factors: update. *Ancient TL 29*, 5–8.

Hammer, Ø., Harper, D. A. T. & Ryan, P. D. 2001: PAST: Paleontological Statistics software package for education and data analysis. *Palaeontologia Electronica 4*, 1–9.

Hardt, J., Lüthgens, C., Hebenstreit, R. & Böse, M. 2016: Geochronological (OSL) and geomorphological investigations at the presumed Frankfurt ice marginal position in northeast Germany. *Quaternary Science Reviews 154*, 85–99.

Head, M. J. 2007: Last Interglacial (Eemian) hydrographic conditions in the southwestern Baltic Sea based on dinoflagellate cysts from Ristinge Klint, Denmark. *Geological Magazine 144*, 987–1013.

Hermsdorf, N. & Strahl, J. 2008: Karte der Eem-Vorkommen des Landes Brandenburg. *Brandenburger Geowissenschaftliche Beiträge 15*, 23–55.

Houmark-Nielsen, M. 2003: Signature and timing of the Kattegat Ice Stream: onset of the Last Glacial Maximum sequence at the southwestern margin of the Scandinavian Ice Sheet. *Boreas 32*, 227–241.

Houmark-Nielsen, M. 2010: Extent, age and dynamics of Marine Isotope Stage 3 glaciation in the southwestern Baltic Basin. *Boreas 39,* 343–359.

Hughes, A. L. C., Gyllencreutz, R., Lohne, Ø. S., Mangerud, J. & Svendsen, J. I. 2016: The last Eurasian ice sheet – a chronological database and time-slice reconstruction, DATED-1. *Boreas 45*, 1–45.

Huntley, D. J. 2006: An explanation of the power-law decay of luminescence. *Journal of Physics Condensed Matter 18*, 1359–1365.

Huntley, D. J. & Baril, M. R. 1997: The K content of the K-feldspar being measured in optical dating or in thermoluminescence dating. *Ancient TL 15*, 11–13.

Huntley, D. J. & Lamothe, M. 2001: Ubiquity of anomalous fading in K-feldspar and the measurement and correction for it in optical dating. *Canadian Journal of Earth Science 38*, 1093–1106.

Jain, M., Buylaert, J. P., Thomsen, K. J. & Murray, A. S. 2015: Further investigation on 'non-fading' in K-Feldspar. *Quaternary International 362*, 3–7.

Jain, M., Duller, G. A. T. & Wintle, A. G. 2007: Dose response, thermal stability and optical bleaching of the 310 degrees C isothermal TL signal in quartz. *Radiation Measurements 42*, 1285–1293.

Kars, R. H., Wallinga, J. & Cohen, K. M. 2008: A new approach towards anomalous fading correction for feldspar IRSL dating — tests on samples in field saturation. *Radiation Measurements 43*, 786–790.

Kenzler, M., Obst, K., Hüneke, H. & Schütze, K. 2010: Glazitektonische Deformation der kretazischen und pleistozänen Sedimente an der Steilküste von Jasmund nördlich des Königsstuhls (Rügen). *Brandenburger Geowissenschaftliche Beiträge 17*, 107–122.

Kenzler, M., Tsukamoto, S., Meng, S., Thiel, C., Frechen, M. & Hüneke, H. 2015: Luminescence dating of Weichselian interstadial sediments from the German Baltic Sea coast. *Quaternary Geochronology 30*, 215–256.

Kenzler, M., Tsukamoto, S., Meng, S., Frechen, M., Hüneke, H. 2017: New age constraints from the SW Baltic Sea area – implications for Scandinavian Ice Sheet dynamics and palaeo-environmental conditions during MIS 3 and early MIS 2. *Boreas 46*, 34–52.

Krbetschek, M. R. 1995: *Lumineszenz-Datierungen quartärer Sedimente Mittel-, Ost- und Nordostdeutschlands.* Ph.D. thesis, TU Bergakademie Freiberg, 122 pp.

Kristensen, P., Gibbard, P., Knudsen, K. L. & Ehlers, J. 2000: Last Interglacial stratigraphy at Ristinge Klint, South Denmark. *Boreas 29*, 103–116.

Kristensen, P. H. & Knudsen, K. L. 2006: Palaeoenvironments of a complete Eemian sequence at Mommark, South Denmark: foraminifera, ostracods and stable isotopes. *Boreas 35*, 349–366.

Lambeck, K., Purcell, A., Funder, S., Kjær, K.K. H., Larsen, E. & Möller, P. 2006: Constraints on the Late Saalian to early Middle Weichselian ice sheet of Eurasia from field data and rebound modelling. *Boreas 35*, 539–575.

Lamothe, M. 2016: Luminescence dating of interglacial coastal depositional systems: Recent developments and future avenues of research. *Quaternary Science Reviews* 146, 1–27.

Landais, A., Dreyfus, G., Capron, E., Jouzel, J., Masson-Delmotte, V., Roche, D. M., Prié, F., Caillon, N., Chappellaz, J., Leuenberger, M., Lourantou, A., Parrenin, F., Raynaud, D. & Teste, G. 2013: Two-phase change in CO_2, Antarctic temperature and global climate during Termination II. *Nature Geoscience 6*, 1062–1065.

Larsen, N. K., Knudsen, K. L., Krohn, K. L., Kronborg, C. F., Murray, A. S. & Nielsen, O. B. 2009: Late Quaternary ice sheet, lake and sea history of southwest Scandinavia – a synthesis. *Boreas 38*, 732–761.

Livingstone, S. J., Piotrowski, J. A., Bateman, M. D. & Ely, J. C. 2015: Discriminating between subglacial and proglacial lake sediments: an example from the Dänischer Wohld Peninsula, northern Germany. *Quaternary Science Reviews 112*, 86–108.

Ludwig, A. O. 1964: Stratigraphie des Pleistozäns der Ostseeküste von der Lübecker Bucht bis Rügen. *Geologie 13*, 1–143.

LUNG M-V (State Bureau for Environment, Natural Protection and Geology) 2016: Bore log report Hy Damshagen 1/69. Available at: https://www.umweltkarten.mv-regierung.de/atlas/script/index.php.

Lüthgens, C. & Böse, M. 2011: Chronology of Weichselian main ice marginal positions in north-eastern Germany. *Quaternary Science Journal (Eiszeitalter und Gegenwart) 2–3*, 236–247.

Lüthgens, C., Böse, M., Lauer, T., Krbetschek, M., Strahl, J. & Wenske, D. 2011: Timing of the last interglacial in Northern Europe derived from Opticallly Stimulated

Luminescence (OSL) dating of a terrestrial Saalian–Eemian–Weichselian sedimentary sequence in NE-Germany. *Quaternary International 241*, 79–96.

van der Meer, J. J. M. 1993: Microscopic evidence of subglacial deformation. *Quaternary Science Reviews 12*, 553–587.

Mejdahl, V., Shlukov, A. I., Shakhovets, S. A., Voskovskaya, L. T. & Lyashenko, H. G. 1992: The effect of shallow traps: a possible source of error in TL dating of sediments. *Ancient TL 10*, 22–25.

Meng, S., Börner, A., Strahl, J. & Thieke, H.-U. 2009: Bio- und lithostratigraphische Untersuchungen an limnisch-fluviatilen Sedimenten aus dem Eem-Interglazial im unteren Peenetal (NE-Deutschland). *Brandenburger Geowissenschaftliche Beiträge 16*, 63–78.

Menzel-Harloff, H. & Meng, S. 2015: Spätsaalezeitliche und eemzeitliche Makrofaunen aus dem Kliffaufschluss Klein Klütz Höved (NW-Mecklenburg) mit Erstnachweisen von *Belgrandia germanica* (Gastropoda: Hydrobiidae), *Pupilla loessica* (Gastropoda: Pupillidae) und *Lagurus lagurus* (Mammalia: Cricetidae) für Mecklenburg-Vorpommern. *Quaternary Science Journal (Eiszeitalter und Gegenwart) 44*, 82–94.

Menzies, J., van der Meer, J. J. M. & Rose, J. 2006: Till–as a glacial "tectomict", its internal architecture, and the development of a "typing" method for till differentiation. *Geomorphology 75*, 172–200.

Miall, A. D. 1985: Architectural-element analysis: a new method of facies analysis applied to fluvial deposits. *Earth-Science Reviews 22*, 261–308.

Miall, A. D. 1996: *The Geology of Fluvial Deposits: Sedimentary Facies, Basin Analysis, and Petroleum Geology*. 582 pp. Springer, Berlin.

Murray, A. S. & Funder, S. 2003: Optically stimulated luminescence dating of a Danish Eemian coastal marine deposit: a test of accuracy. *Quaternary Science Reviews 22*, 1177–1183.

Murray, A. S., Svendsen, J. I., Mangerud, J. & Astakhov, V. I. 2007: Testing the accuracy of quartz OSL dating using a known-age Eemian site on the river Sula, northern Russia. *Quaternary Geochronology 2*, 102–109.

Murray, A. S., Thomsen, K. J., Masuda, N., Buylaert, J. P. & Jain, M. 2012: Identifing well-bleached quartz using the different bleaching rates of quartz and feldspar luminescence signals. *Radiation Measurements 47*, 688–695.

Murray, A. S. & Wintle, A. G. 2000: Luminescence dating of quartz using an improved single-aliquot regenerative-dose protocol. *Radiation Measurements 32*, 57–73.

Murray, J. W. 1979: British nearshore foraminiferids. *In* Kermack, D.M. & Barnes, R.S.K. (eds.): *Synopses of the British Fauna (new series) 16*, 62 pp. Academic Press, London.

Müller, H. 1974: Pollenanalytische Untersuchungen und Jahresschichtenzählungen an der eem-zeitlichen Kieselgur von Bispingen/Luhe. *Geologisches Jahrbuch A 21*, 149–169.

Müller, U. 2004a: Weichsel-Frühglazial in Nordwest-Mecklenburg. *Meyniana 56*, 81–115.

Müller, U. 2004b: Jung-Pleistozän – Eem-Warmzeit bis Weichsel-Hochglazial. *In* Katzung, G. (ed.): *Geologie von Mecklenburg-Vorpommern*, 234–242. E. Schweizerbart'sche Verlagsbuchhandlung, Stuttgart.

Nielsen, J. K., Helama, S., Rodland, D. & Nielsen, J. K. 2007: Eemian marine molluscs and barnacles from Ristinge Klint, Denmark: hydrodynamics and oxygen deficiency. *Netherlands Journal of Geoscience 86*, 95–115.

Novenko, E. Y., Seifert-Eulen, M., Boettger, T. & Junge, F. W. 2008: Eemian and Early Weichselian vegetation and climate history in Central Europe: A case study from the Klinge section (Lusatia, eastern Germany). *Review of Palaeobotany and Palynology 151*, 72–78.

Obst, K., Nachtweide, C. & Müller, U. 2017: Late Saalian and Weichselian glaciations in the German Baltic Sea documented by Pleistocene successions at the southeastern margin of the Arkona Basin. *Boreas 46*, 18–33.

Oppo, D. W., McManus J. F., Cullen, J. L. 2006: Evolution and demise of the Last Interglacial warmth in the subpolar North Atlantic. *Quaternary Science Reviews 25*, 3268–3277.

Pint, A., Frenzel, P., Fuhrmann, R., Scharf, B. & Wennrich, V. 2012: Distribution of *Cyprideis torosa* (Ostracoda) in Quaternary athalassic sediments in Germany and its application for palaeoecological reconstructions. *International Review of Hydrobiology 97*, 330–355.

Prescott, J. R. & Hutton, J. T. 1994: Cosmic ray contributions to dose rates for luminescence and ESR datin: Large depths and long-term time variations. *Radiation Measurements 23*, 497–500.

Prescott, J. R. & Robertson, G. B. 1997: Sediment dating by luminescence: a review. *Radiation Measurements 27*, 893–992.

de Raaf, J. F. M., Boersma, J. R. & Van Gelder, A. 1977: Wave-generated structures and sequences from a shallow marine succession, Lower Carboniferous, County Cork, Ireland. *Sedimentology 24*, 451–483.

Rattas, M., Kalm, V., Kihno, K., Liivrand, E., Tinn, O., Tänavsuu-Milkeviciene, K. & Sakson, M. 2010: Chronology of Late Saalian and Middle Weichselian episodes of ice-free lacustrine sedimentation recorded in the Arumetsa section, southwestern Estonia. *Estonian Journal of Earth Sciences 59*, 125–140.

Reineck, H.-E. & Singh, I. B. 1975: *Depositional Sedimentary Enivronments*. 439 pp. Springer, Berlin.

Rühberg, N. 2004: Kliffs im Bereich der Wismar-Bucht. *In* Katzung, G. (ed.): *Geologie von Mecklenburg-Vorpommern*, 298–300. E. Schweizerbart'sche Verlagsbuchhandlung, Stuttgart.

Sanchez Goñi, M. F., Turon, J.-L., Eynaud, F., Shackleton, N. J. & Cayre, O. 2000: Direct land/sea correlation of the Eemian, and its comparison with the Holocene: a high-resolution palynological record off the Iberian margin. *Geologie en Mijnbouw 79*, 345–354.

Seidenkrantz, M.-S., Knudsen, K. L. & Kristensen, P. 2000: Marine late Saalian to Eemian environments and climatic variability in the Danish shelf area. *Netherlands Journal of Geosciences 79*, 355–343.

Steinich, G. 1995: Ein marines Eem-Vorkommen im Binnenland Vorpommerns (Ton-Tagebau Grimmen, westlich Greifswald). *Eiszeitalter und Gegenwart 45*, 15–23.

Stoops, G. 2010: *Interpretation of Micromorphological Features of Soils and Regoliths*. 752 pp. Elsevier, Oxford.

Strahl, J. 2000: Detailergebnisse pollenanalytischer Untersuchungen an saalespätglazialen bis weichselfrühglazialen Sedimenten aus dem Kiestagebau Hinterste Mühle bei Neubrandenburg (Mecklenburg-Vorpommern). *Brandenburger Geowissenschaftliche Beiträge 7*, 29–40.

Strahl, U. 2004: Kliffs an den Klützer Höveds. *In* Katzung, G. (ed.): *Geologie von Mecklenburg-Vorpommern*, 294–297. E. Schweizerbart'sche Verlagsbuch-handlung, Stuttgart.

Strahl, J., Keding, E., Steinich, G., Frenzel, P. & Strahl, U. 1994: Eine Neubearbeitung der eem- und frühweichselzeitlichen Abfolge am Klein Klütz Höved, Mecklenburger Bucht. *Eiszeitalter und Gegenwart 44*, 62–78.

Strahl, J., Krbetschek, M. R., Luckert, J., Machalett, B., Meng, S., Oches, E. A., Rappsilber, I., Wansa, S. & Zöller, L. 2011: Geologie, Paläontologie und Geochronologie des Eem-Beckens Neumark-Nord 2 und Vergleich mit dem Becken Neumark-Nord 1 (Geiseltal, Sachsen-Anhalt). *Eiszeitalter und Gegenwart 59*, 120–167.

Theisen, B. F. 1966: The life history of seven species of ostracods from a Danish brackish-water locality. *Meddelelser fra Danmarks Fiskeri- og Havundersøgelser N. S. 4*, 215–270.

Toucanne, S., Soulet, G., Freslon, N., Silva Jacinto, R., Dennielou, B., Zaragosi, S., Eynaud, F., Bourillet, J.-F. & Bayon, G. 2015: Millennial-scale fluctuations of the European Ice Sheet at the end of the glacial, and their potential impact on global climate. *Quaternary Science Reviews 123*, 113–133.

Ullerich, H. 1991: Die sandig-siltigen Zwischensedimente am Kliff des Klein-Klütz-Höved (Mecklenburger Bucht). M. Sc. thesis, Ernst-Moritz-Arndt University of Greifswald, 98 pp.

Wansa, S. & Wimmer, R. 1990: Geologie des Jungpleistozäns der Becken von Gröbern und Grabschütz. *Altenburger naturwissenschaftliche Forschungen 5*, 49–80.

Winn, K., Glos, R. & Averdieck, F.-R., Erlenkeuser, H. 2000: On the age of the marine Eem in northwestern Germany. *Geologos 5*, 41–56.

Wintle, A. G. & Murray, A. S. 2006: A review of quartz optically stimulated luminescence characteristics and their relevance in single-aliquot regeneration dating protocols. *Radiation Measurements 41*, 369–391.

Wolff, E. W., Chappellaz, J., Blunier, T. Rasmussen, S. O. & Svensson, A. 2010: Millennial-scale variability during the last glacial: The ice core record. *Quaternary Science Reviews 29*, 2828–2838.

Zhang, J., Tsukamoto, S., Grube, A. & Frechen, M. 2014: OSL and ^{14}C chronologies of a Holocene sedimentary record (Garding-2 core) from the German North Sea coast. *Boreas 43*, 856–868.

4.9 Supplementary information

	Massive clay with lenticularly-bedded, fine-grained sand (lenses) and distinct wavy sand layers		Poorly-sorted, clast-rich, diamictic gravel bed
	Brown-grey, clay rich diamicton		Silt with clay lenses (in black)
	Massive to laminated, organic-rich mud with shell fragments		Dark-brown peat layer
	Massive to faint-laminated, reddish-brown mud interbedded with mm-scale laminae of fine-grained sand		Interbedded fine-grained sand, silt and clay; wave-ripples; locally bioturbated
	Tabular cross-bedded, sandy, fine-grained gravel		Massive, matrix-supported clay-rich diamicton

Fig. S4.1 Expanded table with all results of the pollen analysis from the pollen section at Klein Klütz Höved (Fig. 4.1B) for sample 1 to 45.

▼▼ Tab. S4.1 Expanded table with all results of the pollen analysis from the pollen section at Klein Klütz Höved (Fig. 4.1B) for sample 1 to 45.

sample number	1	2	3	4	5	6	7	8	9	10	11	12	13	14	15
profile meter	0.06-	0.28-	0.40-	0.46-	0.51-	0.56-	0.61-	0.68-	0.73-	0.78-	0.83-	0.88-	0.92-	0.95-	0.99-
taxa	0.08	0.30	0.43	0.48	0.56	0.59	0.66	0.73	0.78	0.83	0.88	0.92	0.95	0.99	1.00
AP (%)															
Juniperus	0.4	2.1	1.5	1.5	2.1	2.4	2.1	1.5	0.6	2.4	1.2	3.6	1.5	3.3	2.7
Salix	-	-	0.9	-	4.1	1.8	1.2	0.9	1.2	0.3	0.6	0.6	0.3	1.8	0.9
Betula	6.4	11.8	4.5	14.9	26.9	33.4	32.5	34.4	23.6	18.5	15.5	21.0	21.8	25.6	17.5
Pinus	(60.4)	(37.1)	(26.4)	(26.0)	(25.1)	(25.1)	(29.0)	(29.8)	(39.7)	(36.4)	(47.5)	(31.1)	(35.0)	(28.6)	(38.9)
Ulmus	(0.4)	(1.5)	(0.6)	(0.6)	(0.6)	(0.9)	(0.6)	(0.9)	(2.1)	(0.6)	(0.6)	(1.5)	(2.1)	(1.8)	(0.9)
Quercus	(2.8)	(0.3)	(0.3)	(0.3)	(0.3)	(1.5)	(0.9)	-	(1.8)	(1.2)	(1.5)	(0.9)	(2.4)	(0.6)	(1.8)
Corylus	(2.4)	(1.2)	-	(1.8)	(2.1)	(1.5)	(1.5)	(0.3)	(2.4)	(0.9)	(0.6)	(1.2)	(0.9)	(1.8)	(0.9)
Alnus	(2.8)	(1.5)	(1.2)	(4.2)	(6.5)	(3.3)	(3.6)	(4.9)	(2.7)	(3.3)	(4.5)	(6.9)	(9.3)	(3.3)	(5.6)
Tilia	(0.4)	-	-	-	-	-	(0.3)	-	-	(0.3)	(0.3)	-	-	-	-
Carpinus	(1.6)	(0.3)	(0.3)	(0.3)	(0.9)	(0.9)	(1.5)	(0.6)	-	(0.6)	(0.6)	(0.3)	(0.6)	(0.6)	(0.3)
Picea	(0.8)	-	(0.3)	(0.9)	(0.3)	(0.6)	(0.3)	(0.9)	(2.1)	(0.6)	(1.5)	(0.6)	(0.3)	(0.6)	(0.6)
Abies	(1.2)	-	(0.3)	-	-	(0.3)	(0.3)	(0.3)	(0.9)	(0.3)	(0.6)	(0.3)	(0.3)	-	(0.6)
Hedera	(0.4)	-	-	-	-	-	-	-	-	-	-	-	-	-	-
Acer	-	-	-	-	-	-	-	-	-	-	-	-	-	(0.3)	-
Fagus	-	-	-	-	-	-	-	-	-	-	-	-	(0.3)	(0.6)	-
Hippophaë rhamnoides	-	0.3	2.4	0.9	1.2	0.6	0.6	0.3	1.2	1.2	1.8	0.3	0.9	0.6	1.2
sum AP (%)	**80.0**	**56.4**	**38.7**	**51.3**	**70.1**	**72.2**	**74.3**	**74.6**	**78.2**	**67.3**	**76.7**	**68.3**	**75.7**	**69.4**	**71.8**
NAP (%)															
Poaceae	5.2	8.1	10.8	10.7	7.4	9.8	7.2	7.8	7.5	8.6	9.8	12.9	6.6	11.6	7.7
Cyperaceae	12.4	15.8	47.4	30.7	16.6	13.1	13.7	12.4	7.8	19.1	8.4	14.4	13.2	11.0	15.1
Calluna	0.4	-	0.6	-	0.3	0.3	-	0.3	0.3	-	-	0.3	-	-	0.3
Ericaceae p.p.	(1.2)	(0.9)	(0.3)	(0.6)	(1.8)	(0.6)	(0.6)	(1.7)	(3.0)	(1.2)	(1.5)	(1.8)	(1.5)	(0.9)	(1.2)
Helianthemum	-	0.3	0.3	0.3	-	-	0.3	-	0.3	0.6	0.3	-	-	-	0.3
Ephedra distachya-type	0.4	-	-	-	-	-	0.3	-	-	-	-	-	-	-	-
Artemisia	-	2.4	1.5	5.4	2.1	1.8	1.5	2.6	1.8	3.0	1.8	2.1	1.8	3.6	1.8
Rumex acetosella-type	-	0.3	-	-	0.3	-	-	-	-	-	-	-	0.3	-	0.3
Chenopodiaceae	0.4	2.7	-	0.6	0.6	0.6	1.2	0.3	0.3	-	0.6	+*	-	0.6	0.3
Caryophyllaceae	-	0.6	-	0.3	0.3	-	-	-	-	-	-	-	-	0.3	-
Cruciferae	-	0.3	-	-	-	-	-	-	-	-	-	-	-	0.3	-
Umbelliferae	-	0.3	-	-	-	-	0.3	-	-	-	-	-	-	-	-
Tubuliflorae	-	0.6	-	-	0.3	0.9	0.3	-	0.3	-	0.6	-	-	0.9	-
Liguliflorae	-	-	0.3	-	-	-	0.3	-	0.3	-	-	-	-	-	-
Galium-type	-	-	-	-	-	0.3	-	-	-	-	-	-	-	0.3	-
Thalictrum	-	0.6	-	-	0.3	0.3	-	-	-	-	-	-	-	-	0.3
Armeria maritima	-	-	-	-	-	-	-	-	-	-	-	0.3	0.3	-	0.3
Polygonum persicaria	-	-	-	-	-	-	-	0.3	-	-	-	-	-	-	-
Plantago	-	-	-	-	-	-	-	-	-	0.3	-	-	-	-	-
Rosaceae p.p.	-	-	-	0.3	-	-	-	-	0.3	-	0.3	-	0.6	0.9	0.6
Filipendula	-	0.3	-	0.3	-	-	-	-	-	-	-	-	-	0.3	-
sum NAP (%)	**20.0**	**43.6**	**61.3**	**48.7**	**29.9**	**27.8**	**25.7**	**25.4**	**21.8**	**32.8**	**23.3**	**31.7**	**24.3**	**30.6**	**28.2**
basis sum (AP + NAP)	**250**	**321**	**333**	**335**	**338**	**335**	**335**	**346**	**335**	**335**	**335**	**334**	**334**	**336**	**337**

sample number	1	2	3	4	5	6	7	8	9	10	11	12	13	14	15
profile meter	0.06-	0.28-	0.40-	0.46-	0.51-	0.56-	0.61-	0.68-	0.73-	0.78-	0.83-	0.88-	0.92-	0.95-	0.99-
taxa	0.08	0.30	0.43	0.48	0.56	0.59	0.66	0.73	0.78	0.83	0.88	0.92	0.95	0.99	1.00
swamp- and waterplants, ferns, mosses (%)															
Potamogeton	-	0.3	-	0.3	0.6	0.3	0.6	-	-	-	-	0.3	-	0.3	-
Myriophyllum spicatum	-	-	-	0.3	-	0.6	0.6	0.9	-	1.5	0.3	-	-	-	-
Nymphaea	-	-	-	-	-	-	-	0.3	-	-	-	-	-	-	-
Ceratophyllum (leaf spines*)*	-	-	-	-	0.3	0.3	0.3	0.9	0.6	0.3	0.3	0.3	0.6	0.3	-
Ranunculus trichophyllos-type	-	-	-	-	0.6	0.3	-	1.2	0.9	0.9	-	-	-	-	-
Typha-/*Sparganium*-type	2.4	0.9	1.2	1.5	1.8	2.7	0.9	1.5	1.5	1.5	0.6	2.7	3.9	2.1	3.0
Ranunculaceae	-	-	0.3	-	-	-	-	-	-	-	-	-	-	-	-
Ranunculus acer-type	-	-	-	-	-	-	-	-	-	-	0.3	-	-	-	-
Urticaceae	-	-	-	-	0.3	-	-	-	-	-	-	-	-	-	-
Equisetum	-	0.3	1.5	3.6	2.7	3.0	4.8	6.6	5.1	2.1	5.4	7.2	6.0	5.4	3.6
Botrychium	-	-	-	-	-	-	-	-	-	-	-	-	-	0.3	-
Selaginella selaginoides	1.2	0.9	0.6	2.1	-	1.8	1.5	0.9	0.6	0.6	-	0.6	-	1.2	0.6
Lycopodium annotinum	-	-	-	-	-	-	-	-	-	-	-	-	-	-	0.3
L. compl.-/*clavatum*-type	-	-	0.3	-	-	-	0.3	-	-	-	-	-	-	-	0.3
Polypodium vulgare	-	-	-	-	-	-	-	-	-	-	-	-	-	-	0.3
monolete fern spores, without perispore	4.8	2.7	1.5	1.8	1.5	2.7	3.0	2.4	3.3	2.4	3.9	3.3	7.8	2.7	5.6
Sphagnum	-	1.8	0.6	0.9	0.9	0.9	1.2	1.2	1.5	2.1	1.2	0.9	0.9	1.8	2.4
algae, plancton and other micro remains (%)															
Pediastrum boryanum	7.2	4.4	1.2	17.3	11.8	3.9	7.8	1.5	1.5	17.3	0.3	3.6	6.0	10.7	7.1
P. kawraiskyi	4.4	2.7	0.6	0.6	2.7	1.8	0.9	-	0.3	3.0	1.5	0.6	1.2	2.1	1.2
P. simplex	0.4	-	-	-	-	-	-	-	-	-	-	-	-	0.3	-
Botryococcus	-	++	+	++	++	++	++	+	+	+	++	++	++	++	++
Zygnemataceae	0.4	0.3	-	0.9	0.9	0.3	-	-	0.9	1.2	-	0.9	1.2	0.6	0.6
Spirogyra (*Ovoidites*)	-	-	-	0.3	0.3	0.3	0.9	-	-	-	0.3	0.3	0.3	-	0.6
Spirogyra	-	-	0.3	-	-	-	-	0.3	0.3	0.6	-	-	0.3	-	-
Chrysophyceae	-	-	-	-	-	0.3	-	-	-	-	-	-	-	-	0.9
Turbellaria (fragments)	-	-	-	1.2	-	0.9	0.6	0.6	1.2	-	-	0.3	0.3	0.3	-
Cladocera (fragments)	-	-	-	-	-	-	-	-	-	0.9	-	0.3	0.3	-	0.3
Rotatoria	-	-	0.3	-	-	-	-	-	-	-	-	-	-	-	-
Chironomidae	0.4	0.6	-	0.3	-	-	0.3	-	0.6	2.1	-	0.6	0.3	0.6	0.3
Zenkersches organ (Ostracoda)	-	-	-	-	0.3	-	-	-	0.3	0.3	0.3	-	0.3	-	0.3
Betula-leafhairs	-	-	-	-	0.3	-	-	-	-	0.6	-	-	-	-	-
stomata	-	-	-	-	-	-	0.3	-	-	-	-	-	-	-	-
fungal and moss spores	-	-	+++	-	-	-	-	-	-	-	-	-	-	-	-
varia/indet	-	-	0.6	0.3	-	-	0.3	-	-	-	-	-	0.3	-	0.3

sample number profile meter taxa	1 0.06- 0.08	2 0.28- 0.30	3 0.40- 0.43	4 0.46- 0.48	5 0.51- 0.56	6 0.56- 0.59	7 0.61- 0.66	8 0.68- 0.73	9 0.73- 0.78	10 0.78- 0.83	11 0.83- 0.88	12 0.88- 0.92	13 0.92- 0.95	14 0.95- 0.99	15 0.99- 1.00
certain reworked taxa (Tertiary and older) (%)	**74.0**	**26.5**	**11.4**	**31.3**	**37.3**	**40.0**	**37.0**	**35.3**	**36.5**	**43.6**	**38.5**	**47.6**	**68.0**	**59.2**	**49.0**
thereof															
Taxodiaceae/Cupressaceae-group	43.2	16.2	1.8	19.7	27.2	28.1	24.5	22.5	20.3	33.1	25.4	32.0	46.4	40.8	31.4
Sciadopytis	4.0	2.1	0.6	0.3	1.2	2.1	2.1	1.5	3.3	1.8	3.3	2.7	0.6	3.3	0.9
Rhoipites-type	0.8	·	0.3	·	·	·	·	·	·	·	·	·	·	·	·
Tsuga	·	·	·	·	·	0.3	·	·	·	·	·	·	·	·	·
Symplocus	0.4	·	·	0.3	·	0.3	·	·	·	·	·	·	·	·	·
Carya	0.4	·	0.3	·	0.3	·	0.6	0.3	·	0.6	0.3	0.6	0.6	·	·
Pterocarya	1.2	·	·	0.3	0.3	0.3	0.3	·	·	·	·	·	0.6	0.3	·
Juglandaceae	·	·	·	·	·	·	0.3	·	·	0.3	·	0.6	·	·	·
Myrica-type	0.8	·	0.3	0.3	·	0.3	·	·	0.3	0.6	·	0.6	0.6	0.6	1.2
Nyssa	2.0	0.6	1.2	0.9	·	·	0.3	0.3	0.9	·	0.6	0.3	1.2	1.5	0.9
Liquidambar	·	0.3	0.3	·	·	0.3	0.6	0.6	·	0.3	0.6	0.6	0.3	0.3	0.6
Ilex	·	0.6	·	0.3	·	·	·	0.3	0.6	0.3	·	·	0.3	·	0.3
Normapolles-group	·	·	0.3	·	·	·	·	·	0.3	·	·	0.3	·	·	·
Classopollis	·	·	·	·	·	0.3	0.3	·	0.3	0.3	·	·	·	·	·
Momipites-type	0.4	0.3	·	0.3	0.3	·	0.3	·	·	·	·	0.3	·	·	1.2
Pompeckjoidaepollenites	·	·	·	·	·	0.3	·	·	·	·	·	·	·	·	·
Tasmanales	4.0	1.2	·	2.4	0.3	1.5	0.3	0.6	1.5	0.6	0.3	0.6	0.3	0.9	1.2
Triporates	0.8	·	0.6	·	0.6	·	0.3	0.3	·	0.3	0.3	0.6	0.9	·	0.6
Tricolporates	10.0	2.4	0.6	4.8	5.9	4.8	5.1	6.9	7.8	4.8	6.9	6.9	13.8	9.5	8.9
Tricolpates	1.2	·	0.9	0.3	·	·	0.6	·	·	0.3	·	0.3	0.9	·	0.3
Striates	0.4	·	·	·	·	·	·	·	·	·	·	·	·	·	·
Azolla, massulae (fragments)	·	·	·	·	·	·	·	·	·	0.3	·	·	0.3	0.3	·
Cicatricosisporites	0.4	·	·	·	·	·	·	·	·	·	·	·	·	0.3	·
Osmunda	0.8	0.6	0.6	·	·	·	·	·	·	·	0.3	·	0.6	·	0.3
Triletes	3.2	1.8	1.2	1.2	1.2	1.5	0.9	2.1	1.2	0.3	0.6	1.2	0.9	1.8	1.2
pit structures (wood)	0.4	·	·	·	·	·	·	·	·	·	·	·	·	·	·
others	0.6	·	·	·	·	·	0.3	·	·	·	·	·	·	·	·
Dinozysts	30.0	9.3	4.8	4.8	9.5	11.6	9.8	7.8	6.9	15.2	13.1	7.2	6.6	7.4	6.8
Wetzeliella-group	·	·	0.3	0.3	0.3	·	·	·	0.3	0.6	0.6	·	0.9	·	0.6

(n) = presumably reworked pollen from older interglacial rsp. from Tertiary or older

+* = form out of basis sum   + = form present   ++ = form often present   · = form not present

AP = arboreal pollen   NAP = non-arboreal pollen

sample number: profile meter: taxa	16 1.00- 1.02	17 1.02- 1.07	18 1.07- 1.15	19 1.15- 1.20	20 1.20- 1.23	21 1.23- 1.29	22 1.29- 1.33	23 1.33- 1.38	24 1.38- 1.43	25 1.43- 1.48	26 1.48- 1.53	27 1.53- 1.58	28 1.58- 1.63	29 1.63- 1.68	30 1.68- 1.71
AP (%)															
Juniperus	3.6	3.3	0.9	0.6	3.0	2.7	6.6	11.4	9.0	6.6	+*	5.1	6.0	4.8	5.1
Salix	0.9	1.2	0.6	0.3	0.6	2.4	0.9	2.7	2.4	2.1	1.5	2.4	2.7	3.9	1.2
Betula	29.1	29.0	22.4	31.4	47.2	21.7	22.7	21.2	19.4	32.9	45.5	25.0	27.4	17.9	22.7
Pinus	(30.0)	(28.4)	(31.3)	(33.5)	(16.4)	(26.4)	(30.4)	(24.0)	(22.4)	(24.6)	(18.8)	(31.5)	(23.5)	(26.0)	(30.7)
Ulmus	·	(1.2)	(0.3)	(3.3)	(1.8)	(0.6)	(0.9)	(0.3)	·	(0.6)	(1.8)	(1.2)	(1.2)	·	(0.3)
Quercus	(1.5)	(0.9)	(1.2)	(2.4)	(1.2)	(2.1)	(1.2)	(0.6)	·	(0.9)	(2.4)	(0.6)	(0.6)	(0.9)	(0.3)
Corylus	(0.9)	(0.9)	(0.9)	(0.9)	(0.6)	(1.8)	(0.9)	(0.3)	(0.6)	(0.3)	·	(0.9)	(0.3)	(0.9)	·
Alnus	(2.1)	(7.8)	(10.1)	(9.5)	(3.9)	(4.2)	(3.3)	(2.7)	(3.0)	(3.0)	(8.3)	(4.8)	(3.0)	(1.8)	(3.9)
Tilia	(0.3)	·	·	·	·	·	·	·	(0.3)	·	·	·	(0.3)	·	·
Carpinus	(0.3)	(0.3)	(0.3)	(1.2)	(0.6)	·	·	(0.3)	·	(0.3)	·	·	(0.6)	(0.3)	(0.6)
Picea	(0.3)	(0.6)	(0.6)	·	·	(1.5)	·	(0.6)	(0.9)	(0.3)	(0.3)	(0.6)	(1.2)	(0.6)	(0.3)
Abies	·	·	·	(0.3)	·	(0.3)	·	·	·	·	(0.3)	·	(0.3)	·	·
Acer	·	·	·	·	·	·	·	·	·	·	(0.3)	·	·	·	·
Hippophaë rhamnoides	0.3	3.3	2.7	0.9	1.2	1.5	·	0.9	0.3	0.6	0.3	0.6	·	·	·
sum AP (%)	**69.1**	**76.9**	**71.4**	**84.0**	**76.7**	**64.7**	**67.2**	**65.0**	**58.2**	**73.1**	**79.2**	**72.9**	**66.7**	**57.3**	**65.1**
NAP (%)															
Poaceae	10.4	10.8	2.7	5.3	7.2	6.5	11.9	11.7	22.1	10.8	10.1	11.6	11.6	9.0	11.6
Cyperaceae	16.0	7.2	21.2	5.3	11.9	22.0	13.7	17.7	15.5	13.5	6.8	11.0	14.6	29.0	19.7
Calluna	·	·	0.3	0.6	0.3	0.3	0.3	·	·	·	·	0.3	·	·	·
Empetrum	·	·	·	·	·	·	·	·	·	·	·	·	0.3	·	·
Ericaceae p.p.	·	(0.9)	(1.2)	(2.1)	(1.2)	(1.2)	(0.9)	(1.2)	(1.5)	(0.3)	(0.9)	(0.3)	(0.6)	(0.6)	(0.6)
Helianthemum	·	·	0.6	0.3	0.3	0.6	·	·	·	·	0.9	0.3	·	1.2	·
Artemisia	2.1	2.7	1.5	0.9	1.2	2.1	2.7	1.5	0.9	1.2	0.6	2.1	3.6	1.2	2.1
Rumex acetosella-type	0.6	·	·	0.3	·	·	0.9	·	·	+*	·	·	·	·	·
Chenopodiaceae	·	·	0.3	·	0.3	·	0.3	1.5	·	·	·	0.3	0.3	·	·
Cruciferae	·	0.3	·	·	·	·	·	0.3	0.3	·	·	·	·	·	+*
Umbelliferae	·	·	·	·	·	0.6	·	0.3	·	·	·	·	0.3	0.3	·
Tubuliflorae	0.6	0.6	·	0.3	0.3	0.9	0.9	0.9	0.9	·	0.9	0.3	0.3	·	0.3
Liguliflorae	·	0.3	·	·	·	·	0.3	·	·	·	·	·	·	0.3	0.3
Alchemilla	·	·	·	·	·	·	0.3	·	·	·	·	·	·	0.3	·
Galium-type	0.6	·	·	·	·	·	0.3	·	·	·	·	·	·	·	·
Thalictrum	·	·	0.6	·	0.3	0.9	·	·	·	0.6	·	+*	0.6	·	+*
Gypsophila fastigiata-type	·	0.3	·	·	·	·	·	·	·	·	·	·	·	·	·
Campanula	·	·	·	·	·	·	·	·	·	·	·	·	0.3	·	·
Rosaceae p.p.	0.6	·	0.3	0.9	0.3	0.3	0.6	·	0.6	0.3	0.6	0.3	0.9	0.9	0.3
Filipendula	·	·	·	·	·	·	·	·	·	·	0.3	·	0.3	·	·
Comarum	·	·	·	·	·	·	·	·	·	·	·	·	0.3	·	·

sample number:	16	17	18	19	20	21	22	23	24	25	26	27	28	29	30
profile meter:	1.00-1.02	1.02-1.07	1.07-1.15	1.15-1.20	1.20-1.23	1.23-1.29	1.29-1.33	1.33-1.38	1.38-1.43	1.43-1.48	1.48-1.53	1.53-1.58	1.58-1.63	1.63-1.68	1.68-1.71
taxa															
sum NAP (%)	30.9	23.1	28.6	16.0	23.3	35.3	32.8	35.0	41.8	26.9	20.8	27.1	33.3	42.7	34.9
basis sum (AP + NAP)	337	334	335	337	335	337	335	334	335	334	336	336	336	335	335
swamp- and waterplants, ferns, mosses (%)															
Potamogeton	·	·	0.3	·	·	0.3	·	0.6	0.3	0.6	·	·	0.6	·	0.6
Myriophyllum spicatum	·	·	0.3	0.3	·	·	0.6	0.9	2.1	0.3	·	0.3	·	·	·
Nymphaea	·	·	·	·	·	·	·	·	·	0.6	·	·	·	·	0.3
Nymphaeaceae (ideoblasts)	·	0.3	·	·	·	·	·	·	·	·	·	·	·	·	·
Ceratophyllum (leaf spines)	0.3	·	·	·	0.6	2.7	0.6	0.6	0.9	·	·	·	0.3	1.8	0.3
Ranunculus trichophyllos-type	·	0.3	·	·	0.3	1.2	0.3	1.2	0.9	·	·	0.6	0.6	0.3	·
Hippuris	·	·	·	·	·	·	·	0.3	·	·	·	·	·	·	·
Typha-/Sparganium-type	0.9	0.6	1.5	3.0	1.8	1.5	1.5	4.8	2.1	1.8	1.5	1.5	0.6	1.5	1.8
T. latifolia	·	·	·	·	·	·	0.3	·	·	·	·	·	·	·	·
Ranunculus acer-type	·	0.9	0.6	·	0.3	·	0.3	·	·	·	·	·	·	·	·
Cladium mariscus	·	·	·	·	·	·	·	·	·	·	0.3	·	·	·	·
Urticaceae	·	·	·	0.3	0.3	·	0.6	·	·	·	·	·	·	·	·
Equisetum	6.0	4.5	3.6	3.0	4.2	12.8	29.9	42.8	31.3	10.2	8.0	11.9	7.1	7.5	57.0
Botrychium	·	·	0.3	·	·	·	·	·	·	·	0.3	·	0.3	·	·
Selaginella selaginoides	0.3	0.9	·	·	·	·	·	·	0.6	·	0.3	·	·	·	·
Lycopodium annotinum	·	·	·	·	0.3	·	·	·	·	·	·	·	·	·	·
monolete fern spores, without perispore	2.4	3.0	4.5	11.6	3.3	2.7	2.1	2.7	3.3	2.4	3.0	1.8	2.4	0.6	1.8
Sphagnum	0.6	1.8	1.5	2.4	1.8	0.6	0.9	2.1	2.1	0.9	0.9	1.2	0.9	0.6	1.8
algae, plancton and other micro remains (%)															
Pediastrum boryanum	6.0	1.2	8.1	1.5	7.5	11.3	6.0	10.5	5.7	9.0	2.1	6.0	7.4	2.4	7.8
P. kawraiskyi	1.2	0.6	1.5	·	0.3	3.3	1.5	2.1	1.5	0.9	0.3	0.6	0.9	0.6	1.5
P. simplex	·	·	·	·	·	·	·	·	·	·	·	·	·	·	0.3
P. simplex var. *simplex*	·	·	·	0.3	·	·	·	·	·	·	·	·	·	·	·
Botryococcus	+	+	++	+	+	+	+	++	·	+	+	++	·	+	·
Zygnemataceae	·	0.9	0.3	0.6	0.9	0.3	0.3	0.6	·	0.3	0.3	·	·	·	0.3
Spirogyra (*Ovoidites*)	0.3	0.3	·	·	0.3	·	·	0.6	·	·	·	0.3	0.3	0.3	0.3
Spirogyra	·	0.3	0.3	0.3	·	0.3	·	0.3	0.3	0.6	0.3	0.3	0.3	·	·
Chrysophyceae	0.3	·	0.3	·	0.3	·	0.3	·	·	·	·	·	·	·	·
Turbellaria (fragments)	0.3	·	0.3	·	0.3	0.3	0.3	0.3	·	·	0.6	·	0.6	·	·
Zenkersches organ (Ostracoda)	·	0.6	·	·	0.6	·	·	·	·	·	·	·	0.3	·	·
Cladocera (fragments)	·	·	0.3	·	0.3	·	·	·	·	·	·	·	0.3	·	·
Filinia hofmanni-type	·	·	·	·	·	·	·	0.3	·	·	·	·	·	·	·
Chironomidae	·	·	·	·	·	0.3	·	·	0.6	0.9	·	·	·	·	·
Betula-leafhairs	·	·	·	·	0.3	0.6	·	·	·	0.3	0.3	0.6	·	·	·
stomata	·	·	·	0.6	·	·	·	·	·	·	0.3	·	·	·	·
fungal and moss spores	·	·	·	·	·	·	·	·	·	·	·	+	·	·	·
varia/indet	0.3	·	·	0.3	0.9	·	0.6	·	·	·	·	0.6	0.3	·	·

sample number:	16	17	18	19	20	21	22	23	24	25	26	27	28	29	30
profile meter:	1.00-1.02	1.02-1.07	1.07-1.15	1.15-1.20	1.20-1.23	1.23-1.29	1.29-1.33	1.33-1.38	1.38-1.43	1.43-1.48	1.48-1.53	1.53-1.58	1.58-1.63	1.63-1.68	1.68-1.71
taxa															
certain reworked taxa (Tertiary and older) (%)	24.9	35.9	34.9	74.8	28.4	32.6	38.2	33.5	25.1	37.1	26.8	38.1	28.6	21.5	25.7
thereof															
Taxodiaceae/Cupressaceae-group	16.9	22.8	25.1	51.0	18.2	20.5	20.3	21.2	18.2	23.6	13.7	25.0	17.3	11.0	15.8
Sciadopytis	0.9	1.8	0.3	1.5	1.5	2.1	2.1	2.1	0.3	1.2	0.3	0.9	1.5	1.8	0.9
Rhoipites-type	·	·	·	·	·	·	·	·	·	·	0.6	0.6	0.9	0.9	0.6
Symplocus	·	·	·	·	·	·	·	·	·	·	0.3	·	0.3	·	0.3
Carya	·	0.6	0.6	·	·	·	0.6	0.3	·	0.6	0.3	·	0.3	0.3	·
Pterocarya	·	·	0.6	0.6	·	0.3	0.6	0.9	·	·	·	·	·	0.3	·
Juglandaceae	·	·	·	0.3	·	·	·	·	·	·	·	0.3	·	·	·
Myrica-type	0.3	0.9	1.8	1.2	0.6	0.6	1.2	1.5	0.6	0.3	0.6	0.6	·	0.3	0.3
Nyssa	·	1.2	0.6	2.1	1.2	0.3	0.3	·	0.3	·	1.8	1.2	0.9	1.2	0.6
Liquidambar	·	·	·	0.9	·	·	0.3	·	·	0.3	0.3	·	0.3	·	·
Ilex	0.3	·	0.3	·	·	0.3	0.6	0.6	0.6	·	0.3	0.3	·	0.3	0.6
Normapolles-group															
Classopollis	·	·	·	0.3	·	·	·	·	·	0.3	·	·	0.3	·	·
Momipites-type	·	·	·	·	·	0.3	·	·	·	·	·	·	·	·	·
Tasmanales	0.3	1.5	0.9	0.3	0.9	0.3	0.3	·	·	·	0.3	·	·	·	·
Triporates	0.6	0.3	0.3	0.3	0.3	0.3	1.2	0.3	0.3	1.5	0.9	1.2	0.6	0.9	·
Tricolporates	3.9	5.1	3.9	12.8	3.9	4.4	9.0	5.1	4.5	8.1	5.6	5.6	6.0	2.7	0.9
Tricolpates	0.3	0.6	0.3	0.3	1.2	1.5	0.9	0.3	·	0.6	0.9	0.3	0.3	0.3	0.3
Monocolpates	·	·	·	0.3	·	·	·	·	·	·	·	·	·	·	·
Cicatricosisporites	·	·	·	·	·	·	·	·	·	·	·	·	0.3	·	·
Azolla filiculoides	0.3	·	·	·	·	·	·	·	·	·	·	·	·	·	·
Osmunda	·	0.3	0.3	0.9	0.3	·	·	·	·	·	·	0.6	·	·	0.9
Triletes	1.5	0.9	·	2.1	0.3	1.8	0.9	0.9	0.3	0.6	0.6	1.2	0.3	0.6	0.6
others	·	·	·	·	·	·	·	0.3	·	·	·	·	0.3	·	0.3
Dinozysts	5.3	3.9	11.9	3.9	6.3	4.7	10.1	7.8	4.8	6.9	3.3	8.6	2.4	6.0	6.0
Wetzeliella-group	·	·	0.3	·	·	0.6	0.3	0.3	·	·	·	0.3	·	·	0.3

(n) = presumably reworked pollen from older interglacial rsp. from Tertiary or older
+* = form out of basis sum   + = form present   ++ = form often present   · = form not present
AP = arboreal pollen   NAP = non-arboreal pollen

sample number: profile meter: taxa	31 1.71-1.76	32 1.76-1.81	33 1.81-1.85	34 1.85-1.89	35 1.89-1.93	36 1.93-1.95	37 1.95-1.98	38 1.98-2.03	39 2.03-2.08	40 2.08-2.13	41 2.13-2.17	42 2.17-2.22	43 2.22-2.25	44 2.25-2.29	45 (o. s.)
AP (%)															
Juniperus	6.9	0.9	·	·	·	·	·	·	·	·	·	·	·	·	·
Salix	2.7	0.9	2.7	4.5	3.9	2.7	1.8	0.3	0.3	0.6	·	·	0.6	0.3	0.9
Betula	21.8	9.3	15.2	21.8	18.0	19.7	22.4	29.2	30.6	19.9	11.6	18.0	14.9	12.2	9.5
Pinus	(26.9)	10.1	44.6	42.5	46.4	54.3	37.6	38.4	36.6	29.2	31.4	26.9	26.3	21.7	22.0
Ulmus	(0.3)	·	·	0.3	2.7	2.1	5.1	5.6	6.2	8.3	6.8	5.3	4.2	3.6	4.5
Quercus	·	·	0.3	0.3	0.9	1.5	0.9	8.0	5.1	26.8	35.3	35.2	40.6	43.6	44.3
Corylus	·	·	·	0.3	·	·	·	0.6	0.3	0.6	0.9	0.6	1.8	0.6	1.2
Alnus	(1.8)	·	·	·	·	·	·	0.3	·	0.3	0.9	0.3	0.9	0.9	0.9
Taxus	·	·	·	·	·	·	·	0.3	·	0.6	·	·	0.6	·	·
Fraxinus	·	·	·	·	·	·	·	·	·	0.3	0.9	·	0.9	1.2	0.6
Picea	0.3	·	·	·	·	·	·	·	·	·	·	+*	·	0.3	0.6
Abies	·	·	·	·	·	·	·	·	·	·	0.3	·	·	·	·
Hedera	·	·	·	·	0.3	·	0.3	·	·	0.6	0.6	1.5	1.2	1.2	1.5
Viscum	·	·	·	·	·	·	·	+*	·	·	·	·	·	·	·
Acer	·	·	·	·	·	·	·	·	·	0.3	·	·	0.3	·	0.3
sum AP (%)	60.6	21.2	62.8	69.8	72.2	80.3	68.1	82.7	79.2	87.5	88.7	87.9	92.2	85.5	86.3
NAP (%)															
Poaceae	10.1	74.6	33.0	26.0	24.8	17.6	25.4	13.1	18.4	8.3	8.9	10.1	3.6	9.8	9.5
Cyperaceae	24.8	3.3	4.2	3.9	2.4	2.1	5.7	3.3	1.5	3.0	1.5	1.2	3.3	3.3	1.8
Calluna	·	·	·	·	·	·	·	·	·	·	·	0.3	0.3	·	0.3
Ericaceae p.p.	·	·	·	·	·	·	·	0.3	·	·	·	+*	·	·	·
Artemisia	3.6	0.6	·	0.3	0.3	·	0.6	0.6	·	·	·	·	0.3	0.3	0.6
Rumex acetosella type	·	·	·	·	·	·	·	·	·	0.6	+*	·	+*	+*	0.6
Chenopodiaceae	·	·	·	·	·	·	·	·	0.6	·	0.3	·	0.3	0.6	0.9
Caryophyllaceae	·	·	·	·	·	·	·	·	·	0.3	·	0.3	·	·	·
Tubuliflorae	·	·	·	·	·	·	0.3	·	·	·	·	0.3	·	0.3	·
Liguliflorae	·	·	·	·	0.3	·	·	·	·	0.3	·	·	·	·	·
Thalictrum	0.6	0.3	·	·	·	·	·	·	·	·	·	·	·	·	·
Rosaceae p.p.	·	·	·	·	·	·	·	·	·	·	0.3	·	·	0.3	·
Filipendula	0.3	·	·	·	·	·	·	·	0.3	·	0.3	·	·	·	·
sum NAP (%)	39.4	78.8	37.2	30.2	27.8	19.7	31.9	17.3	20.8	12.5	11.3	12.1	7.8	14.5	13.7
basis sum (AP + NAP)	335	335	336	334	334	335	335	336	336	336	337	338	335	337	336
swamp- and waterplants, ferns, mosses (%)															
Potamogeton	0.3	·	·	·	·	·	·	·	0.3	0.3	0.9	·	·	·	·
Myriophyllum spicatum	·	·	·	·	·	·	·	0.6	0.6	+*	·	·	·	·	·
Nuphar	·	·	·	·	·	0.3	·	·	·	·	0.3	·	·	·	·
Nymphaea	·	·	0.3	·	·	0.3	·	·	·	·	·	·	·	·	·
Nymphaeaceae (ideoblasts)	·	·	0.3	·	0.3	·	·	·	·	·	·	·	·	·	·
Ceratophyllum (leaf spines*)*	·	·	·	·	·	·	1.5	3.6	7.7	1.5	0.3	0.3	+*	·	·
Najas	·	·	0.3	·	·	·	·	·	·	·	·	·	·	·	·
Salvinia natans	·	·	·	·	1.2	1.2	3.9	2.4	1.8	1.5	0.9	1.8	0.6	0.3	0.3
Typha-/Sparganium type	0.9	6.0	6.8	8.1	5.7	3.0	7.2	9.2	6.2	5.1	4.5	5.3	5.4	7.7	4.8

sample number: profile meter: taxa	31 1.71-1.76	32 1.76-1.81	33 1.81-1.85	34 1.85-1.89	35 1.89-1.93	36 1.93-1.95	37 1.95-1.98	38 1.98-2.03	39 2.03-2.08	40 2.08-2.13	41 2.13-2.17	42 2.17-2.22	43 2.22-2.25	44 2.25-2.29	45 (o. s.)
swamp- and waterplants, ferns, mosses (%)															
Typha latifolia	·	·	0.9	2.1	2.4	0.6	·	0.9	·	0.3	·	·	+*	0.6	0.6
Ranunculus acer type	0.3	·	·	·	·	·	·	·	·	·	·	·	·	·	·
Cladium mariscus	·	0.3	·	·	0.3	1.2	1.2	0.3	·	0.3	0.3	·	·	·	·
Urticaceae	·	·	·	·	0.3	0.3	0.3	0.3	·	·	0.3	0.3	0.3	0.3	0.3
Equisetum	125.1	3.9	1.8	0.9	0.3	1.2	0.6	·	·	0.3	0.3	+*	·	·	0.3
Lycopodium	·	·	·	·	·	·	·	0.3	·	·	·	·	·	·	·
*L. complanatum-clavatum-*type	·	·	·	·	·	·	·	·	·	·	·	·	·	·	0.3
Thelypteris palustris	·	·	0.3	·	·	·	1.8	0.3	·	·	·	·	·	·	·
Ophioglossaceae	·	·	·	·	·	·	·	·	0.3	·	·	·	·	·	·
Osmunda	·	·	·	·	·	·	·	·	·	·	·	0.3	·	·	·
Pteridium	·	·	·	·	·	·	·	·	·	+*	1.8	1.2	0.9	2.4	1.8
monolete fern spores, without perispore	0.9	6.0	89.9	100.0	88.9	97.0	50.1	26.2	39.3	16.1	8.0	10.9	5.1	4.2	4.2
Sphagnum	0.3	·	·	·	·	0.3	·	·	0.3	0.3	0.3	·	0.3	·	·
algae, plancton and other micro remains (%)															
Pediastrum boryanum	2.7	·	·	0.3	·	·	2.4	1.2	1.8	21.4	10.1	12.7	16.7	30.3	13.7
P. kawraiskyi	0.6	·	·	·	·	·	0.9	0.9	0.6	9.8	7.1	9.8	4.5	10.7	6.0
P. simplex	·	·	·	·	·	·	·	·	·	1.5	5.6	2.1	7.8	22.6	8.9
P. simplex var. *simplex*	·	·	·	·	·	·	0.3	0.6	0.3	4.2	7.4	5.9	5.4	5.9	3.3
Botryococcus	·	·	·	·	·	·	·	·	·	·	+*	0.6	0.3	0.3	0.3
Zygnematales	0.3	·	0.3	·	0.3	·	0.3	·	·	·	·	·	·	·	·
Spirogyra	0.3	·	0.3	·	·	·	·	·	·	·	·	·	·	·	·
Turbellaria (fragments)	·	·	·	·	·	·	·	0.6	·	·	·	·	0.3	·	·
Mollusca (mouthparts)	·	·	·	·	·	·	·	·	·	·	·	·	·	0.3	·
Cladocera (fragments)	·	·	·	·	·	·	0.3	·	·	·	0.3	0.3	·	·	·
Chironomidae	·	·	·	0.3	·	·	0.6	·	·	0.6	0.3	·	·	·	·
Zenckersches organ (Ostracoda)	·	·	·	·	·	·	·	·	·	·	·	·	·	·	0.6
stomata	0.3	·	·	·	1.2	1.2	·	·	·	·	·	·	·	·	·
fungal and moss spores	·	·	·	·	·	·	·	+*	0.3	·	·	+*	·	·	·
varia/indet	0.3	·	·	·	0.3	·	·	0.3	·	0.3	·	·	0.3	0.3	·

sample number: profile meter: taxa	31 1.71- 1.76	32 1.76- 1.81	33 1.81- 1.85	34 1.85- 1.89	35 1.89- 1.93	36 1.93- 1.95	37 1.95- 1.98	38 1.98- 2.03	39 2.03- 2.08	40 2.08- 2.13	41 2.13- 2.17	42 2.17- 2.22	43 2.22- 2.25	44 2.25- 2.29	45 (o. s.)
certain reworked taxa (Tertiary and older) (%)	9.0	0.3	0.3	-	-	-	-	-	-	0.3	0.9	-	0.9	0.3	0.3
thereof															
Taxodiaceae/Cupressaceae -group	3.6	-	0.3	-	-	-	-	-	-	0.3	0.6	-	0.3	-	0.3
Rhoipites type	0.3	-	-	-	-	-	-	-	-	-	-	-	-	-	-
Myrica type	0.3	-	-	-	-	-	-	-	-	-	-	-	-	-	-
Nyssa	0.3	-	-	-	-	-	-	-	-	-	-	-	+*	-	-
Liquidambar	0.3	-	-	-	-	-	-	-	-	-	-	-	0.3	-	-
Ilex	0.3	-	-	-	-	-	-	-	-	-	-	-	-	-	-
Tricolporates	2.4	-	-	-	-	-	-	-	-	-	0.3	-	0.3	0.3	-
Tricolpates	0.9	-	-	-	-	-	-	-	-	-	-	-	-	-	-
Triletes	0.6	0.3	-	-	-	-	-	-	-	-	-	-	-	-	-
Dinozysts	0.9	-	-	-	-	-	-	0.3	0.3	0.3	0.6	0.3	0.9	0.9	0.6

(n) = presumably reworked pollen from older interglacial rsp. from Tertiary or older
+* = form out of basis sum   · = form not present
AP = arboreal pollen   NAP = non-arboreal pollen   o. s. = orientation sample

Eigenständigkeitserklärung

Hiermit erkläre ich, dass diese Arbeit bisher von mir weder an der Mathematisch-Naturwissenschaftlichen Fakultät der Ernst-Moritz-Arndt-Universität Greifswald noch einer anderen wissenschaftlichen Einrichtung zum Zwecke der Promotion eingereicht wurde.

Ferner erkläre ich, dass ich diese Arbeit selbstständig verfasst und keine anderen als die darin angegebenen Hilfsmittel und Hilfen benutzt und keine Textabschnitte eines Dritten ohne Kennzeichnung übernommen habe.

Greifswald, den 19. April 2017

Michael Kenzler

Curriculum Vitae Michael Kenzler

162

For resons of data protection, the curriculum vitae is not published in the electronic version.

List of publications

Peer reviewed journals

Rother, H., Lorenz, S., Boerner, A., **Kenzler, M.**, Siermann, N., Fülling, A., Hrynowiecka, A., Forler, D., Kuznetsov, V., Maksimov, F. & Starikova A. (submitted): The terrestrial Eemian to late Weichselian sediment record at Beckentin (NE-Germany): first results from lithostratigraphic, palynological and geochronological analyses. *Quaternary International*.

Kenzler, M., Rother, H., Hüneke, H., Frenzel, P., Strahl, J., Tsukamoto, S., Li, Y., Meng, S., Gallas, J. & Frechen, M. (in press): A multi-proxy palaeoenvironmental and geochronological reconstruction of the Saalian-Eemian-Weichselian succession at Klein Klütz Höved (SW Baltic Sea, NE-Germany). *Boreas*

Kenzler, M., Tsukamoto, S., Meng, S., Frechen, M., Hüneke, H. 2017: New age constraints from the SW Baltic Sea area – implications for Scandinavian Ice Sheet dynamics and palaeoenvironmental conditions during MIS 3 and early MIS 2. *Boreas 46 (1)*, 34–52.

Kenzler, M., Tsukamoto, S., Meng, S., Thiel, C., Frechen, M. & Hüneke, H. 2015: Luminescence dating of Weichselian interstadial sediments from the German Baltic Sea coast. *Quaternary Geochronology 30*, 215–256.

Other journals

Kenzler, M. & Deutschmann, A. 2012: Pleistozäne und holozäne Morphogenese der Insel Hiddensee - Exkursion K. *Jahresberichte und Mitteilungen des Oberrheinischen Geologischen Vereins, N.F. 94*, 365–400, Stuttgart.

Kenzler, M. 2010: Neuaufnahme Kliff Glowe-West. *In* Lampe, R. & Lorenz, S. (eds.): *Eiszeitlandschaften in Mecklenburg-Vorpommern, DEUQUA Excursion*, 60–61, Greifswald.

Niedermeyer, R.-O., Kanter, L., **Kenzler, M.**, Panzig, W.-A., Krienke, K., Ludwig, A.O., Schnick, H.H. & Schütze, K. 2010: Excursion C – Rügen Island (I) – Facies, stratigraphy, structural architecture and geological hazard potential of Pleistocene deposits of the Jasmund cliff coast. *In* Lampe, R. & Lorenz, S. (eds.): *Eiszeitlandschaften in Mecklenburg-Vorpommern, DEUQUA Excursion*, 50–71, Greifswald.

Kenzler, M., Obst, K., Hüneke, H. & Schütze, K. 2010: Glazitektonische Deformation der kretazischen und pleistozänen Sedimente an der Steilküste von Jasmund nördlich des Königsstuhls (Rügen). *Brandenburger Geowissenschaftliche Beiträge 17*, 107–122.

Unpublished theses

Kenzler, M. 2011: Comparative investigation of Pleistocene cliff outcrops at Glowe and Kluckow (NW Jasmund / Rügen). Unpublished Bachelor thesis, University Greifswald.

Kenzler, M. 2007: Die glazigenen Sedimente am Stubbenhörn auf Jasmund (Rügen). Unpublished Diploma thesis, University Greifswald.

Conference contributions – orals

Kenzler, M., Frechen, M., Hüneke, H., Stephan, H.-J., Thiel, C. & Tsukamoto, S. 2015: Ein frühweichselzeitlicher Eisvorstoß in Nordeutschland? Vergleich der Aufschlüsse Osterbylund (Schleswig-Holstein) und Klein Klütz Höved (Mecklenburg-Vorpommern). *In* Schriftenreihe des Landesamtes für Umwelt, Naturschutz und Geologie Mecklenburg-Vorpommern-2015, *79. Tagung der Arbeitsgemeinschaft Norddeutscher Geologen p 86*, Güstrow.

Hüneke, H., **Kenzler, M.**, Brumme, J., Gehrmann, A., Beiche, T., Kettler, C., Gallas, J. & Wegener, B. 2015: Methodische Ansätze für eine detailgetreue Rekonstruktion der weichselzeitlichen Sedimentation und Eisdynamik auf Jasmund (Rügen). *In* Schriftenreihe des Landesamtes für Umwelt, Naturschutz und Geologie

Mecklenburg-Vorpommern-2015, *79. Tagung der Arbeitsgemeinschaft Norddeutscher Geologen p 76*, Güstrow.

Kenzler. M., Meng, S., Tsukamoto, S., Thiel, C., Frechen, M. & Hüneke, H. 2014: OSL dating of (glacial-) fluvial/lacustrine MIS 3 sediments from the German Baltic Sea coast. LIAG Austauschsitzung 06.11.2014, Hannover.

Kenzler, M., Meng, S., Tsukamoto, S., Thiel, C., Frechen, M. & Hüneke, H. 2014: OSL dating of MIS3 sediments from the German Baltic Sea coast. The 12th Colloquium on Baltic Sea Marine Geology 08.-12.09.2014, Abstracts p 18, Warnemünde.

Kenzler, M., Meng, S. & Hüneke, H. 2012: The MIS 3 at the cliffs of NW Jasmund. Geohannover 01.-03.10.2012, Hannover.

Hüneke, H., **Kenzler, M.**, Brumme, J. & Beiche, T. 2012: Das Pleistozän von Rügen: Sediment- und Deformationstrukturen aus dem Blickwinkel mikrofazieller Untersuchungsmethoden. 133. Tagung des Oberrheinischen Geologischen Vereins 10.-14.04.2012, Greifswald.

Conference contribution – poster

Kenzler, M., Tsukamoto, S., Frechen, M. & Hüneke, H. 2016: Progressive growth of the Scandinavian Ice Sheet across the south-western Baltic Sea basin during Marine Isotope Stage 2. 35th International Geological Congress 27.08.-04.09.2016, paper number 4398, Cape Town.
https://www.americangeosciences.org/sites/default/files/igc/4398.pdf

Beiche, T., Hüneke, H. & **Kenzler, M.** 2015: Die Genese der rhythmisch geschichteten und rhythmisch brekziierten Seesedimente von Dwasieden (Pleistozän, Jasmund, Rügen). *In* Schriftenreihe des Landesamtes für Umwelt, Naturschutz und Geologie Mecklenburg-Vorpommern-2015, *79. Tagung der Arbeitsgemeinschaft Norddeutscher Geologen p 13*, Güstrow.

Kenzler, M., Tsukamoto, S., Frechen, M., Hüneke, H. & Meng, S. 2015: Die chronostratigraphische Neubewertung ausgewählter Kliffaufschlüsse der Halbinsel Jasmund (Rügen) basierend auf OSL Datierungen. *In* Schriftenreihe des Landesamtes für Umwelt, Naturschutz und Geologie Mecklenburg-Vorpommern-

2015, *79. Tagung der Arbeitsgemeinschaft Norddeutscher Geologen p 85*, Güstrow.

Kenzler, M., Tsukamoto, S., Frechen, M., Hüneke, H. & Rother, H. 2015: Luminescence dating of a Saalian to Weichselian sequence from the northern German Baltic Sea coast. UK Luminescence and ESR Meeting 2015; SUERC, 08.-10.07.2015; Glasgow.

Kenzler, M., Meng, S., Tsukamoto, S., Thiel, C., Frechen, M. & Hüneke, H. 2014: OSL dating of Weichselian sediments from the Jasmund peninsula (southwestern Baltic Sea). Deutsches Lumineszenz- und ESR Treffen, Gießen / Rauischholzhausen 14.-16.11.2014, Gießen.

Kenzler, M., Ash, J., Deutschmann, A., Meschede, M. & Hüneke, H. & IODP Expedition 347 Scientists. 2014: The mysteries of carbonate concretions of the Late Weichselian Baltic Ice Lake rhythmites drilled during IODP Exp. 347 at the Landsort Deep. The 12th Colloquium on Baltic Sea Marine Geology 08.-12.09.2014, Warnemünde.

Kenzler, M., Meng, S., Tsukamoto, S., Thiel, C., Frechen, M. & Hüneke, H. 2014: OSL dating of (glacial-) fluvial / lacustrine MIS3 sediments from the German Baltic Sea coast. 14th International Conference on Luminescence and Electron Spin Resonance Dating in Montreal 07.-11.07.2014, Abstracts p 95, Montreal. http://www.baltec.uni-greifswald.de/documents/kenzler_2014.pdf

Kenzler, M. & Meschede, M. 2013: Micromorphological techniques and glaciogenic sediments – tool for analysis of soft - rock core samples? IODP/ICDP meeting in Freiberg 25.-27.03.2013, Abstracts p 108, Freiberg. http://www.baltec.uni-greifswald.de/documents/kenzler_2013.pdf

Kenzler, M., Meng, S. & Hüneke, H. 2012: The MIS 3 at the cliff of Kluckow (Jasmund /SW Baltic Sea coast). GV and Sediment Meeting 23.-28.10.2012, Hamburg.

Kenzler, M., Obst, K., Hüneke, H. & Schütze, K. 2009: How stable is the cliff north of the 'Königsstuhl' (Jasmund/Rügen)? – Coastal evolution during the last 50 years. International Conference on Climate Change, 25.-28.05.2009, Szczecin.

Kenzler, M., Hüneke, H., Obst, K. & Schütze, K. 2008: Late Pleistocene glacial records of ice-marginal and proglacial deposits: A case study from Rügen (southern coast of the Baltic Sea). Meeting Int. Assoc. Sedimentologists, 01.-03.09.2008, Bochum.

Acknowledgments